

Functional and Clinical Significance of EPLIN in the Progression of Gastrointestinal Cancers



Thesis submitted to Cardiff University for the degree of PhD

PhD Candidate: Jianyuan Zeng

Supervisor Team: Prof Wen G. Jiang, Dr Rachel Hargest, (Dr Andrew J. Sanders),
Dr Lin Ye

July 2022

Acknowledgement

Here I would like to thank Prof Wen G. Jiang for offering me this opportunity to study this PhD project and chase my dream at CCMRC, Cardiff University. Your wisdom, support and professional advice guided me to move forward and be a better researcher. Thank you again for helping me embrace this wonderful research world.

I would like to thank CCMRC team for all your support through my PhD study. CCMRC is like a big family where everyone helps and takes care of everyone. A huge thank to Dr Andrew Sanders, you are always there whenever I got confused and lost. You taught me a lot more than laboratory techniques and scientific knowledges, but also how to be a good researcher and how to sail in this academic sea. Working with you is definitely my pleasure and I cannot say thank you enough for everything you have done for me. Wisdom words from you and Prof Jiang will be with me through my whole academic career. I would also like to thank Dr Lin Ye for your supports and advice for my PhD study, it means a lot to me. Thank you to Dr Rachel Hargest for your professional clinical advice, you have taught me a lot. I also want to say thank you to Dr Tracey Martin for your supports and Mrs Fiona Ruge for helping me with IHCs and your kindness and smile everyday make my day in the lab more enjoyable. Dr Jane Lane, thank you for formatting my writing works. I am particularly grateful to all members in the team, the host laboratory and the host School that had helped me during my study of which the majority part was during the COVID pandemic and national lockdowns. The helps both in person, in organising the shifts, maximising each possible time slot in the laboratory have allowed the progress of my study to a timely completion.

I would like to thank all my peer in CCMRC, Henson, Amy, Channing, Wendy, Laijian, Yiming, Ziqian and Yali. Working with you is enjoyable and thank you for your help. I would also like to thank Amy, Henson and Alicia for being such good friends, your support made me see light at the end of the tunnel and made my journey more joyful.

Finally, a huge thank to my family, my parents and my sister. I would not be able to study my PhD project without your endless support and love. Karl, my dearest partner, thank you for being there for me when I was sad and confused. You are my rock and I can always turn to you when I need a hug. I cannot do this without you and I am looking forward to the future life that I will spend with you.

Publications and presentations

Full papers

Zeng J, Jiang WG, Sanders AJ.

Epithelial Protein Lost in Neoplasm, EPLIN, the Cellular and Molecular Prospects in Cancers. *Biomolecules*. 2021 Jul 16;11(7):1038. doi: 10.3390/biom11071038.

Gong W, Zeng J, Ji J, Jia Y, Jia S, Sanders AJ, Jiang WG.

EPLIN Expression in Gastric Cancer and Impact on Prognosis and Chemoresistance. *Biomolecules*. 2021 Apr 8;11(4):547. doi: 10.3390/biom11040547

Presentations and publications

Jianyuan Zeng, Andrew James Sanders, Tracey Amanda Martin, Wen Guo Jiang

The influence of mechanical and chemical insult on the integrity of vascular endothelial cells and associated impact on Epithelial Protein Lost In Neoplasm (EPLIN) and potential partner protein network. San Antonio Breast Cancer Symposium. 8th- 11th, December, 2020, San Antonio, USA (Online)

Jianyuan Zeng, Andrew Sanders, Rachel Hargest, Lin Ye, Wen G. Jiang

Expression of HSP60 on Colorectal Cancer and Implication in chemotherapeutic responses. ESMO 24th World Congress on Gastrointestinal Cancer. 29th June-2nd July, 2022, Barcelona, Spain (In person)

Jianyuan Zeng, Wen Jiang, Rachel Hargest, Zhongtao Zhang, Jun Li, Andrew Sanders

Clinical implication of Epithelial Protein Lost In Neoplasm (EPLIN) in Colorectal Cancer. ASGBI Congress, 10th-12th June, 2020, Glasgow, UK (Online)

Summary

Colorectal cancer and pancreatic cancer rank as the 4th and 10th most common cancer types in the UK, and both are a deadly threat to people, thus also they have become a heavy social burden. Poor survival rates at the more aggressive stages and frequently reported drugs resistance encouraged researchers to try to gain more understanding of the development of such cancers and hunt for novel bio markers to developing treatments to improve outcomes. My PhD study focussed on establishing the functional and clinical implication of EPLIN on colorectal cancer and pancreatic cancer, as well as its impact on drug resistance. Potential interacting partners and signalling events were also investigated to understand possible the mechanistic network of EPLIN in colorectal cancer.

EPLIN expression was downregulated in human clinical colorectal cancer tissues at transcript and protein level and its downregulation worsened clinical outcomes of colorectal cancer patients. By manipulating expression of EPLIN in colorectal cancer cell lines, EPLIN regulates cellular growth, adhesion, migration and invasion negatively. Protein microarray revealed potential interacting partners and related signalling events of EPLIN. Further I followed up with two of the priority partners, HSP60 and Her2, and performed co-IP assays as well as manipulated EPLIN/HSP60 expressions in colorectal cancer cells to reveal that EPLIN and HSP60 had a negative correlation with Her2 but not a close protein-protein interaction. High level of HSP60 was observed in colorectal cancer at transcript and protein level. Clinical implication of such molecules was also investigated by revisiting a colorectal cancer cohort, the higher level of Her2 led to worse overall survival (OS) and disease-free survival (RFS), while the combination of aberrant expression of EPLIN/Her2/HSP60 resulted in worst clinical outcomes within control groups and was identified as one of the factors to affect the OS and RFS as well. Moreover, inhibition of EPLIN and HSP60 in colorectal cancer cell lines led to dysregulation of cells' response to chemotherapeutic and EGFR/Her2 targeted therapeutic agents. Such dysregulation might be related to the correlated relationship between these molecules or mitochondrial metabolism. In my study, I also demonstrated that EPLIN was related to carcinogenesis in pancreatic cancer. Its expression was upregulated in tumour samples at transcript and protein level and related to aggressiveness. The presence of EPLIN led to worse clinical outcomes of pancreatic cancer patients.

In conclusion, my study explored and demonstrated EPLIN's implication on clinical outcomes, cellular functions and drugs resistances as well as shed light on mechanisms of action of EPLIN in colorectal cancer. This study also challenges the tumour suppressor role that EPLIN plays, and suggests it promotes the development of pancreatic cancer.

Abbreviations

5-FU	5-fluorouracil
AJ	Adherens junctions
AJCC	American Joint Committee on Cancer
APC	Adenomatous Polyposis Coli
ARCaP	Androgen refractory cancer of prostate
Arv1	ACAT-related protein required for viability 1
AS	Age standardised
ATF	Activating transcription factor
AXIN	Axis inhibition proteins
BMI	Body mass index
BRAF	B-Raf proto-oncogene, serine/threonine kinase
BRCA	Breast Cancer gene
BSA	Bovine serum albumin
CA19-9	Cancer antigen 19-9
CAF	Cancer-Associated Fibroblasts
CAMs	Cell-cell adhesion molecules
Capeox	Capecitabine with oxaliplatin
CAPIRI	Capecitabine, irinotecan
CAPOX	Capecitabine, oxaliplatin
CAPP2	Colorectal Adenoma/Carcinoma Prevention Programme 2
CCMS	Colon cancer molecular subtyp
CCND1	Cyclin D1
CCS	Colon cancer subtype
CDH1	E-cadherin
CDK6	Cyclin Dependent Kinase 6
CDKN2A	Cyclin Dependent Kinase Inhibitor 2A
CEA	Carcinoembryonic antigen
CIMP	CpG island methylator phenotype
CIN	Chromosomal instability
CLASP2	Cytoplasmic Linker Associated Protein 2
cLP	Classical lamellipodia
co-IP	Co-immunoprecipitation
CRC	Colorectal cancer
CRCA	Colorectal cancer assigner
CRCSC	Colorectal cancer subtyping consortium
CTC	CT colonography
CTCs	Circulating tumour cells
CTLA4	Cytotoxic T lymphocyte antigen 4
CTNNA1	α -catenin
CTNNB1	β -catenin
CTNND1	p120
DEPC	<i>Diethyl pyrocarbonate</i>
DFS	Disease-Free Survival
DMEM	Dulbecco's Modified Eagle's medium
DMSO	Dimethyl sulfoxide
DTX	Docetaxel
DVL	Dishevelle
EC	Endothelial cell
ECIS	Electric Cell Impedance Sensing
ECM	Extracellular matrix
EDAC	Epithelial defence against cancer

EGFR	Epidermal growth factor receptor
eIF4E	Eukaryotic Translation Initiation Factor 4E
EMR	Endoscopic resection
EMT	Epithelial mesenchymal transition
EPLIN	Epithelial protein lost in neoplasm
ErbB2	Epidermal Growth Factor Receptor 2
ERK	Extracellular signal- regulated kinase
ESD	Endoscopic submucosal dissection
F-actin	Filament actin
FAK	Focal adhesion kinase
FAP	Familial Adenomatous Polyposis
FCS	Foetal Calf Serum
FIT	Faecal immunochemical test
FOBT	Faecal occult blood test
FOLFIRI	5-FU, LV with irinotecan
FOLFOX	5-FU, LV and oxaliplatin
G-actin	Globular actin
GDP	Guanosine diphosphate
GEO	Gene Expression Omnibus
GI	Gastrointestinal
GRB2	Growth factor receptor bound protein 2
GSK3 β	Glycogen synthase kinase three β
GTP	Guanosine triphosphate
HDACs	Histone deacetylases
HGF	Hepatocyte growth factor
HGNC	HUGO Gene Nomenclature Committee
HIF-1	Hypoxia inducible factor-1
HNPCC	Hereditary Non-Polyposis Colorectal Cancer
HSP	Heat Shock Protein
HUVEC	Human umbilical vascular endothelial cell
IARC	The International Agency for Research on Cancer
ICI	Immune checkpoint inhibitor
IFN- γ	Interferon γ
IGF-1	Insulin like growth factor-1
IgG	Immunoglobulin G
IHC	Immunohistochemistry
IPMN	Intraductal papillary mucinous neoplasm
IR	Ionizing radiation
JAIL	Junction-associated intermittent lamellipodia
JUN	Jun Proto-Oncogene, AP-1 Transcription Factor Subunit
KRAS	Kirsten Rat Sarcoma Viral Oncogene Homolog
LC-MS/MS	Liquid chromatography-tandem mass spectrometry
LCK	Lymphocyte Cell-Specific Protein-Tyrosine Kinase
LDL-C	Low-density lipoprotein cholesterol
LGR5	Leucine-rich repeat-containing G-protein coupled receptor 5
LncRNA	Long noncoding RNA nuclear paraspeckle assembly
NEAT1	transcript 1
Lonsurf	5-FU, LV, irinotecan, capecitabine, trifluridine and tipiracil
LS	Lynch syndrome
LUZP1	Leucine Zipper Protein 1
LV	Leucovorin
MAPK	Mitogen-activated protein kinase
MCN	Mucinous cystic neoplasm

MEC	Mammary epithelial cell
MET	Metabolic equivalent of tasks
MHC	Major histocompatibility complex
MMR	DNA mismatch repair
MRI	Magnetic resonance imaging
MRLC	Myosin regulatory light chain
MSI	Microsatellite instability
MTT	Thiazolyl Blue Tetrazolium Bromide
MUTYH	mutY DNA glycosylase
NAC	Neoadjuvant chemotherapy
NADH	Nicotinamide adenine dinucleotide
NADPH	Nicotinamide adenine dinucleotide phosphate
NCCN	National Comprehensive Cancer Network
NCI	National Cancer Institute
NCIN	National Cancer Intelligence Network
NHOK	Normal human oral keratinocytes
NPC1L1	Niemann-Pick C1-Like Protein 1
NPI	Nottingham Prognosis Index
OR	Odds Ratio
ORF	Open reading frame
OS	Overall Survival
PADC	Pancreatic ductal adenocarcinoma
PAF	population attributable fraction
PanIN	Pancreatic intraepithelial neoplasia
PBS	Phosphate-buffered saline
PCR	Polymerase Chain Reaction
PD1	Programmed cell death 1
PDGF	Platelet produced platelet-derived growth factor
PDQ	Physician Data Query
PET-Scan	Positron emission tomography scan
PIP2	Phosphatidylinositol 4, 5 biphosphate
PIP3	Phosphatidylinositol 3, 4, 5 triphosphate
PKA	Protein kinase A
PMs	Peritoneal macrophages
PNETs	Neuroendocrine pancreatic tumours
PrEC	Prostate epithelial cell
PRSS1	Serine Protease 1
PTEN	Phosphatase and tensin homologue protein
PVDF	Polyvinylidene fluoride
PXN	Paxillin
qPCR	Quantitative PCR
RFS	relapse-free survival
RR	Relative risk
SBRT	Stereotactic body radiotherapy
SCCHN	Squamous cell carcinoma of head and neck
SDS	Sodium dodecyl sulphate
SDS-PAGE	Sodium dodecyl sulfate-polyacrylamide gel electrophoresis
SIPA1L1	Signal Induced Proliferation Associated 1 Like 1
SOS	Son of seven-less
SPINK1	Serine Peptidase Inhibitor Kazal Type 1
Src	Proto-oncogene tyrosine protein kinase
STAT3	Signal transducer and activator of transcription 3
STK11	Serine/Threonine Kinase 11

TAM	tumour-associated macrophages
TCF/LEF	T-cell factor/lymphoid enhancer factor family
TCGA	The Cancer Genome Atlas
TCR	T cell receptor
TFAP2A	Transcription Factor AP-2 Alpha
TGF- β	Transforming growth factor- β
TMA	Tissue microarrays
TME	Tumour Microenvironment
TNF- α	Tumour necrosis factor α
TNM	Tumour, regional lymph nodes and distant metastasis
VCL	Vinculin
VEGF	Vascular endothelial growth factor
VEGFR	VEGF receptor
WB	Western Blot
WRFC	World Cancer Research Fund Classifications

Table of Contents

ABBREVIATIONS-----	5
CHAPTER1-----	16
INTRODUCTION-----	16
1.1 Colorectal cancer-----	17
1.1.1 Large intestine-----	17
1.1.1.1 Anatomy-----	17
1.1.1.2 Histology of the colonic wall-----	18
1.1.1.3 Blood supply and lymphatic drainage-----	18
1.1.1.4 Function of colon and rectum-----	19
1.1.1.4.1 Formation, storage and elimination of faeces.-----	19
1.1.1.4.2 Absorption of water and electrolytes-----	19
1.1.1.4.3 Microflora are involved in production of vitamins and carcinogenesis.-----	19
1.1.2 Incidence of colorectal cancer-----	20
1.1.3 Carcinogenesis of CRC-----	23
1.1.3.1 Molecular pathways-----	23
1.1.3.2 Tumour microenvironment-----	26
1.1.4 Risk factors for CRC-----	27
1.1.4.1 Obesity-----	28
1.1.4.2 Alcohol-----	28
1.1.4.3 Smoking-----	28
1.1.4.4 Lack of physical activity-----	28
1.1.4.5 Lack of dietary fibre-----	29
1.1.4.6 Radiation-----	29
1.1.4.7 Type II diabetes and gastrointestinal diseases-----	30
1.1.4.8 Medication-----	31
1.1.4.9 Hereditary syndrome-----	31
1.1.4.10 Hereditary non-polyposis colorectal cancer-----	31
1.1.4.11 Familial Adenomatous Polyposis-----	32
1.1.5 Diagnosis and staging of CRC-----	32
1.1.5.1 Clinical features and diagnosis of colorectal cancer-----	32
1.1.5.2 Staging of colorectal cancer-----	32
1.1.6 Treatment of CRC-----	35
1.1.6.1 Surgery-----	35
1.1.6.2 Radiotherapy-----	35
1.1.6.3 Chemotherapy and targeted therapy-----	35
1.1.6.4 Immunotherapy-----	36
1.2 Metastasis of Colorectal Cancer-----	37
1.2.1 Metastatic cascade-----	37
1.2.1.1 Lymphatic spread-----	37
1.2.1.2 Haematogenous spread-----	37
1.2.1.3 Peritoneal dissemination (transcoelomic metastasis)-----	38
1.2.2 Genes and key pathways-----	40
1.2.2.1 Tumour suppressors-----	40
1.2.2.1.1 <i>Adenomatous Polyposis Coli (APC)</i> -----	40
1.2.2.1.2 p53-----	40
1.2.2.1.3 TGF- β -----	40
1.2.2.2 Tumour promoting genes-----	41
1.2.2.2.1 KRAS/BRAF-----	41

1.2.2.2.2 PI3KCA	41
1.2.2.3 Key Pathways	41
1.2.2.3.1 Canonical Wnt signalling pathway	41
1.2.2.3.2 TGF- β signalling pathway	42
1.2.2.3.3 EGFR/MAPK & PI3K/AKT signalling pathway	43
1.2.3 Epithelial Mesenchymal Transition (EMT)	45
1.2.4 Prognosis of CRC and challenges for unmet clinical needs	46
1.3 Pancreatic Cancer	47
1.3.1. Overview of pancreas	47
1.3.2. Incidence and mortality of pancreatic cancer	47
1.3.3 Risk factors & genetic factors	48
1.3.3.1 Risk factors	48
1.3.3.2 Genetic factors	48
1.3.4 Diagnosis and treatment	49
1.3.5. Urgent need	49
1.4 Epithelial Protein Lost in Neoplasm (EPLIN)	50
1.4.1 Discovery	50
1.4.2 Location	50
1.4.3 Structure of the EPLIN coding gene, <i>LIMA1</i>	51
1.4.4 Function and Functional Interacting Partners of EPLIN	53
1.4.4.1 EPLIN regulates actin dynamics	53
1.4.4.2 Functional interaction partners of EPLIN	54
1.4.4.2.1 EPLIN stabilizes adherens junction via cadherin-catenin complex	54
1.4.4.2.2 EPLIN is required for cytokinesis	55
1.4.4.2.3 EPLIN is a direct target of the p53 family	57
1.4.4.2.4 Phosphorylation of EPLIN by ERK is required in EGF induced EMT	58
1.4.4.2.5 EPLIN interacts with FAK & Src	61
1.4.4.2.6 EPLIN interacts with Plectin, Cav-1 and paxillin	61
1.4.4.3 Impact on endothelial cells	65
1.4.4.4 EPLIN, implications in other biological processes and diseases	69
1.4.5 Role in cancer	78
1.4.5.1 Breast cancer	79
1.4.5.2 Prostate cancer	80
1.4.5.3 Melanoma, oesophageal cancer, ovarian cancer, pulmonary cancer & SCCHN	82
1.4.5.4 Gastric cancer	83
1.4.5.5 Colorectal cancer	83
1.5 Hypothesis and Aims	84
CHAPTER2	89
MATERIALS & METHODS	89
2.1 Materials	90
2.1.1 Cell lines	90
2.1.2 General cell culture plastics, hardware and software	91
2.1.3 General compounds	92
2.1.4 Primers	94
2.1.5 Antibodies	95
2.2 Cell culture	96
2.2.1 Preparation of chemical solutions used for cell culture	96
2.2.1.1 Cell Culture Medium	96

2.2.1.2 Phosphate-buffered saline (PBS)	96
2.2.1.3 Trypsin EDTA	96
2.2.2 Culturing cells	96
2.2.3 Cell Detachment, passaging and cell counting	97
2.2.3.1 Cell detachment and passaging	97
2.2.3.2 Cell counting	97
2.2.4 Storage of cells in liquid nitrogen and cell thawing	98
2.2.4.1 Storage of Cells in Liquid Nitrogen	98
2.2.4.2 Cell thawing	98
2.2.5 Transfection	98
2.2.5.1 Plasmid preparation and extraction	98
2.2.5.2 Generation of EPLIN α overexpression cell lines using electroporation-based transfection	100
2.2.5.3 Generation EPLIN knockdown cell lines using shRNA-based transfection	100
2.2.5.4 Generation HSP60 knockdown cell lines using siRNA-based transfection	100
2.2.5.5 Generation EPLIN manipulated cell lines using UltraCruz [®] based transient transfection	101
2.2.6 Thiazolyl Blue Tetrazolium Bromide (MTT) based Killing curve	101
2.2.7 MTT-growth assay	102
2.2.8 Matrigel adhesion assay	102
2.2.9 Matrigel invasion assay	103
2.2.10 Wound healing assay	104
2.2.11 Electric cell-substrate impedance sensing (ECIS) based cell migration assay	104
2.2.12 Cytotoxicity assays	106
2.2.13 Mitochondrial metabolic assays	106
2.2.13.1 Griess Reagent System	106
2.2.13.2 NAD(P)H-Glo [™] Detection System	106
2.3 Molecular biology	107
2.3.1 Preparation of chemical solutions used for molecular biology	107
2.3.1.1 DEPC (Diethyl pyrocarbonate) water	107
2.3.1.2 75% Ethanol DEPC water	107
2.3.1.3 GoScript [™] Reverse Transcription Mix, Oligo (dT)	107
2.3.1.4 Primers	107
2.3.1.5 Tris-Boric-Acid (TBE) electrophoresis buffer	107
2.3.2 RNA Extraction	108
2.3.2.1 RNA isolation	108
2.3.2.2 RNA quantification	108
2.3.3 Reverse transcription of RNA	109
2.3.4 Polymerase Chain Reaction (PCR)	109
2.3.5 Agarose gel electrophoresis and DNA visualisation	110
2.3.5.1 Agarose gel electrophoresis	110
2.3.5.2 DNA visualisation	110
2.3.6 Real time quantitative PCR (qPCR)	111
2.4 Protein extraction and analysis	112
2.4.1 Protein extraction	112
2.4.2 Protein quantification	112
2.4.3 Sodium dodecyl sulfate-polyacrylamide gel electrophoresis (SDS-PAGE)	113
2.4.4 Transfer to polyvinylidene fluoride (PVDF) membrane	113
2.4.5 Immuno-Blotting	114
2.4.6 Co-immunoprecipitation	114
2.5 Tissue collection and processing	115
2.5.1 Colorectal cancer cohort	115
2.5.2 Pancreatic cancer cohort	116
2.6 Immunohistochemical (IHC) staining and analysis	116

2.7 Kinex™ antibody-based protein microarray	117
2.8 statistical analysis	121
CHAPTER-3	122
CLINICAL SIGNIFICANCE OF EPLIN IN COLORECTAL CANCER (CRC)	122
3.1 Introduction	123
3.2.1 Tissue collection and processing	125
3.2.2 RNA extraction	125
3.2.3 Reverse transcription of RNA	125
3.2.4 Real time quantitative PCR (qPCR)	125
3.2.5 Immunohistochemical (IHC) staining and analysis	125
3.2.6 Statistical analysis	125
3.3 Results	126
3.3.1 Analysis of EPLIN expression within online GEO datasets	126
3.3.2 Transcript expression of EPLIN in clinical CRC cohorts	130
3.3.2.1 Quantitative Polymerase Chain Reaction (qPCR) for the first clinical cohort	130
3.3.2.2 qPCR Analysis of EPLIN transcript expression in the second clinical Cohort.	132
3.3.3 Implications of EPLIN expression on patients' survival	133
3.3.4 Analysis of The Cancer Genome Atlas (TCGA) database	136
3.3.5 EPLIN protein expression in clinical CRC tissue	139
3.3.5.1 Immunohistochemical staining of EPLIN expression in clinical CRC	139
3.3.5.2 Tissue microarray (TMA)	141
3.4 Discussion	146
CHAPTER-4	150
FUNCTIONAL SIGNIFICANCE OF EPLIN IN COLORECTAL CANCER (CRC) CELLS	150
4.1 Introduction	151
4.2 Methods	153
4.2.1 cell culturing	153
4.2.2 Thiazolyl Blue Tetrazolium Bromide (MTT) based Killing curve	153
4.2.3 Transfection	153
4.2.4 MTT cells growth assay	153
4.2.5 Matrigel cells adhesion assay	153
4.2.6 ECIS based cells migration assay	153
4.2.7 Matrigel cells invasion assay	154
4.3 Results	154
4.3.1 EPLIN expression screening in CRC cell lines	154
4.3.2 Transfection of CRC Cell lines	157
4.3.2.1 Killing Curve and Transfection Process	157
4.3.2.2 Confirmation of over-expression of EPLIN α in RKO cell lines.	159
4.3.2.3 Confirmation of knockdown of EPLIN in HRT-18 cell lines	161
4.3.3 Implication of EPLIN expression on cell growth	163
4.3.4 Implication of EPLIN expression on cell adhesion	165
4.3.5 Implication of EPLIN expression on cell migration	168
4.3.6 Implication of EPLIN expression on the <i>in vitro</i> invasiveness of colorectal cancer cells	171

4.4 Discussion -----	174
CHAPTER-5 -----	177
IDENTIFICATION OF KEY SIGNALLING PATHWAYS INVOLVING EPLIN IN COLORECTAL CANCER -----	177
5.1 Introduction -----	178
5.2 Methods -----	178
5.2.1 Kinex™ antibody protein microarray -----	178
5.2.2 Cell culture-----	179
5.2.3 Protein extraction and quantification-----	179
5.2.4 Immunoprecipitation -----	179
5.2.5 Western blotting -----	179
5.3 Results -----	179
5.3.1 Searching for EPLIN interacting proteins and protein kinases in colorectal tissues -----	179
5.3.2. Comprehensive analysis of signalling pathways from the most prominent priority EPLIN interacting proteins in colon tissues by way of Reactome analysis -----	185
5.3.3 Interaction of EPLIN with the Heat Shock Protein (HSP) family proteins-----	188
5.3.4 Interaction of EPLIN with the EGFR family proteins-----	191
5.3.5 Potential signalling pathways involved by the EPLIN interacting candidates -----	194
5.3.6 Investigation of interaction among EPLIN, HSP60 and Her2 in CRC cell lines -----	196
5.3.7 Investigation into potential regulatory relationships between EPLIN, HSP60 and Her2 in colorectal cancer cell lines-----	200
5.4 Discussion -----	203
CHAPTER 6 -----	205
6.1 Introduction -----	206
6.2 Methods -----	208
6.2.1 Tissue collection and processing-----	208
6.2.2 RNA extraction-----	208
6.2.3 Reverse transcription of RNA -----	208
6.2.4 qPCR-----	208
6.2.5 IHC and TMA -----	208
6.2.5 Statistical analysis-----	208
6.3 Results -----	208
6.3.1 Transcript expressions of HSP60 in clinical CRC cohort.-----	208
6.3.2 Transcript expressions of HER2 in clinical CRC cohorts. -----	210
6.3.3 Correlation of Hers, HSP60 and EPLIN in clinical CRC cohort-----	212
6.3.4 Implications of Her2, HSP60 and EPLIN on patients' overall survival.-----	215
6.3.5 Implications of Her2, HSP60 and EPLIN on patients' relapse-free survival.-----	219
6.3.6 HSP60 protein expression profile in CRC tissues -----	222
6.4 Discussion -----	226
CHAPTER 7 -----	229

IMPLICATION OF EPLIN, HSP60 AND HER2 ON DRUG SENSITIVITY IN COLORECTAL CANCER 229

7.1 Introduction	230
7.2 Methods	231
7.2.1 Cell culture and transfection	231
7.2.2 RNA extraction, reverse transcription and qPCR	231
7.2.3 Cytotoxicity assays	231
7.2.4 Griess Reagent System	231
7.2.5 NAD(P)H-Glo™ Detection System	231
7.2.6 Statistics	231
7.3 Results	232
7.3.1 <i>Implication of EPLIN, HSP60 and Her2 on chemotherapeutic resistance in the TCGA colorectal cancer cohort</i>	232
7.3.1.1 All chemotherapies combined	232
7.3.1.2 Bevacizumab	233
7.3.1.3 Capecitabine	235
7.3.1.4 Irinotecan	236
7.3.1.5 5-fluorouracil (5-FU)	237
7.3.1.6 Oxaliplatin	238
7.3.2 Implication of EPLIN and HSP60 on response to chemotherapeutic agents in colorectal cancer cells	239
7.3.2.1 5-fluorouracil (5-FU)	241
7.3.2.2 Docetaxel	243
7.3.2.3 Oxaliplatin	245
7.3.3 Implication of EPLIN and HSP60 on EGFR/Her2 targeted therapy in colorectal cancer cells	247
7.3.3.1 AG825	247
7.3.3.2 Neratinib	249
7.3.3.3 Afatinib	251
7.3.3.4 Lapatinib	253
7.3.3.5 Regulatory relationship between EPLIN, HSP60 and Hers family	255
7.3.4 Implication of manipulating EPLIN/HSP60 on mitochondrial metabolism	258
7.3.4.1 Implication of manipulation of EPLIN/HSP60 on NAD(P)H	258
7.3.4.2 Implication of manipulation of EPLIN/HSP60 on nitrite production in cells	259
7.4 Discussion	260
CHAPTER 8	264
EPLIN EXPRESSION PROFILE IN PANCREATIC CANCER AND ITS CLINICAL IMPLICATION	264
8.1 Introduction	265
8.2 Methods	265
8.2.1 Pancreatic cancer clinical cohort	265
8.2.2 QPCR	266
8.2.3 IHC and TMA	266
8.2.4 Statistics	266
8.3 Results	266
8.3.1. Expression profile of EPLIN gene transcript in pancreatic ductal cancer clinical cohort	266
8.3.2 Expression profile of EPLIN in pancreatic adenocarcinoma from TCGA database	268
8.3.3 Implication of EPLIN on patients' overall survival in the pancreatic cancer clinical cohort	270
8.3.4 Implication of EPLIN expression on patients' survival in TCGA pancreatic ductal adenocarcinoma data set	271

8.3.5 Protein expression profile of EPLIN in pancreatic cancer tissues.....	272
8.4 Discussion	277
CHAPTER 9	280
GENERAL DISCUSSION	280
9.1 Clinical implication of EPLIN in colorectal cancer	281
9.2 EPLIN regulates cellular functions in colorectal cancer	282
9.3 Potential novel interacting partners and signalling pathways of EPLIN in colorectal cancer	283
9.4 Clinical implication of Her2, HSP60 and EPLIN on colorectal cancer	284
9.5 EPLIN and HSP60 have the potential to regulate responsive efficiency of chemotherapeutic and EGFR/Her2 targeted therapeutic agents	284
9.6 Potential novel signalling pathway of EPLIN in colorectal cancer	285
9.7 EPLIN plays a different role in pancreatic cancer	286
9.8 Future work	287
REFERENCES	288
SUPPLEMENT MATERIALS	308
Supplement-1. Human Colorectal cancer TMA	308
Supplement-2. TMA of human pancreatic cancer.	315

Chapter1

Introduction

1.1 Colorectal cancer

1.1.1 Large intestine

1.1.1.1 Anatomy

Colorectal cancer (CRC) refers to cancer that occurs in the colon and rectum (Cancer Research UK 2020). The colon and rectum are found in the lower digestive tract and are located in the peritoneal cavity along with other visceral organs, such as the liver, stomach, kidney, duodenum and small intestine. The initial part of the large intestine, the caecum, forms the connection between the colon and small intestine, and it connects to the small intestine with the addition of an appendix. The colon can be separated into four distinct parts due to the physiological bending (Figure 1.1), namely the ascending colon (that includes the right colonic (hepatic) flexure), the transverse colon (that includes the left colonic (splenic) flexure), the descending colon and the sigmoid colon. The rectum then connects to the sigmoid at the end of the lower digestive tract (Azzouz and Sharma 2020). Recent studies have suggested the large intestine should be separated into three parts based on their blood supply and lymphatic drainage - the proximal colon (caecum, ascending colon and transverse colon), the distal colon (descending colon) and the rectum, since the anatomical location where CRC has developed is associated with different subtypes, genders, age, ethnicity and hereditary syndromes (Keum and Giovannucci 2019).

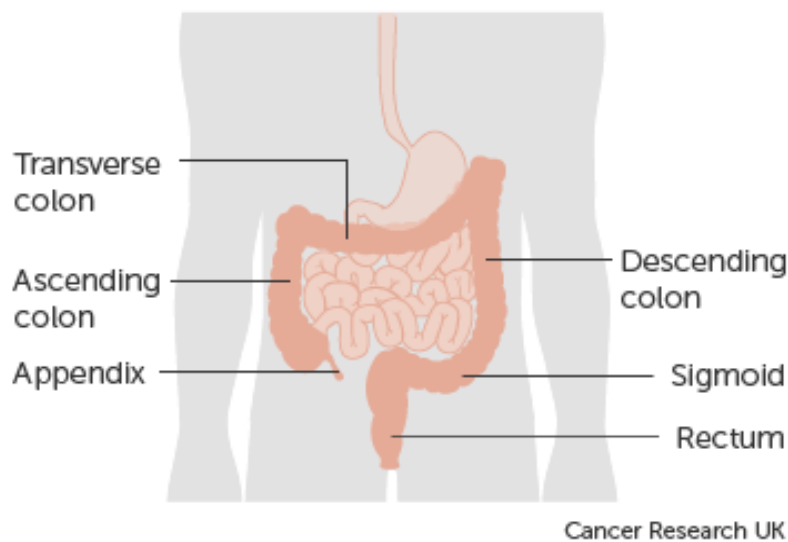


Figure 1.1 Anatomy of Large Intestine. (Credit: Cancer Research UK)

1.1.1.2 Histology of the colonic wall

The colonic wall is comprised of the following layers, namely the mucosa, submucosa, muscularis propria, the subserosa and serosa. Unlike the small intestine, the surface of the colon mucosa does not have circular folds but is instead made up of columnar cells and goblet cells. The mucosa also contains a layer called lamina propria. The submucosa is formed of loose connective tissue, vessels, lymphatics, nerves and adipocytes. The muscularis propria, which is found outside the mucosa and submucosa, is made from two different types of smooth muscle, the internal-circular smooth muscle and the external-longitudinal smooth muscle. Beneath the muscularis, the colonic wall is covered by the subserosa and serosa. The transverse colon, sigmoid, anterior wall of the ascending colon and the descending colon are covered by serosa, while the posterior walls of the ascending colon and descending colon are covered by the fibrous tissue of the retroperitoneum. The external longitudinal smooth muscle can be thicker in some parts of the colon and as a result forms three longitudinal taenia coli on the external surface of the colon. Since the taenia coli is shorter than the colon it attaches to, small pouches, namely Haustra are formed due to the sacculation. Another characteristic colon has is epiploic appendages, a type of fat-filled protrusion which is covered by serosa and lays along the outer surface of the colon (Li and Zeng 2018; Patil and Zhang 2022).

1.1.1.3 Blood supply and lymphatic drainage

The mesocolon carries blood and lymphatic vessels to the non-retroperitoneal sections of the large intestine, particularly the transverse colon. Blood vessels and lymphatics throughout the mesocolon establish connections between vessels that are derived from the submucosa of the colon, the circulatory system and the lymphatic system. The ileocolic artery, which provides the blood supply to the right side of the colon, is the terminal branch of the superior mesenteric artery, while the left side of colon, sigmoid and rectum are supplied by left colic, sigmoid and superior rectal arteries which all arise from the inferior mesenteric artery. The junction of the proximal two-thirds and distal third of the transverse colon is the site of overlap between right and left blood supplies. This marks the site of junction of the embryological midgut and hindgut and hence their arterial supply – superior mesenteric and inferior mesenteric respectively. Veins also run alongside the arteries, converging to form the superior mesenteric vein and inferior mesenteric vein respectively. The inferior mesenteric vein is a branch of the splenic vein, and the splenic vein and superior mesenteric vein unite to form the portal vein (Beauchemin and Huot 2010).

Lymph fluid is mainly transported to the lymph nodes of the colon and paracolon lymph nodes via lymphatic vasculatures. The lymph fluid drains to either ileocolic nodes, right colic nodes, middle colic nodes, left colic nodes or sigmoid nodes, dependent on where the lymph fluid has originated. Thereafter, lymph fluid is transported to the superior mesenteric nodes and inferior mesenteric nodes from right or left sides respectively (Beauchemin and Huot 2010).

1.1.1.4 Function of colon and rectum

1.1.1.4.1 Formation, storage and elimination of faeces.

As part of the digestive system, the colon and the rectum, which are also known as the large intestine, play a vital role in the digestive process. One of the main functions of the colon is forming and transporting faeces, which will be excreted through the rectum. During this process, the muscularis of the large intestine helps to achieve two different types of movement, haustral contraction and mass movement. When partly digested food material (chyme) in the small intestines passes to the colon, it is stored in the haustra, activating haustral contraction, and subsequently the colonic wall will contract to slowly move chyme to the next haustra. While Mass movement is a coordinated peristalsis wave that goes all the way through the stomach, small bowel and colon. Thus, this is a stronger movement compared to haustral contraction, and this transports the chyme to the rectum faster (Williams and Dickey 1969; Azzouz and Sharma 2020).

1.1.1.4.2 Absorption of water and electrolytes

As chyme is passed to the small intestine, most of the water and nutritional content is absorbed before proceeding into the large intestine. The ascending colon absorbs a significant amount of the water and some electrolytes and nutritional molecules by osmotic pressure. The indigestible residue left in the colonic lumen forms faeces as the end product. The colon also absorbs sodium, potassium and chloride ions (Williams and Dickey 1969; Azzouz and Sharma 2020).

1.1.1.4.3 Microflora are involved in production of vitamins and carcinogenesis.

The colon is inhabited by over 1000 types of microbes, ninety five percent of which are bacteria (Rajilic-Stojanovic and de Vos 2014). Some of these residents, including *Escherichia coli*, anaerobic *Bacillus*, *Streptococcus*, and *Staphylococcus*, play a vital role in producing essential vitamins that are required by the human body. This is achieved by fermentation and, as a result, Vitamin K and B vitamins are produced and absorbed into the blood circulation. Additionally, bacteria in the colon can supplement vitamins in short supply

within the individual (Azzouz and Sharma 2020). Routy *et al* illustrated that *Akkermansia muciniphila* benefits immunotherapy against CRC (Routy et al. 2018). However, besides these positive impacts on human health, a large number of residents of the bacterial community in the colon work the opposite way to promote development of CRC. These bacteria can support carcinogenesis directly by accumulating in the tumour microenvironment, for example *F. nucleatum*, *S. gallolyticus*, *C. difficile*, and *P. anaerobius*, or promote development of CRC indirectly by inducing immune aberration or secondary metabolites, for example, *B. fragilis* and *E. coli* (Xu et al. 2020). Therefore, this rich population of bacteria within the colon have distinct roles, some of which protect human health, while others take part in promoting development of CRC.

1.1.2 Incidence of colorectal cancer

CRC is the fourth most common cancer in the UK (2017), with around 42,317 new cases occurring each year during 2015-2017 and accounts for 11% of overall cancer diseases cases in 2017 within the UK. Meanwhile, around 16,300 deaths were reported from CRC per year during this period and accounted for approximately 10% of all cancer related deaths in 2017. This makes it the 2nd most common cause of cancer death in the UK. Analysis of the data based on gender, revealed 44% of CRC cases occurred in females and 56% in males. In 2017, it was reported that 10% of all new cancer cases in females and 13% of all new cancer cases in males were CRC. In terms of mortality, 10% of all female and male cancer deaths were the result of CRC. Within these cases, 45% occurred in females while 55% occurred in males (Cancer Research UK, 2020).

Incidence rates of CRC, based on European age-standardised (AS) rates, have generally been stable since the 1990s, although they have slightly reduced by 4% during the last decade. During the last decade, incidence rates of CRC diminished by 6% in males and 2% in females. Mortality rates (AS) of CRC have also decreased by more than 44% since the 1970s, where the number of deaths in females has decreased by 50%, while the number of deaths in males decreased by 41%. Over the last decade, overall CRC mortality rates decreased by 13%, of which a 12% reduction was seen in females and 15% in males (Cancer Research UK, 2020) (Figure 1.2 A). Approximately 78.3% of CRC patients in England were alive for one year or longer, whilst 58.4% of patients survived CRC for five years or more (2013-2017). Predicted survival rates of CRC patients (AS) for ten years or more is approximately 52.9% in England (2013 to 2017). It is worth noting that the survival rates have steadily improved in the last 40 years in the UK, from 22% to 57% (Cancer Research UK, 2020). Although the overall survival rates have been improved and mortality

rates are decreasing, the five-year-survival rate remains unsatisfactory and in fact has dropped to 10% among patients in TNM stage 4 (Figure 1.2 B) (Cancer Research UK, 2020).

According to the National Cancer Intelligence Network (NCIN) and Cancer Research UK, the incidence rates of CRC are also related to ethnicity. CRC incidence rates (AS) of white males and white females are significantly higher than in the population of Asian and Black ethnicities, with 54.1 cases in white males, and 55.3 cases in white females per 100,000 compared to 34.0 to 34.8 cases for males and females of other ethnicities respectively (National Cancer Intelligence Network (NCIN), 2020) (Cancer Research UK, 2020). Amongst all the new CRC cases during 2015-2017, more than 44% of them occurred in people aged 75 years and above, and the peak rate was found in patients aged 85-89 years (AS). In 2015-2017 in the UK, approximately 58% of deaths occurred in patients aged 75 and above and it reached the peak at 90 and above (Cancer Research UK, 2020). Although the data from Cancer Research UK showed the rate of CRC incidence in the UK, based on AS, has been stable since the end of last century, incidence rates in the 25- to 49-year-old age group (AS) have increased by 41% between 1993-2017 (Figure 1.2C) (Cancer Research UK, 2020). Multiple studies have revealed that the rate of patients under 50 years of age with CRC, so called early-onset colorectal cancer, has increased in the USA and European countries over the past two decades, and a greater proportion of these cases are rectal cancers (Pearlman et al. 2017; Vuik et al. 2019; Siegel et al. 2020). The underlying reasons behind this increase remain elusive, but may be related to variation of risk factors, including obesity, diet patterns, smoking, family history, alcohol consumption, and gene mutation (Pearlman et al. 2017).

Taken together, the overall incidence rates have been stable over decades and overall survival rates have been improved along with decreasing mortality rates. Interestingly, there is evidence to indicate the rising incidence rates of early onset CRC and poor prognosis of advanced stages of CRC. Given the current screening techniques mainly diagnose CRC in TNM3/4, which have a pessimistic prognosis (Altobelli et al. 2019), it may potentially raise the incidence rates. Hence, novel potential therapeutic targets are needed in the near future to help fight against CRC.

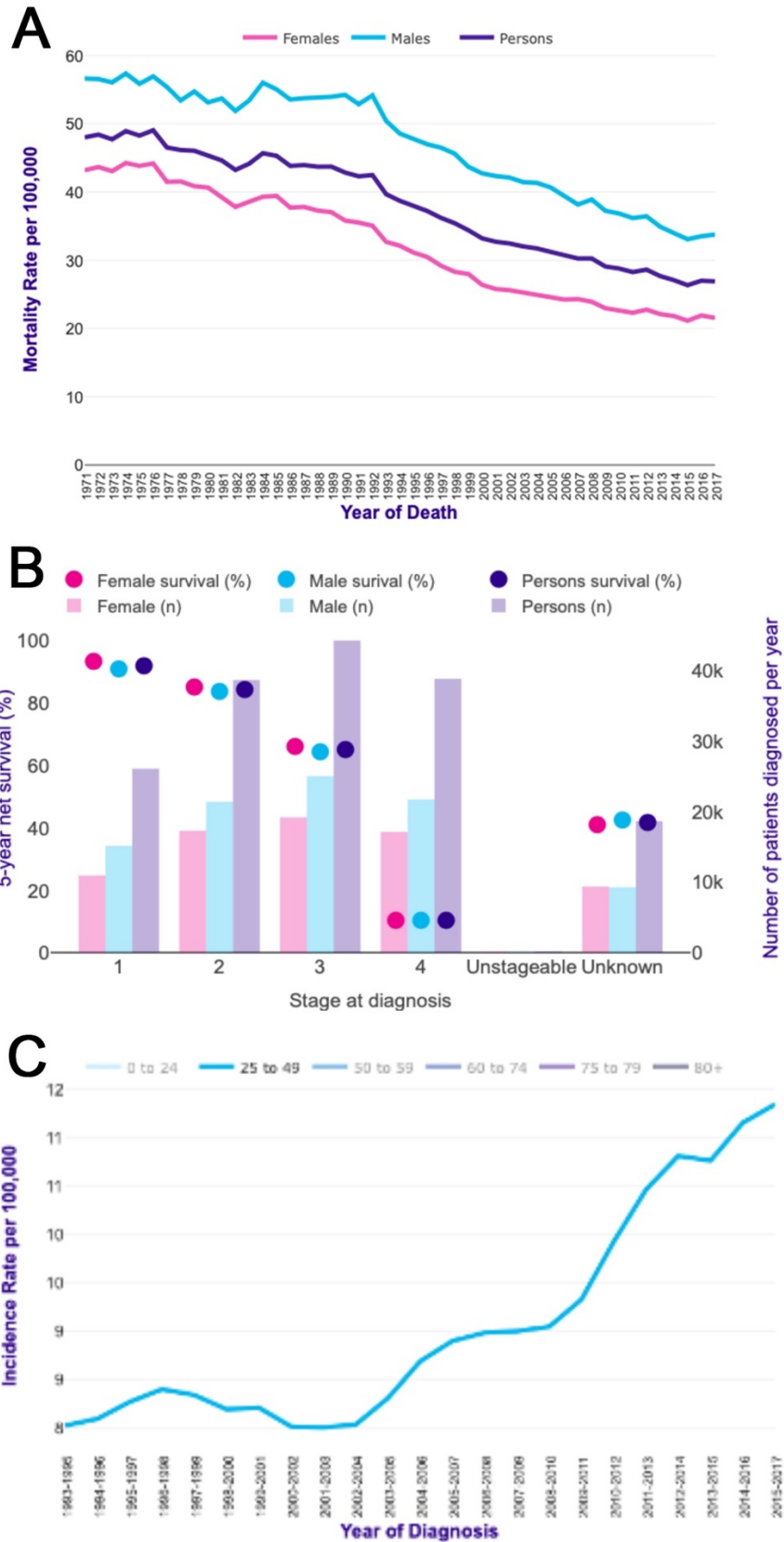


Figure 1.2 A. Bowel Cancer (C18-C20), European Age-Standardised Mortality Rates per 100,000 Population, UK, 1971-2017. B. Bowel cancer five-year net survival by stage, with incidence by stage (all data: adults diagnosed 2013-2017, followed up to 2018) (Credit: Cancer Research UK) C. Bowel Cancer (ICD-10 C18-C20), European Age-Standardised Incidence Rates (25-49 age group), UK, 1993-2017. (Credit: Cancer Research UK.)

1.1.3 Carcinogenesis of CRC

The carcinogenesis of CRC follows certain pathological routes, the most well-established being the adenoma-adenocarcinoma sequence (Fearon and Vogelstein 1990). Over 90% of CRCs develop from epithelial cells in the mucosa via the adenoma-adenocarcinoma sequence, with others arising from neuroendocrine, squamous cell carcinoma, adenosquamous carcinoma, spindle cell carcinoma and undifferentiated carcinomas (Fleming et al. 2012). The adenoma-adenocarcinoma sequence can be summarised as the process whereby benign tumours (adenomas) transformed to malignant cells which form a malignant neoplasm and proliferate to invade through the colonic wall, which results in dissemination to other tissues or distant organs via local spread, lymphatic spread or hematogenous spread (Beauchemin and Huot 2010).

Whilst the development of CRC maybe sporadic or hereditary, in both situations CRC must go through the process of cancer development, initiation, promotion, progression and metastasis (Carethers and Jung 2015; Keum and Giovannucci 2019). During the initiation and promotion phases, genetic damage occurs which induces abnormal cell proliferation and the subsequent abnormal neoplastic transformation. During this phase, the *Adenomatous Polyposis Coli (APC)* is one of the early changes in launching this carcinogenetic process, where mutation/depletion of the *APC* gene results in uncontrol growth of epithelial cells and transforms them into adenoma. Mutation of Kirsten Rat Sarcoma Viral Oncogene Homolog (*KRAS*) and *B-Raf* proto-oncogene, serine/threonine kinase (*BRAF*) allows adenoma to continue to proliferate. In the progression phase, genetic changes induce the cells' transformation to malignant cancer cells, which have aggressive characteristics to develop to cancer and to disseminate (metastasise). These genetic changes include mutation of *TP53* and *SMAD4*, members of tumour suppressor families and also tumour supporting genes such as *PIK3CA*. These aberrations support the transformation from adenoma to malignant tumour and further dissemination. In the final phase, cancer cells metastasise to nearby tissues and distant organs from the primary location through several pathways and metastatic cascades (discussed later in section 1.2.1) (Carethers and Jung 2015; Huang et al. 2018; Keum and Giovannucci 2019).

1.1.3.1 Molecular pathways

During these carcinogenic phases, genetic and epigenetic abnormalities occur and can be summarized as three molecular carcinogenesis characteristics, namely chromosomal instability (CIN), CpG island methylator phenotype (CIMP) and microsatellite instability (MSI) (Ionov et al. 1993; Pino and Chung 2010).

Approximately 85% of CRC cases are reported to be attributed to the chromosomal instability (CIN) aberration, which mainly includes the aberration and imbalances of chromosomal copy number (aneuploidy) and structure (Ionov et al. 1993; Carethers and Jung 2015). During this process, tumour suppressors, such as *APC* and tumour protein p53 TP53, or oncogenes such as *KRAS* and *BRAF*, act as key genes to activate the Wnt and MAPK pathways and promote the development of CRC. They also lead to the most classical adenoma-carcinoma sequence (discussed later) (Harada and Morlote 2020).

As its name describes, CpG island methylator phenotype (CIMP) mainly includes CpG island hypermethylation. CpG islands refer to the repetitive CG dinucleotides, which occur in the promoter region of some cancer suppressor genes, with a key role to diminish their expression (such as *MLH1*.*MINT1,2&3*) (Keum and Giovannucci 2019). Microsatellite instability (MSI) is aberration of the length of microsatellites (1-6 pairs Short Tandem Repeats (STRs) in genome), which is the result of the unsuccessful DNA mismatch repair (MMR) system, induced by silencing of DNA mismatch-repair genes, and the hypermethylation of promoter regions (Pawlik et al. 2004; Nojadeh et al. 2018; Keum and Giovannucci 2019). Since the process of MSI also includes hypermethylation, which diminishes the expression of DNA mismatch repair (MMR) genes, *MLH1*, *MSH2*, *MSH6*, or *PMS2* and leads to high level of MSI, they overlap substantially and are correlated (Weisenberger et al. 2006; Keum and Giovannucci 2019). These three aberrations may occur in combination or individually (Bardi et al. 2004). Carethers and Jung (2015), reported that the detected rate of incidence of CIMP-positive and MSI-high, in sporadic CRC, is around 20% and 15% respectively (Carethers and Jung 2015).

The carcinogenic pathways of CRC, including the adenoma-carcinoma sequence, serrated pathway, and inflammatory pathway, have been established (Keum and Giovannucci 2019). In these different pathways, several genes, as mentioned above, and signalling pathways, such as *APC*, *KRAS*, *p53*, *BRAF*, *PIK3CA*, *SMAD4*, Wnt/ β -catenin and MAPK, act as critical players during CRC development (Huang et al. 2018; Keum and Giovannucci 2019).

Based on the carcinogenic pathways discussed above, subtypes of CRC could be identified as CIN, CIMP and MSI in which they could be divided into negative, positive, high or low respectively. MSI-high and CIMP-high are more common in proximal colon while CIN-positive is more usual in distal colon (Missiaglia *et al.* 2014). There are a number of molecular classifications based on gene expression and methodological differences, including the colon cancer subtype (CCS) system, the colorectal cancer assigner(CRCA)

system, the colon cancer molecular subtype (CCMS) system, the CRC intrinsic subtypes and the colorectal cancer subtyping consortium (CRCSC)(De Sousa et al. 2013; Marisa et al. 2013; Sadanandam et al. 2013; Roepman et al. 2014; Sadanandam et al. 2014; Rodriguez-Salas et al. 2017). Based on gene expression profiles published previously (De Sousa et al. 2013; Sadanandam et al. 2013), Sadanandam *et al.* (2013), analysed and gathered the relationships within these classifications, and other studies, to demonstrate a novel classification, CRCSC (Table 1.1), which includes four subtypes, CMS1, CMS2, CMS3 and CMS4 (Sadanandam et al. 2014). CCMS system has been indicated to determine molecular characteristics of CRC, while another classification, The Cancer Genome Atlas (TCGA), is designed to determine mutation rate of oncogenes, thus it has been established as a tool to select and formulate suitable treatment strategies (Dariya et al. 2020).

Table 1.1 Colorectal Cancer Subtyping Consortium (CRCSC). (Rodriguez-Salas et al. 2017; Sadanandam et al. 2014; Stintzing et al. 2019).

Colorectal Cancer Subtyping Consortium (CRCSC)	
CMS1	Hypermuted tumour with immune cell infiltration, MSI-high/CIMP, less popularity of SCNAs (somatic copy number alterations) and commonly BRAF mutation.
CMS2	Tumour that presents as CIN or MSS (microsatellite stable) with EGRF amplification. It is also related to mutation, overexpression of TP53 and activation of Wnt/MYC signalling.
CMS3	Tumour which frequently presents as CIMP, low CIN with less popularity of SCNAs, around 30% are hypermuted. It is associated with moderate activation of EGRF, Wnt/MYC signalling pathway, metabolic abnormalities, mutation of KRAS & P13K and overexpression of IGBP2.
CMS4	Tumour mainly presents as CIN with mesenchymal characteristics, activation of TGF- β signalling pathway and complement-mediated inflammation.

In cases where adenoma appears as the precancerous lesion, adenoma-carcinoma sequence, which is the most classical pathway, is presented as a pathway to progress to CRC (Huang et al. 2018). During this process, mutation of the *APC* gene results in the inactivation of the APC protein, a key event considered as the trigger of CRC development. The inactivation of the APC protein dismantles the protein complex, which contains APC, β -catenin, and GSK3-beta. With a mature and normal APC protein, the APC/ β -catenin/GSK3-beta protein complex targets β -catenin for protein degradation. However, mutation of the *APC* gene and APC inactivation, results in β -catenin accumulation in the cytoplasm of the cells and leads to the activation of Wnt/ β -catenin signalling, in which Wnt protein binds to Frizzled family receptor and Axin is removed from the destruction complex. The accumulated β -catenin is then translocated into the nucleus and oncogenic

transcription begins, resulting in cellular growth and proliferation (Eklof et al. 2013; Harada and Morlote 2020). The mutation of *KRAS* allows the growth and development of cells and adenoma, while TP53 is suppressed in the later stage to contribute to the development to malignant tumour (Huang et al. 2018).

The serrated pathway describes serrated adenomas as a precursor to develop to CRC and relates to CIMP-high and MSI CRC. In this particular pathway, normal mucosa is transformed to hyperplastic polyps, by the activation of BRAF at the early stage and cell proliferation through the MAPK pathway. This would finally result in development of CRC (Kedrin and Gala 2015; Keum and Giovannucci 2019).

In another suggested pathway, the inflammatory pathway, normal mucosa proceeds through indefinite dysplasia, low-grade dysplasia, high-grade dysplasia and results in the development of CRC. During this process, mutation of p53 occurs at the early stage while the inactivation of APC does not frequently appear (Itzkowitz and Yio 2004; Keum and Giovannucci 2019).

1.1.3.2 Tumour microenvironment

The mutation of genes and associated pathological pathways contribute to the progression of CRC, while crosstalk between the Tumour Microenvironment (TME) and CRC cells is also essential for carcinogenesis and the development of CRC. The TME is a rather complicated network which is composed of stromal cells, immune cells and extracellular matrix (ECM) (Roma-Rodrigues et al. 2019; Dariya et al. 2020; Kasprzak 2021). Stromal populations exist across the colon epithelium, with fibroblasts being one of the most common, which serve in stabilizing cells' morphology and maintaining communication between cells. Transformation from fibroblasts to Cancer-Associated Fibroblasts (CAF) is induced by the efferent pathway. CAFs then are responsible for secreting components such as EGF, HGF, miR-200b through the afferent pathway, to promote uncontrolled proliferation and angiogenesis of the carcinogenetic process, with the help of blood & lymphatic veins, mesenchymal stromal cells and immune cells (T-/B-lymphocytes and tumour-associated macrophages (TAM)). Moreover, normal cells which are adjacent to the TME can be transformed into tumour cells with the help of exosomes (Roma-Rodrigues et al. 2019; Dariya et al. 2020).

During the development of CRC, the immune system is also a crucial participant. On one hand, immunosurveillance allows immune cells to detect, recognise then eliminate tumour cells. For instance, natural killer cells are able to kill tumour cells by a number of ways

including secreting cytotoxic cytokines, including Interferon γ (IFN- γ) and tumour necrosis factor α (TNF- α) (Zhang et al. 2018a). On the other hand, immunoediting gives tumour cells a chance to develop resistance to elimination and escape immunosurveillance, further allowing tumour cells to proliferate and invade. For example, Tissue Associated Macrophages (TAMs) play a role in promoting tumour cell growth and the progression of epithelial mesenchymal transition (EMT), which leads to metastasis (discussed later in Chapter 1.2.4). T lymphocytes have the ability to induce apoptosis which eliminates tumour cells, but can also promote tumour cell growth by releasing supporting cytokines (Dariya et al. 2020). Extracellular matrix (ECM) remodelling is also induced by cross talk with the TME under its influence, ECM results in desmoplasia which supports development of CRC (Kasprzak 2021).

Communication within the TME can be regulated by gap junction channels which are regulated by chemokines and cytokines, ECM, exosomes and microvesicles. This crosstalk allows proliferation, angiogenesis and invasion of tumour cells, which leads to metastasis, poor prognosis and therapeutic resistance (Dariya et al. 2020). Hence, besides molecular aberrations, the TME is a vital influencer in carcinogenesis and development of CRC.

1.1.4 Risk factors for CRC

Currently, approximately 54% of the population attributable fraction (PAF) of CRC cases could be prevented (Brown et al. 2018). From the statistics described above, it is clear that the elderly population are at more risk of developing CRC compared to younger groups. It has been suggested that the genetic damage of cells becomes accumulative through ageing. The genetic damage could be caused by a genetic mutation process or by additional risk factors. The International Agency for Research on Cancer (IARC)/World Cancer Research Fund Classifications (WCRF) reported that consumption of alcohol and tobacco, exposure to X-rays, gamma-radiation, obesity, and adult attained height are considered high risk factors related to CRC (InternationalAgencyforResearchonCancer 2020). In addition, the WCRF/AICR report has also confirmed that insufficient fibre intake from the daily diet of an individual, as well as lack of physical activity also play a role in increasing the risk of CRC (Cancer Research UK, 2020). Moreover, type II diabetes, gastrointestinal diseases and hereditary factors have also been outlined to be associated with incidence of CRC (Gala and Chung 2011; Keum and Giovannucci 2019).

1.1.4.1 Obesity

Brown *et al.* (2018), reported that in 2015, 11% PAF of CRC cases in the UK were associated with obesity (Brown *et al.* 2018). Body mass index (BMI) is a value calculated from the weight of the body divided by the square of the body height. BMI is used to define obesity levels of an individual, based on different standards for females and males. An umbrella study of meta-analyses demonstrated that the risk of incidence of colon cancer is increased by 30% in males and 12% in females respectively, when BMI increased per 5 kg/m². For rectal cancer the risk increased by 9% in males (95% CI, 1.09 vs 1.30), but there was no significant correlation in females (Kyrgiou *et al.* 2017). It has also been reported that the incidence risk of CRC is associated with waist circumference. Individuals with a larger waist circumference have a higher risk (46%) of developing CRC compared to those with a smaller waist circumference (Ma *et al.* 2013).

1.1.4.2 Alcohol

Brown *et al.* also reported that 6% PAF of CRC cases in the UK in 2015 were associated with alcohol consumption (Brown *et al.* 2018). A meta-analysis study revealed that individuals who drank more than 50g (6+ units) of alcohol each day had a 33% increased risk of developing CRC compared to non or occasional drinkers (Choi *et al.* 2018). The risk increased by 7% per unit/10g of alcohol intake each day (Fedirko *et al.* 2011; Vieira *et al.* 2017).

1.1.4.3 Smoking

The same study also showed that 7% PAF of CRC cases in the UK (2015) were associated with smoking (Brown *et al.* 2018). A number of studies have demonstrated that the risk of developing CRC is significantly correlated with smoking. The younger an individual starts smoking the higher the risk of CRC incidence for the individual in future years. There is an increased risk of 17-21% for those who are currently smoking, and 17-25% for former smokers, when compared with those who have never smoked. Other meta-analysis studies revealed that the risk of CRC incidence would increase by 7-11% with every 10 cigarettes consumed each day (Huxley *et al.* 2009; Liang *et al.* 2009; Tsoi *et al.* 2009; Cheng *et al.* 2015).

1.1.4.4 Lack of physical activity

The World Cancer Research Fund/American Institute for Cancer Research have revealed that levels of physical activity are also associated with the incidence of CRC, with a clear and negative correlation. Five MET (metabolic equivalent of tasks)-hours of various types of

physical activities each week decreases the risk of developing colon cancer by 8% (RR 95%CI 0.92 (0.86-0.99) (Keum and Giovannucci 2019). A cohort study showed that the risk of digestive system malignancies, including CRC, would reduce with a recommended 30 MET-hours per week of aerobic exercises (RR 0.68, 95% CI 0.56-0.83)(Schmid and Leitzmann 2014; Keum and Giovannucci 2019). Aleksandrova *et al.* (2017), also revealed that the high strength of physical activity (more than 91 MET-hours per week compared to less than 91 MET-hours per week) has a negative correlation with the risk of colon cancer incidence (95% CI 0.57 to 0.96) (Aleksandrova *et al.* 2017). Indeed, physical exercises could reduce and prevent obesity, as revealed by a study from Ruiz-Casado *et al.*, demonstrating that it could also have a positive impact on the motility of the digestive and immune system, inflammation and metabolic hormones (Ruiz-Casado *et al.* 2017; Keum and Giovannucci 2019). A meta-analysis study also revealed that increased time of occupational sitting and TV viewing (2 hours each day) would increase the risk of CRC incidence by 7% (RR 1.07, 95% CI 1.05-1.10) and 4% (95% CI 1.08–1.22) respectively. Indeed, physical exercise has been shown to reduce the rates of CRC incidence and 5% PAF of bowel cancer cases in the UK in 2015 is associated with the lack of physical activity (Brown *et al.* 2018).

1.1.4.5 Lack of dietary fibre

Besides the level of physical activity being associated with the incidence of CRC, Brown *et al.* (2018), also reported that 28% of CRC cases in the UK in 2015 were related to a lack of intake of dietary fibre (Brown *et al.* 2018). Indeed, Vieira *et al.* (2017), revealed that, not only consumption of alcohol, processed meat and red meat play an important role in increasing risks of developing CRC, but also reported that the risk would decrease by 17% if 100g of whole grains were included in the diet each day (95% CI = 11-21%, I² = 0%, heterogeneity= 0.30, 6 studies) (Vieira *et al.* 2017). As part of the digestive system, the large intestine's main function is processing chyme into faeces. By increasing intake of dietary fibre, the time of chyme transportation will decrease, therefore the chance of the colorectal epithelium being exposed to carcinogens will also decrease. Fibre interacts with the intestinal microbiota which also contribute to this (Holscher 2017; Keum and Giovannucci 2019), indicating that intake of fibre may play a role as a protector in incidence of CRC.

1.1.4.6 Radiation

Another risk factor associated with CRC incidence is possible harm from radiation. It has been reported, that 0.7% of new cancer cases were attributed to exposure to medical ionizing radiation (IR) in 2015 in France, in which colon cancer comprised 290 cases. The risk of IR is related to the doses of radiation that a target organ accepted (Marant-Micallef *et*

al. 2019). In the UK, Brown *et al.* (2018), also reported that exposure to radiation had a connection with CRC incidence, revealing 2% of CRC cases were attributed to ionising radiation (Brown *et al.* 2018). Pelvic radiation therapy has been established to have a positive correlation with the risks of rectal cancer as secondary tumours (RR 1.43 95% CI 1.18-1.72) (Rombouts *et al.* 2018).

1.1.4.7 Type II diabetes and gastrointestinal diseases

Besides the risk factors described above, CRC is associated with other diseases and certain medicines. Meta-analyses revealed that the rates of CRC increased by 22-30% in type II diabetes patients, compared with those who were diabetes-free (Larsson *et al.* 2005; Jiang *et al.* 2011; Kramer *et al.* 2012; Luo *et al.* 2012; Wu *et al.* 2013). Females who take metformin regularly for diabetes were found to have a smaller chance of developing CRC (Cardel *et al.* 2014).

Adenoma is one of the most frequent precancerous lesions which may eventually turn into CRC directly, with approximately 85-90% of CRC cases reported to originate from adenomas. Conteduca *et al.* (2013), demonstrated that in patients who had advanced adenomas with a size more than 1 cm in diameter, the risk of developing CRC was 30-50% higher than those with non-advanced adenomas (Conteduca *et al.* 2013), although the chance of adenomas progressing to CRC was less than 10% (Conteduca *et al.* 2013; Keum and Giovannucci 2019). Martinez *et al.* (2009), conducted a pooled analysis to report that approximately 1% of patients who were suffering from larger adenomas, or adenomas with high-grade dysplasia, had been diagnosed with CRC around 4 years after having their adenomas removed (Martinez *et al.* 2009). Serrated polyps are another vital precancerous type which can develop into CRC. These include hyperplastic polyp, serrated adenoma, sessile serrated adenoma and mixed polyp. It is very interesting to note that between 10-15% of CRC, which are not related to heredity origin, are reported to come from serrated polyps (Conteduca *et al.* 2013; Keum and Giovannucci 2019). A study of patients with ulcerative colitis, with 14 years follow up, revealed that patients who suffered from ulcerative colitis had a higher risk (2.4-fold) (95% CI 2.1-2.7) of developing CRC (Lakatos and Lakatos 2012). A 70% increase in CRC was seen in patients who suffered from Crohn's colitis (Inflammatory bowel disease), compared with those without (Lutgens *et al.* 2013), and 80% of individuals diagnosed with low-risk polyps at first colonoscopy, compared with those that had no polyps, had an increased risk of CRC (Hassan *et al.* 2014).

1.1.4.8 Medication

Recently, it has been shown that the rates of CRC incidence of in aspirin users are 17% lower when compared with those who have never taken aspirin (Qiao et al. 2018). A Colorectal Adenoma/Carcinoma Prevention Programme 2 (CAPP2) randomised trial, with a follow-up of up to four years, revealed that the risk of CRC incidence in patients with lynch syndrome is associated with the intake of aspirin. The risk decreased by 63% compared to those who were given a placebo instead (HR 0.63 95% CI 0.35-1.13)(Burn et al. 2011).

1.1.4.9 Hereditary syndrome

Hereditary factors may contribute to CRC. Wilschut *et al.* (2010) analysed thirteen colonoscopy studies to reveal that individuals who had a family history of CRC had a higher risk of adenomas, which is one of the main precancerous lesions of CRC, when compared with those without (OR 1.7, 95% CI 1.4-3.5) (Wilschut et al. 2010), with the rate between CRC and family history up to 25%(Gala and Chung 2011).The time required to develop to Stage 4 CRC may be reduced in hereditary CRC compared with sporadic CRC (Keum and Giovannucci 2019). Although the rate of the correlation between CRC and hereditary syndromes only accounts for around 2-5% of CRC cases (Jasperson et al. 2010), studies found that, in individuals who had at least one relative in the family with CRC history, the risk of CRC incidence increased by 2.24% (95% CI 2.06-2.43) and the risk increased to 3.97% (95% CI 2.60-6.06) for those who had at least two relatives with CRC history. Butterworth *et al.* (2006), also revealed that this association gets stronger with ageing (Butterworth et al. 2006).

There are several types of hereditary colorectal cancer syndromes, the most common two being Lynch syndrome (LS), also named Hereditary Non-Polyposis Colorectal Cancer (HNPCC) (Lynch and Lynch 2004), and Familial Adenomatous Polyposis (FAP) (Snyder and Hampel 2019).

1.1.4.10 Hereditary non-polyposis colorectal cancer

Accounting 2-4% cases of colorectal cancer, HNPCC is highly linked to MSI-high and frequently located at proximal colon (Smyrk and Lynch 1999). And it has been reported to link with several gene mutations, including DNA mismatch-repair (MMR) genes, MLH1, MSH2, MSH6 (Lynch and Lynch 2004), PMS2 (Aaltonen et al. 1998; Snyder and Hampel 2019). Inhibition of EPCAM, an upstream players of MSH2, was also reported to be related to HNPCC (Steinke et al. 2013). South et al. demonstrated that familial ovarian cancer

patient with negative testing of the BRCA family (BRCA1 and BRCA2), had increased risk of getting HNPCC (Steinke et al. 2013).

1.1.4.11 Familial Adenomatous Polyposis

As another more common syndrome, patients with FAP account for less than 1% of CRC cases (Gala and Chung 2011). However, FAP could be dangerous, as 95% of FAP patients develop polyps by the age of 35 and can develop numerous adenomatous polyps rapidly leading to CRC (Snyder and Hampel 2019). FAP is reported to be associated with the mutation of the APC gene (Snyder and Hampel 2019). Mutation of mutY DNA glycosylase (MUTYH) gene was reported to contribute to a subtype of FAP, Attenuated FAP (Castellsague et al. 2008; Half et al. 2009).

1.1.5 Diagnosis and staging of CRC

1.1.5.1 Clinical features and diagnosis of colorectal cancer

Physician Data Query (PDQ) database from National Cancer Institute's (NCI's) summarised colorectal cancer could alter bowel habit and presents clinical symptoms on intestinal tract. Typical symptoms include haematochezia, diarrhoea, constipation, altered shape of faeces and chronic abdominal pain. Weight loss of unknown cause, weakness and vomiting could also present on patients with colorectal cancer (National Cancer Institute 2022).

Diagnosis of colorectal cancer should determine primary tumour, pathologic information, molecular profile and whether metastasis occurs. Diagnostic tools such as CT colonography (CTC) or optical colonoscopy are suggested to be performed for patients with suspected CRC, and CRC should be diagnosed ideally histologically, through biopsy (Cunningham et al. 2017). Besides, magnetic resonance imaging (MRI), positron emission tomography scan (PET scan), x-ray could aid to determine metastatic sites. While carcinoembryonic antigen (CEA) assay and testing of tumour markers for instance, cancer antigen 19-9 (CA19-9), could also assist diagnosing colorectal cancer (Biller and Schrag 2021). Faecal occult blood test (FOBT) and faecal immunochemical test (FIT) detect haemoglobin while multitarget stool DNA testing screens abnormal DNA to assist diagnosing colorectal cancer (Levin et al. 2008).

1.1.5.2 Staging of colorectal cancer

The staging of CRC can be identified based on two classification, Dukes and TNM staging. Dukes' staging system was established by Dr Cuthbert Dukes in 1932 and used for rectal

cancer (Dukes 1932), and the system was adapted and developed by Astler and Coller (Astler and Coller 1954) as well as Turnbull (Langman et al. 2017) in later years and utilised for colon and rectum cancer (Table 1.2). Dukes' staging classifies tumour by measuring invasiveness through mucosa and bowel wall, but it does not clarify the degree of nodal involvement.

American Joint Committee on Cancer (AJCC) developed TNM (Tumour, Regional lymph nodes and distant metastasis) staging system to classify malignant tumour including colorectal cancer. In colon cancer guidelines published by National Comprehensive Cancer Network (NCCN) in 2022, TNM8 staging system was utilised (Table 1.3).

Table 1.2 Dukes' Classification (Dukes 1932; Astler and Coller 1954; Langman et al. 2017)

Dukes' Classification	
Dukes' A	tumour limited to the bowel wall and negative for lymph node invasion
Dukes' B	tumour spread beyond the muscularis propria; negative for lymph node invasion
Dukes' C1	lymph node(s) involved but tumour did not break through the bowel wall
Dukes' C2	tumour broke through all the layers of bowel and lymph node(s) involved
Dukes' D	Distant metastasis occurs

Table 1.3 TNM8 Classification

TNM8 Classification	
Tx	Primary tumour cannot be assessed
T0	No evidence of primary tumour
Tis	Tumour is involved in lamina propria but not through muscularis mucosae
T1	Tumour invades through the muscularis mucosae but not muscularis propria
T2	Tumour invades the muscularis propria
T3	Tumour invades through muscularis and get into pericorectal tissues
T4	Tumour invades through the visceral peritoneum (T4a) Tumour invades or adheres to adjacent organs or structures (T4b)
Nx	Regional lymph nodes cannot be assessed
N0	No regional lymph node metastatic disease
N1	Metastatic disease in 1 (N1a) to 3 (N1b) regional lymph nodes. Or no regional lymph nodes are positive, tumour deposits are present (N1c)
N2	4 to 6 regional lymph nodes are present (N2a) 7 and more regional lymph nodes are present (N2b)
M0	No evidence of distant metastatic disease
M1	Tumour metastasis to one site or organ but not peritoneum (M1a). Tumour metastasis to two or more sites or organ but not peritoneum (M1b). Tumour metastasis to peritoneum (M1c)

1.1.6 Treatment of CRC

1.1.6.1 Surgery

Surgery is one of the main curative treatments for CRC either alone or in combination with other therapies. Operations include endoscopic resection (EMR), endoscopic submucosal dissection (ESD), segmental colonic resection and palliative surgery. The method of surgery is different based on the site and stage of CRC and the condition of the patient's health (Ahmed 2020).

1.1.6.2 Radiotherapy

For CRC patients who have liver metastasis but are not suitable for surgery, stereotactic body radiotherapy (SBRT) is performed, to restrict the proliferation and growth of tumour tissue. Multiple studies have supported that SBRT effectively contributes to local control and overall survival (Kobiela et al. 2018; Petrelli et al. 2018).

1.1.6.3 Chemotherapy and targeted therapy

As described previously, the development of CRC is associated with multiple mutated genes and carcinogenesis pathways. On this principle, chemotherapy and targeted therapy have been developed to target certain key mutated genes and vital pathways. The drugs used, 5-FU (5-fluorouracil) with LV (leucovorin), capecitabine, FOLFOX (5-FU, LV and oxaliplatin), Capeox (capecitabine with oxaliplatin) (Lee et al. 2012), FOLFIRI (5-FU, LV with irinotecan), CAPIRI (capecitabine, irinotecan), CAPOX (capecitabine, oxaliplatin), Lonsurf (5-FU, LV, irinotecan, capecitabine, trifluridine and tipiracil), are main strategies of chemotherapy or adjuvant chemotherapy for CRC. The choice and combination is dependent on TNM stage (Ahmed 2020). Among these strategies, 5-FU, pyrimidine analogue is one of the most common chemotherapy drugs for CRC, which acts as an inhibitor which targets synthesis of DNA and RNA (Liu et al. 2020). It is, however, noted that 5-FU based therapy is often found to suffer from therapy resistance at an earlier stage and from peritoneal metastasis (Guo et al. 2018; Van der Jeught et al. 2018). For instance, research has reported that long noncoding RNA nuclear paraspeckle assembly transcript 1 (LncRNA NEAT1) is related to the promotion of drug resistance by downregulating expression of miR-34a and thus elevates autophagy (Liu et al. 2020). By analysing 440 CRC patients with a PCR based method, Wang *et al.* (2018), reported that mutation of PIK3CA leads to greater resistance against 5-FU based chemotherapy. Similar influences were obtained *in vivo* and *in vitro* (Wang et al. 2018). Liu *et al.* (2019) elucidated that EMT contributes to promote resistance against oxaliplatin therapy (Liu et al. 2019).

Targeted therapy is used for targeting certain types of CRC, based on carcinogenesis and mutated genes. To target vascular endothelial growth factor (VEGF), bevacizumab is recommended, while for VEGF receptor (VEGFR), ramucirumab is the option. Cetuximab and panitumumab target epidermal growth factor receptor (EGFR) (Ahmed 2020), and KRAS and BRAF mutations have been established as a axis of anti EGFR treatment (Van der Jeught et al. 2018). On the other hand, bevacizumab, ramucirumab, regorafenib and aflibercept focus on angiogenesis(Ahmed 2020). Certain biological and genetic factors, for example anti-EGFR drugs and BRAF mutation have been linked to drug resistance(Van der Jeught et al. 2018).

1.1.6.4 Immunotherapy

Immunotherapy, including immune checkpoint therapy, has played a critical role in treating CRC with high gene mutations and metastatic CRC in recent years (Ganesh et al. 2019). CRC can be divided into two individual groups, based on the differences in carcinogenesis; mismatch-repair-deficient or high level of microsatellite instability (dMMR-MSI-high) and mismatch-repair-proficient or low level of microsatellite instability/microsatellite stable (pMMR-MSI-low), this can be a method to guide the choice of immunotherapy. In the immune system, T cell receptor (TCR) on T cell surfaces binds to the peptides and major histocompatibility complex (MHC) class 1, which exists on the surfaces of both normal and cancer cells. T cells distinguish enemy and alliance through modulation by multiple co-stimulatory or co-inhibitory signalling pathways. These include inhibitory receptors on T cells, such as programmed cell death 1(PD1) and cytotoxic T lymphocyte antigen 4 (CTLA4), activating receptors on T cells such as CD28, CD134, CD357, CD137, ICOS, CD 27 and CD40L and their ligands on the surface of tumour cells. When inhibitory receptors on T cells bind to their ligands on tumour cells, the killing function of T cells will be silenced and/or lead to T cell apoptosis(Ganesh et al. 2019).

During the process of immune checkpoint inhibitor (ICI) treatment, ICIs target and bind to inhibitory receptors on immune cells, including T cells such as CTLA4 and PD1 or their ligands (in this case, CD80/CD86 and PDL1 respectively) on tumour cells. Therefore, T cells will be activated and have the potential to destroy tumour cells(Ganesh et al. 2019). The FDA has approved the strategy of pembrolizumab and nivolumab to target PD1,while ipilimumab to target CTLA4 with nivolumab is effective for treating dMMR-MSI-H CRC (Ganesh et al. 2019).

1.2 Metastasis of Colorectal Cancer

The process of metastasis is defined as tumour cell dissemination to other distant locations, subsequent proliferation and formation of new tumours. The process of metastasis is rather complicated and includes several essential steps within a cascade (known as the metastatic cascade), which include gaining the invasive ability to disseminate themselves to surrounding matrix (local invasion), spreading to distant organs through the circulatory systems (blood vessels or lymphatic vessels) and re-establishing in distant sites in the body. Lots of elements and factors from the microenvironment, the process of angiogenesis, various signalling pathways, and EMT contribute to the metastasis of CRC (Pretzsch et al. 2019). There are a number of routes that cancer cells can metastasise through (outlined in section 1.2.1).

1.2.1 Metastatic cascade

1.2.1.1 Lymphatic spread

Tumour cells, shed by the primary tumour, gain access to the lymphatics around the primary tumour site, due to imbalance of interstitial fluid pressure when the primary tumour develops through the serosa of the colonic wall. Another possibility is that tumour cells can enter the lymphatics through opening of lymphatic vessels due to surgery or anastomotic leakage induced by infection (Sleeman 2000; Pretzsch et al. 2019). After gaining access to the lymphatics, tumour cells are transported to regional nodes through lymphatic vessels. Tumour cells can then stay at the node for a certain length of time. The surviving tumour cells in the lymph nodes could proliferate and initiate micro-metastasis ranging in size from 0.2mm to 2mm. Tumour cells can also be filtered in draining nodes and grow and proliferate in a clustered manner, leading to a larger metastatic lesion, greater than 2mm in size. In this situation, continuous proliferation of tumour cells can cause extracapsular extension, or tumour cells can spread from one lymphatic node to surrounding downstream nodes. Furthermore, following access to lymphatic vessels present within the primary tumour region, tumour cells may be drained into larger lymphatic vessels and eventually enter the blood circulation via the thoracic duct. However, those tumour cells in metastatic lymph nodes could eventually adhere to the peritoneum and achieve peritoneal metastasis (Beauchemin and Huot 2010).

1.2.1.2 Haematogenous spread

Tumour cells from CRC which gain the ability to disseminate, intravasate to the venules of the primary tumour region by promoting the formation of new vessels, commonly referred to as tumour angiogenesis (Weis and Cheresh 2011). They are then transported to the portal

vein where they face the challenge from the hepatic sinusoid and enter the circulatory system. For rectal cancer, tumour cells can achieve haematogenous spread based on where they originate, with tumour cells from the upper and mid-rectum disseminating via the portal vein while those from the lower third via the inferior vena cava (Beauchemin and Huot 2010).

After entering the circulatory system, circulating tumour cells (CTCs) may form clusters with blood cells including platelets and neutrophils, disseminating in the body through the blood stream. Platelet produced platelet-derived growth factor (PDGF) and transforming growth factor (TGF- β) act to protect tumour cells from natural killer cells by inhibiting their function and, at the same time, platelets can also create protective cloaks to protect tumour cells directly. During their dissemination through the circulation and at the secondary site, tumour cells are able to extravasate through vasculature. For CRC, the main destination of haematogenous dissemination is the liver. Upon surviving natural killer cells and other immune responses and supported by Kupffer cells, hepatic endothelial cells and platelets, CTCs can enter liver tissue via hepatic microcirculation (Lambert et al. 2017; Pretzsch et al. 2019). During this process, neutrophils also support extravasation by forming a neutrophil extracellular trap to help tumour cells to adhere to endothelial cells and extravasate to liver tissue (Lambert et al. 2017; Pretzsch et al. 2019). After forming liver metastases, CRC tumour cells can continue to disseminate to the systemic circulation to achieve metastases in other organs including the lungs and bones (Beauchemin and Huot 2010).

1.2.1.3 Peritoneal dissemination (transcoelomic metastasis)

The main destination of local spread for tumour cells in CRC is the peritoneal cavity. The overall pathology of the peritoneal transcoelomic metastasis involves detachment of tumour cells (from the metastatic lymph nodes or invasion and penetration of the colorectal wall), transport to the peritoneal surface through certain routes, seeding at the surface of the peritoneum, re-invasion through the peritoneum and formation of tumour (Lemoine et al. 2016; Pretzsch et al. 2019). Tumour cells, whose destination is the peritoneum, have to gain a number of characteristic traits, such as enhanced motility and invasive capacities, and leave the primary tumour region through detachment. At this phase, tumour cells may leave the primary tumour region spontaneously at T4 stage or due to the imbalance of interstitial fluid pressure and be shed into the peritoneal cavity. Another route is accidental seeding during surgery, when tumour mass are accidentally sectioned through during the surgical procedure (Lemoine *et al.* 2016; Pretzsch et al. 2019).

The metastatic activities of tumour cells are believed to be at least partly attributed to the change of epithelial characteristics and the loss of cell-cell adhesion which are the results of EMT (Mittal 2018). Downregulation of E-cadherin and cell-cell adhesion molecules (CAMs), up-regulation of N-cadherin, and some regulated components such as EGFR are involved in EMT (discussed in section 1.2.4) (de Cuba et al. 2012; Lemoine et al. 2016; Mittal 2018). When tumour cells are free in the peritoneal cavity, they tend to adhere to the peritoneal surface (Lemoine et al. 2016), with evidence indicating a pivotal role for integrins, CD44, ICAM1, VCAM1, L1CAM and mucins on cancer cells in this process (Lemoine et al. 2016; Sluiter et al. 2016). Following adherence to the surface of the peritoneum, the next step for tumour cells is to invade both the protective protein layer of the peritoneum, mainly the hyaluronans and the cellular coating namely peritoneal mesothelium. Hepatocyte growth factor (HGF), the ligand for the proto-oncogene cMET receptor, is a key factor responsible for promoting the process of invasion (Ma et al. 2003; Lemoine et al. 2016); this, other stromal derived factors and other elements from microenvironment are also crucial players in the invasion process. For instance, peritoneal macrophages (PMs) change to their subtype 2 (M2) at the later stage of CRC to release ECM degrading components. CAFs induce TGF- β and PDGF. These stromal microenvironment produced factors, such as HGF, also contribute to the beginning of invasion to create a suitable microenvironment for tumour cells to invade stroma (Karagiannis et al. 2012; Mikula-Pietrasik et al. 2018; Pretzsch et al. 2019). Besides, peritoneal fibroblasts, sub-peritoneal fibroblasts and peritoneal adipocytes are also reported to support invasion phases (Kojima et al. 2014; Zhang et al. 2015; Mikula-Pietrasik et al. 2018; Pretzsch et al. 2019). Following invasion, another vital step of metastasis occurs, the proliferation and formation of tumours in the peritoneum. In this phase, tumour cells need to proliferate and recruit/develop their own vessels to gain nutrition for further development. Therefore, growth factors and elements which contribute to angiogenesis play essential parts in this stage. EGFR, TGF- α , and insulin like growth factor-1 (IGF-1) have been reported to be up-regulated in metastatic CRC (mCRC) and have a positive role in metastatic progression (Lemoine et al. 2016). The peritoneal-blood barrier leads to hypoxia in cells and the mediation of hypoxia inducible factor-1 (HIF-1), which in turn up-regulates VEGF. These key events collectively contribute to the activation of signalling pathways including MAPK and PI3K, to enhance the proliferation, migration and survival of tumour cells and to promote tumour-endothelial interactions (Dimova et al. 2014; Lemoine et al. 2016; Maishi and Hida 2017; Pretzsch et al. 2019).

1.2.2 Genes and key pathways

As discussed earlier, the development of CRC is characterised in one part by the adenoma-carcinoma sequence (Pino and Chung 2010). During the sequence, there are genes that act as tumour repressors to inhibit the process of development of carcinogenesis and metastasis of CRC such as *APC*, *p53*, *SMAD4*, *TGF- β* , *PTEN*, to name some. On the other hand, there are other genes which support the carcinogenesis and metastatic events, such as *KRAS*, *BRAF*, *PIK3CA*, etc. Mutation of these genes could lead to activation/inactivation of some clinical pathways and eventually support the development and metastasis of CRC.

1.2.2.1 Tumour suppressors

1.2.2.1.1 Adenomatous Polyposis Coli (*APC*)

APC is considered to be a guard against CRC carcinogenesis, and its mutation has been identified as one of the earliest events in CRC incidence (Powell et al. 1992; Aghabozorgi et al. 2019). *APC* is part of the destruction complex which is involved in the canonical Wnt signalling pathway (Zhan et al. 2017) and also helps to inhibit the incidence and development of CRC. Mutated *APC* leads to activation of the Wnt signalling pathway and the inhibition of the destruction complex, upregulation of β -catenin and transcriptional factor TCF4 and further promoting tumour development and metastasis in CRC (Hankey et al. 2018).

1.2.2.1.2 p53

p53, a classic tumour suppressor, is a transcriptional factor which is associated with cell cycle arrest, apoptosis and senescence (Li et al. 2015b). Mutation of p53 has been reported among 40-50% of sporadic CRC cases (Takayama et al. 2006) and is considered as another signature aberration in the initiation of CRC development (Li et al. 2015b), as well as late stages of advanced CRC (Vogelstein et al. 1988). When interacting with certain family members of microRNA (miRNA) (miR-125b, miR-34, etc), p53 fulfils part of its function by inhibiting the Wnt pathway and the EMT process. Mutated p53 could lead to the loss of its function as a protector and results in up-regulation of the Wnt pathway, the EMT process and p53 pathways and finally cause cell proliferation, tumour growth, and invasion (Li et al. 2015b).

1.2.2.1.3 TGF- β

The role TGF- β plays in CRC differs across different stages of CRC carcinogenesis. At the early stage, it represses the proliferation of both cancerous and normal epithelial cells, but it acts in an opposite role in the later stages of CRC (Zubeldia et al. 2013). Downregulation of

TGF- β will lead to the inactivation of the TGF- β /Smad pathway and eventually results in tumour progression. Mutations in TGF- β will also lead to the loss of Smad4 and this is followed by activation of signal transducer and activator of transcription 3(STAT3) to support EMT (Pretzsch et al. 2019) and activation of RAS-MAPK and PI3K-AKT pathways (Villalba et al. 2017). Staudacher *et al.* elucidates that by binding to its receptor, TGF- β also contributes to activate Notch and the Wnt signalling pathways which support development of CRC (Staudacher et al. 2017).

1.2.2.2 Tumour promoting genes

1.2.2.2.1 KRAS/BRAF

KRAS and BRAF are two regulators of the EGFR-RAS-RAF-MEK-ERK pathway. The mutation of these two genes will lead to activation of the pathway mediated by the ligands of EGFR (EGF/FGF), which results in promotion of cell proliferation (Carethers and Jung 2015) and the EMT process (Pretzsch et al. 2019). Mutations at differing sites of KRAS lead to different outcomes. For example, mutation of KRAS was reported to be related to late staged and metastatic CRC when it occurred at exon 2 codon 12 (Li et al. 2015a), while another study discovered a close relationship between poor clinical outcomes and mutant KRAS in exon 2 codon 13 (Chen et al. 2014). BRAF V600E, the most common mutant form of BRAF, has also been established to be associated with poor prognosis (Day et al. 2015).

1.2.2.2.2 PI3KCA

PI3KCA encodes p110 α protein, a catalytic subunit of the PI3K protein being pivotal for signal transduction through AKT pathway. Mutation of the *PI3KCA* gene and *AKT1* will eventually result in activation of the pathway and promote cell growth, survival and proliferation (Slattery et al. 2018b).

1.2.2.3 Key Pathways

Multiple pathways are involved in CRC carcinogenesis and metastasis. Some of the classical and common pathways, including canonical Wnt pathway, TGF- β /Smad pathway, and EGFR signalling pathways (RAS-RAF-MEK-ERK-MAPK & PI3K/AKT) are briefly outlined here (Figure 1.3).

1.2.2.3.1 Canonical Wnt signalling pathway

When the canonical Wnt pathway is inactivated, APC, axis inhibition proteins (AXIN) and glycogen synthase kinase three β (GSK3 β) form a destruction complex. This complex

targets β -catenin then results in phosphorylation and ubiquitination which leads to proteasomal degradation. Furthermore, a complex containing T-cell factor/lymphoid enhancer factor family (TCF/LEF) and transducin-like enhancer (TLE)/Groucho presents in the nucleus that targets and inhibits associated gene expression with the help of histone deacetylases (HDACs). If Wnt ligands bind to frizzled or LRP receptors, the pathway will be activated, which leads to Dishevelled (Dvl) up-regulation and transposition to the membrane, to silence the destruction complex. This leads to β -catenin accumulation in the cytoplasm and translocation to the nucleus, where it interacts with TCF/LEF family and results in the promotion of multiple cellular processes such as proliferation and survival (Zhan et al. 2017), while also supporting EMT progression and metastasis (Brocardo and Henderson 2008; Novellasdemunt et al. 2015). Activated Wnt pathways also upregulate expression of a well-established metastatic marker, c-MYC (Rennoll and Yochum 2015), whose upregulation has been reported to be related to cellular differentiation, proliferation and transformation (Jeong et al. 2018). It has also been previously argued that induced upregulation of c-MYC is also associated with prognosis (Toon et al. 2014). Jeong *et al.* demonstrated that activation of the Wnt pathway also induces aberrant expression of c-Jun, cyclin D1 (CCND1) EGFR, leucine-rich repeat-containing G-protein coupled receptor 5 (LGR5), CD44 and CD133, which results in promotion of CRC progression (Jeong et al. 2018).

1.2.2.3.2 TGF- β signalling pathway

TGF- β ligand binds and interacts with its receptor, type II TGF- β receptor (TGFBR2) and therefore, activates the TGF- β signalling pathway. Following activation, TGFBR2 recruits type I TGF- β receptor (TGFBR1) and phosphorylation occurs. Activation of TGFBR1 includes phosphorylation of receptor-associated SMAD (R-SMAD) proteins, SMAD2 and SMAD3 which results in formation of a complex through binding of these proteins to SMAD4. The interaction between R-SMAD and TGFBR1 can be promoted by a number of proteins such as SARA and Axin, or can be inhibited by DPR2, PP2A EIF2A, EIF3/TRIP1 and STRAP. This complex then migrates to the nucleus and regulates targeted gene expression (Jeong et al. 2018).

This regulation of target genes induced by the TGF- β signalling pathway leads to dysregulation of fundamental cellular events, such as reduced proliferation of epithelial populations in colon and supports apoptosis and differentiation (Marmol et al. 2017; Jeong et al. 2018). Hence, activation of this pathway promotes carcinogenesis of CRC.

1.2.2.3.3 EGFR/MAPK & PI3K/AKT signalling pathway

Epidermal growth factor receptor (EGFR), which is also known as ErbB-1 (HER1) is a transmembrane protein which is a member of the ErbB family and serves as a receptor tyrosine kinase (Hirsh 2018). MAPK is responsible for activating a series of phosphorylation and extracellular signal regulated kinases (RAS, RAF, MEK, ERK), belonging to the MAPK family (Slattery et al. 2018a). In binding to its ligand, EGF activates the EGFR/MAPK signalling pathway. An adaptor complex, formed by growth factor receptor bound protein 2 (Grb2) and the son of seven-less (SOS), is bound with EGFR and induces transformation of RAS-GTP (guanosine triphosphate) from RAS GDP (guanosine diphosphate) after activation of the pathway. Activated RAS then triggers phosphorylation of the downstream component including RAF, MEK and ERK. Phosphorylated ERK is then transferred to the nucleus and contributes to activation of transcription factors e.g., activating transcription factor (ATF) which is followed by regulation of expression of target genes such as c-MYC, c-Jun and c-fos (Jeong et al. 2018).

The PI3K/AKT pathway is also one of the essential signalling pathways that contributes to development of CRC. This pathway can be activated by EGFR, activating extracellular factors through receptor tyrosine kinases or promoting activated RAS (Koveitypour et al. 2019). Grb2 is responsible for recruiting PI3K and inducing production of phosphatidylinositol 3, 4, 5 triphosphate (PIP3) by phosphorylating phosphatidylinositol 4, 5 biphosphate (PIP2) (Yu and Cui 2016). This phosphorylation can be regulated by a tumour suppressor, Phosphatase and tensin homologue protein (PTEN) which is also a vital negative mediator of the pathway (Papadatos-Pastos et al. 2015). When PIP2 is converted, PIP3 binds to AKT and translocates it to the membrane domain, AKT is then phosphorylated by PDK1 which results in mediating cellular functions such as proliferation, survival and invasiveness by regulating associated proteins or activating mTOR (Yu and Cui 2016).

Hence, activation of these pathways contributes to the progression of CRC, by mediating cellular migration, angiogenesis, invasion, metastasis and inhibition of apoptosis (Slattery et al. 2018b; Koveitypour et al. 2019). Jeong *et al.*, (2018), illustrates crosstalk between the Wnt pathway and the EGRF pathway, mutations of APC and KRAS are upregulated jointly which contribute to the development of CRC including carcinogenesis, progression and metastasis (Jeong et al. 2018).

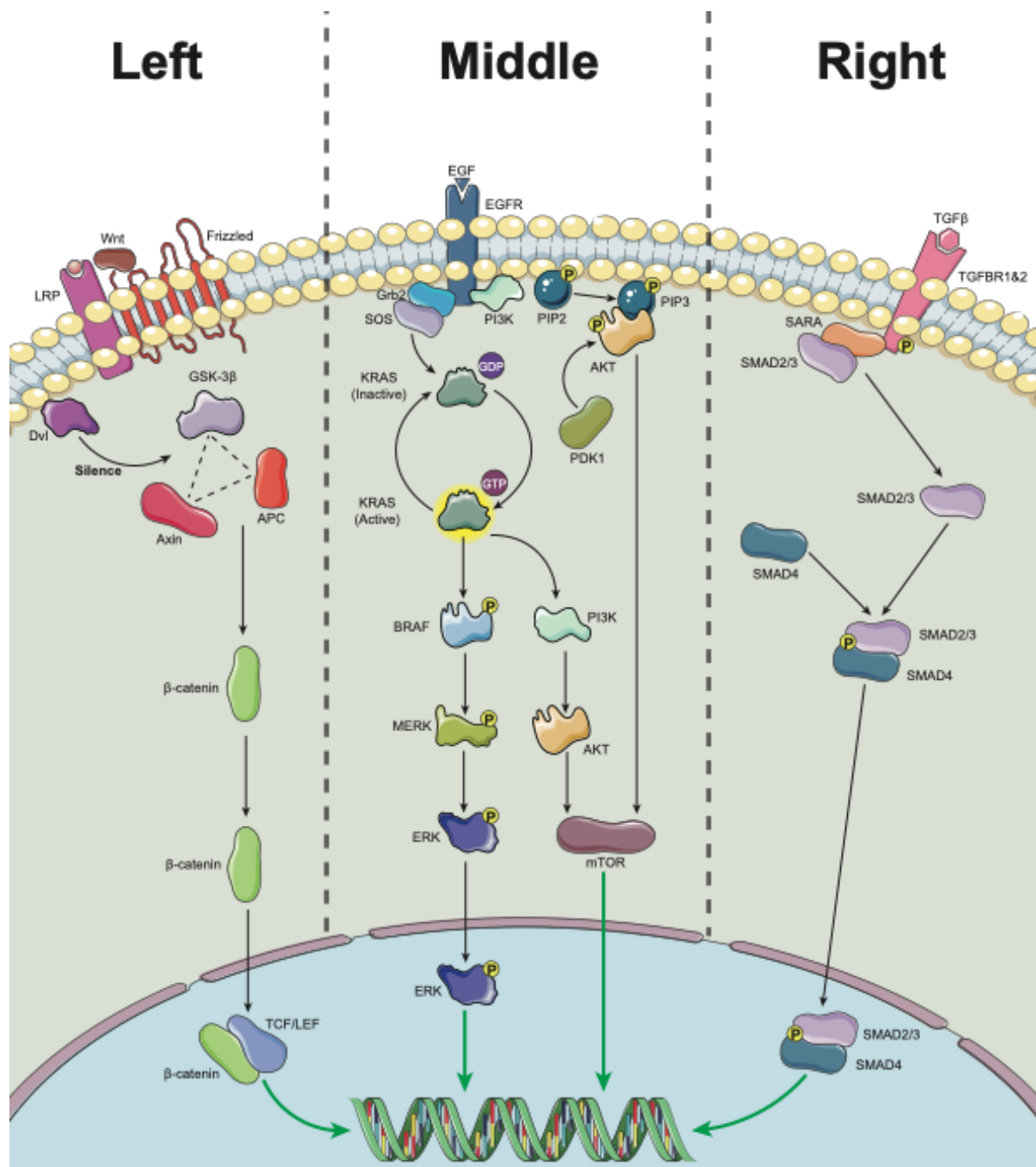


Figure 1.3 Main signalling pathways that participate in CRC Development. (Left) Canonical Wnt Signalling Pathway. (Middle) EGFR & PI3K/AKT Signalling Pathway. (Right) TGF-β Signalling Pathway. Icons were obtained from SMART-Servier Medical ART (<https://smart.servier.com>) and graphics of pathways were designed and created by using Adobe Illustrator 2021 (Adobe, California, USA).

1.2.3 Epithelial Mesenchymal Transition (EMT)

As discussed above, carcinogenesis and development of CRC can be described as a progression through normal mucosa-adenoma-adenocarcinoma (Pretzsch et al. 2019). This process is a complicated network and amongst the significant cellular and molecular events, EMT seems to play a key part (Mittal 2018). EMT has been established to be important in early embryonic and organ development (Shook and Keller 2003), wound healing and development of cancer (Vu and Datta 2017). In terms of carcinogenesis and cancer development, the role played by EMT in the early stages of tumour formation remains controversial. However, compelling evidence has implicated EMT as having a vital impact on metastasis in cancer including CRC (Vu and Datta 2017; Mittal 2018).

The main process of EMT in promoting metastasis in cancer cells is attributed to its ability to down regulate genes that encode adherence junction proteins and stabilize epithelial cells (e.g. E-cadherin, occludins, claudins), while upregulating genes that promote mesenchymal adhesion (e.g. N-cadherin, vimentin, fibronectin). This results in disruption of cell-cell junctions of tumour cells and loss of the apical-basal polarity of epithelial derived cancer cells, which in turn leads to the reorganization of their cytoskeletal structure and, by doing so, develop their potential to migrate and invade (Cao et al. 2015; Vu and Datta 2017).

EMT can be regulated by transcription factors (SNAIL/SULG, ZEB1/2, TWIST1/2, FOXC2, TCF4, SOX2, etc.) and/or by elements present in, or derived from, the microenvironment, including miRNAs (has-miR-31-5p, miR-200, miR-21, miR-31, miR-9) (Vu and Datta 2017; Mittal 2018). A number of signalling pathways are involved in the process of EMT (Vu and Datta 2017; Mittal 2018) including those outlined previously. For example, the canonical Wnt pathway can be activated by downregulation of CLDN3, NDRG1, AOC and AXIN2. After degradation of the destruction complex, β -catenin is increased in the cytoplasm and transported to the nucleus where it binds to transcription factor TCF-4 leading to accumulation of ZEB and SNAI-1, which can subsequently repress the expression of E-cadherin and hence promote EMT. When the TGF- β signalling pathway is activated, loss of Smad-4 results in accumulation of STAT-3 which again would lead to increase of ZEB1, N-cadherin, vimentin and a decrease of E-cadherin (Pretzsch et al. 2019). In EGFR signalling pathways, including RAS/RAF/MEK/ERK/MAPK and PI3K/AKT, the activation of the RAS/RAF/MEK/ERK/MAPK pathway leads to up-regulation of SNAI1/2; the activation of the PI3K/AKT pathway will either lead to inhibition of the destruction complex to promote the Wnt pathway, or increase NF- κ B, both resulting in up-regulation of SNAI-1 which will repress E-cadherin and promote EMT (Pretzsch et al. 2019).

1.2.4 Prognosis of CRC and challenges for unmet clinical needs

The five-year-survival rate of CRC patients in the UK is 58.4% (95%CI 58.0-58.8) from 2013 to 2017 (Office for National Statistics, 2020). According to Cancer Research UK's statistics, net survival for males and females has been improved from 25% to a predicted 59% and from 24% to a predicted 58% respectively during this period (Cancer Research UK, 2020). Thanks to the availability of screening programmes, including colonoscopy and available therapeutic options including surgery, chemotherapy, radiotherapy, targeted therapy and immunotherapy, the survival rate for CRC has been improved over the years (Ahmed 2020). However, with regard to development and late stages of CRC, Siegel *et al.*, (2014), reported that the five-year-survival rate of mCRC is only 12% (Siegel *et al.* 2014) and, in fact, the five-year-survival rate drops to 10% among patients in TNM4 (Van der Jeught *et al.* 2018).

Development of CRC is coordinated through numerous complicated networks, with a wide range of biological and clinical factors impacting on the outcome and prognosis of the patients. CRC with peritoneal metastasis has been reported to have poor prognosis, by resistance to 5-FU based chemotherapy (Klaver *et al.* 2012). Mutation of genes and transcription factors such as APC, TWIST1, SNAI2, vimentin, CLD3, NDRG1, VEGF, HGF, p53, KRAS and BRAF, lead to poor survival and prognosis (Dimova *et al.* 2014; Li *et al.* 2015b; Lemoine *et al.* 2016; Sluiter *et al.* 2016; Vu and Datta 2017; Van der Jeught *et al.* 2018; Ahmed 2020; Harada and Morlote 2020).

Therefore, CRC, especially advanced CRC, has become a huge health and social burden. The development of CRC and progression to advanced metastatic disease is complicated, requiring additional research to understand the underlying mechanisms, identifying the vital players that can influence the progression and, hopefully, gain valuable insight towards development of new therapeutic strategies.

1.3 Pancreatic Cancer

1.3.1. Overview of pancreas

Pancreatic cancer refers to malignant tumours generated from the pancreas. Located at the upper part of the abdominal cavity, it connects the liver and gallbladder via the common bile duct and duodenum through the pancreatic duct. The pancreas is part of the gastrointestinal (GI) system and an essential component of the digestive system (Cancer Research UK, 2022). Regulating glucose homeostasis by secreting hormones (notably insulin) and promoting the disassembly of carbohydrates, lipids and proteins by releasing pancreatic juices, which are rich in enzymes, are the two main functions of the organ. The pancreas is therefore very well known as being an endocrine organ and an exocrine organ respectively (Shih et al. 2013). As a consequence of the endocrine and exocrine nature of the gland, cancers derived from the pancreas are largely divided into two main groups (Grant et al. 2016):

1. Exocrine (nonendocrine cancers) which make up over 90% of pancreatic cancers. This group contains the largest portion of all the pancreatic cancers including pancreatic ductal adenocarcinoma (PADC), which is the dominant type of pancreatic cancer, squamous cell carcinoma, adenosquamous carcinoma, and colloid carcinoma. The latter three are less common.
2. Neuroendocrine pancreatic tumours (PNETs). These are tumours secreting hormones, for example insulioma which produces insulin, gastrinoma producing gastrin, glucagonoma producing glucagon, and rarely somatostatinoma and VIPoma. PNETs make up about 5% of all the pancreatic malignancies.

1.3.2. Incidence and mortality of pancreatic cancer

Ranking as the 10th most common cancer type across the UK (female: 48 percent; male: 52 percent) (2016-2018), incidence rates of pancreatic cancer have been increased by 17 percent since 1993-1995. The incidence is also age related like colorectal cancer and most other cancer types. Besides the increasing incidence rate, 79 percent of patients are diagnosed at more aggressive stages (stage III or IV) (Cancer Research UK, 2022). The survival rate of pancreatic cancer is very poor. For example, the European age-standardised (AS) mortality rates have increased by 5 percent over the last decade. Along with the worrying low 5-year survival rates in England (male: 6.5 percent; female: 8.1 percent. 2013-2017), which has not been improved since the 1970s (Cancer Research UK, 2022), pancreatic cancer has become an urgent health burden and requires better understanding to shed light on better clinical outcomes.

1.3.3 Risk factors & genetic factors

A number of environmental, dietary and genetic factors are known to link to the development of pancreatic cancer, although most of the factors are not specific to pancreatic cancer.

1.3.3.1 Risk factors

As discussed above, incidence and mortality rates of pancreatic cancer are related to age and sex. According to research by the International Agency for Research on Cancer (IARC) and the World Cancer Research Fund, tobacco smoking and obesity are classified as sufficient evidence for increasing incidence rates of pancreatic cancer, while red meat and processed meat products, intake of alcohol and radiation are listed as limited evidence (Lauby-Secretan et al. 2016). Moreover, diseases such as pancreatitis, gallstones, diabetes and metabolic syndrome are also reported to be involved in promoting incidence rates of pancreatic cancer (Cancer Research UK, 2022).

1.3.3.2 Genetic factors

It is clear that pancreatic cancer is connected to the existence of benign pancreatic tumours, including pancreatic intraepithelial neoplasia (PanIN), intraductal papillary mucinous neoplasm (IPMN) (Grant et al. 2016) and mucinous cystic neoplasm (MCN) (Ansari et al. 2016). Certain genetic factors have also been shown to be pancreatic cancer risk factors. For example, mutation of oncogenes or tumour suppressors contribute to the development of pancreatic cancer. Mutation or dysfunction of KRAS, p53, Smad4 and Cyclin Dependent Kinase Inhibitor 2A (CDKN2A) have been illustrated as the most common genetic alterations related to the incidence of PDAC (Grant et al. 2016; Collisson et al. 2019). During the development of PDAC, a number of signalling pathways contribute to promote its progression, namely DNA repair, cell cycle, RNA processing, ROBO SLIT, KRAS, TGF β , WNT, SWI/SNF and Chromatin signalling pathways (Collisson et al. 2019).

Most of the incidence of pancreatic cancer is sporadic (approximate 90%), while around 10% of the cases are related to certain gene mutations within the family heritage (Ansari et al. 2016). These include mutation/alteration of specific genes such as Serine/Threonine Kinase 11 (STK11), Serine Protease 1 (PRSS1), Serine Peptidase Inhibitor Kazal Type 1 (SPINK1), p16, APC, Breast Cancer gene 1 (BRCA1), Breast Cancer gene 2 (BRCA2), MLH1 and MSH2, abnormalities of the genes are found to support hereditary pancreatic cancer (Li et al. 2004; Klein 2013).

1.3.4 Diagnosis and treatment

Current diagnostic methods of pancreatic cancer largely rely on fine needle aspiration biopsy and medical imageology, including ultrasonography, endoscopic retrograde cholangiopancreatography, endoscopic ultrasonography, CT and MR scans (Goral 2015). Although these methods are more than 90 percent sensitive to detect pancreatic cancer, most cases are diagnosed at more advanced stages, a key factor contributing to poorer clinical outcomes for patients. One of main reasons for the late diagnosis is a consequence of late presentation due to lack of specific and early symptoms to alert the patients.

When it comes to choices of treatment, surgical resection is one of most effective ways to remove resectable tumours, which account for a very small proportion of tumours. While chemotherapeutic treatments such as 5-FU, Gemcitabine, paclitaxel, FOLFIRINOX (folinic acid, 5-FU, irinotecan and oxaliplatin), leucovorin and OFF (oxaliplatin, folinic acid/leucovorin and 5-FU) have been reported to be effective as first-line or second-line treatment regimens (Ansari et al. 2016), more and more studies have reported drug resistance events against gemcitabine (Zeng et al. 2019). Other novel treatments, such as immunotherapy and targeting therapy against cancer metabolism, are also being reported but their clinical benefits require extensive assessment (Ansari et al. 2016).

1.3.5. Urgent need

Pancreatic cancer, the 10th most common cancer type in the UK (2016-2018), with its increasing incidence rates and low 5-year survival rates, has become a heavy social burden. Worrying facts urge us to explore deeper into pancreatic cancer, to hunt novel potential biomarkers to target pancreatic cancer and develop targeted therapeutic strategies, in order to improve prognosis and clinical outcomes. Pancreatic cancer was investigated in my study for the purpose of first to use it as an alternative gastrointestinal cancer type to compare with the findings from colorectal cancer which is the main focus of my study and second to explore the impact of EPLIN in this cancer type that has not been investigate for its expression of EPLIN.

1.4 Epithelial Protein Lost in Neoplasm (EPLIN)

1.4.1 Discovery

EPLIN (Epithelial Protein Lost In Neoplasm), also known as actin binding protein1 and LIMA1, a cytoskeletal protein, was first identified during early studies by Chang *et al.* who conducted a cDNA representational analysis (cDNA-RDA) and a cDNA array hybridization to identify differential gene expressions between normal oral epithelial cells and cancer cells. After comparing NHOK, a primary normal human oral keratinocyte cell line, and HOK18L, an HPV-immortalized oral cancer cell line, 345 clones were detected and 69 genes represented 99 non-redundant clones, after 212 redundant clones were excluded (Chang *et al.* 1998). Among these 99 clones, Clone 21(EPLIN), a cDNA fragment which was expressed preferentially in HNOK, was downregulated in oral cancer cells. Similar relationships between epithelial normal and cancer cells were also observed when prostate cancer cell lines, xenograft tumours and breast cancer cell lines were compared to their relative normal epithelial cells (Maul and Chang 1999). Furthermore, high abundance of EPLIN mRNA was also detected in other epithelial cells including placenta, kidney, pancreas, prostate, ovary, spleen, and heart. In contrast, low levels of EPLIN were detected in primary aortic endothelial cells and dermal fibroblasts. EPLIN contains an open reading frame (ORF) which is characterised by a LIM Domain (Maul and Chang 1999). The LIM Domain is a putative protein-protein interaction domain whose function is involved in protein interactions(Kadmas and Beckerle 2004). A sequence analysis was performed to describe the ORF of EPLIN and it indicated that EPLIN has two isoforms, EPLIN α has an ORF of 600 aa while EPLIN β has an additional 160 aa at the amino terminus. An immunoblot analysis described the size of polypeptides of EPLIN, identifying 90 kDa and 110 kDa polypeptides which represented EPLIN α and EPLIN β respectively (Maul and Chang 1999).

1.4.2 Location

EPLIN has been found to be frequently lost, or downregulated, in cancer cells and preferentially expressed in normal epithelial cells including MEC (mammary epithelial cell), PrEC (prostate epithelial cell), NHOK (normal human oral keratinocytes)(Chang *et al.* 1998; Maul and Chang 1999; Jiang *et al.* 2008; Sanders *et al.* 2011; Collins *et al.* 2018) and colon polyps (Lee *et al.* 2006). Low EPLIN expression was also detected in primary aortic endothelial cells and dermal fibroblasts. An immunofluorescence analysis indicated the location of EPLIN by revealing EPLIN has a similar staining pattern, when compared to actin fibres, and an overlap pattern with paxillin at the periphery of the cytoplasm(Maul and Chang 1999). In keeping with this, later studies demonstrated that EPLIN colocalises with stress fibre, circumferential belt and actin filaments in prostate cancer cells (Zhang *et al.* 2011;

Zhang et al. 2013). This location of EPLIN indicates that EPLIN may play a role in actin dynamics.

However, the location of EPLIN is not fixed, when mouse EPLIN is phosphorylated by ERK, which is stimulated by platelet-derived growth factor (PDGF) in NIH 3T3 cells, it is also found to relocate to peripheral and dorsal ruffles of stress fibres during disassembly of stress fibres and membrane ruffling (Han et al. 2007). The location of EPLIN implicates that EPLIN might play a role in maintaining the cytoskeleton and the stability of the cell matrix.

EPLIN can also be co-localised with interacting partners to bring about certain functions. For example, it has been demonstrated, using immunoprecipitation, that when RasV12 cells were surrounded by normal cells, EPLIN was co-immunoprecipitated and partly co-locates with Cav-1, plectin and paxillin (Ohoka et al. 2015; Kadeer et al. 2017; Kasai et al. 2018). Similarly, immunofluorescence revealed that in this circumstance, EPLIN was not only profoundly expressed at the apical and lateral areas in RasV12 transformed cells, but also appeared in cytoplasmic domains and on the inner surface of RasV12 cells, where they interacted with each other. When RasV12 transformed cells were cultured alone, in the absence of normal cells, EPLIN was mainly located at the lateral domains but not as widely as it was located when RasV12 cells were in the presence of normal cells (Ohoka et al. 2015).

The locations of EPLIN are associated with its unique functions. EPLIN co-locates with stress fibres and the actin belt, when EPLIN is phosphorylated, this co-location seems to be disrupted which implicates a possible role in actin cytoskeleton and associated dynamics. In other cases, EPLIN co-locates with a number of interacting proteins to fulfil certain cellular functions.

1.4.3 Structure of the EPLIN coding gene, *LIMA1*

In *Homo sapiens*, the EPLIN coding gene, *LIMA1*, locates to Chromosome 12q13, (data from HGNC (HUGO Gene Nomenclature Committee) (Chen et al. 2000)). The EPLIN gene transcript has two differential isoforms, a 600aa EPLIN α and EPLIN β which has an additional 160aa at the 5' end, both generated from an alternative mRNA splicing event (Maul and Chang 1999). The whole EPLIN gene *LIMA1* sequence spans approximately 100kb, including 10 introns and 11 exons in which EPLIN β occupies all 11 exons while EPLIN α consists of exon4 to 11. The promoter of EPLIN β exists near the beginning of Exon 1 while EPLIN α 's locates downstream of Exon3 and near Exon 4 (Figure 1.4), with both

sharing the same stop codon, located in exon 11 (Wang et al. 2007). The fact that two isoforms have unique promoters indicate that they might be regulated independently.

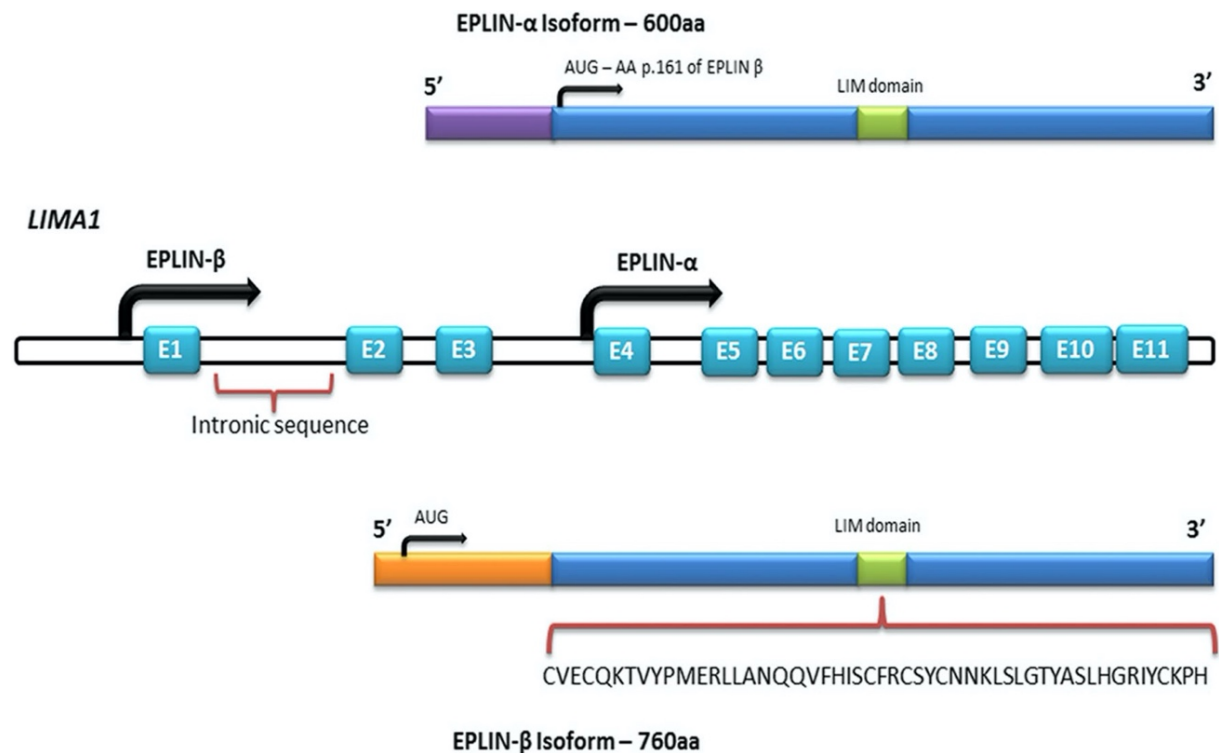


Figure 1.4 Structure of EPLIN α and EPLIN β . Graphic was obtained from Collins et al. Cancer Metastasis Rev (2015) 34:753–764 (Collins et al. 2015)

As indicated previously, the central region of EPLIN contains a LIM Domain. The LIM Domain is a putative protein-protein interaction domain with two zinc fingers which has the ability of attracting related protein targets. The size of the LIM Domain is approximately 55 amino acids, and the sequence has been identified as CX₂CX₁₆₋₂₃HX₂CX₂CX₂CX₁₆₋₂₁CX₂(C/H/D). Multidimensional NMR spectroscopy and X-ray crystallography have been carried out to establish the structure of the LIM Domain (Figure 1.5), and both identified zinc fingers include two orthogonally packed antiparallel β -hairpins, in which β -hairpins 1&2 exist in the first zinc finger while β -hairpins 3&4 present in the other (Kadmas and Beckerle 2004).

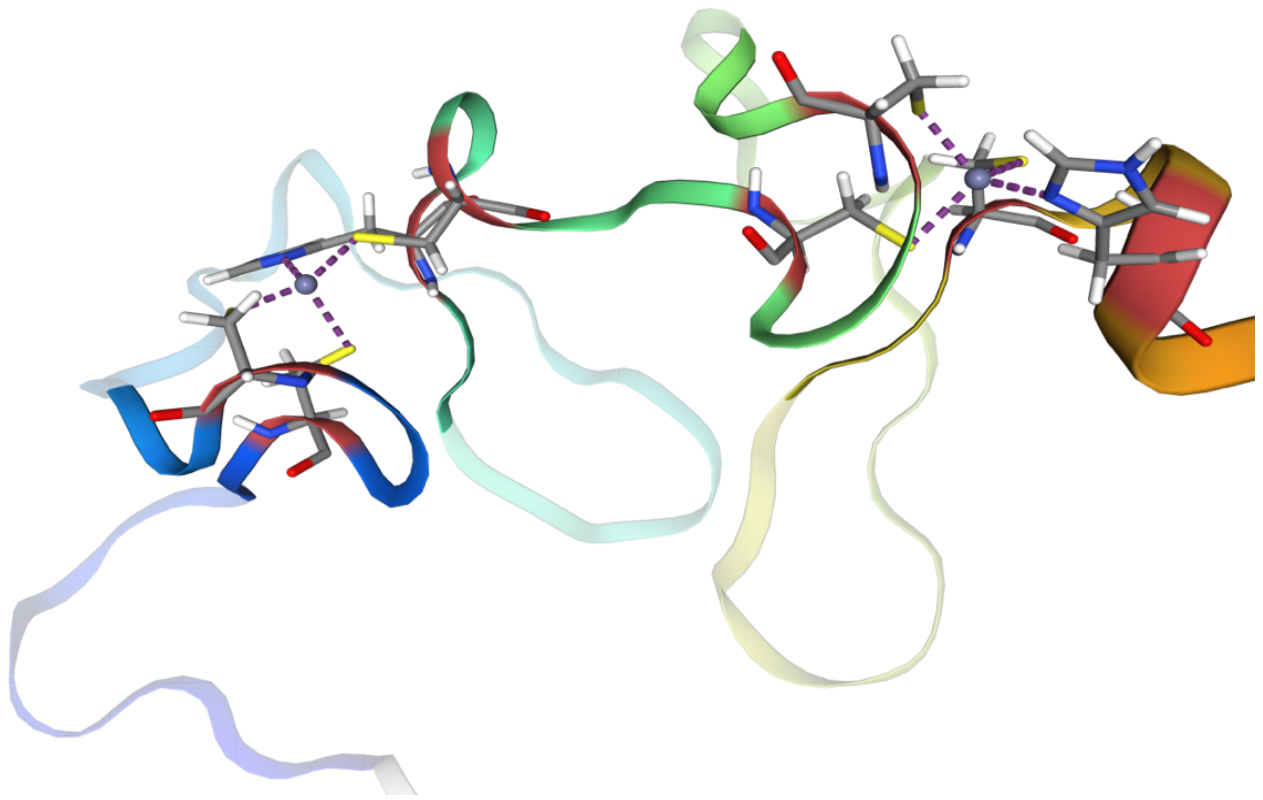


Figure 1.5 Three-Dimensional (3D) Structure of LIM Domain and Zinc Fingers. (PDB ID:2D8Y). Photo is generated and captured from SWISS-MODEL. (<https://swissmodel.expasy.org/repository/md5/d8feaf28e2f35b287ff6967600629b94>)

1.4.4 Function and Functional Interacting Partners of EPLIN

1.4.4.1 EPLIN regulates actin dynamics

The cytoskeleton, which maintains cellular structure and is involved in cellular motility, is formed by the interaction of microtubules, microfilaments and intermediate filaments.

Similarly, actin constitutes a crucial part of the cell cytoskeleton, of which there are two different types, F-actin (filament actin) and G-actin (globular actin), and three subtypes: α , β and γ . G-actin participates in the nucleation of the composition process of microtubules, and F-actin is formed at this stage, subsequently, the microtubule structure will be stabilized by the continuous forming of F-actin and elongation (Lodish H 2000).

Multiple studies reveal that EPLIN co-locates with actin stress fibres, the circumferential actin belt and actin filaments (Maul and Chang 1999; Zhang et al. 2011; Zhang et al. 2013). The localization of EPLIN to the actin cytoskeleton might be essential to suppress anchorage-independent growth of transformed cells; the amino terminal of EPLIN was found to be crucial for this (Song et al. 2002). A study by Maul *et al.* revealed that enhanced amounts

and thickness of stress fibres were observed when EPLIN was overexpressed in MCF-7 cells. Similarly, EPLIN α was found to have two distinct actin binding sites, which are flanked on each side of the LIM Domain, both capable of being activated separately. The existence of two actin binding sites indicates that EPLIN has the ability to cross-link and bundle actin filaments and therefore can stabilize the structure of filaments. Moreover, EPLIN contributes to the inhibition of actin depolymerization and EPLIN α is capable of inhibiting membrane ruffling by activating Rac1 and branching nucleation through the Arp2/3 complex (Maul et al. 2003). In keeping with this, phosphorylation of the C-terminal of EPLIN leads to weaker affinity for EPLIN to bind actin filaments and occurrence of stress fibre disassembly and membrane ruffling (Han et al. 2007). Similarly, Zhang *et al.* using confocal microscopy, demonstrated that downregulation of EPLIN in ARCaP_E cells led to the increase of F-actin structures (Zhang et al. 2011).

The location and apparent function of EPLIN indicates that EPLIN is essential for the stabilization of actin dynamic and that it might play an important role in maintaining the structure of the cytoskeleton.

1.4.4.2 Functional interaction partners of EPLIN

1.4.4.2.1 EPLIN stabilizes adherens junction via cadherin-catenin complex

As described above, EPLIN has the ability to bind actin directly due to two actin binding domains. Adherens junctions (AJ) are cell-cell junctions containing several different types of catenins (e.g., α , β and γ (also known as p120)), cadherin and associated proteins. The AJ is capable of linking epithelial cells around their apical parts and together they compose the zonula adherens and adhesion belt. Therefore, the AJ is involved with controlling epithelial morphogenesis. Cadherins are present on the outside surface of the plasma membrane and communicate with cadherins from neighbouring cells so that they can attach with each other. On the other side of the membrane, a cadherin-catenin complex is bonded with the plasma membrane by the p120 catenin. The cadherin-catenin complex is formed by the presence of E-cadherin, α -catenin and β -catenin, forming a stable structure. Another crucial feature of the AJ is that it links to F-actin and the actin cytoskeleton. To achieve this, it requires vinculin to connect the cadherin-catenin complex to actin filaments (Bruser and Bogdan 2017).

Immunoprecipitation analysis showed that both isoforms of EPLIN can be co-precipitated with α catenin, β catenin or E-cadherin from DLD-1 cells. Similarly, a GST pull-down assay gave further insight into the role of EPLIN within this complex. This showed that EPLIN only be precipitated with GST- α -catenin, but not by the other two elements (β catenin or E-

cadherin) on their own. However, in the presence of GST- α -catenin, EPLIN could also be co-precipitated with GST- β -catenin, and furthermore GST-E-cadherin cytoplasmic domain could similarly be co-precipitated if both GST- α -catenin and GST- β -catenin were present (Abe and Takeichi 2008). This indicates that EPLIN could only associate with α -catenin and furthermore that it could be linked with the cadherin- β -catenin- α -catenin complex through α -catenin. The study further showed that when EPLIN was absent, the stable organization formed by the cadherin- β -catenin- α -catenin complex was completely disorganised, changing from the honeycomb like organised pattern to a blurred dis-ordered shape. Taken together, this implicates an important and necessary role for EPLIN in the formation of the apical actin belt and demonstrates EPLIN's role in maintaining this structure, through its linking ability to the cadherin- β -catenin- α -catenin complex (Abe and Takeichi 2008). Zhang *et al.*, (2011), has also implicated a similar role for EPLIN demonstrating that the depletion of EPLIN led to decreased E-cadherin on prostate cancer cell membrane (Zhang et al. 2011).

Since EPLIN can associate with the cadherin- β -catenin- α -catenin complex via α -catenin, and as EPLIN can not only link to F-actin (due to its two actin binding sites), but also inhibit the depolymerization of actin, EPLIN has the capacity to build a connection between AJs and F-actin, making it an essential component to maintain and support the AJs, actin cytoskeleton and also influence cell motility.

1.4.4.2.2 EPLIN is required for cytokinesis

The actin-cross-linking property that EPLIN exhibits raises the question as to whether EPLIN also has an impact on other cellular activities involving the actin family. Indeed, recent studies have elucidated that EPLIN takes part in the process of cytokines being associated with several interacting partners (Chircop et al. 2009; Sundvold et al. 2016).

Chircop *et al.* knocked down EPLIN in Hela cells, and observed multinucleation after one round of division, which implicates failed cytokinesis, suggesting an important role for EPLIN in cytokinesis. EPLIN was found to be immunoprecipitated with myosin-IIb and cortical actin in Hela and MCF-7 cells, two essential components to form a contractile ring, and promotes membrane ingression of cytokinesis (Maupin and Pollard 1986; Chircop et al. 2009). EPLIN was also immunoprecipitated with Sept2, a regulator of cytokinesis associated with actin at the cleavage furrow, more during division compared to interphase (Kinoshita 2003; Chircop et al. 2009). Additionally, immunofluorescence assays revealed accumulation of EPLIN in the cleavage furrow along with cortical actin in telophase of cytokinesis, when myosin-II was inhibited. EPLIN was noticed to be collocated with cortical actin in the arrested furrow

caused by myosin-II inhibitor. Following knocking down EPLIN in HeLa cells, Chircop *et al.* reported a reduction in accumulation of not only actin, Sept2 and activated myosin-II, myosin regulatory light chain (MRLC) at the cleavage furrow in the late stage of cytokinesis, but also Cdc42 and RhoA, two GTPase members that regulate Sept2 and myosin respectively (Chircop *et al.* 2009).

In agreement with these, Sundvold *et al.* identified that EPLIN also interacts with another novel protein, ACAT-related protein required for viability 1 (Arv1), that accumulates in the cleavage furrow during telophase of cytokinesis, to promote membrane ingression by helping the formation of the contractile ring. Depletion of Arv1 in HeLa cells results in failure of cytokinesis as multinucleation was observed. Liquid chromatography-tandem mass spectrometry (LC-MS/MS) analysis and immunoprecipitation assays elucidated EPLIN as a potential interacting partner of Arv1. Immunofluorescence assays showed EPLIN collocated with Arv1 at the cleavage furrow in HeLa cells. When EPLIN was silenced, the intensity of immunofluorescent Arv1 was decreased, when compared to mock models, while EPLIN was not affected after knockdown of Arv1. This suggests that EPLIN works as an upstream regulator of Arv1 thus recruiting it to cleavage furrow to ensure a successful process of cytokinesis (Sundvold *et al.* 2016).

Hence, EPLIN has been demonstrated to be essential for cytokinesis as it promotes recruitment of key players of cytokinesis including actin, myosin, Sept2, RhoA, Cdc42 and Arv1 to the cleavage furrow to facilitate this cellular process (Figure 1.6).

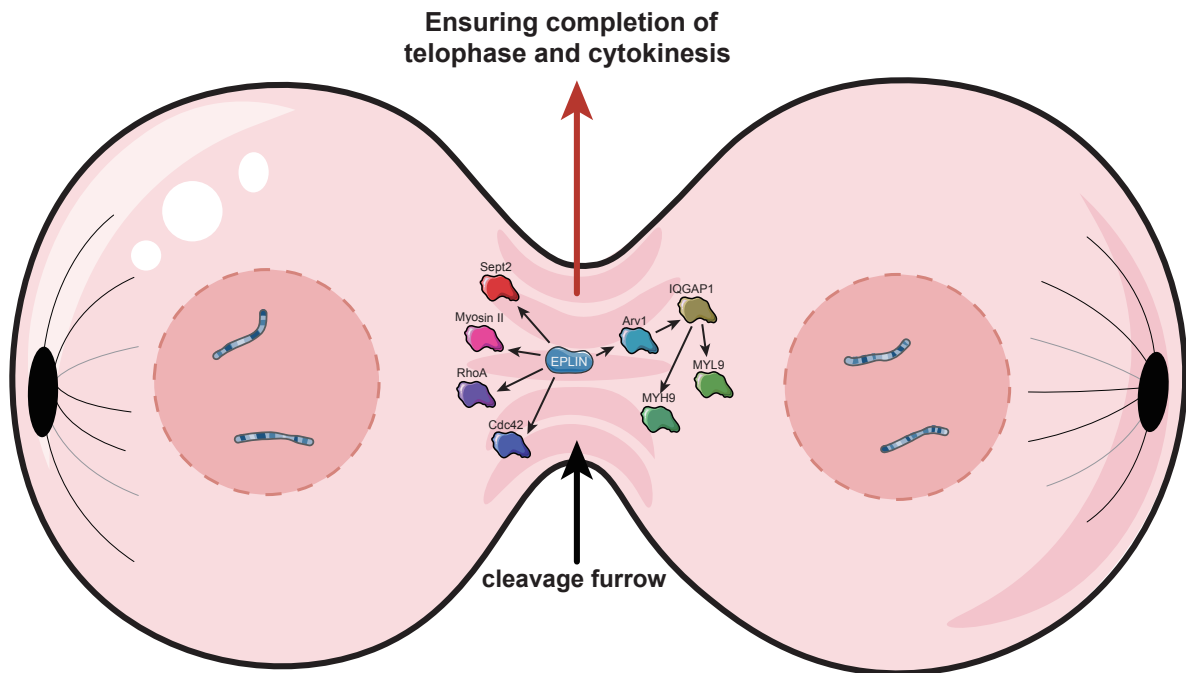


Figure 1.6 EPLIN is essential for cytokinesis. EPLIN localizes at the cleavage furrow and recruits Myosin 66 II, Sept2, RhoA, Cdc42 and Arv1. Arv1 then attracts myosin heavy chain 9 (MYH9) and myosin 67 light chain 9 (MYL9) via IQ- motif-containing GTPase-activating protein (IQGAP1) to support cells 68 division during telophase, icons were obtained from SMART-Servier Medical ART (<https://smart.servier.com>) and graphics of pathways were designed and created by using Adobe Illustrator 2021 (Adobe, California, USA).

1.4.4.2.3 EPLIN is a direct target of the p53 family

p53 is a universally known tumour suppressor which is associated with cancerous metastasis and chemotherapy resistance. A few studies have also indicated that EPLIN has a direct connection with the p53 family, which acts as a tumour suppressor during the progression of cancer (Steder et al. 2013; Ohashi et al. 2017). DNp73, a mutant isoform with a shortly defective N-terminal region produced by the TP73 gene, has the ability to inhibit the expression of a p53 family members, p73, and has found to be related to the development of melanoma cancer (Steder et al. 2013). A report by Steder et al. showed that expression of EPLIN alters under the influence of variation of DNp73 and after comparing their microarray and CHIP-Seq results, they suggested that DNp73 acts as a regulator of EPLIN. When DNp73 was overexpressed in melanoma cells, both isoforms of EPLIN were downregulated and confirmed by immunofluorescence and immunoblotting approaches. Further reporter assays demonstrated that DNp73 induced depletion of EPLIN by interacting

with wild type p73. Moreover, pAKT and pSTAT3 were found to be activated and elevated after knocking down EPLIN by selected shRNA, or forced expression of DNp73 in melanoma cells, in company with a decrease of E-Cadherin and increase of Slug, both related to EMT. Furthermore, the overexpression of EPLIN in melanoma cells was seen to have the opposite effect. Steder *et al.* also demonstrated that this certain relationship between DNp73 and EPLIN resulted in activation of insulin like growth factor 1 receptor (IGF1R) signalling. Hence, depletion of EPLIN induced by DNp73 was responsible for activation of AKT, STAT3 and IGF1R pathways and further brings biological impacts on melanoma cells (discuss later in Chapter 1.3.5.3) (Steder *et al.* 2013).

Further study by Ohashi *et al.* revealed that EPLIN is a direct target of the p53 family. By conducting western blotting using two over-expressed p53 family members in two p53-null cell lines (H12999 & Saos-2), EPLIN was found to have a positive relationship with p53, p63 γ and p73 β in transcript levels, due to transactivation by p53 family binding to RE-1/RE-2 regions (RRRCWWGYYY RRRCWWGYYY) of EPLIN, with its mRNA expression downregulated in these cancer cells as well, when compared to their normal tissues in online datasets. Further analysis found that EPLIN's protein expression was enhanced in the presences of the p53 family. Endogenous wild-type p53 also induced increasing protein expression of EPLIN through nutlin-3a in colon, breast and lung cancer cells, and demonstrated that EPLIN was downregulated in p53 mutant cancer (Ohashi *et al.* 2017). Such findings support that p53, as a direct regulator of EPLIN, is one of the essential interacting partners of EPLIN.

1.4.4.2.4 Phosphorylation of EPLIN by ERK is required in EGF induced EMT

Enhanced cellular migration is commonly associated with an increased metastatic tendency and aggressive nature in cancer cells. Actin dynamics and organisation of the actin cytoskeleton are a crucial part of this process. Behind the mechanism of cell migration, one of the necessary steps is the extracellular stimuli transduction by intracellular elements. Mitogen-activated protein kinase (MAPK) family is one example, extracellular signal-regulated kinase (ERK) being a family member.

ERK can be activated, in response to stimulation of various growth factors, through the Ras-Raf-MEK pathway, translocating to the nucleus where it is able to phosphorylate a range of effector molecules such as protein kinases. ERK was reported to possess a key role in various cell activities, including cell migration (Huang *et al.* 2004; Han *et al.* 2007). EPLIN has been identified as a substrate for ERK mediated phosphorylation by Han *et al.*, (2007),

They revealed several key connections between ERK and mouse EPLIN (m-EPLIN). Firstly, ERK could phosphorylate both isoforms of m-EPLIN at Ser360, Ser602 and Ser692 *in vitro* and *in vivo*. Further work, using a co-sedimentation assay demonstrated that the actin binding ability of m-EPLIN was weakened when its C-Terminal region was phosphorylated by ERK. Secondly, when stimulated with PDGF, the location of m-EPLIN was found to move from the stress fibres to peripheral and dorsal ruffles where Ser360 and Ser602 were phosphorylated and stress fibre disassembly was observed at this stage. Furthermore, ERK phosphorylation of m-EPLIN was revealed to be essential for stress disassembly, membrane ruffling and cell migration, as a non-ERK-phosphorylatable mutant of m-EPLIN inhibited the impact of PDGF (Han et al. 2007). Later study revealed similar findings between ERK and human EPLIN. Epidermal growth factor (EGF) can activate the ERK1/2 cascade, to induce phosphorylation of EPLIN in epithelial like androgen refractory cancer of prostate (ARCaP_E) cells, an experimental model used for studying metastasis in prostate cancer, on Ser362 and Ser604 (Zhang et al. 2013). These two serine residues are counterparts of Ser360 and Ser602 of mouse EPLIN, which is in line with earlier findings (Han et al. 2007). The phosphorylation caused by EGF in ARCaP_E cells is responsible for protein degradation and ubiquitination of EPLIN as, blocking the ERK1/2 pathway by a proteasome inhibitor MG132 counteracts the decreased half-life (T_{1/2}) of EPLIN, which is caused by EGF (Zhang et al. 2013). Similarly, this phosphorylation of EPLIN can be dephosphorylated by hCDC14A on Ser362 and Ser602 (Chen et al. 2017).

As discussed earlier, EMT is a key process through which epithelial cancer cells obtain the abilities of invasiveness and migration by transforming to a more mesenchymal phenotype. The loss of E-cadherin and the increase of certain target genes including TWIST1&2, ZEB1, SNA1 (Snail) and Slug lead to EMT progression (Steder et al. 2013). Actin dynamics, the cytoskeleton and close interaction and contact with neighbouring cells are important to maintain the steady state of epithelial cells. Given EPLIN's role in regulating actin dynamics and in linking the cadherin catenin complex to the actin cytoskeleton, it was anticipated that EPLIN could also play a role in EMT. Indeed, several studies have revealed the connection between EPLIN and EMT, with key early work being conducted by Zhang *et al.*, (2013). In their study, two experimental models of androgen refractory cancer of prostate (ARCaP) were generated, one displaying low invasive rates and an epithelial like morphology (termed ARCaP_E) and another with more invasive, mesenchymal properties (termed ARCaP_M). Using western blotting and immunocytochemical staining, EPLIN was found to be downregulated in ARCaP_M, and carcinoma of the neck and head (SCCHN), in cellular and mouse experimental models. Furthermore, by depleting the expression of EPLIN in ARCaP_E, the features of ARCaP_E changed to the mesenchymal type, indicative of EMT and in keeping

with this, downregulation of E-cadherin, upregulation of ZEB1 and vimentin, which are key proteins that promote EMT process, were observed. Moreover, increased nuclear β -catenin, implicated in the activation of the Wnt/ β -catenin signalling pathways that also support EMT, as well as miR-205, miR-200b and miR-429, which are also vital for EMT, were also observed (Zhang et al. 2011). Actin disassembly and membrane ruffles were also seen. Another study by the same teams dug deeper to elucidate the relationship between EPLIN and EMT. EGF is able to promote the EMT process in ARCaP via activation of the ERK1/2 pathways and phosphorylation of EPLIN occurs due to this cascade. Meanwhile, EGF can also induce downregulation of E-cadherin *in vitro* and *in vivo* with the presence of phosphorylated EPLIN (Zhang et al. 2013), which is in line with their earlier study (Zhang et al. 2011).

Thus, downregulation of EPLIN, that is attributed to phosphorylation by ERK, is essential for EGF induced EMT. Meanwhile, activation of Wnt/ β -catenin signalling, disruption of EMT related elements, the presences of membrane ruffles and actin cytoskeleton disorganisation implicates a connection between EPLIN and EMT.

Recent studies have questioned this conventional concept that, downregulation of epithelial markers like E-cadherin, upregulation of mesenchymal markers such as N-cadherin and vimentin and complete transformation from epithelial traits to mesenchymal ones, are essential for EMT, as a mesenchymal prototype reversed to gain the epithelial characteristic during the process and these two types of characteristic cells can coexist during this dynamic EMT progression (Beerling et al. 2016; Zhitnyak et al. 2020). Zhitnyak *et al.*, (2020) elucidated that disorganisation of the actin cytoskeleton and E-cadherin based AJs occur at the earlier events of EGF induced EMT in epithelial IAR-20 cells and are essential for the whole process. Formation of pseudopodia and retrograde flow are also detected, which lead to loss of cell-cell contact, while expression of E-cadherin remains unchanged (Zhitnyak et al. 2020). During these early events of EGF induced EMT, disruption of co-location between EPLIN and linear AJ and phosphorylation of EPLIN is observed, which is in line with earlier studies (Zhang et al. 2011; Zhang et al. 2013; Zhitnyak et al. 2020).

In agreement with these findings between EPLIN and EMT, additional research by Steder *et al.*, (2013), also deepens this solid relationship. As a regulator of EPLIN, the presence of DNp73 in melanoma cells, or in invasive tumour xenograft mouse models, leads to the downregulation of EPLIN, and further Human Phospho-RTK Antibody Proteome Profiler Array (R&D Systems) and immunoblotting, demonstrated upregulation of slug, p-AKT, p-STAT3, total and phosphorylated IGF1R along with depletion of E-cadherin, which indicates

that DNp73 regulates the EMT process by inhibiting EPLIN, via activation of IGF1R and AKT/STAT3 signalling pathways (Steder et al. 2013).

Taken together, EPLIN is essential for stabilizing actin dynamics and AJs, whose disorganisation, caused by phosphorylation of EPLIN induced by ERK, leads to early events of EGF induced EMT and further supports the process allowing cells to gain the abilities of directional migration.

1.4.4.2.5 EPLIN interacts with FAK & Src

A later study by Collins *et al.*, (2018), has reported that EPLIN α has a relationship with paxillin, focal adhesion kinase (FAK) & proto-oncogene tyrosine protein kinase (Src). By overexpressing EPLIN α in PC-3 and LNCaP cells, the expression of FAK transcript was up-regulated in overexpressed PC-3 cells, while Src was downregulated in LNCaP cells when compared to their control cell lines respectively. Western blot analysis was similarly performed to reveal that the expressions of pFAK Y925, pPaxillin Y31, pPaxillin Y118 and total paxillin were significantly increased in overexpressed PC-3 cells compared to control PC-3 cells, while the expression of pFAK Y397 was up-regulated and pPaxillin Y118 was decreased in transfected LNCaP cells, when compared to control cells. Moreover, Y419, an important site involved in Src activation, was observed to be significantly decreased following overexpression of EPLIN α in PC-3 cells, using a protein microarray and, subsequently, western blot was carried out to confirm a similar trend between p-Src Y419 and transfected PC-3 cells, when compared to control cells. Additionally, p-Src Y530 was upregulated in PC-3 cell following EPLIN α overexpression. Furthermore, a relationship between EPLIN and Src & FAK was found in CA-HPV-10 cells, as the expression of total FAK and Src Y419 were significantly increased by knocking down EPLIN (Collins et al. 2018).

1.4.4.2.6 EPLIN interacts with Plectin, Cav-1 and paxillin

During the early carcinogenesis period in epithelial tissue, mutation of oncogenes are crucial contributors. Kajita *et al.*, (2014), revealed, by using mammalian epithelial cells, that when Ras-transformed cells are surrounded by normal cells, the normal cells will fight to raise the transformed cells and eliminate them into the apical lumen from the epithelium. This competitive self-defence process was described as apical elimination, also epithelial defence against cancer (EDAC) (Kajita et al. 2014).

It has also been reported that EPLIN interacts with a number of crucial players, which take part in apical elimination of RasV12 transformed cells surrounded by normal cells (Ohoka et al. 2015; Kadeer et al. 2017; Kasai et al. 2018). Immunofluorescence assay demonstrated that EPLIN mainly gathered within the cytoplasm, interphase regions between Ras-transformed cells and normal cells, and also at apical and lateral membrane regions where actin and Cav-1 partly co-localised with EPLIN, while the intensity of EPLIN was decreased in transformed cells when they were cultured alone. By silencing EPLIN, apical elimination was observed to be repressed and a similar influence was also induced by knocking down Cav-1. Furthermore, Cav-1 was found to interact with EPLIN in RasV12 transformed cells when surrounded by normal cells by conducting immunoprecipitation assays, mass spectrometric analysis and western blotting. When EPLIN was knocked down in RasV12 transformed cells, the expressions and activities of Cav-1, myosin-II and protein kinase A (PKA) were inhibited, indicating that EPLIN played a role as a regulator. Additionally, a mutual relationship between EPLIN and filamin-A was also observed, which is reported to be a crucial player of apical elimination (Kajita et al. 2014), with knockdown of either, in the surrounding cells, influencing accumulation of the other. Additionally, the expression of EPLIN was found to be diminished due to addition of cytochalasin D and U0126, which inhibit MEK and actin dynamics. Hence, EPLIN was indicated to be an essential regulator of apical elimination by interacting with Cav-1, PKA, myosin-II and filamin-A and, at the same time, actin dynamic and MAPK pathways are required during this competitive cellular activity (Ohoka et al. 2015). Hence EPLIN acts as an upstream regulator of Cav-1 and participates in EDAC. Saitoh *et al.*, (2017), reported that Rab5, a regulator of endocytosis that has been shown to be involved in cell migration and oncogenesis, has the ability to induce apical elimination by mediating EPLIN, to disorganise the structure of the catenin-cadherin complex, in order to interact with players such as myosin II and PKA, to promote the EDAC elimination process (Saitoh et al. 2017).

Further studies regarding apical extrusion of RasV12 transformed cells by Kadeer's team, (2017), revealed that EPLIN's role in RasV12 cells also had a close connection with plectin, paxillin and tubulin, vital players in this event whose inhibitions lead to repression of apical elimination (Kadeer et al. 2017; Kasai et al. 2018). EPLIN was reported to be co-immunoprecipitated with plectin and paxillin, in Ras-transformed cells when they are surrounded by normal cells. Furthermore, the expression of EPLIN was downregulated when plectin or paxillin was diminished, while the expression of plectin/paxillin was similarly decreased by knocking down EPLIN in Ras-transformed cells. While in close proximity to normal cells. Silent plectin also induced depletion of paxillin and knock down of paxillin also had the same impact on plectin. Thus, a potential paxillin-plectin-EPLIN complex was

established (Kadeer et al. 2017; Kasai et al. 2018). Other studies also implicate the relationship between paxillin and EPLIN in prostate cancer. Immunofluorescence assay exhibited greater intensity of paxillin after overexpressing EPLIN in PC-3 cells (Sanders et al. 2011), with Collins *et al.*, (2018) showing that enhanced expressed EPLIN was related to increased paxillin at the protein level and to its phosphorylation (Collins et al. 2018).

Inhibition of EPLIN was also found to downregulate the expression of tubulin, while the microtubule polymerisation inhibitor nocodazole, caused EPLIN's suppression (Kadeer et al. 2017; Kasai et al. 2018). Acetylated tubulin was observed to be accumulated in surrounded transformed cells and enhanced when HDAC6, a deacetylase which regulates acetylation of tubulin, was inhibited. Paxillin has been reported to regulate acetylated tubulin via HDAC6 (Deakin and Turner 2014), in line with this, inhibition of not only paxillin but also EPLIN, or plectin in normal cell-surrounded ras-transformed cells, also induced downregulation of acetylated tubulin, while additional antagonist of HDAC6 was able to counteract this impact and the apical elimination caused by disruption of paxillin (Kasai et al. 2018). Hence, EPLIN is a positive regulator of apical elimination and, in order to achieve it, a number of vital players in this event are involved, including Cav-1, PKA, myosin-II, plectin and paxillin. Actin cytoskeleton dynamics and MAPK pathways are indicated to affect apical elimination as well and acetylation of tubulin mediated by paxillin-plectin-EPLIN complex, via regulating HDAC6, is one of the mechanisms behind it.

In summary, roles of EPLIN in cancerous epithelium have been explored (Figure 1.7). Firstly, EPLIN directly links to the cadherin-catenin complex via α -catenin and also bundles actin due to its two actin linking sites, facilitating EPLIN specific roles in stabilizing AJs, actin dynamics and the cytoskeleton. Secondly, EPLIN has been reported to interact with several partners, either upstream regulators such as p53, DNp73 and ERK, or downstream participants such as Cav-1 and PKA, to fulfil its role in modifying cellular events that affect developments of cancers. Specific roles of EPLIN in cancers will be discussed in section 1.3.5.

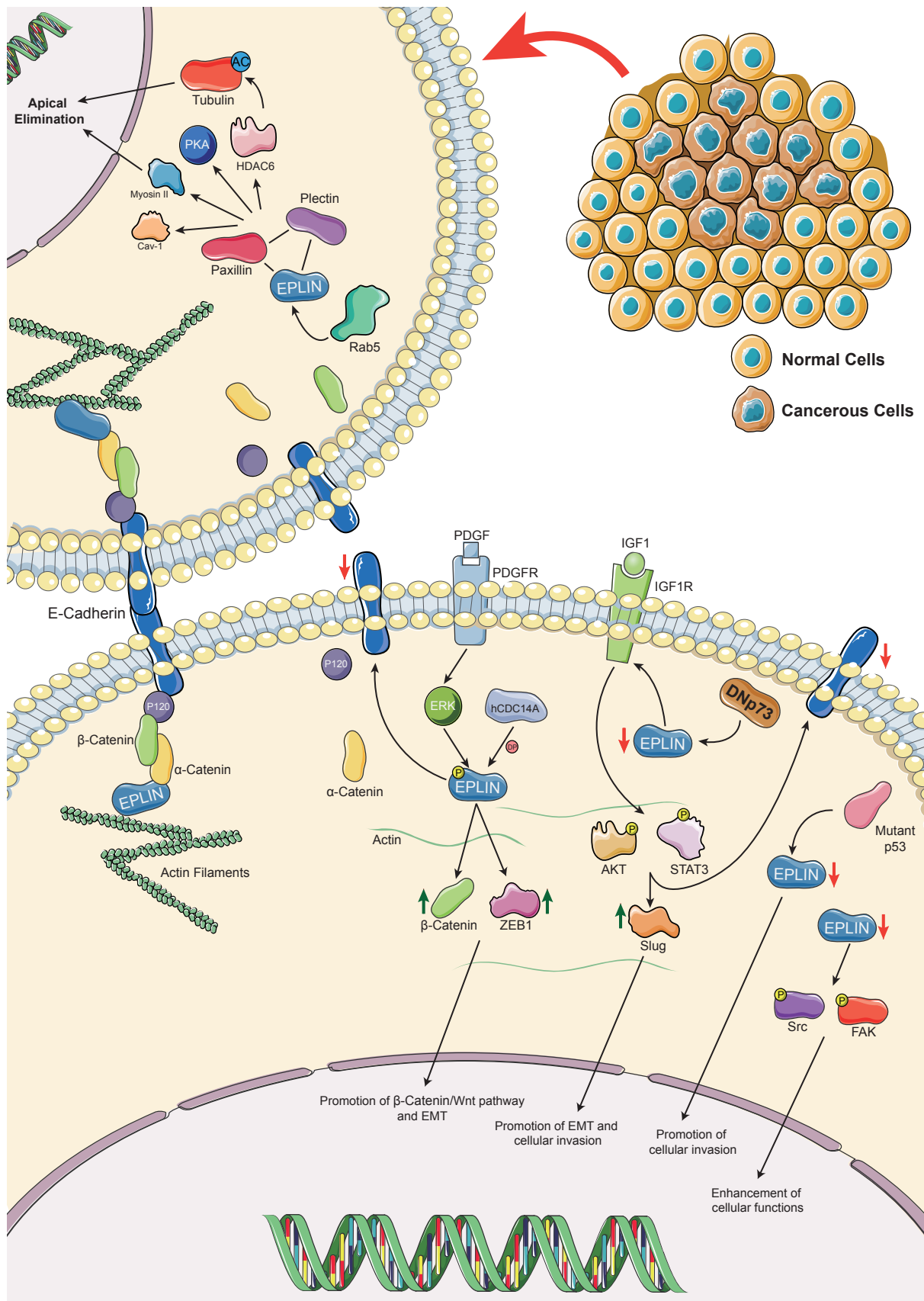


Figure 1.7. Continued on next page

Figure 1.7 EPLIN pathways in epithelium. EPLIN stabilizes AJs and actin dynamics by binding to the cadherin-catenin complex and actin directly. PDGF could induce phosphorylation of EPLIN via ERK signalling pathways and results in disorganization of AJs and interruption of actin dynamics, which further upregulates expression of β -catenin and ZEB1, diminishes expression of E-cadherin which leads to activation of the β -catenin/Wnt pathway and promotion of EMT, further impacting cellular functions. While this phosphorylation of EPLIN is able to be counteracted by hCDC14A. DNp73 induces downregulation of EPLIN which allows IGF1R to interact with its ligand then phosphorylates AKT and STAT3, which increases expression of Slug and decreases expression of E-cadherin, to promote the EMT process. p53 mutation down-regulates expression of EPLIN which results in enhancement of cellular invasiveness. The downregulation of EPLIN has been reported to promote cellular functions, which may attribute to phosphorylation of FAK/Src and activation of the FAK/Src pathways. EPLIN, paxillin and plectin form a complex and Rab5 allows disruption of the cadherin-catenin complex to recruit PKA, Cav-1 and myosin II then acetylates tubulin through HDAC6, which contributes to promotion of apical elimination when Ras-transformed cells are surrounded by normal cells. Icons were obtained from SMART-Servier Medical ART (<https://smart.servier.com>) and graphics of pathways were designed and created by using Adobe Illustrator 2021 (Adobe, California, USA). (Zeng et al 2021).

1.4.4.3 Impact on endothelial cells

EPLIN was initially reported to be diminished or absent in epithelial cancer cells compared to their normal pairs (Chang et al. 1998; Maul and Chang 1999), and had been largely investigated in regard to cellular functions and interacting partners, mainly in epithelial derived cancer cells. Work derived from early studies has led to EPLIN being labelled as a tumour suppressor, as discussed in previous sections. The development and progression of aggressive cancers often requires access to the circulatory system, which facilitates advanced growth of the tumour (Pretzsch et al. 2019). However, EPLIN's role in angiogenesis was not characterised in the early studies. EPLIN bundles actin filaments and connects them to the cadherin-catenin complex via α -catenin and inhibits the branched nucleation caused Arp2/3, contributing to sustaining the cytoskeleton and cell-cell adhesion in epithelial cells (Maul et al. 2003; Han et al. 2007). Similarly, cell junction activities in endothelial cells, which regulate endothelium integrity, are crucial for angiogenesis (Aird 2007; Chervin-Petinot et al. 2012).

Apart from its functional impact on epithelial cancer cells, and given the significance of angiogenesis in cancer metastasis, the impact of EPLIN on endothelial cells has also been explored. Sanders *et al.* (2010), observed that overexpression of EPLIN α in human endothelial HECV cell lines resulted in significantly decreased cell migration, compared to control HECV^{pEF6} and HECV^{WT} cells, by conducting wounding assays. EPLIN α overexpression similarly impacted on cell-matrix adhesion but had no obvious influence on cell growth. By co-injecting either EPLIN α overexpressed HECV cells, or control HECV^{pEF6} cells, together with MDA MB231 cells into nude mice, tumours were observed to grow slower and smaller in the group inoculated alongside the HECV EPLIN α overexpression group, than the control group. Moreover, overexpressed EPLIN α in HECV cell lines resulted in depletion of tubule formation capacity and, through addition of ERK inhibitors, indicated that ERK signalling might play a role in the underlying mechanism (Sanders et al. 2010).

Thus, EPLIN α might be a negative regulator of angiogenesis *in vitro* and *in vivo* and has a possible role in regulating cell migration in endothelial cells. Given the significance of these processes in angiogenesis, questions about EPLIN's role and mechanism in endothelial cells and angiogenesis were asked.

Confocal microscopy and immunoprecipitation assays, in human umbilical vascular endothelial cells (HUVECs), demonstrated that EPLIN co-locates with actin filaments, VE-cadherin, α/β -catenin and vinculin at cell junction regions. Similarly, knocking down EPLIN lead to location changes of vinculin, , from locating dominantly at periphery regions to spreading amorously around the cytoplasm. A GST pull-down assay showed that EPLIN links to the VE-cadherin-catenin complex, via α -catenin. Although muting EPLIN did not affect adhesion, migration and proliferation of HUVECs (Chervin-Petinot et al. 2012). Another study reported that miR-93-5p, a microRNA which is a positive regulator of migration, proliferation and angiogenesis in HUVECs, acted upstream of EPLIN as, inhibiting miR-93-5p significantly upregulated expression of EPLIN, whilst enhancing its expression lead to downregulation of EPLIN in HUVECs, which indicated a negative correlation between these two elements. Such observations were confirmed using luciferase reporters, demonstrating that miR-93-5p manipulates expression of EPLIN by binding to its 3'-UTR sequence. Additionally, the authors discovered that knocking down EPLIN leads to enhanced migration and lumen formation inhibited by miR-93-5p (Liang et al. 2017). This may implicate that the role of EPLIN in HUVECs' cellular functions could be achieved through interacting with other elements. Additionally, Chervin-Petinot *et al.*, (2012), conducted tubule formation assays, to show that knocking down EPLIN increases the number of decreased network length and breakage events, when compared to control groups (Chervin-Petinot et al. 2012). This appears to be consistent with the results from our lab, and that from Liang *et al.*, (2017) (Sanders et al. 2010; Liang et al. 2017), and emphasises the potential negative regulatory role EPLIN plays in endothelial cell junctions and angiogenesis.

EPLIN has two isoforms that generate from two distinct promoters (Chen et al. 2000), with the two isoforms only differing in the N-terminal region, in which EPLIN β has an additional 160aa (Maul and Chang 1999) and share a centrally located LIM domain and two actin binding sites (Maul and Chang 1999; Maul et al. 2003), which are essential for EPLIN's function. Expression of EPLIN- α is frequently diminished in cancer, while EPLIN β has been reported to remain the same or slightly increase (Chen et al. 2000). Thus, when it comes to EPLIN's implication in epithelial cells or cancers, the EPLIN α isoform is often investigated. However, recent investigations on EPLIN's implication in endothelial cell dynamics discloses that the two isoforms act differently in endothelial cells dynamics (Zhitnyak et al. 2020).

Earlier studies from the team, performed a combination of some advanced methods to target both EPLIN isoforms with EGFP/mCherry/Halo in HUVECs and monitor their locations respectively. Hofer *et al.*, (2018), showed they mainly present at cell junctions and EPLIN- α is brighter than EPLIN β (Hofer et al. 2018), which is in agreement with previous reports on the location of EPLIN. Taha *et al.*, (2019), monitored the locations of both isoforms, in the same HUVEC cells, by specific tags and time-lapse recording, revealing that both isoforms are present at cell junctions and stress fibres. However, EPLIN α dominantly presents at branched actin networks, including classical lamellipodia (cLP) and junction-associated intermittent lamellipodia (JAIL). Furthermore, monitoring the expression of both isoforms, in pig aortic and cava vein, suggested that EPLIN β expression is upregulated in aortic endothelial cells rather than in cava vein endothelial cells, while EPLIN α remains the same, with β isoform expression regulated by shear stress strength positively in HUVECs. Regarding EPLIN α , the authors reported that its expression correlated with confluence of cells and protrusion formation, as EPLIN α expression and migration velocities weaken as the cells grow (Taha et al. 2019). These findings suggest potential different functions of the two isoforms in endothelial cells dynamics.

Further monitoring shows that EPLIN α localises with cLP and FAIL, which are components of branched actin networks and could be controlled by the Arp2/3 complex (Zhitnyak et al. 2020). JAIL is responsible for forming and developing endothelial cell junction sites, allowing protrusions to travel to neighbouring cells through the membrane, until interaction with VE-cadherin, then protrusion stops until the next junction site is formed. This regulation of cell dynamics contributes to migration and junctional dynamics related to angiogenesis (Cao and Schnittler 2019; Zhitnyak et al. 2020). A combination method of Spinning disc and confocal microscopy was conducted, to show that EPLIN α and the Arp2/3 complex display at a distance in cells, getting closer to each other as the protrusion develops, the protrusion ending when the two players overlap, whilst both EPLIN and Arp2/3 are disconnected with actin, suggesting a potential role for EPLIN in inhibiting protrusion via the Arp2/3 complex. Pull-down assays reported that part of Arp2/3 was detected in both isoforms, further confirming an interaction between these two; while blocking Arp2/3 leads to inhibition of protrusion and dislocation of EPLIN α . Similarly, inhibition of EPLIN α results in promotion of size and duration of protrusion. These support the concept that EPLIN, especially the α isoform, participates in regulating protrusion progression by interacting with the Arp2/3 complex. Furthermore, overexpressing EPLIN- α in either HUVECs or MCF-7 cells (EPLIN- α absent) terminates JAIL formation quicker, in combination with upregulation of formation of filopodia, which indicates enhancement of actin dynamics. Meanwhile, interruption of VE-Cadherin dynamic is observed, which is responsible for weaker migration and barrier

function (Taha et al. 2019). On the other hand, EPLIN- β is discovered to be associated with stabilization of stress fibres. EPLIN- β tends to protect stress fibre structure more efficiently than EPLIN- α as, dosing an inhibitor to depolymerize stress fibres in overexpressed EPLIN- α / β and control HUVECs, led to a less decreased rate of stress fibres in the overexpressed EPLIN- β group, when compared to others and overexpressed EPLIN- β leads to more formation of stress fibres when compared other control cells (Taha et al. 2019).

Therefore, the role of EPLIN in endothelial dynamics has been investigated (Figure 1.8). Taken together, EPLIN takes part in regulation of endothelial dynamics by binding to VE-Cadherin via α -catenin and actin filaments. Depletion of EPLIN could be induced by miR-93-5p, which contributes to elevation of cellular migration and lumen formation, which is in line with the finding that this downregulation of EPLIN promotes angiogenesis. EPLIN- α mainly locates at JAIL and cLP and plays a role in regulating protrusion progressions by interacting with Arp2/3 and mediating JAIL formation and VE-Cadherin dynamics, further influencing cellular migration and barrier function. EPLIN- β expression is lower in branched actin networks but presents along with stress fibres, and a high level of the β isoform was observed in aortic cells. EPLIN- β plays a role in stabilizing stress fibre in actin dynamics in endothelial cells (EC).

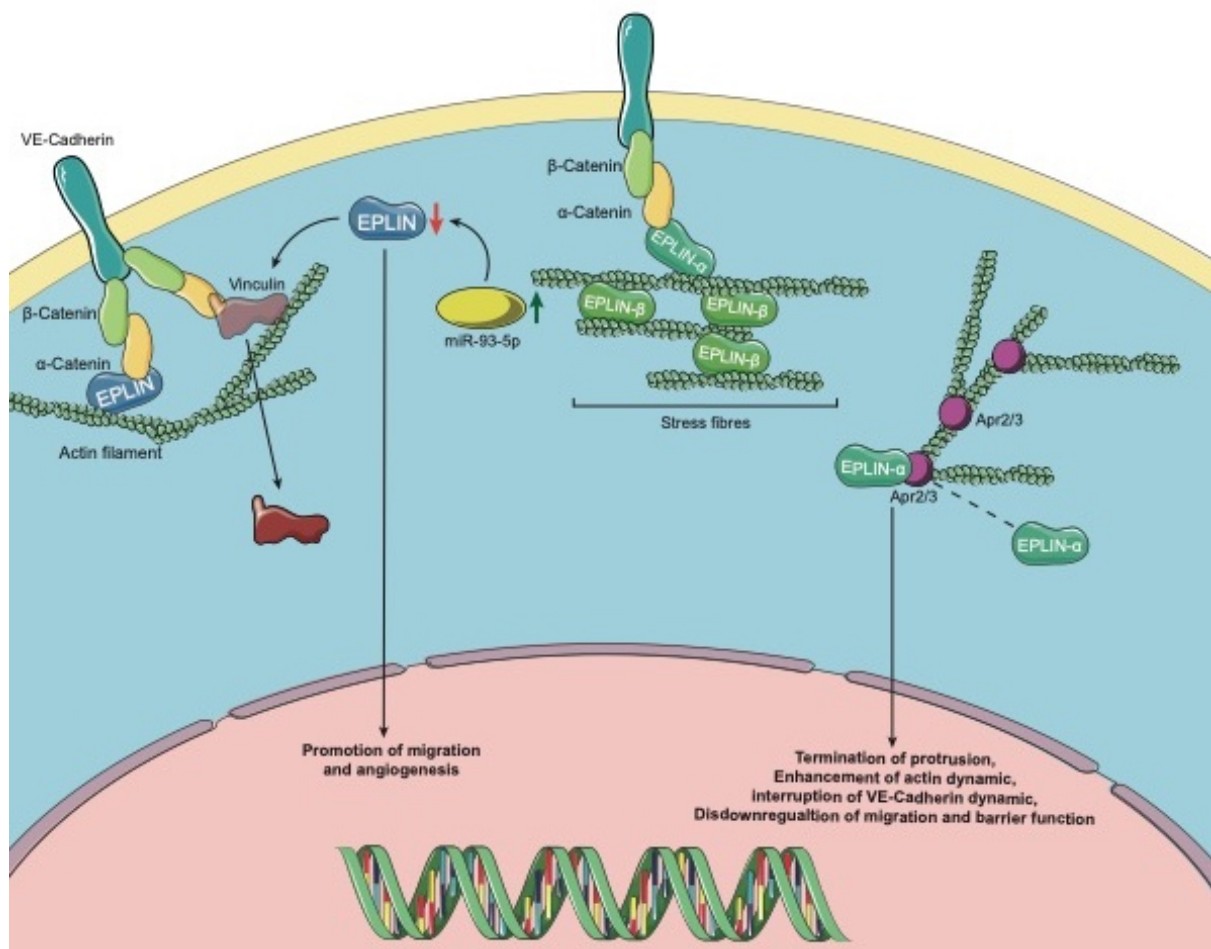


Figure 1.8 EPLIN's role in endothelium. EPLIN sustains cell junctions in ECs by linking to VE-Cadherin via α -catenin. Downregulation of EPLIN could be induced by upregulation of miR-93-5p which leads to translocation of vinculin from the periphery to cytoplasm. Downregulation of EPLIN also results in promotion of cellular migration and supports angiogenesis. EPLIN- α mainly locates at JAIL and cLP which are components of branched actin. EPLIN- α regulates protrusion progression via the Arp2/3 complex, whilst EPLIN- β mainly locates at stress fibres to maintain stability. Icons were obtained from SMART-Servier Medical ART (<https://smart.servier.com>) and graphics of pathways were designed and created by using Adobe Illustrator 2021 (Adobe, California, USA). (Zeng et al 2021).

1.4.4.4 EPLIN, implications in other biological processes and diseases

From earlier studies, one of the most significant findings regarding EPLIN is that it regulates actin dynamics, by colocalising with actin filaments and other actin structural regulators and cross-linking actin filaments, inhibiting branched nucleation through Arp2/3, further affecting cell motility and migration (Maul and Chang 1999; Maul et al. 2003; Abe and Takeichi 2008). As discussed in previous sections, research throughout these years mainly highlighted EPLIN's impacts in cancerous epithelium as well as endothelial dynamics. Interestingly, research has illustrated the fact that, besides its role in tumours, EPLIN also takes part in cellular events in non-cancerous tissues.

Tsurumi *et al.*, (2014), reported strong expression of EPLIN in mesangial cells and downregulated expression in mesangial proliferative nephritis *in vivo*. EPLIN colocalises at focal adhesions with paxillin and their interaction takes part in stabilizing focal adhesion in mesangial cells. PDGF induced MEK/ERK signalling is responsible for disruption of the EPLIN-paxillin complex and translocation of EPLIN from focal adhesion sites to peripheral ruffles. Additionally, depletion of EPLIN results in disorganization of focal adhesions and enhancement of cells' migration via PDGF (Figure 1.9) (Tsurumi et al. 2014).

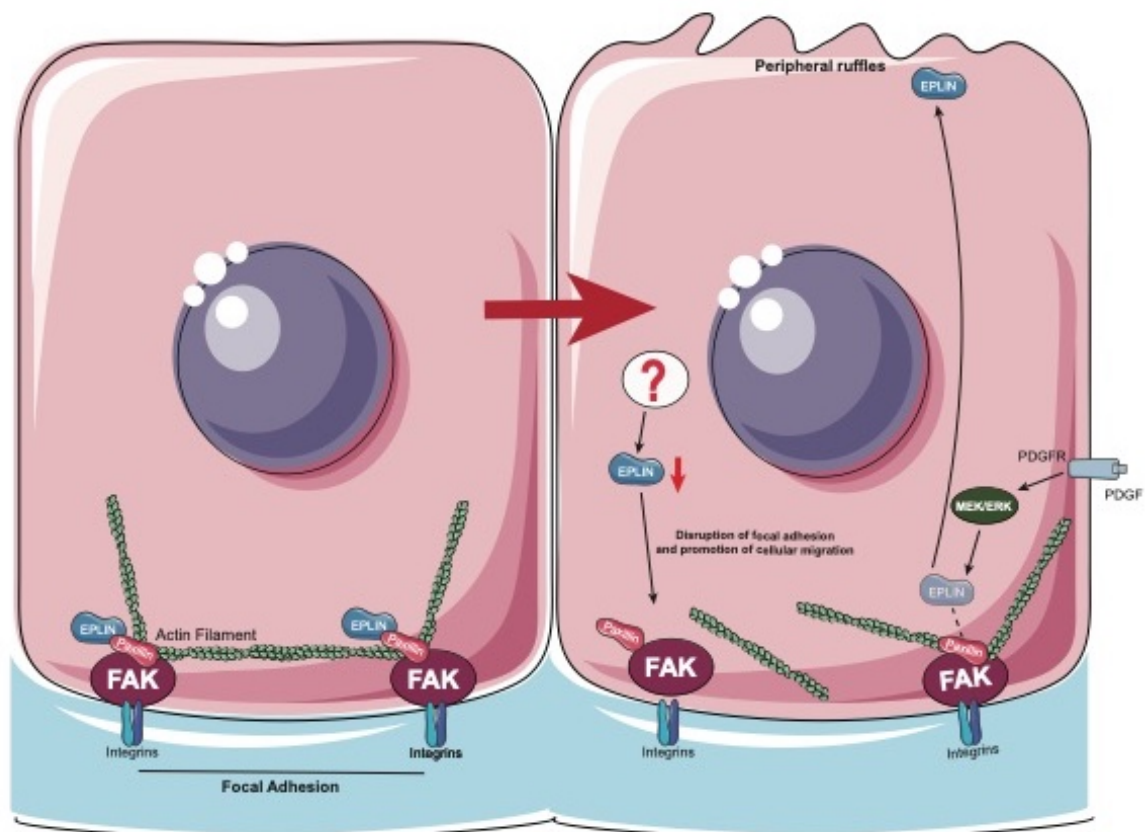


Figure 1.9 EPLIN interacts with Paxillin to form a complex resulting in maintenance of focal adhesion. PDGF induced MEK/ERK signalling pathway leads to disruption of the EPLIN-paxillin complex and translocation of EPLIN from focal adhesion sites to peripheral ruffles. Depletion of EPLIN results in disorganization of focal adhesions and enhancement of cellular migration via PDGF, although upstream participants responsible for EPLIN's depletion remain elusive. Icons were obtained from SMART-Servier Medical ART (<https://smart.servier.com>) and graphics of pathways were designed and created by using Adobe Illustrator 2021 (Adobe, California, USA). (Zeng et al 2021).

Recent study by Goncalves *et al.*, (2020), revealed that EPLIN is involved in another cellular activity, ciliation, by interacting with Leucine Zipper Protein 1 (LUZP1) (Goncalves *et al.* 2020). Cilia are membranous protrusions which originate from the centrosome via complicated mechanisms, including cytoskeleton, membrane traffic, etc. Cilia take part in certain sensory and motional biological functions, whose dysregulation could lead to ciliopathies, including blindness, cystic kidneys, etc (Gupta *et al.* 2015; Mitchison and Valente 2017; Goncalves *et al.* 2020). LUZP1 has been reported as a regulator of ciliogenesis negatively and actin dynamic positively (Gupta *et al.* 2015; Wang and Nakamura 2019).

Goncalves *et al.*, (2020), identified EPLIN as a novel interacting partner of LUZP1 by conducting affinity purification and mass spectrometry assays in a HeLa cells dataset (Yam *et al.* 2008; Goncalves *et al.* 2020). This relationship was confirmed through conducting coimmunoprecipitation (coIP) assays using GFP/FLAG vectors in RPE-1 cells or HEK293 cells. The authors revealed that LUZP1 and EPLIN interact with each other via the C-terminal of LUZP1, as GFP targeted LUZP1 pulled down both isoforms of EPLIN in RPE-1 cells, GFP-EPLIN/FLAG-EPLIN- β pulled down LUZP1 in RPE-1 cells and HEK293 cells respectively. GFP-EPLIN- β was able to pull down FLAG tagged full length and C-terminal LUZP1 in HEK293 cells, and both FLAG-EPLIN and FLAG-LUZP1 were able to pull down actin. Intriguingly, immunofluorescence revealed both EPLIN and LUZP1 co-locate with actin filaments in RPE-1 cells, however, LUZP1 locates at centrosome and basal regions, EPLIN- α locates mainly at the leading edge, where membrane ruffles occur, while EPLIN- β mainly locates along with actin filaments. Hence, a possible functional correlation between these proteins was indicated. Further, accumulation of ciliated cells and longer primary cilia were observed when EPLIN/LUZP1 were knocked down by siRNA in RPE-1 cells, along with increased expression of MyosinVa through immunofluorescence analysis. Aberrant regulation of ciliation, caused by cytochalasin D, could be counteracted by overexpressing EPLIN and LUZP1, while accumulation of Arp2 was also observed. Hence, LUZP1 interacts with EPLIN to contribute to ciliation regulation, possibly through regulating actin structures (Goncalves *et al.* 2020)(Figure 1.10).

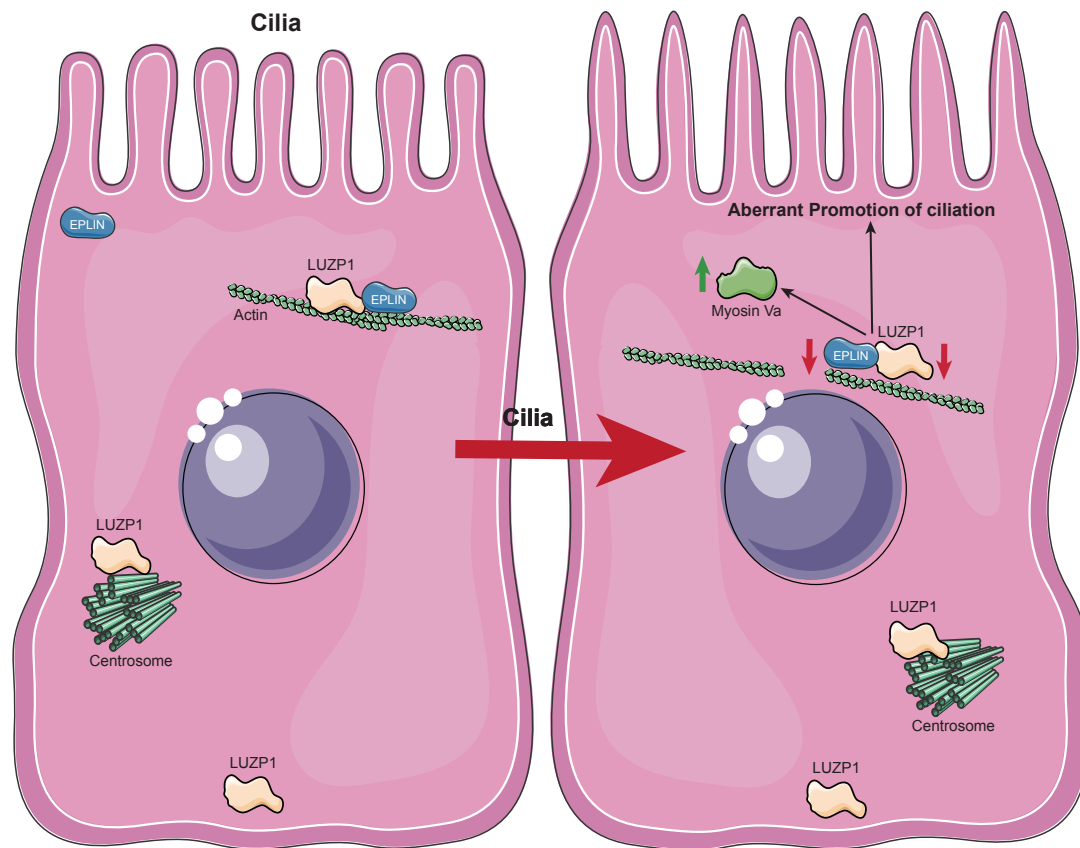


Figure 1.10 EPLIN colocalises and interacts with LUZP1 at actin. Depletion of EPLIN/LUZP1 leads to accumulation of ciliated cells and longer primary cilia, in combination with increasing myosin Va. Icons were obtained from SMART-Servier Medical ART (<https://smart.servier.com>) and graphics of pathways were designed and created by using Adobe Illustrator 2021 (Adobe, California, USA). (Zeng et al 2021).

We introduced above that EPLIN participates in the regulation of ciliation progression through interaction with LUZP1 (Goncalves et al. 2020). Depletion and dysfunction of cilia could result in diseases such as blindness, cystic kidneys etc. (Mitchison and Valente 2017), which together indicate that EPLIN also plays key roles in biological progressions, not only related to carcinogenesis and tumour development, but also other diseases.

Indeed, another study by Zhang *et al.*, (2018b), reported that EPLIN is associated with cholesterol absorption in intestines. A Chinese Kazakh family (n=9), with inherited low level of low-density lipoprotein cholesterol (LDL-C) in plasma, have been established by the group as a study model. A mutation of EPLIN, LIMA1-K306fs, which includes a frameshift variant on exon-7, was identified to be a potential candidate, which is associated with LDL-C in the family, by using whole-exome sequencing and sanger sequencing. Individuals who express LIMA1-K306fs have a significantly lower level of LDL-C and campesterol:lathosterol

ratio when compared to those who do not. By analysing a larger cohort, another mutation of EPLIN, LIMA1-L25I, was also found to have a similar effect. Moreover, the team set up a mouse experimental model, and silenced EPLIN in intestines of the mice which lead to the downregulation of cholesterol uptake, plasma cholesterol, liver 3H-cholesterol and plasma 3H-cholesterol, when compared to control groups. Hence, this implies that EPLIN is a potential positive regulator in LDL-C levels and intestinal cholesterol absorption in humans and mice (Zhang et al. 2018b). To investigate the possible mechanism behind this interesting function, EPLIN was found to be co-localised with myosin Vb and Niemann-Pick C1-Like Protein 1 (NPC1L1), which are known to be essential to cholesterol absorption (Xie et al. 2014; Zhang et al. 2018b), on the brush border in mouse intestines by using co-immunoprecipitation assays. Furthermore, knock down of EPLIN in CRL1601 cells led to a diminishing of both myosin Vb and NPC1L1 and pull-down assays revealed EPLIN interacts with both proteins. Depletion of EPLIN or myosin Vb and mutation of EPLIN in CRL1601 cells led to disruption of NPC1L1's transporting ability, suggesting the NPC1L1-EPLIN complex is needed for cholesterol absorption, as disconnecting the complex lead to weakened transporting ability by NPC1L1 *in vitro* and *in vivo* (Zhang et al. 2018b). Therefore, EPLIN was found to be associated with LDL-C, whose high concentration is responsible for cardiovascular disease, with mutation/downregulation of EPLIN having a positive effect on cholesterol absorption by interacting with NPC1L1 and myosin Vb (Figure 1.11).

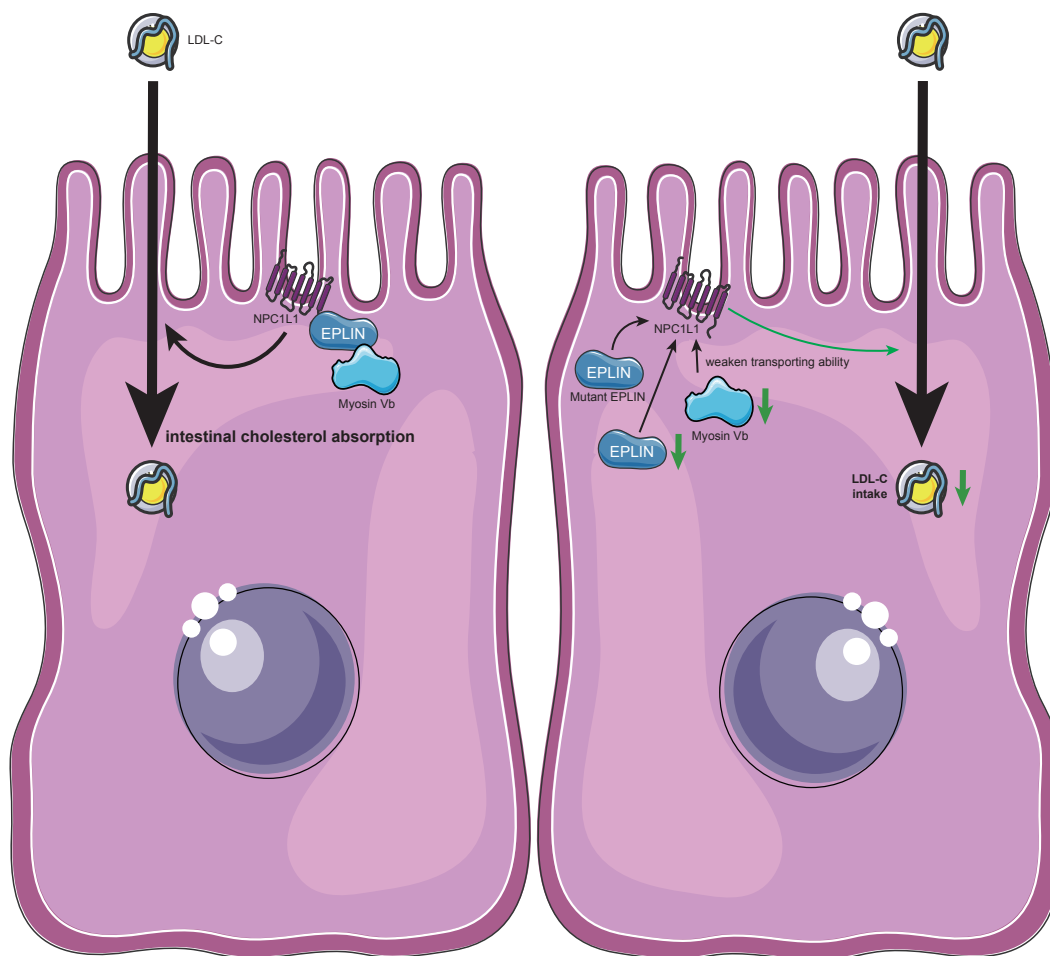


Figure 1.11 EPLIN takes part in LDL-C absorption in intestines. NPC1L1, which is essential for LDL-C intake, interacts with EPLIN which binds to myosin Vb to regulate cholesterol absorption. Mutant or depletion of EPLIN, or downregulation of myosin Vb, diminishes the transporting ability performed by NPC1L1, which results in reduction of LDL-C intake. Icons were obtained from SMART-Servier Medical ART (<https://smart.servier.com>) and graphics of pathways were designed and created by using Adobe Illustrator 2021 (Adobe, California, USA). (Zeng et al 2021).

Hence, EPLIN appears to have a number of significant cellular roles and implications in traits associated with, not only cancer progression in epithelial and endothelial cells, but also focal adhesion, ciliation and cholesterol absorption, in non-cancerous tissues. A number of pathways and interacting partners have been discussed in this section. STRING, a part of the ELIXIR infrastructure, which is one of ELIXIR's Core Data Resources, is carried out here to analyse EPLIN's potential interacting partners across online databases (Figure 1.12). As shown in the Figure, most of the strong linking interacting partners are in line with research discussed above, including proteins that associate with AJs and the cytoskeleton such as VCL (Vinculin), CTNND1 (p120), CDH1 (E-cadherin), CTNNB1 (β -catenin), CTNNA1 (α -catenin) and PXN (paxillin). Interestingly, ATP6V1B1 (ATPase H⁺ Transporting V1 Subunit

B1), PTPLAD1 (HACD3), SIPA1L1 (Signal Induced Proliferation Associated 1 Like 1) and CLASP2 (Cytoplasmic Linker Associated Protein 2), however, their relationships with EPLIN have not yet been explored. Early interacting partners have been summarised in previous reviews focused on EPLIN (Collins et al. 2015; Wu 2017), such partners have been recapped and updated based on recent literature and are summarised in Table 1.4.

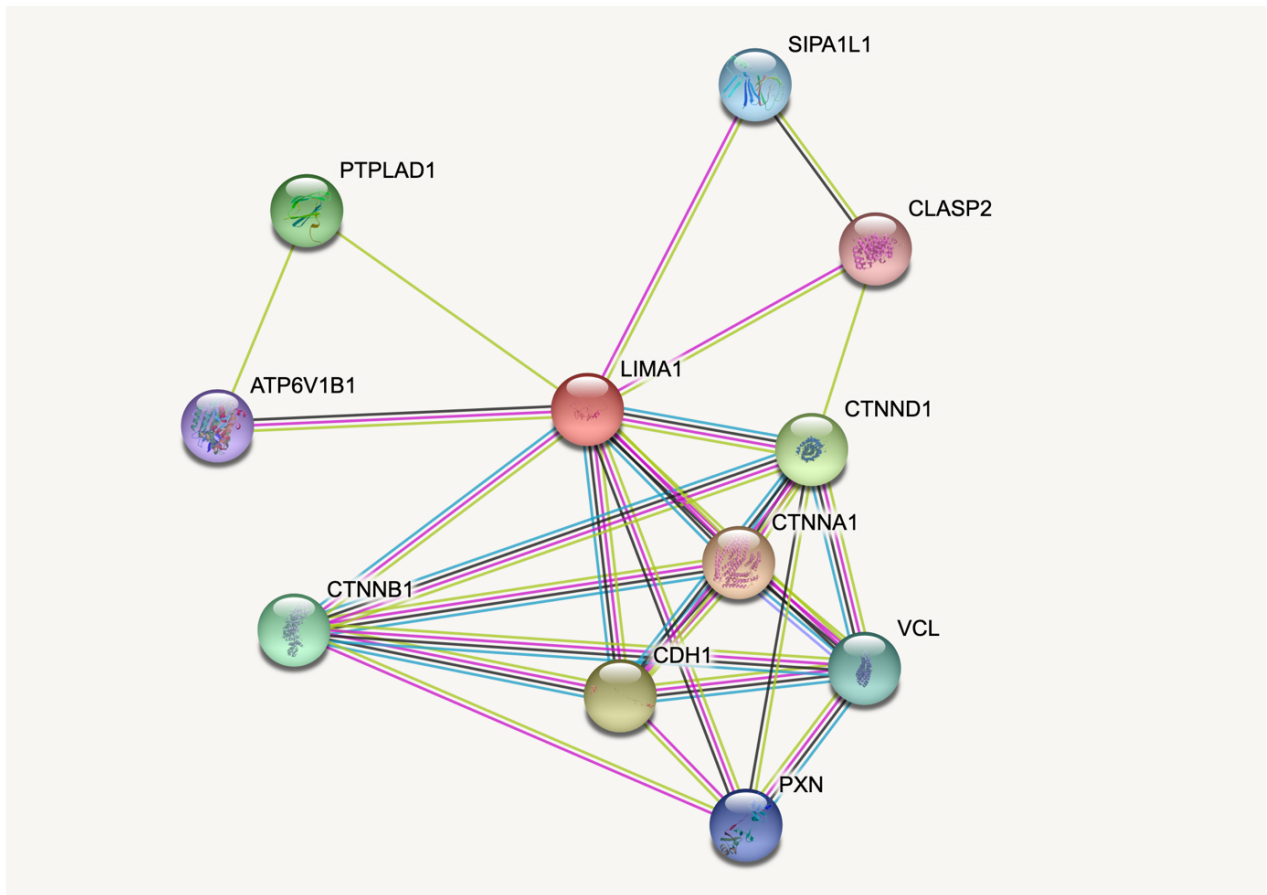


Figure 1.12 Network of Interacting Partners of EPLIN (LIMA1). Picture was collected from the STRING, ELI'IR's Core Data Resources. (<https://string-db.org/cgi/network.pl?taskId=6JcAAZ8RSD9m>)

Table 1.4 Interacting Partners of EPLIN

Interacting Partners	Bio-Significance	references
Actin	Actin is a foundational component of the cytoskeleton which is essential for maintaining the stabilization of epithelial cells. EPLIN can bind F-actin directly, with its two actin-binding sites, in order to regulate actin dynamics. EPLIN is essential for actin accumulation at cleavage furrows during cytokinesis in Hela cells.	(Maul and Chang 1999; Maul et al. 2003; Han et al. 2007; Chircop et al. 2009)
Arp2/3	EPLIN could inhibit the branching nucleation of F-actin via Arp2/3	(Abe and Takeichi 2008; Abu Taha and Schnittler 2014)
α -catenin	α -catenin and β -catenin are part of the cadherin- β -catenin- α -catenin complex, and the complex is also a part of the AJs. EPLIN was revealed to have connection with AJs by binding α -catenin, and the depletion of EPLIN leads to disassembly of the complex and the disorganisation of AJs	(Abe and Takeichi 2008; Zhang et al. 2011; Collins et al. 2015)
β -catenin		
E-cadherin	E-cadherin is an essential, functional part of AJs, they exist on the outside surface of the membrane and epithelial cells form connections with each other to form a belt. EPLIN's downregulation could lead to the disorganisation of AJs.	(Abe and Takeichi 2008)
ERK	ERK can phosphorylate EPLIN on ser 360, 602 and lead to disassembly of actin filaments.	(Han et al. 2007; Zhang et al. 2013)
hCDC14A	Responsible for dephosphorylating EPLIN on Ser362 and Ser604. Knocking down hCDC14A and EPLIN in HCT-16 cell lines leads to promotion of the EMT process.	(Chen et al. 2017)
Rab5	Mutation of Rab5 could downregulate expression of EPLIN in Ras-transformed cells around normal cells which leads to promotion of apical extrusion.	(Saitoh et al. 2017)
Plectin	Plectin was linked to EPLIN when RasV12 cells were surrounded by normal cells and they have positive correlation.	(Kadeer et al. 2017)
Cav-1	Knock-down of EPLIN could diminish the expression of Cav-1 in Ras-transformed cells when they were normal cells.	(Ohoka et al. 2015)
Paxillin	The expression and localization of Paxillin was found to be associated with the expression of EPLIN and they have a positive correction in surrounded Ras-transformed cells. Paxillin, plectin and EPLIN interact to regulate apical elimination. EPLIN and paxillin may form a complex to regulate actin dynamics. The expression of pPaxillin Y118 was downregulated in LNCaP cells, while pPaxillin Y31, total Paxillin and pPaxillin Y118 was increased in PC-3 cells upon EPLIN α over-expression.	(Sanders et al. 2010; Collins et al. 2018; Kasai et al. 2018)

Tubulin	Tubulin and EPLIN have a positive correlation in the apical elimination process. Acylation of tubulin is regulated by paxillin-plectin-EPLIN complex by regulating HDAC6.	(Kadeer et al. 2017; Kasai et al. 2018)
E-box-binding homeobox 1	The expression was observed to increase while EPLIN was downregulated, as an activator of EMT, it implicates a role between EPLIN and EMT.	(Zhang et al. 2011; Zhang et al. 2013)
p53	P53 was demonstrated to have a direct connection and a positive correlation with EPLIN.	(Ohashi et al. 2017)
DNp73	DNp73 could suppress the expression of EPLIN that results in activation of the AKT, STAT3 and IGF1R signalling pathways.	(Steder et al. 2013)
FAK	FAK was reported to have a positive correlation with EPLIN α in PC-3 & LNCaP cells, while the expression of total FAK and Src Y419 was increased in CA-HPV-10 cells by knocking down EPLIN.	(Collins et al. 2018)
Src	P-Src Y419 was depleted in PC-3 cells while p-Src Y530 was up-regulated when EPLIN α was overexpressed. The expression of Src Y419 was increased when EPLIN was knocked down in CA-HPV-10 cells.	(Collins et al. 2018)
Myosin-II and RhoA	Inhibition of EPLIN in Ras-transformed cells downregulated expression of myosin-II. EPLIN immunoprecipitated with activated myosin-II at the cleavage furrow in telophase during cytokinesis in Hela cells, and knocking down EPLIN led to downregulation of activated myosin-II and its regulator, RhoA at the cleavage furrow.	(Chircop et al. 2009; Ohoka et al. 2015)
Sept2 and Cdc42	Sept2 associates with EPLIN at the cleavage furrow during mitosis, whose silence caused reduction of Sept2 and its regulator, Cdc42 at the cleavage furrow.	(Chircop et al. 2009)
Arv1	Like actin, myosin and Sept2, Arv1 collocates at the cleavage furrow with EPLIN and EPLIN's reduction brought downregulation of Arv1	(Sundvold et al. 2016)
LUZP1	LUZP1 interacts with EPLIN to regulate ciliation.	(Goncalves et al. 2020)
NPC1L1	By interacting with NPC1L1 and MyosinVb, EPLIN has been shown to be a potential regulator of cholesterol absorption	(Zhang et al. 2018b)
miR-93-5-p	miR-93-5-p regulates EPLIN expression negatively by binding to its [33] 3'-UTR sequence and associates with migration and angiogenesis in HUVECs.	(Liang et al. 2017)

1.4.5 Role in cancer

As discussed earlier, the progression of cancer includes multiple essential phases. In general, cancer cells must gain abilities to grow uncontrollably, migrate and invade surrounding tissues to develop and metastasise. There are many underlying mechanisms of how cancers develop and metastasise and there is an urgent need to fully understand the process of metastasis, due to its significant implications on patient morbidity and mortality. EPLIN, an actin binding protein, coded by the LIMA 1 gene, was originally identified to be expressed in many epithelial cells including placenta, kidney, pancreas, prostate, ovary, spleen and heart. EPLIN α was initially reported to be downregulated in oral cancer cell lines when compared to normal human oral keratinocytes (NHOK) (8/8), prostate cancer cells (7/7), and breast cancer cells (5/6), while EPLIN β increased or remained the same (Maul and Chang 1999). Further studies subsequently revealed that EPLIN was depleted in a range of cancers including oral cancer (Chang et al. 1998; Maul and Chang 1999), breast cancer (Jiang et al. 2008), prostate cancer (Sanders et al. 2011; Zhang et al. 2011; Collins et al. 2018), colorectal cancer (Song et al. 2002; Lee et al. 2006; Zhang et al. 2011; Ohashi et al. 2017), SCCHN (Zhang et al. 2011), Lung cancer (Liu et al. 2012b), ovarian cancer (Liu et al. 2016) and oesophageal cancer (Liu et al. 2012a).

EPLIN has the ability to regulate actin dynamics by binding actin filaments at two actin binding sites on both sides of the LIM Domain (Maul et al. 2003). EPLIN also links to the Adherens Junction via the cadherin- β -catenin- α -catenin complex, by interaction with α -catenin, and the phosphorylation of EPLIN mediated by ERK would lead to the disassembly of the complex and the disorganisation of the adherens belt and membrane ruffling (Abe and Takeichi 2008). Furthermore, EPLIN was found to play an essential role in EMT, which is a vital step for epithelial cancer cells to gain the ability to metastasise, while the depletion of EPLIN would induce EMT. Similarly, EPLIN is known to interact with a number of significant cancer relevant pathways and proteins. EPLIN is a direct target of the p53 family (Ohashi et al. 2017), whereas DNp73 inhibits the function of the p53 family, causes downregulation of EPLIN and it induces EMT as well as membrane ruffles (Steder et al. 2013). Additionally, EPLIN can regulate the expression/phosphorylation states of Paxillin, FAK and Src differently in PC-3, LNCaP and CA-HPV-10 cells (Collins et al. 2018). Our lab has been working on the clinical significance and mechanism surrounding EPLIN for over a decade, which has helped to establish EPLIN as a tumour and metastasis suppressor, due to its ability to regulate cancer cells' growth, migration, invasion and metastases in breast cancer (Jiang et al. 2008), prostate cancer (Sanders et al. 2011; Collins et al. 2018), ovarian cancer (Liu et al. 2016) and oesophageal cancer (Liu et al. 2012a), and have correlation with

prognosis and survival rate in breast cancer (Jiang et al. 2008). All these findings, taken together with the wider literature, illustrate that EPLIN affects many functional activities of cancer cells, including cell motility, migration, invasion and cancer metastasis.

1.4.5.1 Breast cancer

When EPLIN was first reported in 1999, the study described its depletion in breast cancer (Maul and Chang 1999), providing an early implication that EPLIN might play a role in breast cancer. Subsequently, in 2008, Jiang *et al.*, revealed that the expression of EPLIN was not only downregulated in experimental breast cancer cell lines but also in breast cancer tissues, using a combination of IHC and qPCR normalized against CK19. In this study, through comparison of grade 2 & 3 tumour samples with grade 1, the expression of EPLIN was found to be significantly decreased and a similar trend was also observed among TNM staging (Jiang et al. 2008). Besides, study from Zhang *et al.*, (2011), analysed the ONCOMINE database, demonstrating that the expression of EPLIN was downregulated in lymph node metastases of breast cancer when compared to primary tumour tissue (Zhang et al. 2011). Ohashi et al. revealed that lower level of EPLIN has a linkage with mutant p53 when compared to wild type 53 expressing group by conducting TCGA data sets (Ohashi et al. 2017).

Jiang et al. further analysed the clinical cohort by using NPI (Nottingham Prognosis Index) as an indicator, EPLIN expression was significantly downregulated in poor prognosis groups compared to good prognosis groups. Furthermore, EPLIN was discovered to have a correlation with clinical outcome, with highest levels of EPLIN observed in patient samples who remained disease free, with the expression of EPLIN depleted in samples of local recurrence and those of patients who died of breast cancer. Additionally, Kaplan-Meier survival analysis demonstrated a positive correlation between EPLIN and overall survival (Jiang et al. 2008). Another study also supports these early findings, reporting lower levels of EPLIN are related to poor survival rates (Ohashi et al. 2017).

The study by Jiang *et al.*, (2008), went onto further analyse the cellular impact by overexpressing EPLIN α in MDA-MB-231 cells, which originally displayed a strong ability to invade *in vitro* and in an athymic nude mouse model. Following overexpression, the invasiveness and growth were distinctly reduced in transfected MDA-MB-231 cells and they also grew slower than control cells. Moreover, proliferation of tumour in the athymic nude mouse model was also repressed after overexpressing EPLIN α . The impact of EPLIN α on migration was also explored using an Electric Cell Impedance Sensing (ECIS) assay which demonstrated that MDA-MB-231 cells, that overexpressed EPLIN α , had a weaker resistance

and capacitance than wild type and control cells following wounding and recovery, which was indicative of reduced migratory abilities. This attenuation, caused by overexpressing EPLIN α , was reversed after the addition of an ERK inhibitor (Jiang et al. 2008). Furthermore, following knock down of EPLIN in MCF-7 cells, a wound-healing assay and Boyden chamber assay revealed that the invasive and migratory ability of MCF-7 cells was increased (Zhang et al. 2011). These findings implicate that reduced expression of EPLIN can enhance cell motility and invasion in breast cancer cells and that it plays a role in determining clinical outcome and metastasis, highlighting EPLIN as a potential novel clinical therapeutic.

1.4.5.2 Prostate cancer

EPLIN was found to be downregulated in multiple prostate cancer cell lines and tissues (Maul and Chang 1999; Chen et al. 2000; Sanders et al. 2011; Zhang et al. 2011; Steder et al. 2013; Collins et al. 2018). Sanders *et al.*, (2011), revealed that EPLIN was downregulated in clinical tissues in a small cohort of prostate cancer patients, when compared to normal tissue by conducting IHC staining (Sanders et al. 2011). A similar trend could be seen in tissue microarrays (TMA) and Gene Expression Omnibus (GEO) datasets (Zhang et al. 2011; Collins et al. 2018). Furthermore, analysis of the ONCOMINE database demonstrated that the depletion of EPLIN could be seen in the prostate cancer tissues with lymph node metastasis, compared to paired primary tumour tissues (Zhang et al. 2011). In addition, high levels of TP73 that encodes DNp73 and low levels of EPLIN were observed in metastatic samples when compared to primary prostate cancer (Steder et al. 2013).

Cell growth assays and athymic nude mouse tumour development models were used to examine the impact of EPLIN in tumour development *in vitro* and *in vivo*. Using PC-3 cells, overexpressing EPLIN α and its paired control cell lines, such experiments demonstrated that a negative impact on growth and tumour development was associated with higher EPLIN α expression. Furthermore, Matrigel invasion assays were conducted to illustrate EPLIN α could negatively impact cellular invasion through Matrigel (Sanders et al. 2011; Collins et al. 2018). Similarly, wound healing assays demonstrated that EPLIN α over-expressed PC-3 cells migrated significantly slower than in the control set (Collins et al. 2018). As highlighted previously, Collins *et al.*, (2018), implicated a potential relationship between EPLIN α and FAK /Src, which could alter expression or phospho-expression patterns, though this showed some cell line specificity (Collins et al. 2018). To explore this relationship at the functional level, the authors went on to conduct invasion and wound healing assays, in both EPLIN α over-expression and EPLIN knockdown models, in the presence of inhibitors to FAK and Src. Such work demonstrated a number of differential effects of both FAK inhibitor and the

src inhibitor dasatinib, on migration and invasion rates of control cell lines, compared to the EPLIN manipulated lines, further suggesting links between these molecules, though variations were observed between cell lines (Collins et al. 2018). Thus, the features of EPLIN's impact on PC-3, LNCaP and CA-HPV-10 cells were consistent with the findings relating to breast cancer from Jiang *et al.*, (Jiang et al. 2008), overexpressed EPLIN α could induce downregulation of invasion, migration and growth of PC-3 cells while cellular invasion and migration were up-regulated in CA-HPV-10 when EPLIN was knocked down. These implicate a possible role as a regulator of metastasis, potentially acting through links with Src and FAK in prostate cancer.

Work by Zhang *et al.*, (2011), establishing epithelial like and mesenchymal like cell model systems, has proven vital in establishing EPLIN's role in EMT and prostate cancer (Zhang et al. 2011). In this key study, epithelial type-ARCaP (Androgen refractory cancer of the prostate), (ARCaP_E) and mesenchymal type- ARCaP (ARCaP_M), were used to demonstrate EPLIN's importance in EMT. Downregulation of EPLIN in ARCaP_E was shown to have divisive influences on genes related to EMT and metastasis of prostate cancer, such as the up-regulation of zinc-finger E-box-binding homeobox 1, cAMP-responsive element-binding protein, myeloid cell leukemia-1, MMP-27 and CD44^{high}/CD24^{negative} marker profile ratio and depletion of Krueppel-like factor 5. Western blotting revealed the downregulation of both isoforms of EPLIN in ARCaP_M, compared to ARCaP_E where EPLIN was substantially expressed. Similarly, IHC analysis illustrated a similar pattern in athymic nude mice. A wound-healing assay was also undertaken which suggested that the depletion of EPLIN could lead to enhancement of migration/invasion in ARCaP_E, LNCaP and PC3 cells. Further experiments demonstrated that depletion of EPLIN in prostate cancer cells could also induce downregulation of E-cadherin on the cellular membrane, disorganisation of AJs, actin remodelling and membrane ruffles, which were consistent with the function EPLIN discussed above. Interestingly, inhibition of EPLIN resulted in increased chemotherapeutic resistance to docetaxel and doxorubicin.

In summary, EPLIN has been shown on many occasions to negatively regulate growth, migration and invasion in prostate cancer cells and is strongly implicated in EMT. Taken together with its altered expression, it appears to play an essential role in the progression of prostate cancer, especially metastasis.

1.4.5.3 Melanoma, oesophageal cancer, ovarian cancer, pulmonary cancer & SCCHN

As discussed in section 1.3.4.2, invasive melanoma cells that express DNp73, or forced expression of DNp73 in melanoma cells and mice models, leads to depletion of EPLIN and results in activation of AKT and STAT3 signalling pathways in company with activated IGF1R (Steder et al. 2013). Steder *et al.*, (2013), also reported that low levels of both isoforms of EPLIN in melanoma samples are related to deeper Breslow depth (>4 mm) when compared to high levels of EPLIN (<1 mm). Levels of EPLIN and DNp73 correlate with metastatic melanoma samples, when compared to primary ones, with upregulated expression of TP73, which produces DNp73, and downregulation of EPLIN, observed in metastatic melanoma samples, when compared to primary samples. Boyden chamber assays were performed in cell models that either knocked down or overexpressed EPLIN. Invasiveness was inhibited following forced expression of EPLIN, while reverse influences were noticed when EPLIN was silenced, compared to their mock models respectively (Steder et al. 2013).

Liu *et al.*, (2012a), has reported that EPLIN was decreased in tumour tissues of oesophageal cancer and pulmonary cancer, when compared to normal tissues, by conducting qPCR to analyse EPLIN expression in clinical cohorts of both cancers. Importantly, significant depletion of EPLIN in oesophageal cancer patient samples was observed in TNM4 compared to TNM2, N0 compared to N1 and patients who died compared to disease free patient groups (Liu et al. 2012a). In pulmonary cancer, EPLIN was expressed at a higher level in squamous pulmonary & adenocarcinoma than in small cell cancers and other types of lung cancer such as carcinoid in pulmonary cancer tissues. EPLIN was also found to be downregulated in TNM2 & TNM3, N1 & N2 and locally advanced cancers, with vessel cancerous embolus when compared to TNM1, N0 and primary cancer groups respectively (Liu et al. 2012b). Low levels of EPLIN were found to be related to poor overall survival rates (Ohashi et al. 2017). Additionally, analysis of the ONCOMINE database demonstrated EPLIN to have a negative correlation with lymph node metastasis, in squamous cell carcinoma of head and neck (SCCH) (Zhang et al. 2011).

Meanwhile, by overexpressing EPLIN α in an oesophageal cancer cell line, KYSE150 and a pulmonary cancer cell line, SKMES-1, growth assay, invasion assay, matrix adhesion assay and ECIS were performed to reveal that EPLIN α over-expressed lung cancer cells had a negative correlation with growth and motility, while EPLIN α overexpressed oesophageal cancer cells also displayed reduced growth and invasion but did not display any significant impacts on cell matrix adhesion *in vitro* (Liu et al. 2012a,b). Furthermore, Liu *et al.*, (2016),

investigated the relationship between EPLIN α and ovarian cancer, by knocking down the expression of EPLIN in two epithelial ovarian cancer (EOC) cell lines, SKOV3 and COV504. A growth assay revealed that the growth rate was enhanced at day 3 and day 5, with adhesion and invasion assays demonstrating a greater rate of EOC cellular attachment to Matrigel and enhanced invasion through Matrigel respectively. Moreover, wound-healing assays and ECIS assays were carried out to further demonstrate an enhanced migratory capacity of EOC cells when EPLIN was targeted (Liu et al. 2016).

In summary, the role of EPLIN in Melanoma, Oesophageal Cancer, Ovarian Cancer, Pulmonary Cancer & SCCHN appears to be in keeping largely with its role in prostate and breast cancer, contributing to the notion that it is generally lost in cancer progression and is associated with pro-metastatic traits.

1.4.5.4 Gastric cancer

Recent research by our laboratory elaborates an impact of EPLIN on chemotherapeutic resistance of gastric cancer. By analysing a clinical cohort, which includes 320 gastric cancer patients and 175 healthy individuals, and another clinical cohort containing gastric cancer patients with neoadjuvant chemotherapy (NAC) and peritumoural tissues (158 samples), Gong *et al.*, (2021), reported that samples in T1&T2 groups expressed higher EPLIN compared to T3&T4 groups, in both cohorts, which indicates that EPLIN expression is correlated with tumour invasive depth and metastasis. Intriguingly, patients who are responsive to NAC, which is a key treatment to narrow tumour size for patients in aggressive stages before surgery, have been reported to have higher expression of EPLIN than those who are not responsive to NAC. Moreover, by analysing these two cohorts, patients with higher EPLIN expression have longer Disease-Free Survival (DFS) than those with lower EPLIN expression. Multivariate analysis was performed to elucidate that EPLIN is a significant prognostic indicator for DFS and Overall Survival (OS), while univariate analysis also shows EPLIN is valuable for DFS. Results from datasets from Kaplan-Meier plotter also agree with the finding, among the two clinical cohorts, that patients with higher expression of EPLIN have significant longer PPS, OS and FP(Gong 2021). Hence, EPLIN has been shown to be involved in gastric cancer development, with low levels of EPLIN possibly being responsible for deeper invasion, short survival and worse reaction to NAC.

1.4.5.5 Colorectal cancer

CRC has the 4th greatest incidence rate, is the 2nd most common cause of cancer related death in UK and presents a social health concern, due to its significant patient morbidity and

mortality. The poor patient prognosis is largely attributed to its metastatic ability to disseminate cancer cells to secondary locations. EPLIN has been established as a tumour suppressor in multiple cancer cells though Unexpectedly, only a few reports link EPLIN to colorectal cancer. The findings so far have been based on gene transcript analyses and tend to be inconclusive.

By conducting a cDNA microarray, in a set of micro-dissected cells from formalin-fixed, paraffin-embedded colon tissues, the expression of EPLIN was observed to be depleted in the normal-adenoma-carcinoma sequence, which was a similar trend to some of the other tumour suppressor genes also detected (Lee et al. 2006). Another study discovered the potential role of EPLIN in metastasis in CRC. Zhang *et al.* (2011), ran a search in the ONCOMINE database and found that the expression of EPLIN transcript was downregulated in metastatic CRC, when compared to primary tumours and a further IHC assay revealed the similar disposition in lymph node metastasis from CRC compared to paired primary tumours (Zhang et al. 2011). Chen *et al.*, (2017), also reported that EPLIN mRNA was decreased in colorectal carcinoma when compared with normal colon tissue, by analysing the ONCOMINE database, and found that it has a positive correlation with prognosis in CRC patients, by analysing Genomics Analysis and Visualization Platform (Chen et al. 2017). Furthermore, Ohashi *et al.*, (2017), conducted datasets from The Cancer Genome Atlas (TCGA) and their analysis revealed a similar trend, that EPLIN's expression is downregulated in CRC when compared with normal groups, with low levels of EPLIN related to poor clinical outcomes, which is consistent with discussed studies. Also, expression of EPLIN diminishes in CRC expressing mutant p53, when compared to wild type p53 group(Ohashi et al. 2017). While another study by Steder *et al.*, (2013), also shows that low levels of EPLIN transcript, combined with high levels of DNp73, are related to CRC metastasis (Steder et al. 2013). Taken together, EPLIN has been demonstrated to be a potential protective regulator of incidence and development of CRC, and activities of p53 and DNp73 and signalling pathways they involve may be the potential driver mechanism behind it. Further studies are needed to explore its functional implication and possible related mechanisms.

1.5 Hypothesis and Aims

CRC is the 4th most common cancer type in the UK and one of the main contributors to cancer death. Despite the stable overall incidence rate and decreasing mortality rate over decades, the increasing incidence rate among the 25-49 age group and serious mortality rates among patients who suffered from advanced CRC, contribute to the huge burden to

individual health and society. CRC develops from small adenoma to malignant tumour through a number of carcinogenetic pathological pathways (adenoma-carcinoma sequence, serrated pathway, and inflammatory pathway) and molecular pathways, including CIN, MSI and CIMP. Multiple risk factors influence CRC progression such as smoking, lack of physical activities, obesity, diet, etc. Over 90% of cases are sporadic while around 5% are hereditary.

The development of CRC can be summarized into four phases, initiation, promotion, progression and dissemination. Mutation of a number of tumour supporters or suppressors participate in these processes, such as APC, the guard gene of carcinogenesis; p53, one of the most classic tumour inhibitors; KRAS & BRAF which have been reported to be frequently mutated. Given poor clinical outcomes associated with advanced CRC, we are interested in metastatic progression within CRC. Mutation of genes contribute to the activation of several signalling pathways including the Wnt/ β -catenin pathway, EGFR/PI3K pathways, the notch pathway and the TGF- β pathway and result in promoting proliferation, migration and invasiveness of CRC cells and apoptosis of normal epithelial population. As well as, these gene mutations, signalling pathways and components from the TME trigger the progression of EMT which allows epithelial cells to lose their epithelial like properties and gain mesenchymal characteristic, giving them the potential to invade. Hence, dissemination of CRC occurs. Tumour cells disseminate themselves to surrounding tissues and spread to distant organs (liver, bone) and re-establish via circulatory systems (blood vessels or lymphatic vessels) by metastatic cascades. Essential cascades in CRC include lymphatic spread, hematogenous spread and peritoneal dissemination.

Diagnostic methods for CRC, especially screening programmes, have been successful which contributes to early diagnosis of CRC and reduced mortality rates. Therapeutic methods, including chemotherapy, targeted therapy, immunotherapy, radiotherapy and surgery, are rapidly developing and help promote prognosis. Despite these developing treatments and diagnostic methods, poor clinical outcomes have been reported in late stage of CRC patients. Moreover, increasing evidence points out that resistance against first-line 5-FU based chemotherapy attributes to bio factors, such as LncRNA NEAT1 and PI3KCA. Hence, it is urgent to identify novel biomarkers for CRC and shed light into novel therapeutic strategies.

Pancreatic cancer, a GI cancer as CRC, ranks as the 10th most common cancer type in the UK, with increasing incidence rates and unsatisfied 5-year survival rate, making it one of the most dreadful and heaviest health burden. Similar to CRC, a large portion of pancreatic cancer patients are diagnosed at more aggressive stages, which leads to worse clinical

outcomes. Development of pancreatic cancer links to mutation or dysregulation of oncogenes and tumour inhibiting genes, in which abnormal alterations of SMAD4, KRAS, p53 and CDKN2A have been reported to be the hallmarks of PDAC. Similar to CRC, mutation of SMAD4, KRAS and p53 lead to promotion of EMT and more aggressive cancer developments, which frequently leads to poorer prognosis for pancreatic cancer patients, as discussed above. Meanwhile, activation of certain signalling pathways promotes its development and a deterioration in clinical outcomes as well, such as DNA repair, cell cycle, RNA processing, ROBO SLIT, KRAS, TGF β , WNT, SWI/SNF and Chromatin signalling pathways.

Apart from surgery and immunotherapy, chemotherapy is one of the most essential and widest studied treatments in pancreatic cancer. 5-FU, Gemcitabine, paclitaxel, FOLFIRINOX (folinic acid, 5-FU, irinotecan and oxaliplatin), leucovorin and OFF (oxaliplatin, folinic acid/leucovorin and 5-FU) are the most widely adopted chemotherapeutic strategies. Sadly, as one of the most essential reagents, gemcitabine has been reported to be involved in drug resistance with a largely unknown mechanism. Hence, as well as CRC, pancreatic cancer needed wider research to identify novel markers and potential therapeutic strategies that lead patients to a brighter and better future.

Since its initial discovery, EPLIN has been established as playing key roles in maintaining cellular junctions and actin dynamics. As such, it has implications in regulating many cellular traits altered in cancer progression including proliferation, migration and invasiveness. In keeping with this, EPLIN is found to be dysregulated in a number of human cancers including CRC and its loss is associated with a more pro-metastatic cellular phenotype and EMT, leading to its establishment as a metastasis suppressor. Multiple interacting partners have been searched for and established as contributing to EPLIN's role in regulating these important processes. For example, p53 has been reported to be an upstream player of EPLIN. Mutant p53 leads to downregulation of EPLIN and more aggressive invasion in breast cancer cells. Given that, within an analysis of TCGA database of CRC, EPLIN is correlated with mutant p53, an interesting question about the impact of p53 and EPLIN on cellular functions in CRC has been asked. In clinical aspect, work by our laboratory and other researchers has elucidated that downregulation of EPLIN has been observed in a number of tumours including CRC and is indicative of poor prognosis and metastasis in cancers such as breast cancer and prostate cancer. Intriguingly, Zhang *et al.*, (2011), demonstrate that downregulation of EPLIN leads to greater resistance against docetaxel (DTX) and doxorubicin, mainstream chemotherapeutic drugs in a prostate cancer cell model, which provides early evidence of a potential role of EPLIN in chemotherapy. Recent studies

by our laboratory also supports that EPLIN is a potential influencer for chemotherapy in gastric cancer.

As discussed above, due to the significance of CRC and pancreatic cancer, and the implications of metastatic dissemination of this disease and chemotherapeutic resistance, investigation into novel factors that may predict, or be used as potential therapeutic strategies, to combat metastatic disease are vital. Since EPLIN plays a role in inhibiting tumour progression in a number of cancers and EPLIN has been involved in cellular functions in multiple types of cancer, it has also been implicated to be a potential influencer against chemotherapeutic resistance in prostate cancer and gastric cancer. We draw an intriguing question whether EPLIN is also involved in chemotherapeutic resistance in CRC and pancreatic cancer. Although research has reported a possible linkage between CRC and EPLIN, by analysing available public databases and IHC, there is little effort focused on the cellular impact of EPLIN in CRC cells and the associated mechanisms related to EPLIN's effects in CRC cells. Thus, we are interested in investigating the relationship between CRC/pancreatic cancer and EPLIN.

We hypothesise that EPLIN expression, as with other cancers, will be reduced in CRC and that loss of EPLIN will enhance aggressive cellular traits and has influences on metastasis and chemotherapy of CRC.

The aims of the current study were to explore not only the clinical and functional importance of EPLIN in CRC and pancreatic cancer, but also EPLIN's impact on chemotherapy. Additionally, the study aimed to investigate potential interacting partners related to EPLIN in CRC and the possible mechanism behind it.

Specific project aims were:

- 1) To examine EPLIN expression in clinical cohorts and TMA of CRC cancer and its association with patient clinicopathological information and prognosis.
- 2) To generate EPLIN manipulated cell lines and characterise the effects of EPLIN dysregulation on cellular traits associated with cancer development and metastasis.
- 3) To assess EPLIN's impact on popular chemotherapeutic drugs of CRC in our established CRC cell models.
- 4) To explore underlying mechanisms and potential interacting partners that may account for EPLIN's actions in CRC cell models.

5) To investigate the significance of EPLIN and its associated mechanistic pathways and partners in the key traits identified in the earlier chapters as well as the clinical relevance of such interactions.

6) As an extension of EPLIN's studies in CRC, we also drew attention to another critical GI cancer type, pancreatic cancer, and its clinical relevance with EPLIN, as well as implication of EPLIN on chemotherapeutic resistance in pancreatic cancer.

Chapter2

Materials & Methods

2.1 Materials

2.1.1 Cell lines

Four cell lines from human colorectal cancer, RKO, CaCo2, HT115 and HRT18, three cell lines from human pancreatic cancer, PANC1, MIAPaCa2 and AsPC1 were used in this study. All cells were purchased from American Type Culture Collection (ATCC, Rockville, MD, USA) (LGC Standard, ATCC UK agent), and kept in liquid nitrogen preservation at low passage. Information regarding these cell lines is detailed in Table 2.1. All cell stocks were verified as mycoplasma free using a GENEFLOW kit (Geneflow Ltd., Litchfield, UK).

Table 2.1. Detailed Information of Colorectal Cancer Cell Lines (top) and Pancreatic cancer cell lines (Bottom) used in the present study.

	RKO	HRT-18	HT-115	CaCo2
Organism	Homo sapiens, human	Homo sapiens, human	Homo sapiens, human	Homo sapiens, human
Tissue	Colon	Colon	Colon	Colon
Morphology	Epithelial	Epithelial	Epithelial	Epithelial
Culture Properties	Adherent	Adherent	Adherent	Adherent
Disease	Carcinoma	Ileocecal colorectal adenocarcinoma	colorectal adenocarcinoma	Colorectal adenocarcinoma
Age	Unknown	67	Unknown	72
Gender	Unknown	Male	Male	Male
Mutation	No	No	Unknown	No

	Panc-1	MIAPaca-2	AsPC-1
Organism	Homo sapiens, human	Homo sapiens, human	Homo sapiens, human
Tissue	Pancreas; Duct	Pancreas	Pancreas
Morphology	Epithelial	Epithelial	Epithelial
Culture Properties	Adherent	Adherent	Adherent
Disease	Pancreatic epithelioid carcinoma	Pancreatic carcinoma	Pancreatic adenocarcinoma
Age	56	65	62
Gender	Male	Male	Female
Mutation	unknown	KRAS	Unknown

2.1.2 General cell culture plastics, hardware and software

General cell culture plastics, hardware and software used in this study and their suppliers are given below in Table 2.2.

Table 2.2 General materials and suppliers used in this study

Hardware/Software	Supplier
25cm ² and 75cm ² Flasks	Greiner Bio-One Ltd., Gloucestershire, UK
Universal Tubes	Fisher Scientific UK, Leicestershire, UK
Eppendorf Tubes	Greiner Bio-One Ltd., Gloucestershire, UK
Safety Bio Cabinet	Wolf Laboratories York, UK
Image J	Downloaded from https://imagej.nih.gov/ij
6-well plates	Greiner Bio-One Ltd., Gloucestershire, UK
24-well plates	Greiner Bio-One Ltd., Gloucestershire, UK
96-well plates	Greiner Bio-One Ltd., Gloucestershire, UK
TC translucent inserts for 24-wells plate with 8.0µm pores	Greiner Bio-One Ltd., Gloucestershire, UK
Leica DM IRB Microscope	Leica Microsystems (UK) Ltd., Milton Keynes, UK
Neubauer Haemocytometer	Fisher Scientific UK, Leicestershire, UK
Counting Chamber	
Incubator	Wolf Laboratories, York, UK
Implen nanophotometer	Geneflow Ltd, Litchfield, UK
LT4500 plate reader	Wolf Laboratories, York, UK
SimpliAmpTherm Cycler	Fisher Scientific UK, Leicestershire, UK
Techne, Hybridiser HB-1D drying oven	Wolf laboratories, York, UK
CRYO.STM tubes	Greiner Bio-One, Germany
0.2 µm mini-start filter	Sigma-Aldrich, Pooled, Dorset, UK
MicroAmp Fast Optical 96-Well Reaction Plate with Barcode (0.1ml)	Thermo Fisher Scientific, Waltham, MA, USA
AccuSpin Micro 17R	Fisher Scientific UK, Leicestershire, UK
Step One Plus Real Time PCR System	Thermo Fisher Scientific, Waltham, MA, USA
GenePluserXcell™ electroporation system	Bio-Rad Laboratories, Hercules, CA, USA
G-BOX	Syngene, Cambridge, UK
Electroporation cuvette	Geneflow Ltd, Litchfield, UK
Electrophoresis cassette	Scie-Plas Ltd., Cambridge, UK
Syngene U: Genius 3 Fluorescence UV Transilluminator	Synoptics Ltd., Cambridge, UK
Consort EV243 electrophoresis power supply	Sigma-Aldrich, Pooled, Dorset, UK
Optical seal	PrimerDesign, Southampton, UK
Immobilon P PVDF membrane	Merck Millipore, Hertfordshire, UK
Cryostat	Leica DMB, Milton Keynes, UK
ECIS Ztheta instrument	(Applied Biophysics Ltd, Troy, New Jersey, USA)
GloMax®-Multi Detection System	(Promega, Southampton, UK)
LEICA DFC3000 G microscope with Kubler CODIX system	(Leica DMB, Milton Keynes, UK).

2.1.3 General compounds

General compounds used in this study are listed in Table 2.3 below.

Table 2.3 General compounds included in this study

Material & Reagent	Supplier
Agarose	Melford Laboratories Ltd, Suffolk, UK
Bio-RadDC Protein Assay Reagent A	Bio-Rad Laboratories, Hercules, CA, USA
Bio-RadDC Protein Assay Reagent B	Bio-Rad Laboratories, Hercules, CA, USA
Bio-RadDC Protein Assay Reagent S	Bio-Rad Laboratories, Hercules, CA, USA
1-Bromo-3-chloropropane	Sigma-Aldrich Co, Poole, Dorset, UK
3,3'-Diaminobenzidine (DAB)	Sigma-Aldrich Co, Poole, Dorset, UK
DEPC (Diethylpyrocarbonate)	Sigma-Aldrich Co, Poole, Dorset, UK
DMEM/Ham's F12 with L-Glutamine medium	Sigma-Aldrich Co, Poole, Dorset, UK
RPMI-1640 Medium With L-glutamine and sodium	Sigma-Aldrich Co, Poole, Dorset, UK
Ethanol	Fisher Scientific, Leicestershire, UK
Sybrsafe DNA stain	Fisher Scientific, Leicestershire, UK
Isopropanol	Sigma-Aldrich Co, Poole, Dorset, UK
Methanol	Fisher Scientific, Leicestershire, UK
Antibiotic antimycotic solution (100x)	Sigma-Aldrich Co, Poole, Dorset, UK
TRI Reagent	Sigma-Aldrich Co, Poole, Dorset, UK
Trypsin EDTA	Sigma-Aldrich Co, Poole, Dorset, UK
Tween 20	Melford Laboratories Ltd, Suffolk, UK
10X PBS	Sigma-Aldrich Co, Poole, Dorset, UK
10X running buffer (tris – glycine-sds buffer)	Sigma-Aldrich Co, Poole, Dorset, UK
10X transfer buffer (Tris glycine buffer)	Sigma-Aldrich Co, Poole, Dorset, UK
VECTASTAIN® ABC Kit	Vector Laboratories Inc, Burlingame, CA, USA
10x TBE	Sigma-Aldrich Co, Poole, Dorset, UK
Foetal Calf Serum (FCS)	Sigma-Aldrich Co, Poole, Dorset, UK
Dimethyl sulfoxide (DMSO)	Sigma-Aldrich Co, Poole, Dorset, UK
PureYield™ Plasmid Maxiprep System	Promega, Southampton, UK
Plasmid Transfection Reagent	Santa Cruz Biotechnology, Inc., Dallas, Texas, USA
Transfection Medium	Santa Cruz Biotechnology, Inc., Dallas, Texas, USA
Puromycin	Fisher Scientific, Leicestershire, UK
Thiazolyl Blue Tetrazolium Bromide	Sigma-Aldrich Co, Poole, Dorset, UK
Matrigel	BD Biosciences, Oxford, UK
GoScript™ Reaction Buffer, Oligo (dT)	Promega, Southampton, UK

GoScript™ Enzyme Mix	Promega, Southampton, UK
10x Tris-Boric-Acid (TBE) electrophoresis buffer	Sigma-Aldrich Co, Poole, Dorset, UK
2-propanol	Fisher Scientific, Leicestershire, UK
PCR GoTaq Green master mix	Promega, Southampton, UK
PCR Ranger PCR ladder	Geneflow Ltd., Litchfield, UK
AmplifilourUniprimer™ Universal system	Intergen company, New York, USA
FAST 2x qPCR Master Mix	PrimerDesign, Southampton, UK
Bovine serum albumin (BSA)	Fisher Scientific, Leicestershire, UK
2x laemmli buffer	Sigma-Aldrich Co, Poole, Dorset, UK
BLUeyePrestained Protein Ladder	Geneflow Ltd., Litchfield, UK
10x Tris buffered saline	Sigma-Aldrich Co, Poole, Dorset, UK
EZ-ECL solution A	Geneflow Ltd., Litchfield, UK
EZ-ECL solution B	Geneflow Ltd., Litchfield, UK
N,N,N',N'-Tetramethyl- ethylenediamine (TEMED)	Sigma-Aldrich Co, Poole, Dorset, UK
Tris (hydroxymethyl) aminomethane	Melford Laboratories Ltd, Suffolk, UK
Sodium dodecyl sulphate (SDS)	Melford Laboratories Ltd, Suffolk, UK
Crystal violet solution	Sigma-Aldrich Co, Poole, Dorset, UK
Ammonium persulfate	Sigma-Aldrich Co, Poole, Dorset, UK
30% Acrylamide/Bis-Acrylamide solution	Sigma-Aldrich Co, Poole, Dorset, UK
Horse serum	Sigma-Aldrich, Pooled, Dorset, UK
Gill's Haematoxylin	Vector Laboratories Inc, Burlingame, CA, USA
Xylene	Fisher Scientific, Leicestershire, UK
Rabbit anti-mouse (whole molecule) IgG peroxidase conjugate	Sigma-Aldrich, Pooled, Dorset, UK
Vectors (ORF of Stuffer300)	VectorBuilder Inc., Chicago, IL, USA
Vectors (ORF of EPLIN α)	VectorBuilder Inc., Chicago, IL, USA

2.1.4 Primers

Primers used in this study were designed by the Beacon Design Programme (Biosoft International, Palo Alto, California, USA) or Primer BLAST, and synthesized by Sigma Genesis (Poole, Dorset, UK). Primer details used in RT-PCR and qPCR for this study are listed below in Table 2.4.

Table 2.4 Details of primers used in this study. (Red text indicates the Z – sequence of the qPCR primers)

Name	Sequence	Predicted Product Size
EPLIN F8	TCAAACCTAAGATTCTCCGGG	878 bp
EPLIN R8	CAATAGGGGCATCTTCTACC	
EPLIN β F3	CATTTAATAGACGGCAATGGA	626 bp
EPLIN β R3	CCGGAGAATCTTAGTTTGAGT	
GAPDH F8	GGCTGCTTTTAACTCTGGTA	470 bp
GAPDH R8	GACTGTGGTCATGAGTCCTT	
EPLIN F1	AAGCAAAAATGAAAACGAAG	112 bp
EPLIN zR1	ACTGAACCTGACCGTACAGACACCCACCTTAGCAATAG	
GAPDHF1	AAGGTCATCCATGACAACCTT	1285 bp
GAPDH zR1	ACTGAACCTGACCGTACAGCCATCCACAGTCTTCTG	
Her1 F1	GACCTCCATGCCTTTGAGAA	165 bp
Her1 zR1	ACTGAACCTGACCGTACAGCACAAATTTTTGTTTCCTGA	
Her2 F1	CCTCCTCGCCCTCTTG	103 bp
Her2 zR1	ACTGAACCTGACCGTACACATGTCCAGGTGGGTCT	
Her3 F1	CCCCACACCAAGTATCAGTA	80 bp
Her3 zR1	ACTGAACCTGACCGTACAACACAGGATGTTTGATCCAC	
Her4 F1	CTGCTGAGTTTTCAAGGATG	97 bp
Her4 zR1	ACTGAACCTGACCGTACA AACTTGCTGTCATTTGGACT	
HSP60 F10	TGTAGACCTTTTAGCCGATG	111 bp
HSP60 zR10	ACTGAACCTGACCGTACAACAGTCACACCATCTTTTCT	

Note: Sequence marked red is the Z-sequence added to the reverse primer for quantitative PCR analysis using the Ampliflor Technology and UniPrimer.

2.1.5 Antibodies

Primary and secondary antibodies used for western blotting and immunohistochemistry (IHC) are detailed below in Table 2.5.

Table 2.5 Antibodies used in the current study

Antibody name	Host species	Molecular weight	Final Concentration	Supplier and catalogue number
EPLIN	Mouse	90kDa / 110kDa	1:500	Santa Cruz Biotechnology Sc-136399
GAPDH	Mouse	37kDa	1:1000	Santa Cruz Biotechnology Sc-32233
HSP60	Mouse	60kDa	1:200	Santa Cruz Biotechnology Sc-59567
Neu/Her2/ErbB2	Mouse	185kDa	1:250	Santa Cruz Biotechnology Sc-33684
Rabbit anti-mouse (whole molecule) IgG peroxidase conjugate	Rabbit	Dependent on primary	1:1000	Sigma-Aldrich A5278

2.2 Cell culture

2.2.1 Preparation of chemical solutions used for cell culture

2.2.1.1 Cell Culture Medium

In this study, four colorectal cancer cell lines, RKO, HRT18, HT-115 and CaCo2 were cultured. RKO, HT-115 and CaCo2 cells were cultured in Dulbecco's Modified Eagle's medium (DMEM), supplemented with 10% heat inactivated foetal calf serum (FCS) (Sigma-Aldrich, Poole, Dorset, UK) and 1% of a 100X antibiotic mixture including penicillin, streptomycin and amphotericin B (Sigma-Aldrich, Pooled, Dorset, UK). HRT-18 cells were cultured in RPMI-1640 medium, which was also supplemented with 10% heat inactivated foetal calf serum (FCS) and antibiotics. Both mediums were stored at 4°C for up to one month. All pancreatic cancer cell lines were cultured in Dulbecco's Modified Eagle's medium (DMEM) supplemented with 10% FCS and antibiotics.

2.2.1.2 Phosphate-buffered saline (PBS)

Ten times stock PBS (Sigma) was dissolved in distilled water. Five hundred ml stock was added to 4500 ml distilled water to give 1x stock at pH 7.4. The final product was stored at room temperature after being autoclaved.

2.2.1.3 Trypsin EDTA

Ten times stock Trypsin EDTA solution was purchased from Sigma Aldrich and was diluted to 1x concentration in sterile PBS, aliquoted into universal tubes and stored at -20°C until required.

2.2.2 Culturing cells

Cell lines were cultured in either 25cm², 75cm² flasks (Greiner Bio One Ltd. Gloucestershire, UK) or 6, 24 or 96 well (Greiner Bio-One Ltd., Gloucestershire, UK) plates, dependent on experimental purpose. All cell lines were kept in an incubator at 37°C, 95% humidity and 5% CO₂.

Medium was changed based on the condition of cultured cell lines, including confluence and extent of cell death, in order to maintain healthy cell lines. Cells were washed with 5ml of PBS in order to remove dead cells after aspirating the medium with a sterile glass pipette. Aspirated PBS was then replenished with appropriate medium, either 5ml in 25cm² flasks, 15ml in 75 cm² flasks, 200µl in 96 wells plates, or 1ml in 6 wells plates.

Cells were maintained at a sub-confluent level and were routinely subjected to subculturing to maintain suitable levels as described in section 2.2.2.

2.2.3 Cell Detachment, passaging and cell counting

2.2.3.1 Cell detachment and passaging

Cells were detached from the flasks using trypsin/EDTA, prepared as described above. Excess cells were removed by treatment with trypsin/EDTA solution. In brief, after washing with PBS, various volumes of trypsin/EDTA solution (dependent on culturing flask size) were added to the flasks which were then placed in a 37°C incubator for 5-10 minutes (dependent on cell line), to allow the cells to detach. It is important to wash the cells with PBS in order to remove any residual serum that would subsequently inactivate the trypsin/EDTA. The 5ml cell suspension was then collected into a sterile universal container, topped up with medium to a total of 10ml and then centrifuged at 1,700 rpm for 8 minutes.

The supernatant was carefully aspirated and the resultant pellet resuspended in 3ml of medium. Dependent on future experiments or subculture, 1 ml of the cell suspension was added into a new 25cm² flask, while 2ml was added into a 75 cm² flask, with medium added to make the final volumes described above. The flasks were then returned to the incubator to allow cells to grow to sufficient numbers for future experiments.

2.2.3.2 Cell counting

Cells were detached from the flasks using trypsin/EDTA, as described above. The cell suspension was centrifuged and resuspended in a suitable volume of culture medium, as described above.

For cell counting, a 1mm x 1mm x 0.1mm Neubauer haemocytometer counting chamber was used. After attaching a cover slide onto the chamber, 10 µl of the cell suspension was added to the edge of the slide and, due to the capillary action, the suspension of cells was drawn under the cover slide. Four corners of nine squared areas of the haemocytometer were counted under a microscope under the x10 objective lens. The number of cells was calculated using the formula: number of cells /ml = (total number of cells in 4 counted corners/4) x 10⁴.

2.2.4 Storage of cells in liquid nitrogen and cell thawing

2.2.4.1 Storage of Cells in Liquid Nitrogen

Detachment of cells was undertaken as described in section 2.2.2. The pellet was re-suspended in a final volume of 6 ml solution, including medium containing 10% dimethyl sulfoxide (DMSO), at a density of 1×10^6 cells/ml after centrifugation.

Subsequently, 1 ml of solution was transferred into 5 pre-labelled CRYO.STM tubes (Greiner Bio-One, Gloucestershire, UK), which were then wrapped in tissue paper and frozen at -80°C . For long-termed storage, tubes were kept at -196°C in a liquid nitrogen tank.

2.2.4.2 Cell thawing

To defrost cells for further experiments, CRYO.STM tubes were removed from the liquid nitrogen tank and bathed in water at 37°C for a short period of time to thaw. Next, the cell suspension was transferred into a universal tube containing 10ml of pre-warmed medium, then centrifuged at 1,700 rpm for 8 minutes. Following this the medium was aspirated and the pellet resuspended in 5 ml of medium before being transferred to a flask to incubate for further experiments.

2.2.5 Transfection

2.2.5.1 Plasmid preparation and extraction

Two vectors, containing either the ORF of EPLIN α or a Stuffer300 control sequence, were purchased from VectorBuilder Inc. (Chicago, IL, USA) (Figure 2.1) as frozen bacterial stock and were used to inoculate a larger volume of LB broth containing selective ampicillin ($100\mu\text{g/ml}$), in accordance with the protocol for plasmid extraction.

A PureYield™ Plasmid Maxiprep System (Promega, Southampton, UK) was used to extract plasmid stocks in accordance with the manufacturers guidance. Briefly, 100-250ml solution of *E. coli* bacterial cells, carrying the plasmid, were cultured overnight and centrifuged at $3,000 \times g$ for 10 minutes at room temperature, in batches of 50ml universal tubes, before discarding the supernatant to leave bacterial pellets. The pellets were then resuspended in 12ml of Cell Resuspension Solution before 12ml of Cell Lysis Solution was added and mixed gently, through inversion, then incubated at room temperature for 3 minutes. Subsequently, 12 ml of Neutralization Solution was added to the solution and mixed through inversion for 10-15 times before centrifugation at $3,000 \times g$ for 30 minutes at room temperature to get a cleared solution for DNA purification.

The cleared solution was then transferred into a column stack (top: blue PureYield™ Clearing Column; bottom: white PureYield™ MaxiBinding Column) and connected to the vacuum before applying maximum vacuum. The solution moved through the column stack and DNA became bound to the membrane of the binding column. The membrane was washed with 5ml of Endotoxin Removal Wash (having initially added 5.5ml of isopropanol upon first use) and was drawn through the binding column, under vacuum, followed by a washing step with 20ml of Column Wash solution (having added 30ml of 95% ethanol upon first use) and drying of the membrane through application of the vacuum for 5 minutes.

Following this, the binding column was connected to an Eluator™ Device by placing a 1.5ml Eppendorf tube into the device and connecting to the vacuum. One millilitre of Nuclease-Free Water was added and maximum vacuum applied for 1 minute. Following this, the DNA solution was collected in the microcentrifuge tube and was quantified using an Implen nanophotometer (Geneflow Ltd, Litchfield, UK), before storing at -20°C until further use.

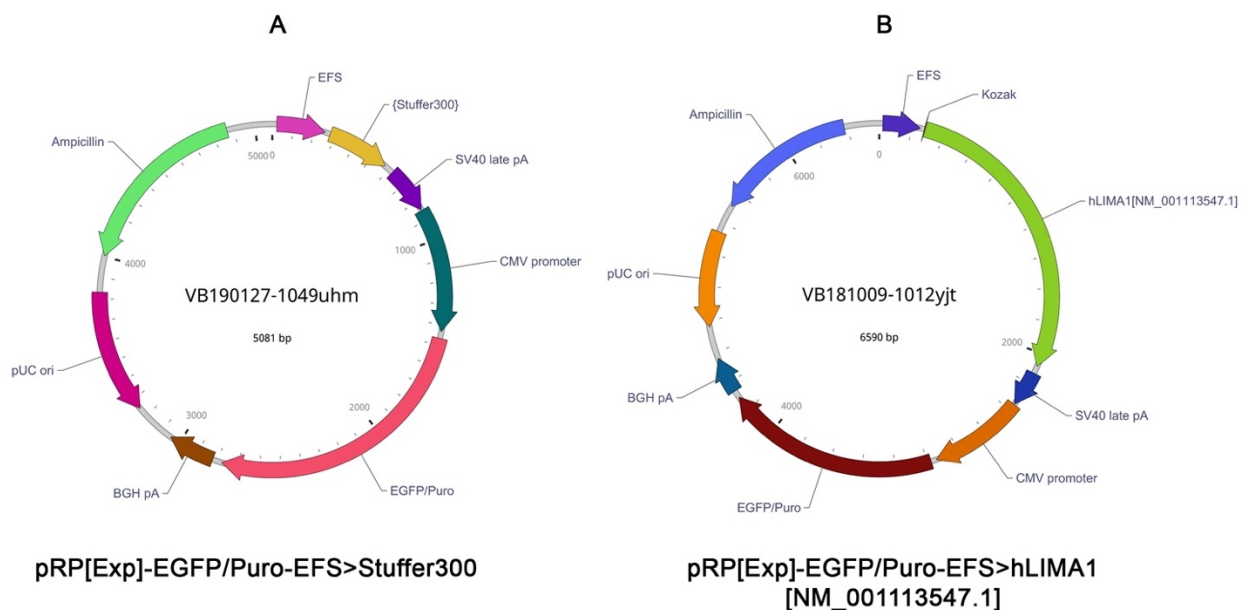


Figure 2.1 Schematic of Plasmid Vectors. A. Plasmid DNA with an inserted ORF of stuffer 300 (ID: VB190127-1049uhm). B. Plasmid DNA with an inserted ORF of hLIMA1[NM_001113547.1] (EPLIN- α). EGFR/Puro, EGFR fused with puromycin antibiotic resistance gene, generates green fluorescence and resistance to puromycin. Ampicillin, ORF of ampicillin resistance gene. EFS, a promoter of human eukaryotic translation elongation factor. CMV promoter, a strong promoter. BGH pA & SV40 late pA, polyA signals that allows transcription termination. pUC ori, a rep_origin of replication which allows plasmid replicate in E. coli. Both were purchased from VectorBuilder Inc. (Chicago, IL, USA).

2.2.5.2 Generation of EPLIN α overexpression cell lines using electroporation-based transfection

One million cells, cultured in antibiotic free medium, were prepared for each transfection. Five micrograms of plasmid DNA was combined and mixed with CRC cells in an electroporation cuvette (Geneflow Ltd, Litchfield, UK) in a final volume of 1ml for each transfection. The solution was incubated for 5 minutes before placing in a BioRad Cell Pulser Xcell electroporation system (BioRad Laboratories, Hertfordshire, UK) and pulsing at 290V and 1000 μ F, before quickly transferring the suspension to prelabelled flasks containing prewarmed medium and placing in the incubator overnight. Subsequently, cells were observed under the microscope before beginning puromycin selection at appropriate concentrations determined by the Killing curves.

2.2.5.3 Generation EPLIN knockdown cell lines using shRNA-based transfection

Cells were cultured in antibiotic free medium in 6 wells plate until they reached 50-70% confluence. shRNA plasmid DNA, Plasmid Transfection Reagent and Transfection Medium were purchased from Santa Cruz Biotechnology, Inc. (Dallas, Texas, USA) and manufacturers guidance was followed. Briefly, solution A and solution B were prepared for the transfection process. Solution A was prepared with 10 μ l of shRNA plasmid DNA and 90 μ l of transfection medium, while solution B was prepared with 3 μ l of transfection reagent and 97 μ l of transfection medium. Once prepared, solution A was added to solution B and mixed gently before incubating in the dark at room temperature for 45 minutes. Subsequently, cells were washed with 2ml of transfection medium twice and supplemented with 200 μ l of the solution A and B complex and 800 μ l of transfection medium, before incubating at 37°C for 5-7 hour. Following incubation, 1ml of cultured medium containing 20% FCS and 2X antibiotics was added into the 6 well plate and the plates incubated for 24 hours. Following this, cell selection was undertaken in accordance with the Killing curve experiments.

2.2.5.4 Generation HSP60 knockdown cell lines using siRNA-based transfection

Cells were seeded in a 6-well plate with antibiotic-free culturing medium and incubated at 37°C with CO₂ to reach 60-80% confluence. For each transfection, siRNA transfection mixture A was made up by gently mixing 2 μ l (20pmols) of HSP60 siRNA (SC-29351, Santa Cruz Biotechnology, Inc. Dallas, Texas, USA) with 100 μ l siRNA transfection medium (sc-36868, Santa Cruz Biotechnology, Inc. Dallas, Texas, USA). Mixture B was prepared by adding 2 μ l of siRNA transfection reagent (SC-29528, Santa Cruz Biotechnology, Inc. Dallas,

Texas, USA) into 100µl siRNA transfection medium and mixing gently. Mixture A was then added into mixture B and mixed gently followed by incubating at room temperature for 45 minutes. After incubation, the cell monolayer was washed with 2ml of siRNA transfection medium and supplemented with mixture A+B and 800µl siRNA transfection medium. The plate was then incubated for 7 hours at 37°C with CO₂. One millilitre of 2 times concentrated normal culturing medium (20% FCS + 2% antibiotic) was added into each well for further incubation for 24 hours at 37°C with 5% CO₂. Medium was aspirated after the 24-hour incubation and each well was supplemented with fresh 1x normal culturing medium, then incubated for another 24 hours before designed experiments were carried out.

2.2.5.5 Generation EPLIN manipulated cell lines using UltraCruz[®] based transient transfection
Transient plasmid transfection was performed by utilizing UltraCruz[®] transfection reagent (SC-395739, Santa Cruz Biotechnology, Inc. Dallas, Texas, USA). Cells were seeded into a 6-well plate and incubated with antibiotic-free culturing medium at 37°C with 5% CO₂ to reach 40-80% confluence. Transfection complex was prepared by mixing solution A (gently mixed 3µg of plasmid with plasmid transfection medium to final volume of 150µl and incubated at room temperature for 5 minutes) with solution B (gently mixed 10µl of UltraCruz[®] transfection reagent with 140µl plasmid transfection medium and incubated at room temperature for 5 minutes), then incubated at room temperature for 45 minutes. Fresh antibiotic-free medium, supplemented with 300µl of the prepared transfection complex, was added followed by incubation for 24 hours at 37°C with 5% CO₂ before designed experiments were performed.

2.2.6 Thiazolyl Blue Tetrazolium Bromide (MTT) based Killing curve

A Killing Curve was performed on RKO, HT-115 and HRT-18 cells, in order to select the right concentration of selective antibiotic for cell transfection and selection. Cells were detached and counted as described in previous sections. Cells were seeded into 5x96 well plates (seeding density: 10,000 RKO and HRT-18 cells, 20,000 HT-115 cells) which represented a reference plate, 24-hour treatment plate, 48-hour treatment plate, 72-hour treatment plate and 114-hour treatment plate respectively.

For the reference plate, 200µl of cell mixture of each cell line was added into 24 wells in 6 repeats respectively. After incubating for 24 hours, 22µl of 5mg/ml MTT solution (Sigma-Aldrich Co, Poole, Dorset, UK) was added into each well for a further 30 minutes to 4 hours incubation. The medium was carefully aspirated and then 100µl DMSO was added into each well after incubation in order to dissolve the crystals formed. The plate was then returned to

the 37°C incubator for 10 minutes and subsequently placed into an LT4500 plate reader (Wolf Laboratories, York, UK) for detection at 540nm.

For the rest of the plates, 4 groups (6 wells each) of different concentrations of puromycin were designed: 0µg/ml, 1µg/ml, 2µg/ml and 5µg/ml for HT-115 and HRT-18 cell lines, whilst 0µg/ml, 0.1µg/ml, 0.2µg/ml and 1µg/ml for the RKO cell line. Two hundred microlitres of cell mixture of each cell line was added into 24 wells in 6 repeats respectively and incubated for 24 hours at 37°C in an incubator. After 24 hours, the medium of each well was aspirated and different concentrations of medium mixed with puromycin were added into each well as designed. The incubation time depended on the designed schedule: 24 hours, 48 hours, 72 hours and 144 hours. After incubation, solutions were removed and the plates were incubated for 30 minutes to 4 hours after 22µl MTT solution was added. Subsequently, media were aspirated and 100µl DMSO was added and mixed for a further 10-minute incubation. Plates were then read in an LT4500 plate reader at 540nm.

Data was collected, normalised, analysed and presented as line charts using excel.

2.2.7 MTT-growth assay

MTT assay was carried out to assess proliferation ability of cells. Cells were detached and cultured as discussed above, and 3,000 cells (200µl of cell mixture) of each cell line were seeded into 3x96 wells plates with 6 repeats. Three plates were marked as reference (day-1), day-3 and day-5.

After incubating for 24/72/144 hours, 22µl of 5mg/ml MTT solution was added into each well for a further 4-hours incubation. The medium was carefully aspirated and 100µl DMSO was added into each well in order to dissolve the crystals formed. The plate was then returned to the 37°C incubator for 10 minutes and subsequently placed into an LT4500 plate reader for detection at 540nm.

Data was collected, normalised, analysed and presented as line charts using excel and GraphPad.

2.2.8 Matrigel adhesion assay

Matrigel adhesion assay was performed in order to measure the cells' adhesive abilities. Matrigel (BD Biosciences, Oxford, UK) was defrosted and diluted with serum free medium (SFM), to reach a final concentration of 0.05mg/ml. The wells of a 96 well plate were coated

with 100µl (5µg) / per well of the Matrigel solution, before drying in the oven at 55 °C for 2-3 hours until the Matrigel had dried. Approximately 40,000 cells (Wang et al. 2013) of each sample were seeded into each well with 6 repeats, after the Matrigel was rehydrated with 100µl SFM for 30 minutes. The plates were then incubated at 37°C with 5% CO₂ for 40 minutes, the medium of each well was aspirated carefully without disturbing the monolayer and PBS was used to wash out unattached cells, before adding 4% formalin to fix attached cells for 10 minutes. Subsequently, 0.5% crystal violet, diluted in distilled water, was added into each well, to cover the monolayer in order to stain attached cells for approximate 3 minutes, before being removed and the crystal violet washed away with water. The plate was then allowed to dry overnight at room temperature. Cells were then observed in 4 random fields of each well under a Leica DM IRB microscope (Leica GmbH, Bristol, UK) (X20) and photographs of each field were captured using a Leica LAS EZ (Leica Microsystems (UK) Ltd, England, UK). Cell counting was completed using Image J software (<https://imagej.nih.gov/ij>) and data was analysed with GraphPad.

2.2.9 Matrigel invasion assay

Invasiveness of cells was investigated by performing Matrigel invasion assays. Matrigel solution was prepared in SFM to a concentration of 0.5mg/ml. The upper chamber of each 8µm pore transwell insert was coated with 50µg (100µl) of Matrigel (BD Biosciences, Oxford, UK). The inserts were placed in a 24-well plate before drying at 55 °C for 2-3 hours in the oven. Dried inserts were then rehydrated with 100µl of SFM, for 30 minutes, before 25,000 cells (200µl) of each cell type, as outlined in (Wang et al. 2013), were seeded into the upper chamber of the insert of duplicate inserts, then 500µl of culture medium was added to each well, to support cells that invaded the insert, followed by incubating for 72 hours at 37 °C with 5% CO₂. After incubating, medium was aspirated carefully before using a cotton swab to remove cells that did not invade through the insert. Invaded cells on the underside of the insert were fixed in 4% formalin solution for 10 minutes followed by staining with 0.5% crystal violet solution. After staining for 5 minutes, redundant crystal violet was washed away with water and the plate was left to dry overnight at room temperature. Stained, invaded cells were visualized in 4 random fields under a Leica DM IRB microscope (Leica GmbH, Bristol, UK) at X20 objective magnification. Photographs of each field were captured using a Leica LAS EZ (Leica Microsystems (UK) Ltd, England, UK). Cell counting was performed by using Image J and data was analysed with GraphPad.

2.2.10 Wound healing assay

Wound healing assays were performed, to test migration ability of samples, by investigating the width of wounded gaps which were refilled through directional migration of cells during closure over time. Each well of a 24-well plate was seeded with 40,000 cells of each sample and incubated till confluent at 37 °C with 5% CO₂. A vertical wound was created in the monolayer of cells of each well by using a 10µl pipette tip and culture medium was replaced with fresh medium. Images of the wounded gap were taken by using Leica LAS EZ (Leica Microsystems (UK) Ltd, England, UK) under a Leica DM IRB microscope (Leica GmbH, Bristol, UK) at X20 objective magnification and marked as 0 hour. Plates were then incubated at 37 °C with 5% CO₂ for 4 hours. At each hour point (1,2,3 and 4), plates were placed under the microscope and photographs of the wounded gap were taken, before returning back to incubation. The widths of each wounded gap (distance between two fronts) from 1,2, and 3 time points were measured by carrying out analysis in Image J and compared with the width at 0 hours, to determine the cellular migration ability of samples. Data was analysed using GraphPad.

2.2.11 Electric cell-substrate impedance sensing (ECIS) based cell migration assay

ECIS based cell migration assay was carried out to investigate cell migration by measuring impedance after wounding. Cell solutions containing 20,000 cells, with the relevant culture medium for each cell model, were seeded, at a volume of 200µl, into 96-well ECIS W961E electrode arrays in 5-6 repeats (Figure 2.2). Electrodes in each well would allow the ECIS system to wound cell monolayers electrically and record impedance. The arrays were then placed on the ECIS Ztheta instrument (Applied Biophysics Ltd, Troy, New Jersey, USA). After incubating for 5 hours to reach confluent monolayers, an electrical wound (2000 mA for 20 seconds) was created in each well by the ECIS, with impedance being measured immediately. Impedance level of each well was recorded continuously over 1000 to 64,000 Hz by the ECIS system for the next 10-24 hours. Data was analysed using ECIS software.

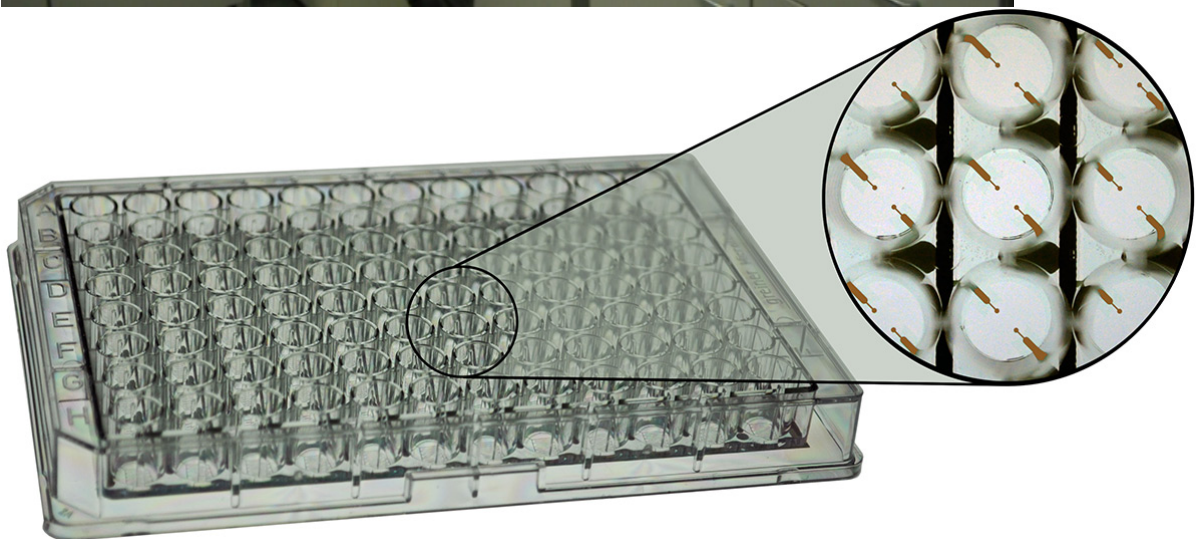


Figure 2.2. *The ECIS instrument and ECIS microarray used in the present.*

2.2.12 Cytotoxicity assays

Cell cytotoxicity assays were carried out to probe the implication of EPLIN/HSP60 on drug resistance in CRC and pancreatic cancer cells. One hundred microlitres of 5,000 cells with culture medium from CRC cellular models, or 3,000 cells from pancreatic cancer cellular models, were seeded into 96 well plates in 6 repeats. This included wells precoated with 100µl serial dilutions of chemotherapeutic drugs/small inhibitors, as well as control wells with fresh culture medium. Plates were then incubated at 37 °C with 5% CO₂ for 72 hours. After incubation, the medium was aspirated and wells were carefully washed with PBS carefully. One hundred microlitres of 4% formalin was added to each well and plates were incubated for 10 minutes at room temperature to fix cells. Formalin was then discarded and each well was stained with 100µl of 0.5% crystal violet solution for another 10 minutes at room temperature before drying. After plates were air-dried, 100µl of 10% acetic acid was added into each well to extract cell bound crystal violet and incubated for 10 minutes at room temperature. Plates were then placed into an LT4500 plate reader for detection at 595nm. Data analysis was performed using Microsoft Excel.

2.2.13 Mitochondrial metabolic assays

2.2.13.1 Griess Reagent System

Griess Reagent System (Promega, Southampton, UK) was applied to detect nitrite (NO₂-) levels in cell models, in order to investigate formation of nitric oxide to reflect cells' metabolic functions. Twenty thousand cells, from cellular models, were seeded into a 96-well plate in triplicate and incubated overnight at 37°C with 5% CO₂. Prior to the experiment, a Nitrite Standard Reference Curve was created by supplementing Sodium Nitrite (100µM) into the 96-well plate in triplicate and performing 6 series two-fold dilution with distilled water. Fifty microlitres of Sulfanilamide Solution was supplemented into each testing sample and incubated, in the dark, for 10 minutes at room temperature. This was followed by adding 50µl of NED solution and further incubation in the dark for 10 minutes at room temperature. The absorbance was then measured using an LT4500 Plate Reader (Wolf Laboratories, York, UK) at 540nm. Data was normalised based on the Nitrite Standard Curve and analysed using Microsoft Excel.

2.2.13.2 NAD(P)H-Glo™ Detection System

NAD(P)H-Glo™ Detection System was used to investigate concentrations of reduced forms of nicotinamide adenine dinucleotide (NADH) and nicotinamide adenine dinucleotide phosphate (NADPH) (Promega, Southampton, UK) (Ward and Thompson 2012). In brief, 20,000 cells of each cellular model were seeded into a CELLSTAR® 96 well plate (Sigma-

Aldrich Co, Poole, Dorset, UK) in triplicate, followed by incubating overnight at 37°C with 5% CO₂. At this point, 50µl of NAD(P)H-Glo™ Detection Reagent, made by mixing together Reconstituted Luciferin Detection Reagent, Reductase and Reductase Substrate provided by the manufacturer, was supplemented into each testing samples. After shaking gently, the plate was incubated at room temperature for 60 minutes, followed by carrying out GloMax®-Multi Detection System (Promega, Southampton, UK) to measure the luciferase signal. Data was analysed using Microsoft Excel.

2.3 Molecular biology

2.3.1 Preparation of chemical solutions used for molecular biology

2.3.1.1 DEPC (Diethyl pyrocarbonate) water

DEPC water was used to help inhibit RNase action. The solution was prepared by adding 500µl diethyl pyrocarbonate (Sigma-Aldrich, Poole, Dorset, UK) to 9.5ml of distilled water before autoclaving and storing at room temperature for further experiments.

2.3.1.2 75% Ethanol DEPC water

Seventy five percent ethanol was used for RNA Isolation. The solution was prepared by mixing 15ml of 99.8% ethanol and 5ml of DEPC water. The solution was prepared before being used in experiments.

2.3.1.3 GoScript™ Reverse Transcription Mix, Oligo (dT)

Ten microlitres of GoScript™ Reverse Transcription Mix was used for cDNA synthesis, prepared by mixing 4µl of Nuclease-Free Water, 4µl of GoScript™ Reaction Buffer, Oligo (dT) and 2µl of GoScript™ Enzyme Mix, the solution was stored at -20°C for further use.

2.3.1.4 Primers

Solutions of forward and reverse primers were prepared at a stock solution of 10µM, Subsequently, for this study, primers were diluted 10 or 100 times by adding 20µl of primer stock into 180µl or 4 µl of primer into 396µl of PCR Water respectively (to give 10µM or 1µM stocks) before mixing and storing at 4°C in the fridge for further experiments.

2.3.1.5 Tris-Boric-Acid (TBE) electrophoresis buffer

The stock of 10x TBE buffer was purchased from Sigma-Aldrich (Poole, Dorset, UK). A solution of 1x TBE for further use was prepared by adding 200ml of 10x TBE buffer into 1800ml of distilled water and storing at room temperature.

2.3.2 RNA Extraction

2.3.2.1 RNA isolation

RNA extraction was undertaken using the TRI Reagent Kit (Sigma-Aldrich, Poole, Dorset, UK) in line with the manufacturer's instructions. In brief, upon reaching approximately 90% confluence, medium was aspirated and 1ml of TRI Reagent was added to the cell monolayer to lyse the cells through gentle agitation. Subsequently, the lysate was transferred to a labelled Eppendorf tube and left to stand at room temperature for 5 minutes. Following this, 100µl of 1-bromo-3-chloropropane (Sigma-Aldrich Co, Poole, Dorset, UK) was added to the lysate and vigorously shaken for 15 seconds, before standing at room temperature for 5 minutes. The sample was then centrifuged at 12,000 x g for 15 minutes at 4°C resulting in separation into three layers: a transparent upper aqueous phase containing RNA, a thin interphase containing DNA and a pink lower organic phase containing protein. For further experiments, the upper phase was used.

The upper phase, which contained RNA, was collected and transferred to a new labelled Eppendorf tube containing 500µl of 2-propanol (Fisher Scientific UK Leicestershire, UK), mixed and left to stand for 5 minutes at room temperature. Subsequently, the sample was centrifuged at 12,000 x g for 10 minutes at 4°C forming a pellet in the bottom of the Eppendorf tube. The supernatant was then carefully removed, leaving the pellet, and supplemented with 1ml of 75% ethanol DEPC, mixed gently and allowed to stand at room temperature for 5 minutes, before being centrifuged at 7,500 x g for 5 minutes at 4°C.

The supernatant was removed from the resulting pellet before drying briefly at 55 °C for a few minutes in the drying oven (Techne, Hybridiser HB-1D drying oven, Wolf laboratories, York, UK), to remove the remaining ethanol.

2.3.2.2 RNA quantification

The pellet was dissolved by adding 50-100µl of DEPC water based on the size of the formed pellet. An Implen nanophotometer (Geneflow Ltd, Litchfield, UK) was used to quantify RNA against a DEPC water blank. After measurement, the concentration of RNA was calculated, allowing for standardisation in future experiments and the RNA stored at -80°C for further experiments.

2.3.3 Reverse transcription of RNA

For reverse transcription, GoScript™ Reverse Transcription System Kit (Promega Corporation, Madison, WI, USA) was used in order to obtain cDNA samples for further use. Ten microlitres of GoScript™ Reverse Transcription Mix (RT Mix) was supplemented with 10µl of RNA solution, which was standardised with PCR water (500ng) and mixed to make up a 20µl solution.

The reverse transcription reaction was performed in a Simplicamp thermocycler (Fisher Scientific UK Leicestershire, UK). The reaction conditions were 25°C for 5 minutes (1 cycle), 42°C for 60 minutes (1 cycle), 70°C for 15 minutes (1 cycle) and hold at 4°C.

Sixty microlitres of PCR water was added to dilute the cDNA sample for further experiments or storage at -20°C.

2.3.4 Polymerase Chain Reaction (PCR)

PCR, a convenient technique to amplify a selected region of target DNA, was used for general screening of cell lines.

PCR was undertaken using the primers outlined in Table 2.4, PCR GoTaq Green master mix (Promega, Southampton, UK), PCR water and sample DNA. A 16µl reaction was prepared as outlined below:

Component	Volume
cDNA sample	1µl
Forward Primer	1µl
Reverse Primer	1µl
PCR water	5µl
2x GoTaq Green Master Mix	8µl

The sample was placed in a Simplicamp Thermocycler after mixing and subject to the following reaction conditions:

Process	Temperature	Time	Cycles
Initialisation	94°C	5 minutes	1
Denaturation	94°C	20 seconds	
Annealing	55°C	20 seconds	32
Extension	72°C	50 seconds	
Final Extension	72°C	10 minutes	1
Final Hold	4°C	∞	1

2.3.5 Agarose gel electrophoresis and DNA visualisation

2.3.5.1 Agarose gel electrophoresis

Agarose gel electrophoresis was undertaken to separate and analyse DNA samples following PCR amplification. During the process, negatively charged DNA was separated electrophoretically and compared to a PCR Ranger PCR ladder (Geneflow Ltd., Litchfield, UK), to allow determination of approximate band sizes.

According to the size of target DNA fragments different agarose gels, containing different concentrations of agarose, were chosen. For EPLIN, EPLIN β and GAPDH, a 1% agarose gel, made from 1g of agarose powder (Melford Chemicals, Suffolk, UK), was used. The solution was heated after adding 100ml of 1x TBE buffer in a microwave until molten. The gel was then allowed to cool slightly before 8 μ l of SYBR Safe DNA Gel Stain (Fisher Scientific UK Leicestershire, UK) was added into the solution. The solution then was poured into an electrophoresis cassette (Scie-Plas Ltd., Cambridge, UK), and combs were placed before letting it stand at room temperature for 30-40 minutes to set firmly. The gel was then transferred to the reaction tank and topped up with 1x TBS buffer, to a level 5mm higher than the surface of the gel, before removing the combs. Eight microlitres of the DNA samples and 5 μ l of the DNA ladder were added into each well respectively.

The gel was then run at 120V, 100mA, 50W for 30 minutes powered by an electrophoresis power supply.

2.3.5.2 DNA visualisation

Once sufficiently separated, the gel was transferred to a Syngene U: Genius 3 Fluorescence UV Transilluminator (Synoptics Ltd., Cambridge, UK). Images of DNA fragments and ladders

were visualised and captured under blue light. The images were saved on the systems and printed with a thermal printer.

2.3.6 Real time quantitative PCR (qPCR)

qPCR was carried out using a MicroAmp Fast Optical 96-Well Reaction Plate with Barcode (0.1ml) (Fisher Scientific UK Leicestershire, UK), Optical seal (PrimerDesign, Southampton, UK) and a Step One Plus Real Time PCR System (Fisher Scientific UK Leicestershire, UK) (Figure 2.3). The Amplifilour Uniprimer™ Universal system (Intergen company, New York, USA) was used. The unknown sample solution of each well was made up by preparing a reaction solution through mixing 5µl of precisionFAST2x qPCR Master Mix (PrimerDesign, Southampton, UK), 0.3µl of Forward primer, 0.3µl of Reverse primer containing the z sequence (at a concentration of 1/10th of the forward primer), 0.3µl of uniprobe and 4.1µl of cDNA sample mixture to a total volume of 10µl. In addition, unknown samples were run alongside a standard set of samples of known transcript copy number (ranging from 10¹ to 10⁸), to allow calculation of relative copy numbers in the unknown samples. After placing the reaction in the Step One Plus Real Time PCR System, the reaction was run as outlined below.

	Stage 1		Stage 2	
Cycle	1		100	
Temperature	95°C	95°C	55°C	72°C
Time	10 minutes	10 seconds	35 seconds	10 seconds



Figure 2.3 Step One Plus Real Time PCR System

2.4 Protein extraction and analysis

2.4.1 Protein extraction

Once cells of a 75cm² flask became 90% confluent, the medium was aspirated and 5ml of PBS was added to wash the monolayer several times. Cells then were harvested, in PBS, using a cell scraper and transferred to a universal tube, before centrifuging at 2,000rpm for 7 minutes. A pellet was formed at the bottom of the tube and based on the size of the pellet, 250µl -400µl of lysis buffer was added to resuspend the pellet after aspirating the supernatant. The solution was transferred to an Eppendorf and placed on a rotating wheel at 4°C for a least an hour. After that, the Eppendorf was centrifuged at 13,000 rpm for 15 minutes at 4°C and a pellet was formed. The pellet was discarded and supernatant was collected and transferred to a labelled Eppendorf, before storing at -20°C for further experiments.

2.4.2 Protein quantification

Protein quantification was performed by carrying out a BioRadDC Protein Assay (BioRad Laboratories, Hertfordshire, UK) in accordance with the manufacturer's instructions. In brief,

a standard set of samples was created through serial dilution of 50mg/ml bovine serum albumin (BSA) stock (Sigma-Aldrich Co, Poole, Dorset, UK), diluted in lysis buffer. Following this 5 µl of each standard point or unknown sample were added into a 96 well plate in duplicate (standards) or triplicate (unknowns). Working reagent A' was prepared by adding 20 µl of reagent S into each ml of reagent A intended for use in the assay. Twenty five microlitres of reagent A' was then added into each well followed by 200 µl of reagent B. The plate was incubated in the dark at room temperature for 15 minutes after mixing. The absorbance was then detected at 620nm in an LT4500 spectrophotometer. A standard curve then was drawn based on the standard data, concentrations of the unknown protein samples calculated and standardised to a consistent concentration. An equal volume of 2x laemmli buffer (Sigma Aldrich, Dorset, UK) was added into each protein sample and the sample was boiled for 5 minutes at 100°C before storing at -20°C for further use.

2.4.3 Sodium dodecyl sulfate-polyacrylamide gel electrophoresis (SDS-PAGE)

SDS-PAGE was used to separate proteins. Two different types of gel, a 5% stacking gel (Table 2.6) and a 10% resolving gel (Table 2.7) were prepared. The resolving gel was added between two glass plates held tightly in a cassette to a level which would allow addition of a comb, before overlaying with ethanol to ensure a smooth edge, and being allowed to set. After the resolving gel was set, the overlaid ethanol was removed, the stacking gel was prepared and added on top of the resolving gel, before placing a comb in the solution and allowing to set. Once both gels were set, the cassette was transported to an electrophoresis tank and supplemented with running buffer (tris – glycine- sds buffer). Then 10 µl of samples and 5 µl of BLUeye Prestained Protein Ladder (Geneflow Ltd., Litchfield, UK) were added and the electrophoresis was run at 120V, 50W and 50mA until sufficient separation was obtained.

2.4.4 Transfer to polyvinylidene fluoride (PVDF) membrane

When the electrophoresis process was finished, the gel was transferred to the Immobilon P PVDF membrane (Merck Millipore, Hertfordshire, UK) (cut to 7.8cm x 7.8cm in size), which was activated with 100% methanol for 1 minute, then incubated in transfer buffer. The membrane with the gel on top was then placed on 3 pieces of filter paper (8cm x 8cm) and covered by 3 more pieces of filter paper (8cm x 8cm). This complex was prepared on a semi-dry transfer apparatus and run at 15V, 500mA, 20W for 50 minutes.

2.4.5 Immuno-Blotting

Following semi-dry transfer, the membrane was blocked in 5% milk solution (5% milk in tris buffered saline [TBS] with 0.1% tween-20) for 1 hour before incubating in 2.5% milk solution, with the desired antibody and concentration (outlined in Table 2.5), at 4°C overnight. The following day, the membrane was washed with 2.5% milk solution 3 times, each round for 15 minutes. After removing the final wash, the membrane was incubated in 2.5% milk solution containing the secondary antibody (see Table 2.5 for 1 hour, followed by washing with TBS containing 0.1% tween (TBS-T) twice, each time for 10 minutes. The membrane was then washed with TBS twice, 10 minutes each, before being incubated in EZ-ECL solution (equal parts of solution A mix with solution B) (Geneflow Ltd., Litchfield, UK) for 3-5 minutes and placed in a G-BOX (Syngene, Cambridge, UK) to capture images of the membrane.

Table 2.6 Recipe of 5% stacking gel (6ml)

H₂O	4.1ml
30% Acrylamide/Bis-Acrylamide solution	1ml
1.5M Tris pH (6.8)	0.75ml
10% SDS	0.06ml
10% ammonium persulfate	0.06ml
TEMED	0.006ml

Table 2.7 Recipe of 8% resolving gel (15ml)

Move 1eH₂O	6.9ml
30% Acrylamide/Bis-Acrylamide solution	4ml
1.5M Tris pH (8.8)	3.8ml
10% SDS	0.15ml
10% ammonium persulfate	0.15ml
TEMED	0.009ml

2.4.6 Co-immunoprecipitation

Co-Immunoprecipitation assay was carried out on colorectal cancer cells to investigate protein-protein interaction (Figure 2.4). Cells were cultured in a T75 flask at 37°C with 5% CO₂ till confluent. Protein was extracted by following the method described in Chapter 2.4.1 with lysis buffer (1% triton100, NP40). After quantification, a portion of protein samples were supplemented with 100µl EPLIN antibody (sc-136399, Santa Cruz Biotechnology, Inc. Dallas, Texas, USA), and put on a rotating wheel at 4°C for an hour. 50µl of protein A/G PLUS-agarose immunoprecipitation reagent (sc-2003, Santa Cruz Biotechnology, Inc.

Dallas, Texas, USA) were added into each samples before rotating at 4°C overnight. Samples were centrifuged at 7,000RPM and 4°C for 5 minutes followed by discarding supernatant. Then washing with 1ml lysis buffer three times. After washing, elution of the protein complex was applied. In brief, 60-100µl of 1x sample buffer was supplemented into each sample and boiled at 100°C for 5 minutes before performing immune-blotting with SDS-PAGE as described in Chapter 2.4.3 & 2.4.4 & 2.4.5.

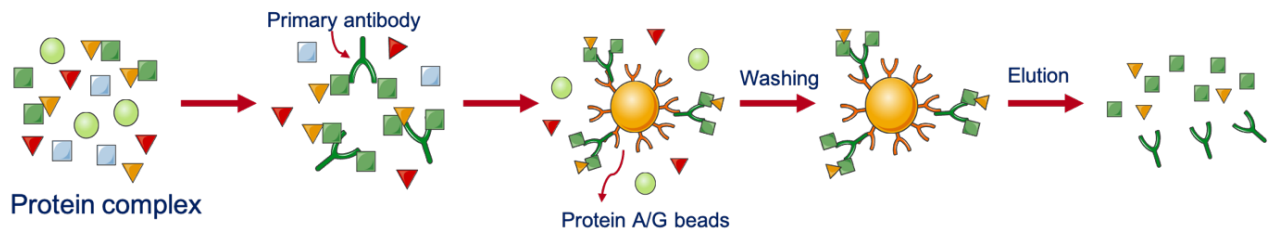


Figure 2.4 Process of co-immunoprecipitation.

2.5 Tissue collection and processing

2.5.1 Colorectal cancer cohort.

Normal human colorectal tissues and human colorectal cancer tissues were collected at the University Hospital of Wales, immediately after surgery from informed, consenting patients. Tissue was recovered from the operating theatre during the procedure by a researcher. This was examined by a consultant pathologist. Samples of colorectal carcinoma, normal matched colorectal tissue (>10cm away from tumour margin) were obtained. Tissue samples were placed in labelled universal containers, frozen in liquid nitrogen and stored in the research laboratory at -80°C until required. Subsequent pathological report was obtained for data stratification. Patients underwent routine clinical, colonoscopic and radiological follow up after the surgery and results were obtained using the hospital clinical portal system and CANISC data. The median follow-up period was 65 months. Ethical approval for the use of tissue was obtained from the South East Wales Local Research Ethics Committee (reference number: SJT/C617/08). The second cohort was collected from the Friendship Hospital of Capital Medical University a Cardiff University institutional partner, by following the same protocol. This was supported by the Capital Medical University Ethics approval.

2.5.2 Pancreatic cancer cohort

To further validate the impact of EPLIN in gastrointestinal malignancies, the study also employed a human pancreatic cancer cohort, part of the institutional collaboration between Cardiff University and Peking University Cancer Hospital. Pancreatic cancer tissues and adjacent normal tissues were obtained from theatre and immediately stored in liquid nitrogen until use. Ethical approval was granted by the Ethics Research Committee of Peking University Cancer Hospital (Ethics approval number: 2006021) and is fully in accordance with the Helsinki declarations. Consents were obtained from the patients. This cohort included 199 patients with pancreatic ductal adenocarcinoma (PDAC), who were followed in the clinics and the current study has a median follow-up period of 12 months.

2.6 Immunohistochemical (IHC) staining and analysis

This was based on staining undertaken for EPLIN, in frozen sections of colorectal tissues, used in the preliminary study. Briefly, fresh frozen tissues (normal and tumour) were sectioned to 6µm in thickness using a cryostat (Leica DMB, Milton Keynes, UK). The sections were mounted on glass slides and fixed for 15 minutes in acetone before air drying. After rehydration and washing with TBS, the sections were permeabilised with 0.1% Saponin/TBS. The sections were then incubated with a blocking solution (10% horse serum) for sixty minutes. This was followed by applying primary antibody for 1hour, stringent washing and then incubation with the relevant biotinylated secondary antibody for 30 minutes. The staining was developed by incubation with avidin-biotin complex (ABC) reagent in VECTASTAIN® ABC Kit (Vector Laboratories, Inc., CA, USA), and subsequent 3'3 diaminobenzidine (DAB) substrate (5mg/ml), each procedure separated by stringent washing. The sections were subsequently counterstained with Gill's haematoxylin (Vector Laboratories Inc, CA, USA) and rehydrated through a series of graded alcohols and cleared in xylene (Fisher Scientific, Leicestershire, UK).

A tissue microarray (TMA) (<https://www.biomax.us/tissue-arrays/Colon/CO2161a>), which contained colon carcinoma and normal colon tissue (code: CO2161a), purchased from US Biomax, Inc. (Derwood, MD, USA) (Supplement-1), was utilised to expand our clinical study by conducting IHC assays in line with instruction presented above. The TMA included 205 cases of adenocarcinoma, 3 signet-ring cell carcinoma, 8 normal tissue, single core per case. Detailed information regarding the TMA is listed below in (Supplement-1).

A tissue microarray (TMA)(<https://www.biomax.us/tissue-arrays/Pancreas/PA2081c>), which contained normal and tumour pancreatic tissues (code: PA2081a), purchased from US Biomax, Inc. (Derwood, MD, USA) (Supplement-2), was utilised to expand our clinical study by conducting IHC assays in line with instructions presented above. The TMA included 192 cores from 96 patients, detailed information regarding the TMA is listed below in (Supplement-2).

Analysis of IHC assays on the TMA slides were conducted as follow. Intensity of staining was scored by two researchers as 0 (negative or little staining in <10% of cells), 1 (faint, weak and partial staining in >10% of cells), 2 (moderate complete staining in >10% of cells), and 3 (strong complete membrane staining in >10% of cells). Scores were grouped based on clinical and pathological information. Chi-square (χ^2) test was conducted to examine the distribution of staining scores.

2.7 Kinex™ antibody-based protein microarray

The interacting network of EPLIN in colorectal cancer was explored on patient's protein samples from the UK colorectal cancer cohort via Kinex™ KAM-880 antibody-based protein microarray (Kinexus Bioinformatics Ltd., Vancouver, BC, Canada). After two pairs of patient's protein was extracted (normal: ID126 & 128; tumour: ID127 & 129) from fresh frozen paired human colorectal tissues (normal colon tissue and colon cancer tissue) and quantified to the same concentration by utilising methods described in Chapter 2.4.1 & 2.4.2, samples were precipitated with EPLIN antibody (immunoglobulin G (IgG) monoclonal, Sc-136399, Santa Cruz Biotechnology, Inc. Dallas, Texas, USA) following the method described in Chapter 2.4.6. Precipitated samples were sent to Kinexus Bioinformatics Ltd., and applied on Kinex™ KAM-880 antibody-based protein microarray which contains 877 antibodies (Figure 2.8).

Each array slide has two array spotted (Figure 2.5). After samples were applied and incubated with the pre-labelled antibodies (Figure 2.6 and Figure 2.7), fluorescent signals were detected and strength of intensity was demonstrated in different colour (From high to low: red, orange, yellow, green and blue.). Analysed reports of enhanced/reduced protein kinases and potential signalling events were generated by the company.

Table 2.8 The antibodies used in the KAM900P antibody protein microarrays. Image obtained from Kinexus Bioinformatics Ltd.

KAM-900P Content	Total %	Total Number
Total number of pan-specific antibodies	30%	265
Total number of phosphor-specific antibodies	70%	613
Total Number of Antibodies	100%	878
Total number of protein kinase pan-specific antibodies	25%	216
Total number of protein kinase phosphosite-specific antibodies	50%	443
Total number of protein phosphatase pan-specific antibodies	0.2%	2
Total number of protein phosphatase phosphosite-specific antibodies	0.7%	6
Total number of transcription factor pan-specific antibodies	1.7%	15
Total number of transcription factor phosphosite-specific antibodies	4%	37

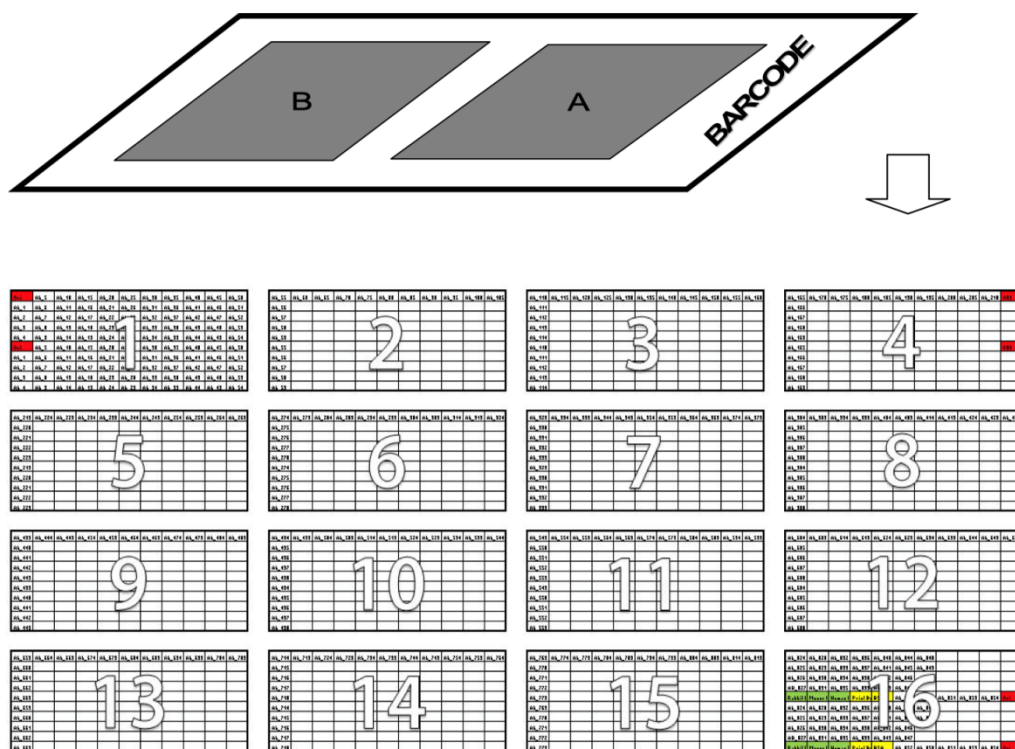


Figure 2.5 Antibody layout on the KAM900P- protein microarray.

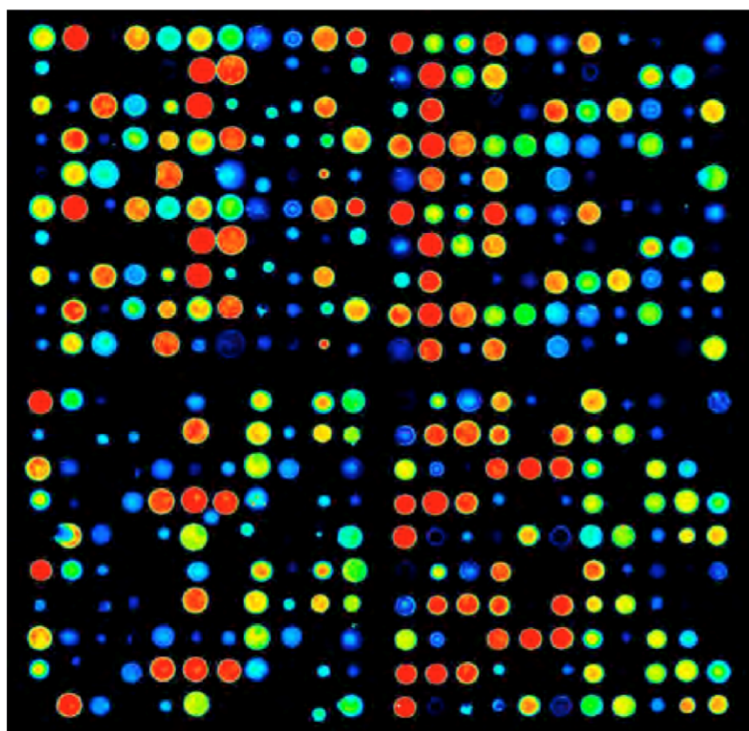


Figure 2.7 An example of closeup examination of the antibody array. Image obtained from Kinexus Bioinformatics Ltd.

Key parameter in the protein microarray analyses.

The following are the key parameters collected and used for the data analyses:

Globally Normalized Signal Intensity – Background corrected intensity values are globally normalized. The Globally Normalized Signal Intensity is calculated by summing the intensities of all the net signal median values for a sample.

Flag – An indication of the quality of the spot, based on its morphology and background. The flagging codes used in the reports are as follows:

- 0: acceptable spots
- 1: spots manually flagged for reasons and may not be very reliable
- 3: poor spots defined by various parameters

%CFC - The percent change of the treated sample in Normalized Intensity from the specified control.

$$\text{Calculation} = (\text{Globally Normalized Treated} - \text{Globally Normalized Control}) / \text{Globally Normalized Control} * 100$$

% Error Range - A parameter to show how tightly the “Globally Normalized Net Signal Intensity” for adjacent duplicate spots of the same protein in the sample compare to each other.

Calculation = $\frac{ABS(\text{Globally Normalized Spot 1} - \text{Globally Normalized Spot 2})}{\text{Globally Normalized Spot 2}} \times 100$

Log2 (Intensity Corrected) - Spot intensity corrected for background is log transformed with the base of 2.

Calculation = $\text{Log}(\text{Average Net Signal Median}, 2)$

Z Scores - Z score transformation corrects data internally within a single sample.

Z Score Difference - The difference between the observed protein Z scores in samples in comparison.

Z Ratios - Divide the Z Score Differences by the SD of all the differences for the comparison.

2.8 statistical analysis

Several statistical software was used to conduct statistical analyses in this study. Minitab (Minitab Ltd. Coventry, UK) was carried out to analyse transcript expression of interested genes in clinical cohorts in comparison to clinical pathological information by using Mann Whitney test and Kruskal Wallis ANOVA on RANKS test. SPSS version 26 (IBM, Armonk, New York, USA) was utilised to perform Kaplan-Meier survival curve, Spearman's correlation analysis and Cox regression multivariate analysis in clinical cohorts. GraphPad (Prism 8) (GraphPad Software, San Diego, CA, USA) was carried out to analyse experimental data by performing normality test, two-tailed t test, Spearman's correlation analysis and Chi-square(χ^2)test. Detailed test methods for each dataset are also sated in the repspevtive result chapters.

Chapter-3

Clinical significance of EPLIN in Colorectal cancer (CRC)

3.1 Introduction

Epithelial Protein Lost In Neoplasm (EPLIN) which is also known as LIMA-1, actin-binding protein-1, was initially reported to be downregulated in oral cancer cells, compared to normal cells, by Maul et al. in the late 1990s (Chang et al. 1998; Maul and Chang 1999), and is encoded by a single gene, *LIMA-1*. EPLIN has two isoforms, a 600aa EPLIN α and EPLIN β which has an additional 160aa at the amino terminus (Maul and Chang 1999). Multiple studies have explored this fascinating protein since then and it has been established as a tumour suppressor in many types of cancers and their metastatic progressions, such as prostate cancer (Maul and Chang 1999; Sanders et al. 2011; Zhang et al. 2011; Collins et al. 2018), breast cancer (Maul and Chang 1999; Jiang et al. 2008; Zhang et al. 2011), oral cancer (Maul and Chang 1999), oesophageal cancer (Liu et al. 2012a), pulmonary cancer (Liu et al. 2012b), melanoma (Steder et al. 2013), CRC (Song et al. 2002; Lee et al. 2006; Zhang et al. 2011; Ohashi et al. 2017), and SCCHN (Zhang et al. 2011).

In the last two decades, researchers have shed light on the clinical implications of EPLIN. Jiang *et al.*, (2008), first found that EPLIN had a correlation with clinical metastatic breast cancer. By analysing clinical datasets, via IHC and qPCR, in comparison with clinical pathological data, the authors revealed that expression of EPLIN was not only attenuated in breast cancer when compared to healthy patients, but also diminished in metastatic breast cancer, which is associated with more advanced TNM stages. Furthermore, they found that lower levels of EPLIN implicated poor prognosis and poor survival rates (Jiang et al. 2008). Other studies have shown consistency with this early study, for example, using analysis profiles from the ONCOMINE database, low levels of EPLIN were found to be related to lymph node metastatic breast cancer (Zhang et al. 2011), poor survival rates (Zhang et al. 2011; Ohashi et al. 2017) and mutant p53 (Ohashi et al. 2017). In prostate cancer, the expression of EPLIN was reported to be downregulated in clinical prostate cancer compared to their control groups respectively and have relevance with metastasis throughout IHC, TMA or analysis of Gene Expression Omnibus (GEO) datasets (Sanders et al. 2011; Zhang et al. 2011; Steder et al. 2013; Collins et al. 2018). Similar trends were observed in melanoma, oesophageal cancer, lung cancer and SCHN. Transcript levels of EPLIN were revealed to be diminished in clinical melanoma, oesophageal cancer and lung cancer in comparison with healthy groups respectively (Liu et al. 2012b,a; Steder et al. 2013; Ohashi et al. 2017). Low levels of EPLIN were reported to be correlated with higher TNM stages, lymph node metastasis, and poor clinical outcomes in oesophageal cancer and lung cancer (Liu et al. 2012b,a; Ohashi et al. 2017). Additionally, research by Steder *et al.*, (2013), also elucidated that attenuated EPLIN was related to metastatic melanoma and SCCHN along

with higher levels of DNp73 (Steder et al. 2013), while Zhang *et al.*, (2011), observed downregulation of EPLIN in lymph node metastatic SCCHN when compared to primary cancer (Zhang et al. 2011).

Hence, in selected tumour types, EPLIN has been established as a tumour suppressor, as its expression is frequently diminished or lost in multiple cancers, when compared to their healthy control groups. Furthermore, lower levels of EPLIN have been identified to be related to metastasis and poor clinical outcomes in various cancer types.

Although the overall incidence and mortality rates of CRC have decreased over the last decade, poor clinical outcomes in aggressive stages, risk factors, higher incidence rates in 25-49 groups and chemotherapeutic resistance contribute to make it the 4th most common cancer type and 2nd commonest cause of cancer death in the UK in 2017. Given EPLIN's role in the development of multiple types of cancer, several studies have implicated that this candidate tumour suppressor may participate in CRC development (Lee et al. 2006; Zhang et al. 2011; Steder et al. 2013; Ohashi et al. 2017). Most of these studies have been focused on the analyses of EPLIN transcript and only limited information is available on the EPLIN protein (Zhang et al. 2011). These reports have indicated a possible relationship between low levels of EPLIN transcript and poor clinical outcome of the patients

Therefore, EPLIN seems to play a similar protective role in CRC as it does in some other cancer types. In this chapter, we focussed on exploring EPLIN's clinical significance in CRC using several clinical cohorts, available online datasets and TMAs.

3.2 Methods

3.2.1 Tissue collection and processing

Methods have been outlined in chapter 2.5.

3.2.2 RNA extraction

Methods have been outlined in chapter 2.3.2.

3.2.3 Reverse transcription of RNA

Methods have been outlined in chapter 2.3.3.

3.2.4 Real time quantitative PCR (qPCR)

Methods have been outlined in chapter 2.3.6.

3.2.5 Immunohistochemical (IHC) staining and analysis

Methods for IHC and detail information of TMA have been outlined in 2.6.

3.2.6 Statistical analysis

Methods have been outlined in chapter 2.8.

3.3 Results

3.3.1 Analysis of EPLIN expression within online GEO datasets

Three individual sets of Gene Expression Omnibus (GEO) datasets, GDS2609, GDS4396 and GDS4382 were searched on NCBI. GDS2609 is a dataset of normal-appearing colonic mucosa and early-onset colorectal cancer (CRC) (reference series: GSE4107) (Hong et al. 2007). GDS4396 is a dataset of unresectable, primary colorectal cancer and metastatic lesions (reference series: GSE28702) (Lambert et al. 2017) and GDS4382 is a dataset of paired CRC tumours and adjacent non-cancerous tissues (reference series: GSE32323) (Khamas et al. 2012). Three different probes, which recognise LIMA-1 (EPLIN) (222456_s_at, 222457_s_at, 217892_s_at) were used to detect and analyse the expression of EPLIN. All analysis was performed on the GPL570 platform (Affymetrix Human Genome U133 Plus 2.0 Array).

GDS4328

Three individual probes of EPLIN were used in this data set (222456_s_at, 222457_s_at and 217892_s_at). Box plots were generated (Figure 3.1) and Mann Whitney test was performed on each probe within the profile. As shown, the expression of EPLIN in normal tissue (n=17) from these three probe sets was significantly higher than the expression in CRC (n=17) ($p < 0.0001$ for 217892_s_at, $p = 0.0004$ for 222457_s_at, $p = 0.0076$ for 222456_s_at).

GDS2609

Three probes of EPLIN (222456_s_at, 222457_s_at and 217892_s_at) were used to explore EPLIN expression in early-onset CRC. Three box plots were drawn based on the three probe sets and Mann Whitney test was carried out. As shown in Figure 3.2, EPLIN expression in the healthy control group (n=10) was significantly higher than its expression in early-onset CRC (n=12) in each probe set ($p = 0.0008$ for 217892_s_at, $p = 0.0006$ for 222456_s_at, $p = 0.0008$ for 222457_s_at). The observed trend was in line with that in GDS4328 dataset.

GDS4396

The same probes were also used in this dataset to detect the expression of EPLIN in primary tumour of CRC and metastatic CRC. Box plots were generated and Mann Whitney tests were performed (Figure 3.3). As shown in Figure 3.3, median values of metastatic lesions (n=6) in three probe sets were higher than those of the primary lesion (n=23), but no statistical significance was noted.

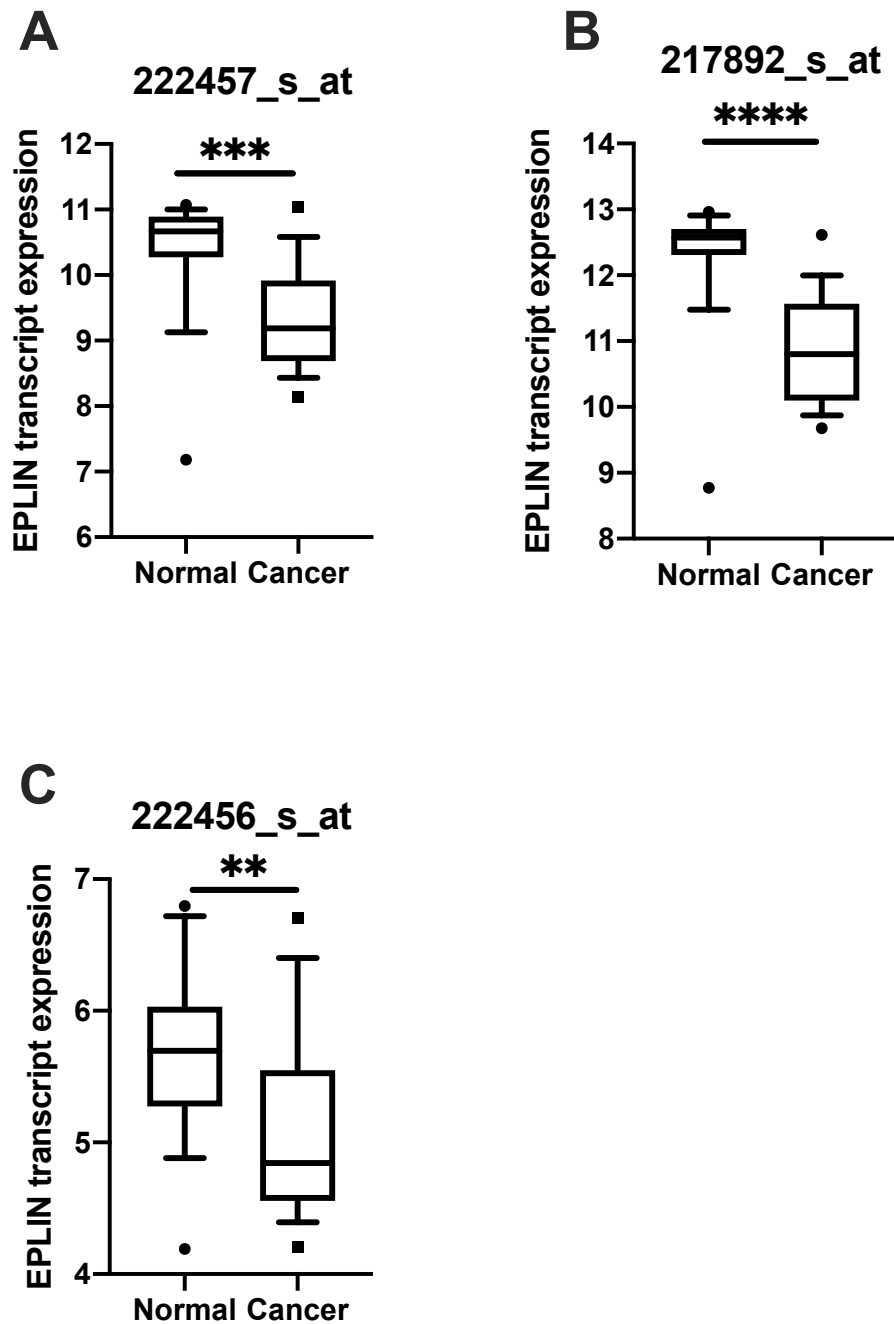


Figure 3.1 GEO profile dataset (GDS4382) comparing LIMA1 expression in cancer (n=17) compared to normal (n=17) samples using 3 different probes (A) 222457_s_at, (B) 217892_s_at and (C) 222456_s_at. Box plot data shown is median expression, Q1 and Q3 values from each dataset, whiskers represent 5th and 95th percentiles with outliers shown. **** represents $p < 0.0001$, *** represents $p < 0.001$, ** represents $p < 0.01$

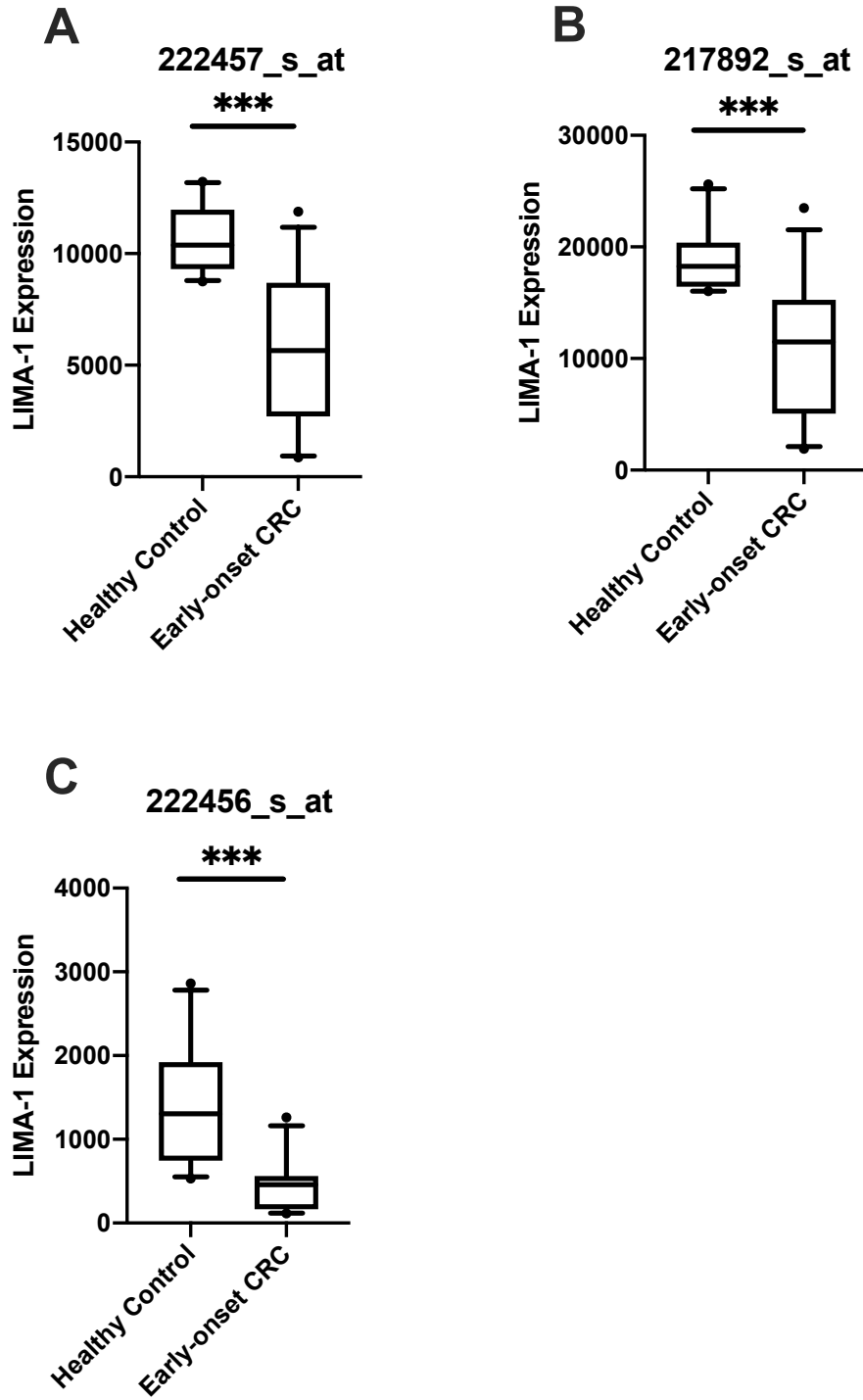


Figure 3.2 GEO profile dataset (GDS2609) comparing LIMA1 expression in healthy controls (n = 10) compared to early onset CRC (n = 12) using 3 different probes (A) 222457_s_at, (B) 217892_s_at and (C) 222456_s_at. Box plot data shown is median expression, Q1 and Q3 values from each dataset, whiskers represent 5th and 95th percentiles with outliers shown., *** represents $p < 0.001$

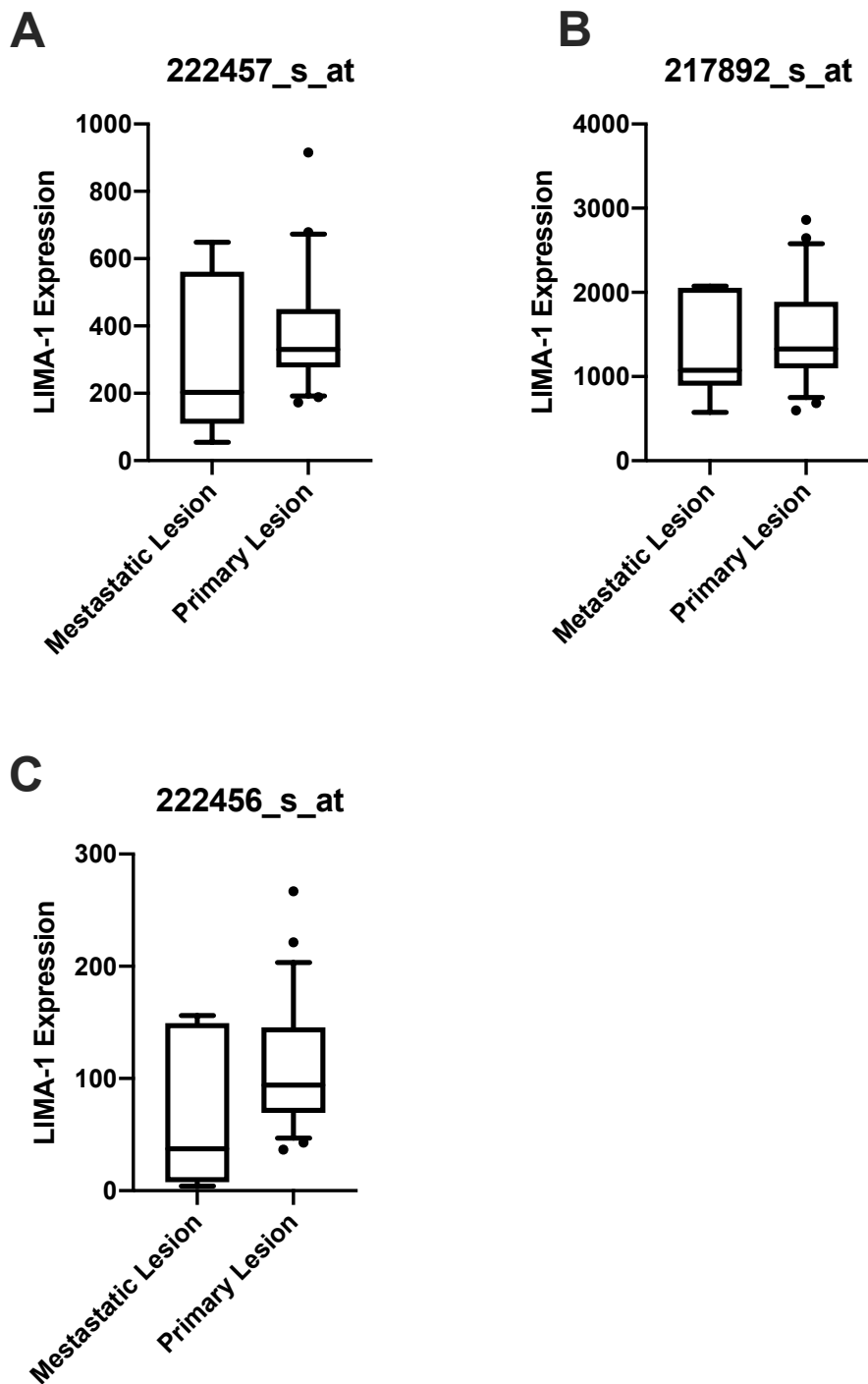


Figure 3.3 GEO profile dataset (GDS4396) comparing LIMA1 expression in metastatic lesion (n=6) compared to primary lesions (n=23) using 3 different probes (A) 222457_s_at ($p=0.1925$), (B) 217892_s_at ($p=0.5109$) and (C) 222456_s_at ($p=0.1139$). Box plot data shown is median expression, Q1 and Q3 values from each dataset, whiskers, where $n > 8$, represents 5th and 95th percentiles with outliers shown.

3.3.2 Transcript expression of EPLIN in clinical CRC cohorts

Here, we assessed the expression level of the EPLIN transcript in two independent colorectal cancer cohorts, available in our laboratory.

3.3.2.1 Quantitative Polymerase Chain Reaction (qPCR) for the first clinical cohort

Tissues and pathological data were collected following ethical approval from the University Hospital of Wales, Cardiff. RNA extraction, quantification, standardisation and reverse transcription were performed to collect cDNA for qPCR. Mann Whitney and Kruskal Wallis ANOVA on RANKS were carried out to analyse the data which is outlined in Table 3.1.

In total, 174 samples were analysed and EPLIN expression in tumour samples (n=94) was found to be significantly diminished when compared to its expression in normal tissue (n=80), with the median relative transcript copy numbers of 137 vs 6515 respectively (p<0.001). There were no significant differences in analysis of differentiation, TNM stage, T stage, Dukes stage, nodal involvement, non-metastasis vs distant metastasis, disease free vs incidence, non-recurrence vs local recurrence or alive vs died of CRC cases (all p > 0.05). Among these, the analysis of different TNM stages suggested a positive correlation between TNM stage and the median relative transcript copy number of EPLIN, in which the median relative transcript expression of EPLIN in TNM1 (n=9) was 4 while in TNM4 (n=6) was 21580, with a borderline significant trend observed within this group (p = 0.051), potentially limited by the low sample numbers. Interestingly, transcript level of EPLIN in invasive samples (n=26, median=182) was higher than it in non-invasive samples (n=50, median=17.2) and it reached statistical significance (p=0.0323). This finding required an investigation in a larger cohort to confirm.

Table 3.1 Transcript expression profile of EPLIN in comparison to clinical pathological information of the Cardiff CRC cohort.

Characteristic	Sample number (n)	Median transcript expression	Q1	Q3	p – value
Tumour	94	137	3	9745	
Normal	80	6515	140	1352500	<0.001 ^a
Differentiation					0.122 ^b
High	2	10848	*	*	
Moderate	54	18	1	7222	
Low	14	609	27	15319	
TNM stage					0.051 ^b
TNM1	9	4	0	11007	
TNM2	30	26	1	8208	
TNM3	26	103	5	1800	
TNM4	6	21580	1633	37877	
T stage					0.879 ^b
T1	2	13602	*	*	
T2	10	49	0	16073	
T3	40	73	2	7774	
T4	18	140	13	5039	
Dukes stage					0.382 ^b
Dukes A	7	95	0	21600	
Dukes B	33	10	1	7498	
Dukes C	32	146	11	13004	
Nodal involvement					0.517 ^b
N0	39	16	1	8050	
N1	16	162	6	13004	
N2	15	142	21	2130	
Metastasis					0.5910 ^a
No metastasis	50	35	3	8208	
Distant metastasis	19	95	0	9325	
Incidence					0.5249 ^a
Disease free	35	29	3	8050	
With incidence	23	95	0	1197	
Recurrence					0.9494 ^a
No Recurrence	58	29	2	7222	
Local Recurrence	7	139	0	235	
Survival					0.9107 ^a
Alive	36	32	4	1849	
Died	22	103	1	9374	
Non invasive	50	17.2			
Invasive	26	182			0.0323 ^a

Note:^a Mann Whitney; ^b Kruskal Wallis ANOVA on RANKS

3.3.2.2 qPCR Analysis of EPLIN transcript expression in the second clinical Cohort.

Tissues and pathological information from the Capital Medical University (CMU) cohort were collected following ethical approval. RNA extraction, quantification, standardisation and reverse transcription were carried out to obtain cDNA for further qPCR analysis. Similar to the Cardiff cohort discussed above, data was collected and analysed by carrying out Mann-Whitney and Kruskal Wallis ANOVA tests (Table 3.2). This cohort contained a larger sample size (n=416). From the results, it can be seen that the median relative transcript copy number value of EPLIN expression in tumour samples (n=275) was decreased compared to normal samples (n=141) (median relative transcript expression: 437 vs 1216 respectively), this was found to be statistically significant (p<0.001). Again, we also analysed EPLIN expression among these samples based on different pathological characteristics. No significant differences could be found in terms of level of differentiation, pTNM stage, T stage, Dukes stage, nodal involvement and non-metastasis vs metastasis cases.

Table 3.2 Transcript expression profile of EPLIN in comparison to clinical pathological information of the China CRC cohort

Characteristic	Sample number (n)	Median transcript expression	Q1	Q3	p - value
Tumour	275	437	152	1742	<0.001 ^a
Normal	141	1216	266	4056	
Differentiation					0.893 ^b
High (1)	55	414	145	1232	0.813 ^b
Mid (2)	158	381	135	1582	
Low (3)	24	580	161	2029	
pTNM stage					0.813 ^b
pTNM1	15	245	105	1031	0.874 ^b
pTNM2	107	481	133	1742	
pTNM3	111	421	148	1300	
pTNM4	21	383	166	3009	
T stage					0.874 ^b
T1	0	*	*	*	0.818 ^b
T2	20	459	188	2466	
T3	128	388	122	1899	
T4	107	420	155	1593	
Dukes stage					0.818 ^b
Dukes A	14	404	87	1146	0.578 ^b
Dukes B	119	420	144	1713	
Dukes C	109	421	149	2099	
Dukes D	16	312	142	993	
Nodal involvement					0.578 ^b
N0	135	414	133	1490	0.486 ^a
N1	91	421	145	2127	
N2	32	376	165	889	
Metastasis					0.486 ^a
No metastasis	190	387	132	1383	0.486 ^a
With metastasis	16	208	142	879	

Note:^a Mann Whitney; ^b Kruskal Wallis ANOVA on RANKS

3.3.3 Implications of EPLIN expression on patients' survival

The relationship between EPLIN expression and patients' survival was also explored in the Cardiff cohort. As shown in Figure 3.4, patients with high levels of EPLIN tended to have a longer overall (top) and disease-free survival (bottom). Patients with high EPLIN expression (above median level) had a mean overall (OS) and disease-free survival (DFS) of 132.1 months and 129.4 months respectively, compared with those with low levels of expression at 84.7 months and 74.2 months respectively. Although these are interesting trends, they were not found to be statistically significant ($p=0.34$ and $p=0.21$ for OS and DFS respectively). This is largely due to the size of cohort which weakened the statistical power. Due to the length of follow-up, we were unable to compute survival with our second clinical cohort.

Therefore, we also analysed an independent cohort online to seek more evidence of the impact of EPLIN on patients' survival. To undertake this, we accessed the Kaplan-Meier Plotter (www.kmplot.com), which also has data on rectal adenocarcinoma. As shown in Figure 3.5, patients with high levels (best cut off value according to KM plot) also had a longer overall survival (Figure 3.5 left) and longer disease-free survival (Figure 3.5 right). In this case, the relationship between EPLIN and disease-free survival was significant, $p=0.023$. Overall, this independent data is in support of the findings from the Cardiff cohort. Unfortunately, again, the study was limited by sample size.

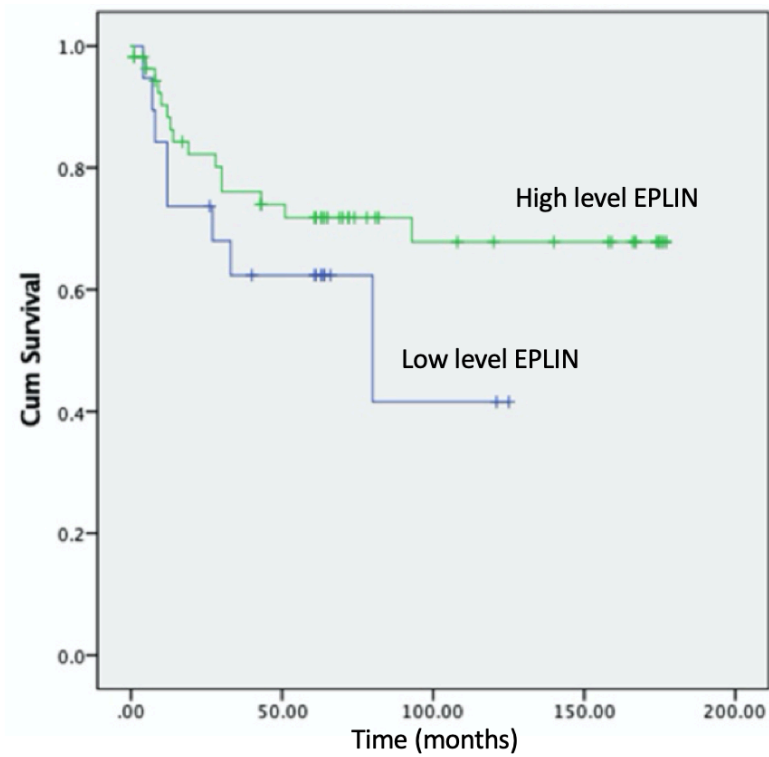
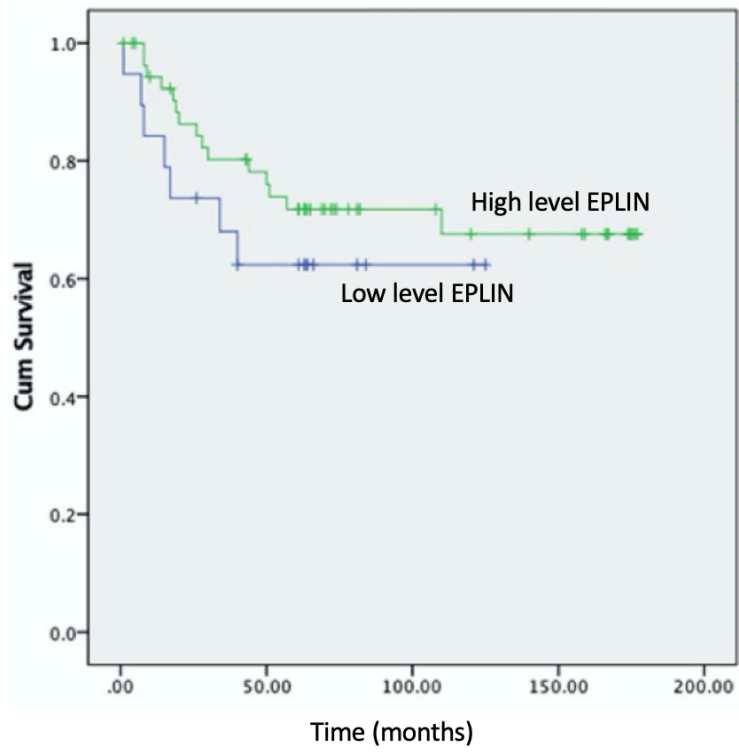


Figure 3.4 Survival Curve showing impact of EPLIN expression on patient survival in the Cardiff clinical cohort. Patients with high levels of EPLIN tended to have a longer overall (top) and disease-free survival (bottom).

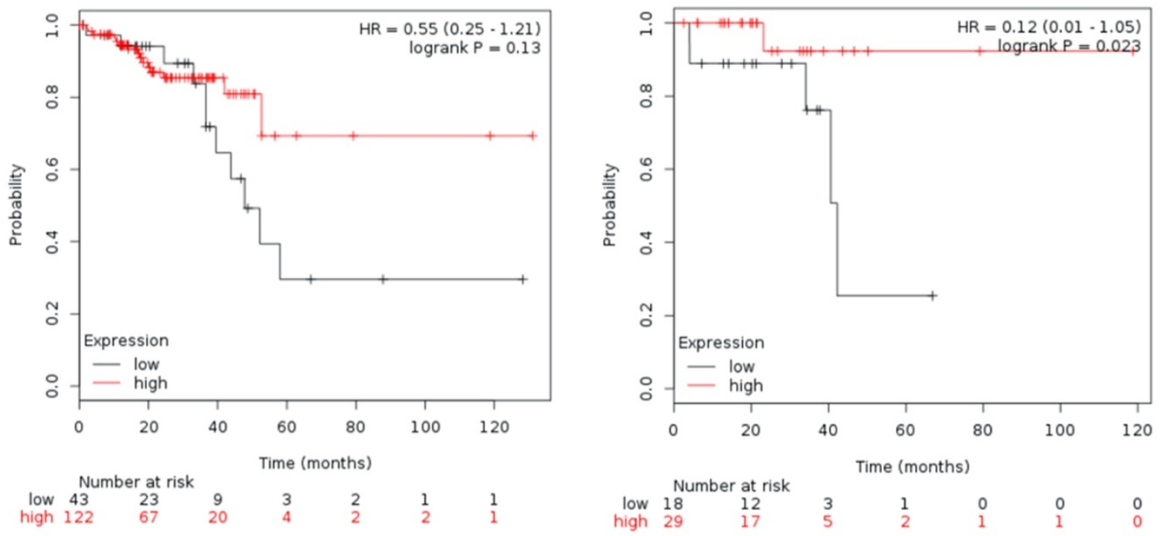


Figure 3.5 Survival Curve showing impact of EPLIN expression on survival of rectal adenocarcinoma patients. Data was collected from Kaplan-Meier Plotter(www.kmplot.com). Patients with high levels of EPLIN tended to have a longer overall (Left) and disease-free survival (right).

3.3.4 Analysis of The Cancer Genome Atlas (TCGA) database

In addition to exploring online GEO databases and our available clinical cohorts, analysis of TCGA database was also conducted. An earlier study has investigated the TCGA dataset of CRC and reported the relationship between EPLIN expression and CRC (Ohashi *et al.* 2017), which is in line with the results from our current study. In order to investigate the role of EPLIN in clinical CRC from a larger sample, an analysis of EPLIN expression in colon adenocarcinoma (COAD) TCGA dataset based on individual cancer stages via UALCAN platform (Chandrashekar *et al.* 2017) was performed (Figure 3.6). As Figure 3.6 shows, EPLIN expression within the normal group (n=41) was significantly higher than in each pathological stage (p<0.05 vs normal group). Although there was a trend that EPLIN expression decreased as CRC became more aggressive, no significant differences between stages were noticed.

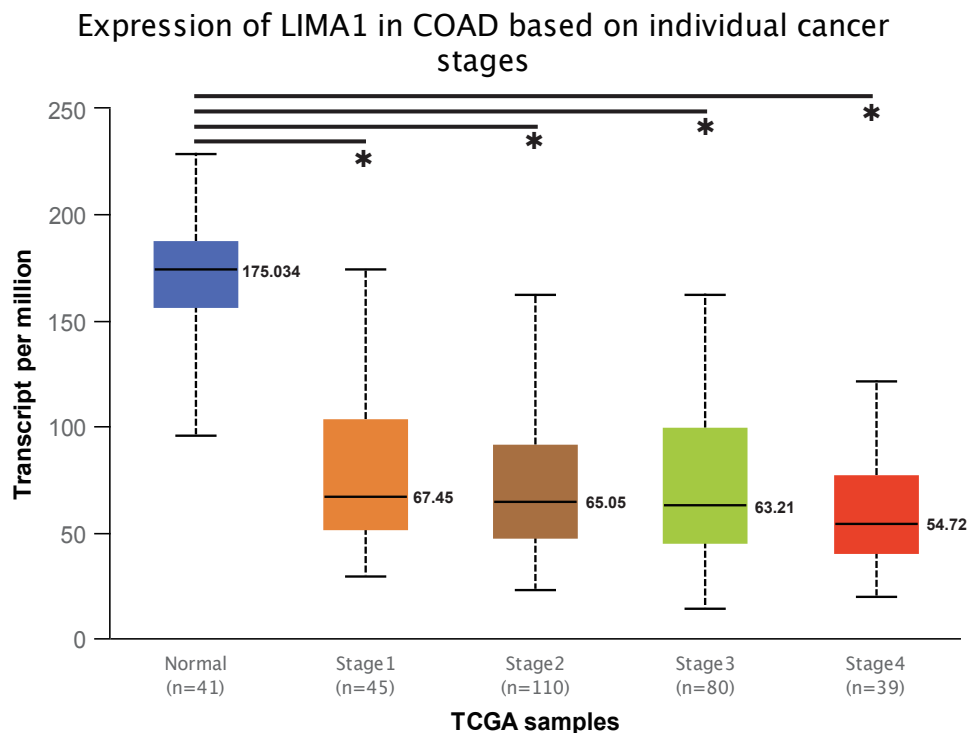


Figure 3.6 Expression of EPLIN (LIMA1) in COAD based on pathological stages. EPLIN expression was significantly higher in normal tissues compared to other pathological stages (* represents p<0.05). Non-significance was observed between each pathological stage. Box plot data shown is median expression, Q1 and Q3 values from each dataset, whiskers represent 5th and 95th percentiles with outliers shown. Box plot was obtained from UALCAN platform (Chandrashekar *et al.* 2017) (<http://ualcan.path.uab.edu/cgi-bin/TCGAExResultNew2.pl?genenam=LIMA1&ctype=COAD>), and modified with Adobe Illustrator.

In addition, we also accessed a TCGA colorectal adenocarcinoma (COADREAD) normalized mRNA sequence (data version 2016_01_28) from FIREBROWS, a service from Broad Institute of MIT & Harvard. The main focus of studying this sequence was to investigate the relationship between EPLIN and biomarkers that have been elucidated to be essential for development of CRC. Here we highlighted some vital players in CRC development which had a significant correlation with EPLIN (Figure 3.7). As bivariate correlation assay combined with Spearman's test demonstrates in Figure 3.7, EPLIN significantly correlated either positively or negatively with some signature biomarkers for CRC development. Among these genes, OCLN (occludin), CLDN3 (claudin 3), FN1 (fibronectin1), SNAI1, TWIST1, FOXC2 (Forkhead Box C2), NDRG1 (N-MYC downstream regulated gene 1) have been reported to be regulators of the EMT process (Pretzsch et al. 2019). APC, a classic tumour suppressor of CRC, takes part in the Wnt signalling pathway as well as β -catenin (Zhan et al. 2017), while BRAF participates in CRC development by supporting its progression (Carethers and Jung 2015). Loss of SMAD4 is associated with the TGF- β signalling pathway and EMT (Pretzsch et al. 2019) and PTEN is a tumour suppressor regulating the PI3K/AKT pathway (Papadatos-Pastos et al. 2015). Hence, this indicates a potential role of EPLIN in progression of CRC via EMT and signalling pathways.

Correlation between EPLIN and Genes in CRC TCGA dataset

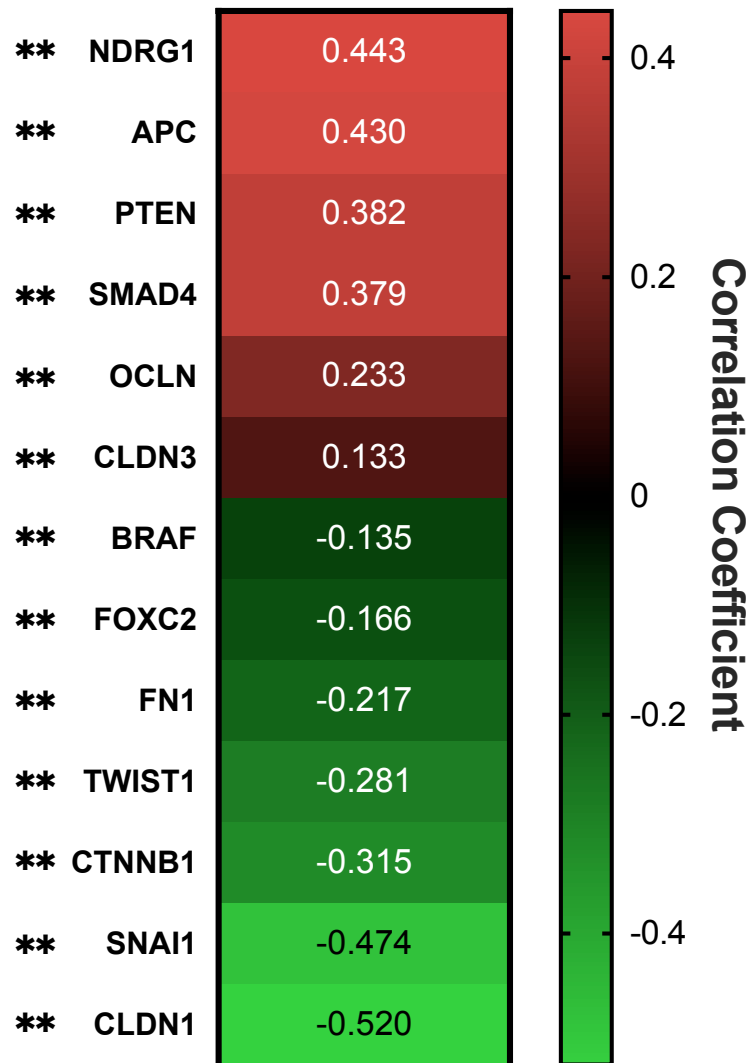


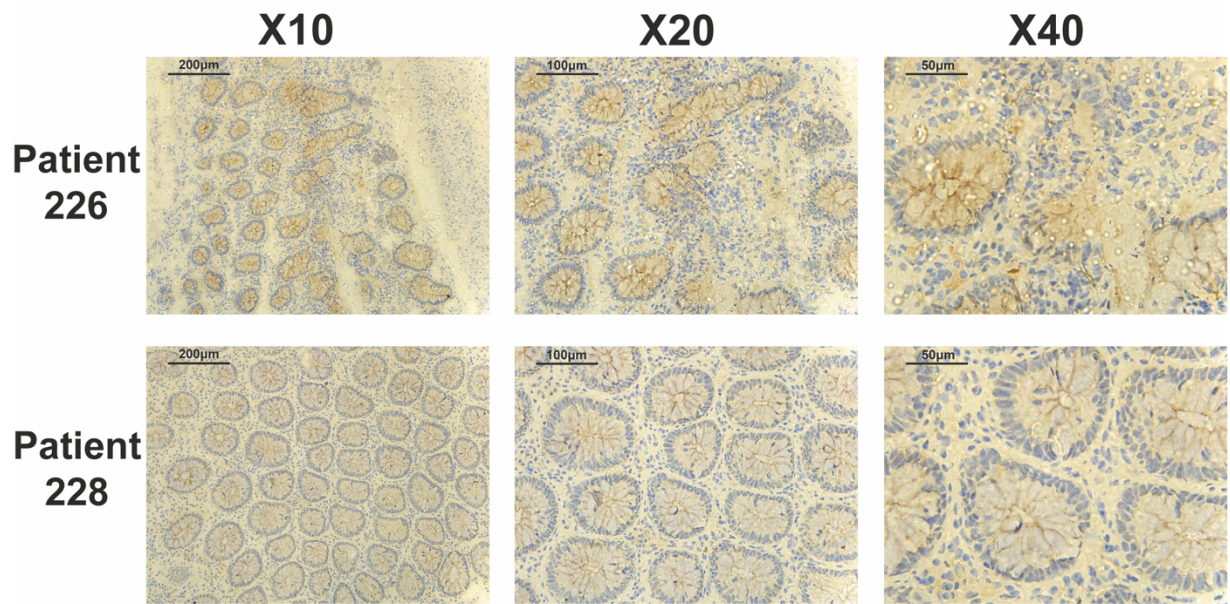
Figure 3.7 Correlation between EPLIN and genes in CRC TCGA dataset. EPLIN correlates with multiple genes that take part in EMT or signalling pathways which result in promoting progression of CRC. TCGA colorectal adenocarcinoma (COADREAD) normalized mRNA sequence (data version 2016_01_28) was obtained from FIREBROWS. Bivariate correlation assay combined with Spearman's test was performed by SPSS Statistics (version26), heatmap was drafted by GraphPad. ** represents $p < 0.01$

3.3.5 EPLIN protein expression in clinical CRC tissue

3.3.5.1 Immunohistochemical staining of EPLIN expression in clinical CRC

Apart from analysing EPLIN expression at the transcript level in two clinical cohorts and based on the data collected from online datasets, we also utilised preliminary data from a historic IHC analysis using our historical fresh frozen colorectal tissue sections, to explore its protein expression level from a set of samples previously available in our lab. However, the size of this IHC cohort was limited (tumour n=8; normal n=6). Therefore, the point of carrying out this set of samples was to give us an initial indication of expression profiles in normal and tumour tissues, rather than an extensive analysis. Preliminary data is shown in Figure 3.8 and indicated that the staining of EPLIN in normal tissues was stronger than in tumour tissues, though this initial observation required additional follow up and verification in larger, more detailed cohorts.

Normal



Cancer

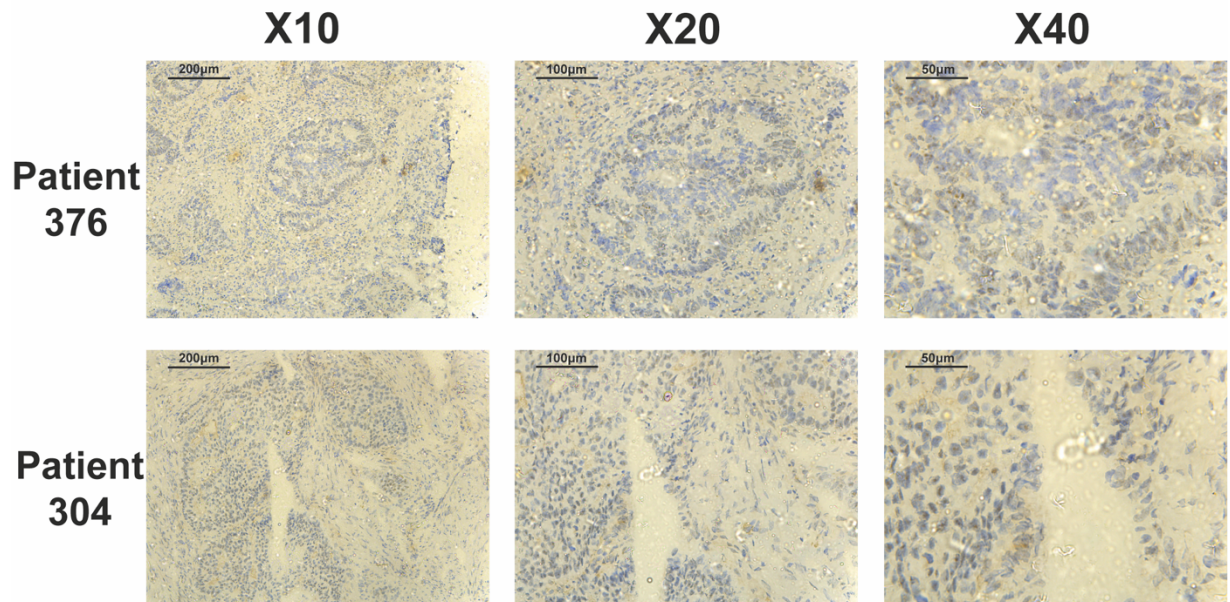


Figure 3.8 Preliminary IHC analysis of EPLIN expression in limited number of normal ($n = 6$ patients) and cancerous ($n = 8$ patients) sections obtained from the Cardiff clinical cohort. Representative images shown from 2 patients at multiple magnifications.

3.3.5.2 Tissue microarray (TMA)

As described above, EPLIN expression was shown to be stronger in normal tissues compared to tumour tissues in a small preliminary cohort. We subsequently purchased a TMA of colon cancer and normal colon tissue including pathology grade, TNM and clinical stage (n=216) (code:CO2161a) (Detail information of each core is given in Chapter 2.6) from US Biomax (supplied through, Insight Biotechnologies, Middlesex, UK). EPLIN antibody (sc136339) (2µg/ml) was used to detect EPLIN expression using IHC staining as described in Chapter 2.6. Scoring of staining intensity was conducted by 2 researchers according to the method described in Chapter 2.6. Analysis of scores in comparison to pathological information was shown in Table 3.3. Representative pictures of the TMA were shown in Figure 3.9 and clinicopathological information related to the presented sections has been summarised in Table 3.4.

EPLIN expression was generally weak or absent in a number of the tissues. However, as Table 3.4 shows, negative to weak staining accounted for 50% in the normal tissues (4 out of 4), while such staining accounted for 59.4% (104 out of 175) in the adenocarcinoma tissues and 80% (24 out of 30) in the mucinous adenocarcinoma tissues. However, there were no significant difference when the adenocarcinoma and the mucinous adenocarcinoma groups were respectively compared with the normal tissue group (both $p > 0.05$). Furthermore, EPLIN expression was generally weak or absent in a number of the tissues (Figure 3.9). However, normal tissues were observed to have some intense areas of staining in a number of the sections and a number of tumour tissues generally weaker intensity than the normal ones as shown in Figure 3.9. This indicated the tumour tissues had weaker staining of EPLIN than the normal tissues.

Intriguingly, we noticed that less aggressive CRC tissues tended to have stronger EPLIN expression than more aggressive ones. Over fifty five percent (55.6%) of the tissues in stage-1 (10 of 18) was negative to weak, while it was 60.9% in stage-2 (70 of 115), 68.6% in stage-3 (48 of 70) and 75% in stage-4 (3 of 4) (Table 3.4). However, the staining in these groups did not reach statistical significance ($p = 0.6085$). As Figure 3.9 demonstrates, EPLIN expression was overall stronger in less aggressive groups (stage I and stage IIB) rather than more aggressive ones (stage IIIC and stage IV). For instance, B12 (Stage I) and A15 (Stage IIB) had stronger EPLIN expression than B10 (Stage IIIC) and E9 (Stage IV). Additionally, in each pathological stage, we also assessed EPLIN expression in CRC tissues relating to histological differentiation namely, well differentiated (Grade 1), moderately differentiated (Grade 2) and poorly differentiated (Grade 3). According to World Health Organization

(WHO) Classification, Grade 1 CRC contains over 95% gland formation, gland formation between 50%-95% is rated as Grade 2, while Grade 3 represents less than 50% gland formation (Bosman et al. 2010; Barresi et al. 2015) which also reflects aggressiveness. As shown in Table 3.4, 51.5% of the tissues in Grade-1 group (17 of 33) was rated as negative to weak, while it accounted for 66.3% and 67.3% in Grade-2 (65 of 98) and Grade-3 group (37 of 55) respectively. Again, chi-square test did not reach statistical significance. Figure 3.9 shows some of the representative cases in that EPLIN expression appeared to decrease as the grade elevated. For example, Stage IIB group, A15 (Grade 1) had the strongest staining of EPLIN, whereas EPLIN expression in D18 (Grade 2) was stronger than J14 (Grade 3).

Taken together, although chi-square test analysis did not result in significance, a trend of a weaker EPLIN staining in tumour tissues than that in normal colorectal tissues was nonetheless observed. Interestingly, EPLIN expression in more aggressive CRC tissues tended to be weaker than less aggressive CRC. A larger tissue cohort is thus needed in order to fully classify the EPLIN protein expression profile in colorectal cancer.

Table 3.4 Analysis of EPLIN staining in the colorectal cancer TMA (CO2161a).

	Total Number	Intensity		Statistical significance	
		Negative to weak (0-1)	Moderate to strong (2-3)	Chi value	p
Pathology					
Normal tissue	8	4	4		
Adenocarcinoma	175	104	71	0.281	0.596 ^a
Mucinous adenocarcinoma	30	24	6	2.931	0.0869 ^a
Signet ring cell carcinoma	3	2	1	0.2444	0.621 ^a
Stage				1.830	0.6085 ^b
I	18	10	8		
II	115	70	45		
III	70	48	22		
IV	4	3	1		
Differentiation				2.227	0.3284 ^c
Grade1	33	17	15		
Grade2	98	65	33		
Grade3	55	37	18		

Note: ^aCompared with the normal tissue group; ^bOverall chi-square analysis among stage groups; ^cOverall chi-square analysis among differentiation groups.

Table 3.3 Information of representative samples of TMA (co2161a)

Position	Age	Sex	Organ/Anatomic Site	Pathology diagnosis	TNM	Grade	Stage	Type
A15	64	M	Colon	Adenocarcinoma	T4N0M0	1	IIB	Malignant
B10	71	M	Colon	Adenocarcinoma	T4N2M0	1	IIIC	Malignant
B12	49	M	Colon	Adenocarcinoma	T2N0M0	1	I	Malignant
C7	72	M	Colon	Adenocarcinoma	T2N0M0	-	I	Malignant
C16	43	F	Colon	Adenocarcinoma	T1N0M0	2	I	Malignant
D18	69	M	Colon	Adenocarcinoma	T4N0M0	2	IIB	Malignant
E9	51	F	Colon	Adenocarcinoma	T4N0M1	2	IV	Malignant
E17	69	M	Colon	Adenocarcinoma	T4N2M0	2	IIIC	Malignant
F2	72	M	Colon	Adenocarcinoma	T4N2M0	-	IIIC	Malignant
F9	66	F	Colon	Adenocarcinoma	T4N0M0	2	IIB	Malignant
J3	48	F	Colon	Adenocarcinoma	T4N1M1	3	IV	Malignant
J14	75	M	Colon	Adenocarcinoma	T4N0M0	3	IIB	Malignant
J15	50	M	Colon	Adenocarcinoma	T2N0M0	3	I	Malignant
K9	53	M	Colon	Adenocarcinoma	T3N2M1	3	IV	Malignant
K10	48	F	Colon	Adenocarcinoma	T4N2M0	3	IIIC	Malignant
L10	48	F	Colon	Signet ring cell carcinoma	T4N0M1	-	IV	Malignant
L12	40	M	Colon	Chronic colitis tissue	-	-	-	Normal
L13	21	F	Colon	Chronic colitis tissue	-	-	-	Normal
L14	28	M	Colon	Colon tissue	-	-	-	Normal
L17	45	M	Colon	Colon tissue	-	-	-	Normal

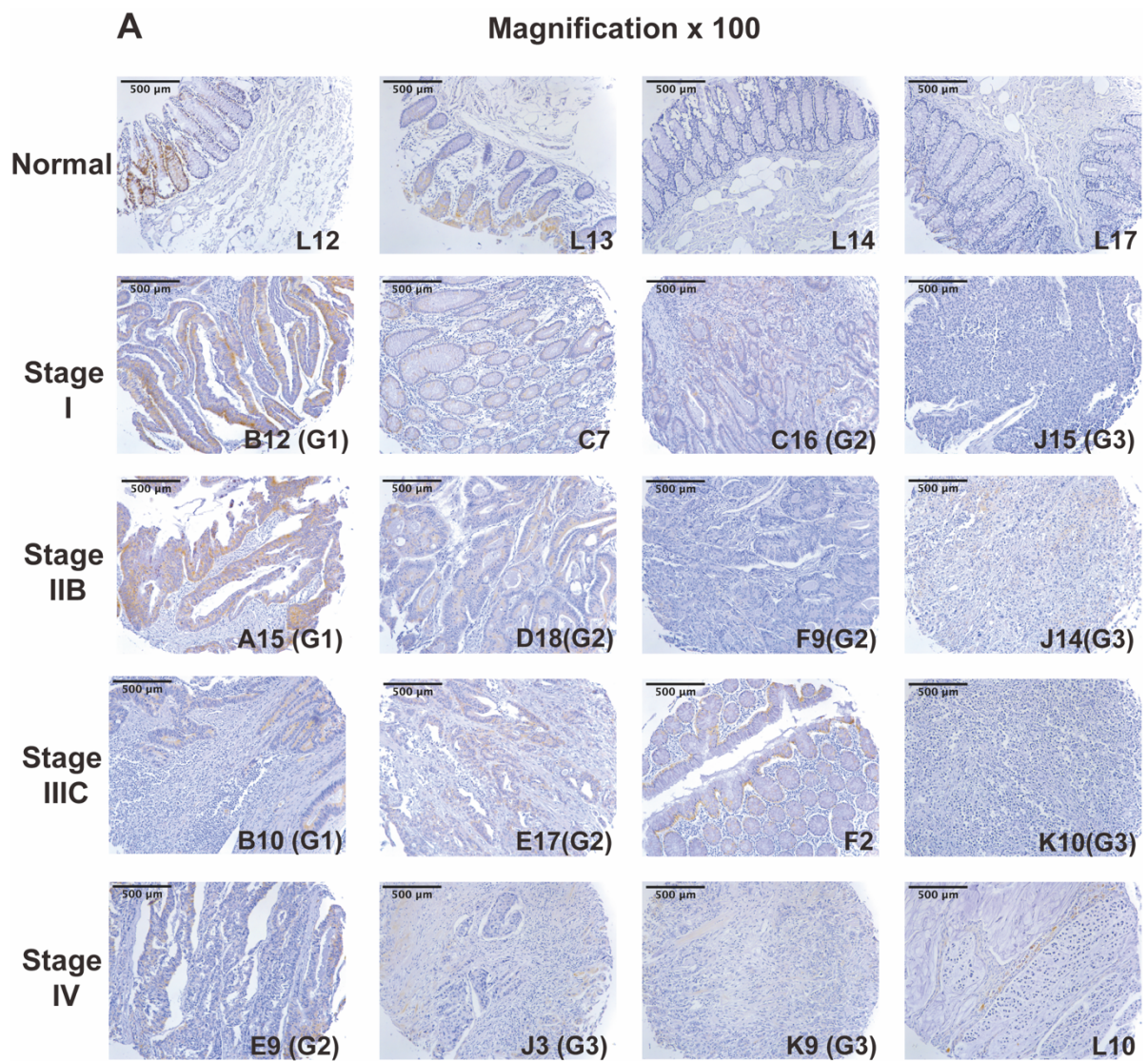


Figure 3.9 Representative pictures of TMA (co2161a). A. Photos were taken under a Lecia DM IRB Microscope (Leica GmbH, Bristol, UK) at X100 objective magnification. B. Photos were taken under a Lecia DM IRB Microscope (Leica GmbH, Bristol, UK) at X200 objective magnification. G1-3 stands for histological grade of CRC tissues.

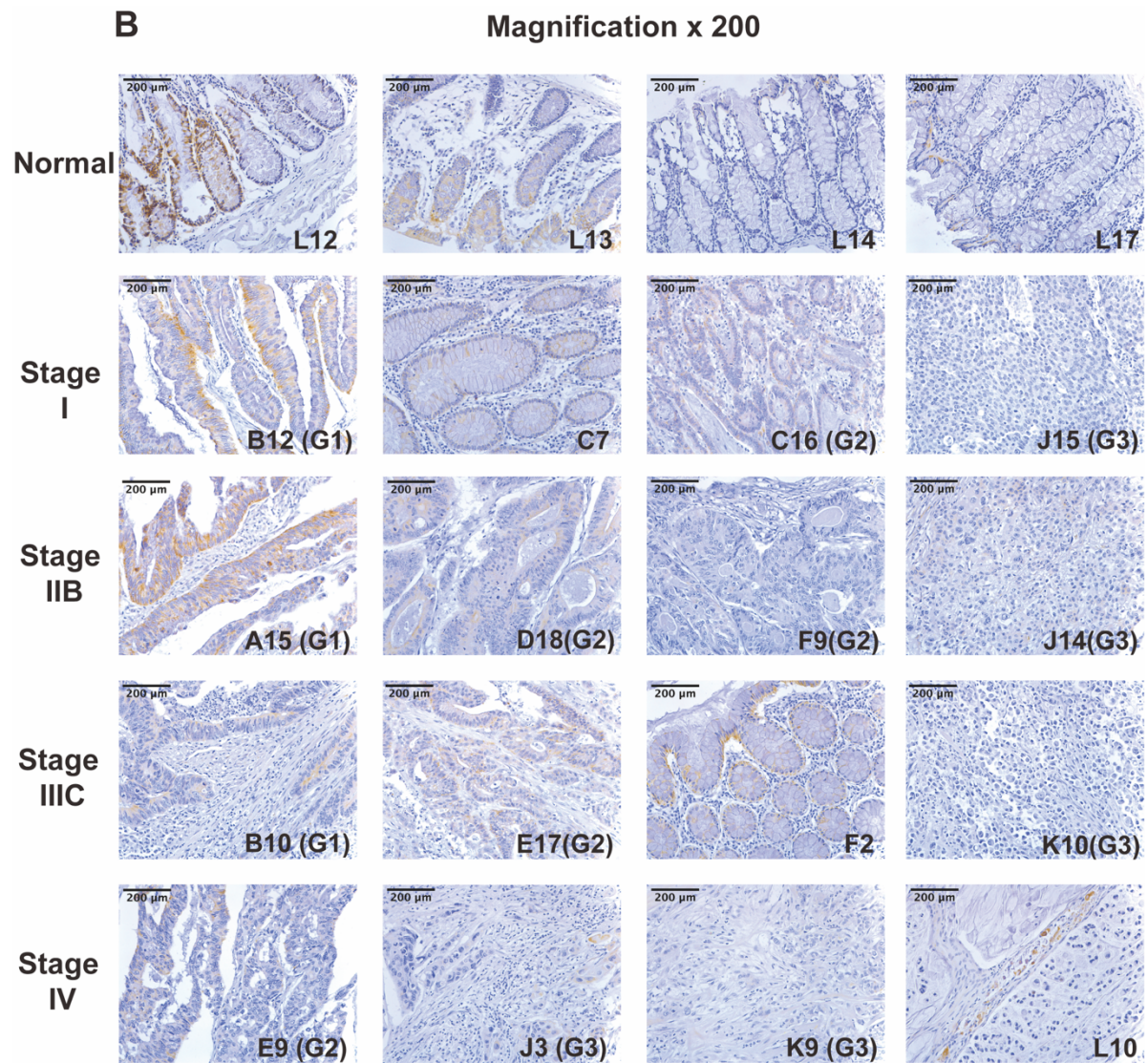


Figure 3.9 Representative pictures of TMA (co2161a) (Continue). A. Photos were taken under a Leica DM IRB Microscope (Leica GmbH, Bristol, UK) at X100 objective magnification. B. Photos were taken under a Leica DM IRB Microscope (Leica GmbH, Bristol, UK) at X200 objective magnification. G1-3 stands for histological grade of CRC tissues.

3.4 Discussion

Multiple studies have indicated that EPLIN acts as a tumour suppressor in a number of cancers, with lower levels of EPLIN related to metastasis and poor clinical outcomes. Early studies of EPLIN in CRC seem to be in line with EPLIN's role in other cancer types but these studies are limited, restricted by sample sizes. Therefore, we are curious about exploring EPLIN's clinical significance in larger sized cohorts, which will strengthen this potential protective role EPLIN plays in CRC.

Indeed, our initial results have demonstrated some interesting findings. We analysed the expression of EPLIN in three CRC GEO datasets, two CRC clinical cohorts, a TCGA online dataset and a TCGA mRNA sequence. Within these three GEO datasets, each contained three individual probes. EPLIN expression was found to be significantly downregulated in cancerous tissues compared to normal tissues, and its expression was also diminished in tumour tissues of early-onset CRC compared to healthy controls. However, there was no significant difference in EPLIN expression between primary tumour and metastatic tumours. We also analysed two clinical cohorts collected and prepared by our institute or collaborators, one from Cardiff (n=174) and another from China (n=416) by carrying out RNA extraction, reverse transcription and qPCR transcript analysis from collected samples. In the Cardiff cohort, the expression of EPLIN in tumour samples (n=94) was significantly lower than in normal samples (n=80) ($p < 0.001$). While in the China cohort, EPLIN expression was again significantly diminished in tumour samples (n=275) when compared to its expression in normal samples (n=141). There was no other significant finding ($p > 0.05$) based on pathological characteristics in either cohort. Interestingly, in the Cardiff cohort, expression of EPLIN showed a positive correlation with TNM stage and it nearly reached statistical significance ($p = 0.051$), which is somewhat opposite to the proposed tumour suppressor role of EPLIN. One of the reasons for that might be the small size of the sample. Only 4 samples were characterized as TNM1 and 6 samples as TNM4. While in the China cohort, there was no significant difference among TNM stage, and we could not find any significant connection between expression of EPLIN in primary tumour nor in metastatic cancer. Our analysis from the GEO datasets and clinical cohorts shared the same trend, highlighting significant reductions of EPLIN expression in tumour samples against normal samples, and this finding is in line with previous findings in CRC by Lee et al. and Ohashi et al. (Lee et al. 2006; Ohashi et al. 2017) and previous studies in multiple cancers (Maul and Chang 1999; Maul et al. 2001; Jiang et al. 2008; Sanders et al. 2010; Zhang et al. 2011; Liu et al. 2012a; Collins et al. 2015; Liu et al. 2016; Collins et al. 2018). Taken together, this strongly implicates that EPLIN plays a role in carcinogenesis of CRC and further supports the observed loss of

EPLIN in cancer. EPLIN was found to be associated with growth, proliferation, invasion and migration of cancer cells which are related to metastasis in several cancers (Jiang et al. 2008; Sanders et al. 2011; Zhang et al. 2011; Liu et al. 2016; Collins et al. 2018). Interestingly, our cohorts did not indicate significant expression differences in patients who had metastasis compared to those who did not. A similar trend was seen in the GEO data set, comparing EPLIN expression between primary and metastatic tumours, again showing no significant differences. To gain more information about the relationship between EPLIN and metastatic CRC from a larger size of sample, a COAD TCGA dataset was also explored on UALCAN platform, although a trend of decreasing EPLIN expression in combination of pathological stages was observed, no statistical significance was shown. Interestingly, based on these clinical data, EPLIN seems to have little connection with metastatic CRC, an analysis of a CRC TCGA mRNA sequence offers us a brighter picture of the potential role EPLIN plays in CRC progression, especially in metastasis. We performed a bivariate correlation assay combined with Spearman's test to try to pick up clues about EPLIN's role in CRC development. Several essential players were investigated to show correlation with EPLIN. NDRG1, CLDN3, OCLN, FOXC2, FN1, TWIST1, CLDN1, SNAI1 and CTNNB1 have been reported to associate with EMT, with SNAI1, TWIST1, APC, PTEN also reported to be associated with not only activation of signalling pathways that result in developing CRC, but also poor clinical outcome (Chen et al. 2014; Papadatos-Pastos et al. 2015; Zhan et al. 2017; Pretzsch et al. 2019). Therefore, this emphasizes a potential role of EPLIN in promoting CRC development. Indeed, recent studies also implicate that EPLIN participates in CRC and promotes its invasiveness. Ohashi *et al.*, (2017), analysed TCGA datasets to show that a low level of EPLIN is related to mutant p53, which is one of the key mutant players, especially in more aggressive CRC (Ohashi et al. 2017). Another study demonstrated low levels of EPLIN not only correlate with high levels of DNp73, a mutant form of p73 that inhibits p73 to promote cancer development, but is also related to metastatic CRC (Steder et al. 2013). These implicate a possible mechanistic link between the p53 family and EPLIN in CRC, since p53 mutation has been demonstrated to be strongly associated with aggressive CRC (Li et al. 2015b), thus supporting the idea that EPLIN may play an essential role in promotion of CRC.

Moreover, previous *in vitro* and *in vivo* work has suggested altered EPLIN expression, particularly the alpha isoform is associated with changes in traits characteristic of metastatic potential such as migration, invasion and EMT in a number of different cancers (Jiang et al. 2008; Zhang et al. 2011; Liu et al. 2012a; Liu et al. 2016). Similarly, with the use of other datasets, several studies have implicated altered expression is associated with metastatic potential in clinical analysis of other cancer types, such as prostate cancer (Zhang et al.

2011; Collins et al. 2018). Furthermore, studies focused on EPLIN and clinical CRC appear to be in line with our clinical analysis and findings in other types of cancer. Analysis of TCGA mRNA sequence also demonstrates EPLIN associates with other players which have impacts on EMT, signalling pathway activation, as well as poor clinical outcome. Hence, this observation from clinical cohorts may be due to sample size or may represent a cancer specific trend. Further information with regard to this will be investigated in the later part of the study. Interestingly, survival curves from the Cardiff cohort and an independent dataset from KMplot have implicated that high level of EPLIN is associated with DFS and OS. However, data from the Cardiff CRC cohort did not reach statistical significance, while DFS data from KMplot was found to be significant, but not that for OS. Although the dataset from KMplot is rectal adenocarcinoma, it still partly implicates the influences on CRC. This finding indicates a possible role of EPLIN in influencing patients' clinical outcome and prognosis in CRC, as it has previously been revealed in other types of cancer, such as breast cancer (Jiang et al. 2008) and further highlights the potential usefulness of EPLIN in a clinical capacity.

In order to understand more about EPLIN's role in clinical CRC, we conducted IHC analysis of a limited Cardiff cohort (n=14) available in our lab and supplemented with a TMA containing additional samples (n=216). The TMA contained a small number of sections from metastatic patients and a larger number of those with nodal involvement. In the Cardiff cohort, normal tissues were observed to have a stronger expression of EPLIN than tumour tissues. While exploring our TMA samples, some interesting findings were noted. In worse clinical stages, EPLIN expression was generally stronger than in less aggressive stages. Also, EPLIN expression was related to tumour differentiation, with EPLIN expression in well-differentiated sections appearing to be stronger than in poorly differentiated sections. Hence, this early analysis may indicate EPLIN is associated with metastatic CRC and agrees with our findings, obtained through analysing the TCGA cohort and results from studies in other tumour types. The TMA analysis presented some interesting findings but also had a number of limitations. For example, during such analysis it has been noted that pathological appearances of some samples did not match with labelled information provided by the manufacturer (e.g.F2). This may potentially have arisen due to repeated sectioning of the company or limitations to tumour burden of the original sample. However, it highlights the need for future, consultation with clinical pathologists to verify clinical information and fully explore the significance of EPLIN throughout this TMA. Despite this, the data gained from the analysis demonstrates EPLIN expression in tumour tissues was weaker than it in healthy tissues and its expression in more aggressive CRC tissues was weaker than less aggressive

CRC. Therefore, we are in the process of seeking pathologist support before finalising analysis.

In conclusion, downregulation of EPLIN contributes to the carcinogenesis of CRC and poor clinical outcomes of patients. EPLIN also appears to be associated with the metastasis of CRC, to achieve this, EPLIN possibly interacts with other potential partners. Our clinical findings support an important role for EPLIN in CRC development and progression and further work within this study will dig deeper to investigate the role of EPLIN in cellular functions and the mechanisms behind it.

Chapter-4

Functional significance of EPLIN in Colorectal Cancer (CRC) cells

4.1 Introduction

From the preceding chapters, it is clear that EPLIN has an important role in multiple cancer types and has a clinical link to CRC. Analysis of clinical cohorts, online datasets and TMA suggested that the dysregulation of EPLIN in transcript and protein levels may lead to the progression of CRC, as well as poor clinical outcomes.

Metastasis in CRC is one of the main contributors to the cause of death from CRC. Metastases originate at the original tumour site, where cancer cells proliferate and gain the potential to dissociate from each other, invade through the matrix to surrounding environments (local invasion), propagate to adjacent tissues and distant organs via circulatory systems and metastatic cascades then establish in distant sites to regrow. In this aggressive process, dysfunction or dysregulation of multiple tumour protectors and tumour suppressors such as APC, BRAF and p53, activate certain signalling pathways to achieve proliferation, migration and invasion to promote metastasis (Pretzsch et al. 2019). The focus of this study is EPLIN which is well-established as a tumour suppressor in multiple cancers but not yet in CRC (Zhang et al. 2011; Zhang et al. 2013). The analysis of their clinical CRC cohorts and online datasets does not keep in line with the findings that EPLIN is downregulated in metastasis of multiple cancers, when compared to primary tumours including some reports on CRC (Jiang et al. 2008; Sanders et al. 2011; Liu et al. 2012a; Steder et al. 2013; Collins et al. 2018). This may be attributable to a few factors including the nature of the samples, the nature of tests (namely protein versus transcript), the technology platform (namely gene chip, QPCR vs RNAseq), and the size of the datasets.

EPLIN has been shown to have a link with EMT via certain signalling pathways (Zhang et al. 2011; Steder et al. 2013; Zhitnyak et al. 2020) and diminished levels of EPLIN are related to several established regulators of cancerous development, such as ERK, mutant p53 and DNp73 in many types of cancer including CRC (Steder et al. 2013; Ohashi et al. 2017). It would suggest that EPLIN is involved in cancer development and progression and that there is need to further explore how EPLIN impacts on the biological functions of colorectal cancer cells, unknown in the past, and how the cellular impact may contribute to the clinical development of this important cancer type. This study aimed to develop CRC cancer cell models with different EPLIN expression profile in order to seek further scientific evidence and support for the role of EPLIN in colorectal cancer.

EPLIN has two isoforms, EPLIN α and EPLIN β . It was believed that the α subtype is the likely main contributor to its role as a tumour suppressor. EPLIN has been demonstrated to be a

negative controller of functional activities in multiple cancer cells including proliferation, migration and invasion which allows tumours to gain aggressive potential to migrate.

EPLIN negatively regulates growth of cancer cells including breast cancer, prostate cancer, oesophageal cancer, lung cancer and ovarian cancer. With an aggressive MDA-MB-231 breast cancer cell line, Jiang *et al.*, (2008), established that the cell line, when overexpressing EPLIN α , had a reduced rate of proliferation *in vitro* and a reduced tumour growth rate *in vivo*, when compared with control groups (Jiang et al. 2008). Overexpressing EPLIN α in PC-3 cells, a prostate cancer cell line, also reduced cell growth (Sanders et al. 2011; Collins et al. 2018). Studies in this laboratory have further revealed a similar impact on oesophageal cancer, pulmonary cancer and ovarian cancer (Liu et al. 2012b,a; Liu et al. 2016).

EPLIN has also been shown to be a negative regulator of cellular invasion in breast cancer, prostate cancer, melanoma cancer, oesophageal cancer and ovarian cancer. Invasive ability was reduced in MDA-MB-231 cells following overexpression of EPLIN α (Jiang et al. 2008). Knocking down EPLIN in MCF-7 cells lead to increasing invasion (Zhang et al. 2011). Multiple prostate cancer cell models to overexpress EPLIN or knock down EPLIN in PC-3, LNCaP and ARCaP_E cells showed that EPLIN has a negative impact on invasion of prostate cancers (Sanders et al. 2011; Zhang et al. 2011; Collins et al. 2018). Stederet *al.*, (2013), reported that downregulation of EPLIN lead to deeper Breslow depth (>4 mm) in melanoma which implicates enhanced invasion. The authors also revealed that EPLIN negatively regulated invasion of melanoma cells in their EPLIN transfected cell models (Steder et al. 2013). This regulation trait is also reported in ovarian cancer and oesophageal cancer as knocking down EPLIN in SKOV3 and COV504 cells lead to enhanced invasion (Liu et al. 2016), while forced expressing EPLIN α had the opposite impact on KYSE150 cells (Liu et al. 2012a).

EPLIN negatively mediates migration of cancer cells including breast cancer, prostate cancer pulmonary cancer and ovarian cancer. By forced expression of EPLIN α in MDA-MB-231 cells and performing ECIS assay, migration ability was weakened when compared with the control groups and this impact was counteracted after inhibiting ERK (Jiang et al. 2008). Migration was enhanced after knocking down EPLIN in MCF-7, PC-3, LNCaP and ARCaP_E cells conducting wound-healing assays compared with control groups (Zhang et al. 2011). Collins *et al.*, (2018), demonstrated that overexpression of EPLIN suppressed migration in PC-3 cells (Collins et al. 2018). When it comes to lung cancer and ovarian cancer, EPLIN

was also demonstrated to regulate cellular migration negatively (Liu et al. 2012b; Liu et al. 2016).

Unexpectedly, given the well-established influence of EPLIN on cellular functions in some cancer types, its functional implications on CRC cells have not been explored in the past and the overall mechanisms by which EPLIN may regulate the functions of colorectal cancer cells remain unknown. In this chapter, I first successfully established experimental CRC cells models by either overexpressing EPLIN α or knocking down total EPLIN. These cell models were used to carry out several functional assays to probe EPLIN's functional impacts including growth, adhesion, invasion and migration and further used to conduct mechanism studies, including cell signalling and drug responses of the cancer cells, to be presented in later chapters.

4.2 Methods

4.2.1 cell culturing

Please refer to Chapter 2.2.2.

4.2.2 Thiazolyl Blue Tetrazolium Bromide (MTT) based Killing curve

Please refer to Chapter 2.2.6.

4.2.3 Transfection

For Stuffer300 and overexpressed EPLIN plasmids preparation, please refer to Chapter 2.2.4.1. Electroporation-based transfection please refer to Chapter 2.2.4.2. For transfection by using shRNA-based technique, please refer to Chapter 2.2.4.3.

4.2.4 MTT cells growth assay

Please refer to Chapter 2.2.7.

4.2.5 Matrigel cells adhesion assay

Please refer to Chapter 2.2.8.

4.2.6 ECIS based cells migration assay

Please refer to Chapter 2.2.11.

4.2.7 Matrigel cells invasion assay

Please refer to Chapter 2.2.9.

4.3 Results

4.3.1 EPLIN expression screening in CRC cell lines

All 4 colorectal cancer cell lines were cultured from a low passage up to passage 18, and RNA extractions were performed at different passages of all cell lines. After reverse transcription, PCR & qPCR was conducted to explore EPLIN transcript expression in these cell lines. Three different sets of RNA samples were collected at different passage in this study and a representative PCR screen is shown in Figure 4.1 A1. Following each screen of the individual sets, EPLIN and EPLIN β expression was quantified using image J (National Institutes of Health, USA) and semi-quantification band densitometry, normalised against GAPDH, combined to display mean percentage HRT-18 (which was taken as 100%) expression across the replicates (Figure 4.1 A2 and A3). Data was analysed in Excel and GraphPad. The expression of EPLIN in RKO was found to be the weakest among these 4 cell lines, while strongest expression was seen in HRT18 and HT-115 cell lines. The expression of EPLIN in RKO was approximately 41% of HRT-18's ($p < 0.05$) and the expression of EPLIN β in RKO was less than 10% of HRT18's ($p < 0.001$). In HT-115, the expression of EPLIN was around 99% of HRT-18 while the expression of EPLIN β was near 93% of HRT-18, with neither result reaching statistical significance ($p > 0.05$). In CaCo-2, EPLIN β 's expression was approximately 52% of HRT-18 ($p < 0.05$), while EPLIN's was around 70% of HRT-18 without statistical significance ($p > 0.05$). Quantitative PCR was then performed to verify the expression profiles of EPLIN in these CRC cell lines (Figure 4.1 B). Three different sets of cDNA of CRC wild type-cell lines were used, data was normalised by GAPDH and analysed in Excel and GraphPad. Similar expression profiles were seen in the qPCR analysis as in the PCR analysis. The expression of EPLIN in HRT-18 was then set as 100% and a One-way ANOVA test was performed to check the statistical significances among the four cell lines. The expression of EPLIN in RKO was approximately 30% of its expression in HRT-18 and this was found to be statistically significant ($p < 0.05$).

EPLIN protein has two isoforms, a 600 aa EPLIN α and EPLIN β which has an additional 160 aa. The molecular weight of EPLIN α is 90kDa while EPLIN β is 110 kDa (Maul and Chang 1999). Due to the similarities, it is difficult to distinguish the alpha isoform from the beta isoform using PCR. Therefore, western blot was carried out to detect the expression of EPLIN α and EPLIN β at the protein level, where a clearer distinction can be made between

the two isoforms. Protein bands were analysed using Image J and plotted using GraphPad (Figure 4.2).

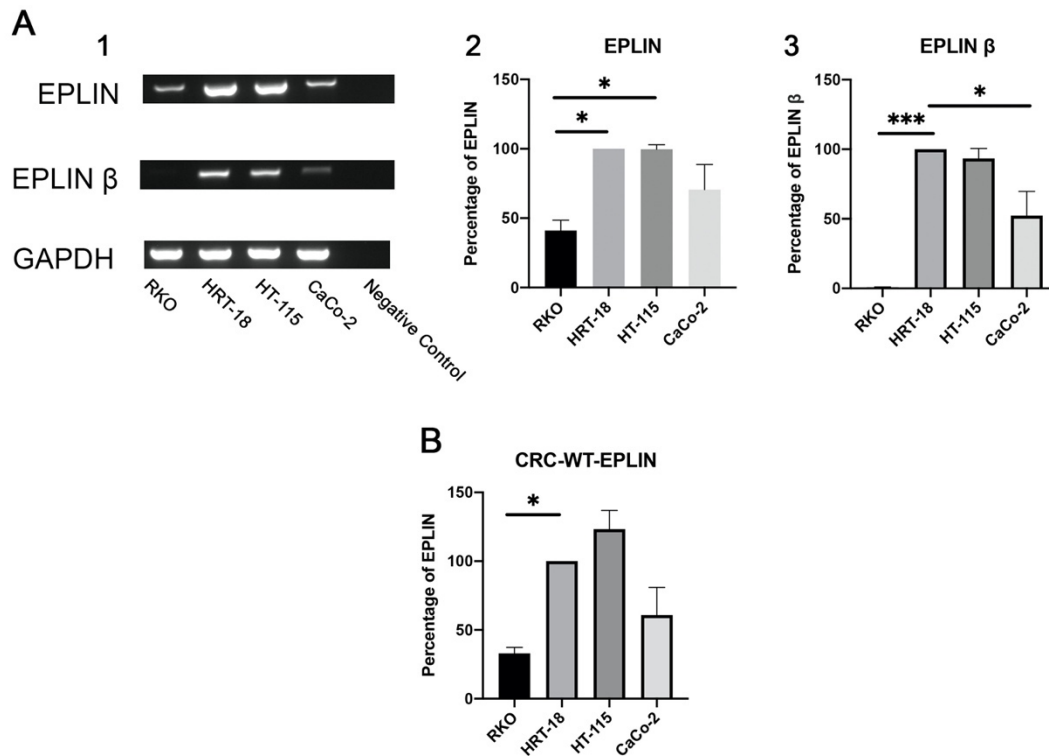


Figure 4.1 PCR and qPCR Screenings of CRC-WT-Cell Lines. (A) 1. Representative images of PCR screening of wild type CRC cells (RKO, HRT-18, HT-115 & CaCo-2). 2&3. Data from three different sets of samples were combined for analysis and the expressions of HRT-18 were regarded as 100% for comparison. Data shown is mean + SEM, n=3. One-way ANOVA Tests were carried out to show significances between cell lines. (B) The expressions of HRT-18 were set to 100% and the rest of the samples compared to it. Data shows mean + SEM. N=3. * represents $p < 0.05$, *** represents $p < 0.001$.

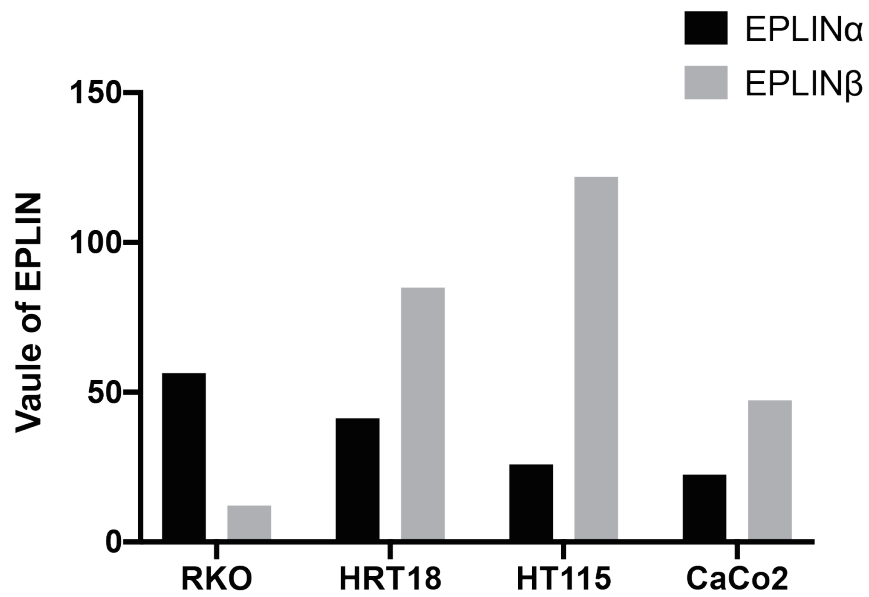
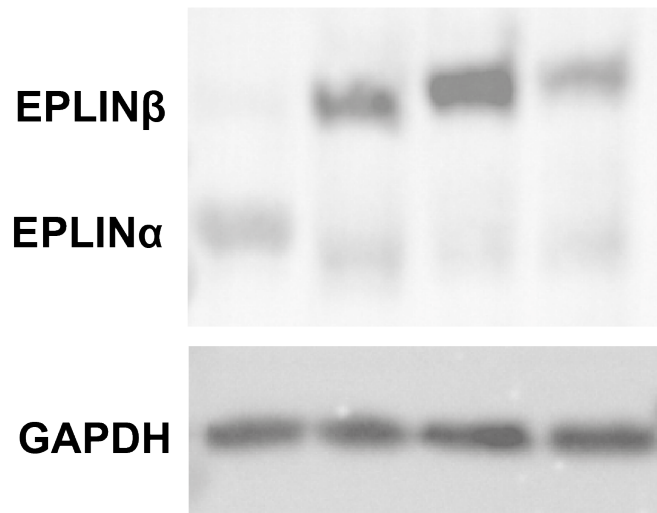


Figure 4.2 Western Blot analysis of EPLIN expression in CRC Wild Type Cell lines. Western blot was performed to explore EPLIN protein expression in the CRC cell lines. Image (top) obtained using G-BOX (Syngene). Integrated density of protein bands was determined using Image J.

4.3.2 Transfection of CRC Cell lines

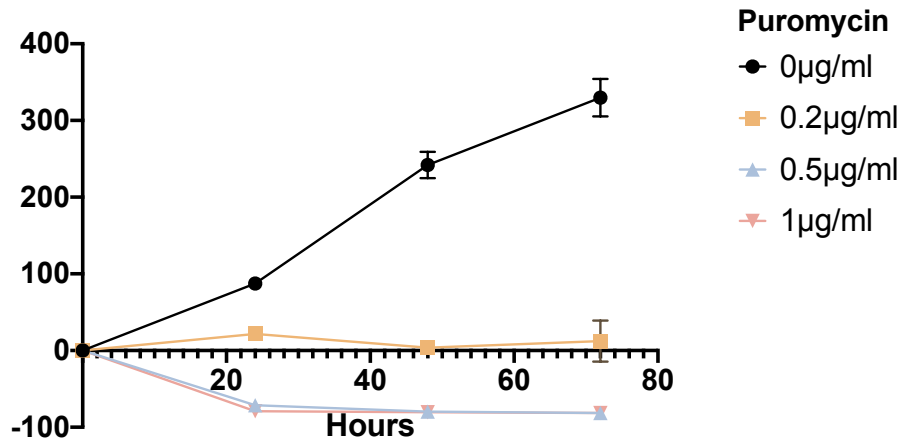
From the EPLIN expression profiling in the colorectal cancer cell lines, all cell lines were positive for EPLIN α while RKO was almost negative for expressing EPLIN β . RKO, an epithelial cell line that originated from poorly differentiated colon carcinoma, and HRT18, an epithelial adenocarcinoma cell line, were chosen to establish cell models by genetically manipulating EPLIN expression.

4.3.2.1 Killing Curve and Transfection Process

To establish the most appropriate concentration of the antibiotics used to select the transfected cells, killing curves were carried out to identify appropriate puromycin selection and maintenance conditions for the manipulated cell lines, after transfection was performed. As shown in Figure 4.3 and Table 4.1&2, the experimental killing lasted for 72 hours after different concentrations of puromycin were added. After treating with puromycin for 24 hours, the number of viable cells in 1 μ g/ml of puromycin in RKO was decreased around 79%. At the 72-hour time point, the number of viable cells in 0.5 μ g/ml of puromycin in RKO was decreased by approximately 81% while 2 μ g/ml of puromycin in HRT-18 decreased around 80% of cells compared to nil puromycin control group. Therefore, the concentrations of puromycin chosen for selection after transfection in RKO cells lines was 0.5 μ g/ml while it was 2 μ g/ml for the HRT-18 cells. Upon establishing the concentrations of puromycin for selection, it was decided that the maintenance medium for the stably transfected cells would use puromycin at a concentration of 0.2 μ g/ml.

With the two cell lines, RKO and HRT-18, selected to create EPLIN over-expressed and EPLIN knockdown models respectively, two different methods of transfections were performed. For RKO, electroporation was carried out to transfect the cells with the expression plasmid which contained the full coding sequence for human EPLIN α or a control plasmid Stuffer 300 (VectorBuilder, Chicago, IL, USA). On the other hand, shRNA-EPLIN or control plasmid (Insight Biotechnologies Ltd., Middlesex, UK) were transfected into HRT-18 cells by way of chemical transfection using Plasmid Transfection Reagent (SC-108061, Santa Curz Biotechnologies Ltd., (CA, USA), purchased via Insight Biotechnologies Ltd., Middlesex, UK) in accordance with the manufacturers' guidance. Following transfection, cells were subject to intense selection using Puromycin at the pre-determined concentrations, followed by subjecting the cells to the maintenance medium (with 0.2 μ g/ml puromycin). This allowed the surviving cells to repopulate to sufficient number for the subsequent verification of efficacy of the knockdown or over-expression.

RKO cells growth



HRT18 cells growth

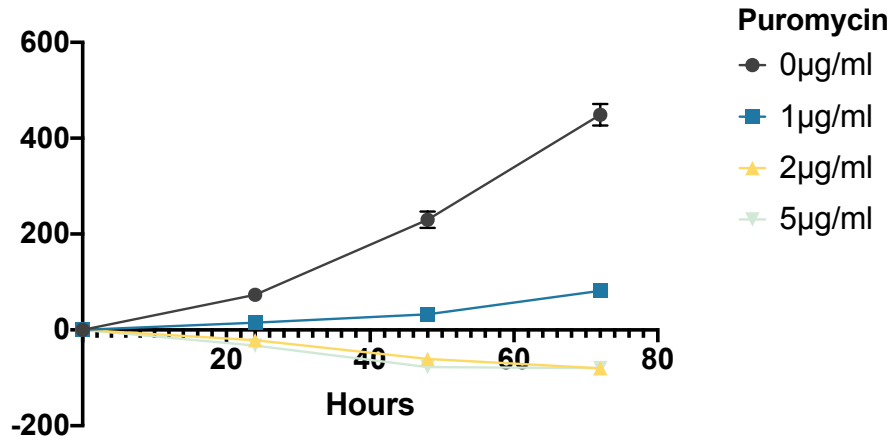


Figure 4.3 Killing Curve of RKO (top) & HRT-18 (bottom) Cells Lines. Killing Curve was performed in these two cell lines for up to 72 hours. Data was analysed and charts were drafted by Excel, mean +/- SD, 6 repeated wells for each concentration.

Table 4.1 Percentage of RKO cells growth against reference plater (data shown as mean, n=6)

	0 Hour	24 Hours	48 Hours	72Hours
0ug/ml	0	87.33032%	241.9934%	329.8402%
0.2ug/ml	0	21.65939%	3.856165%	12.32932%
0.5ug/ml	0	-71.2249%	-79.7221%	-81.4039%
1ug/ml	0	-79.2176%	-80.2907%	-81.4279%

Table 4.2 Percentage of HRT cells growth against reference plater (data shown as mean, n=6)

	0 Hour	24 Hours	48 Hours	72 Hours
0ug/ml	0	73.18327%	229.9831	448.9874%
1ug/ml	0	14.99781%	32.68543	48.6833%
2ug/ml	0	-21.5688%	-60.7624	-80.1649%
5ug/ml	0	-32.6165%	-77.635%	-79.7981%

4.3.2.2 Confirmation of over-expression of EPLIN α in RKO cell lines.

As described in Chapter 2.2.4.1, both control and expression plasmids carry sequences of EGFP/Puro sequences that serves as a fluorescence marker for transfection. As Figure 4.4 shows, both RKO cell models expressed clear and strong GFP fluorescence signals to indicate the success of transfection.

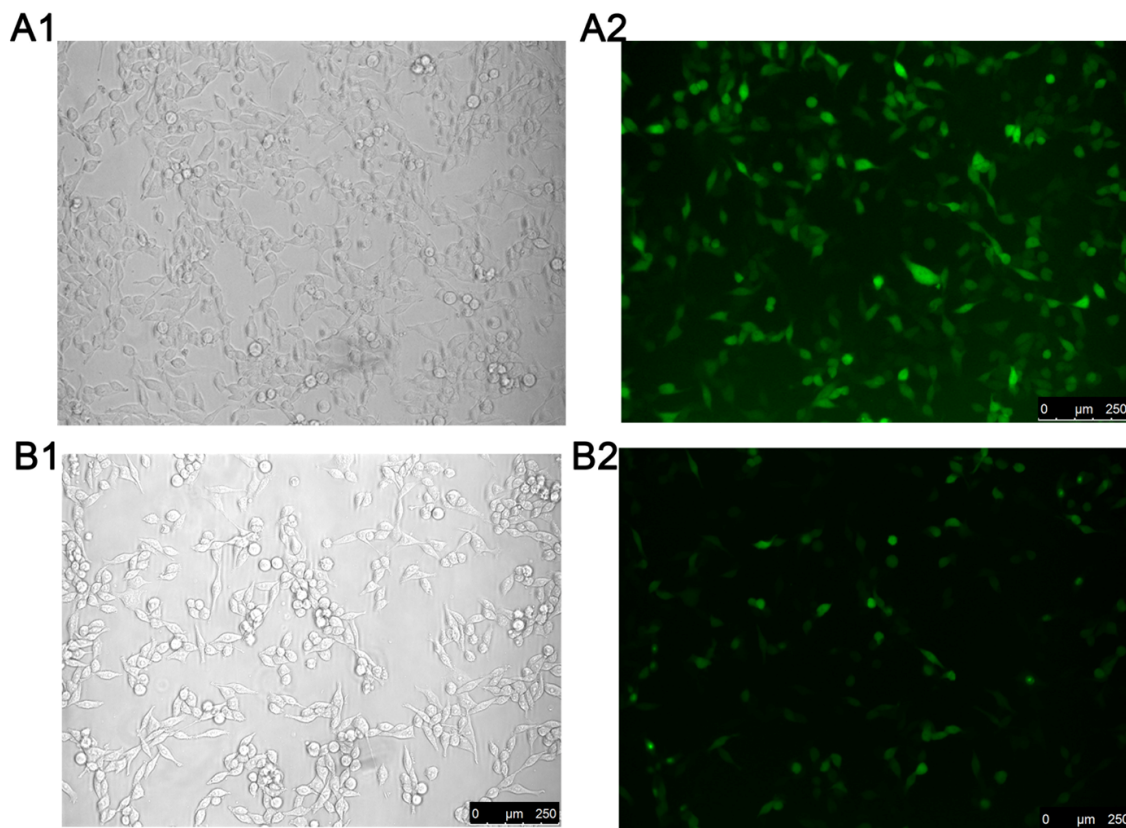


Figure 4.4 GFP fluorescence signals indicate successful transfection in RKO cell lines. (A1) Bright field picture of RKO-Stuffer Control model. (A2) Fluorescence images of RKO-Stuffer Control model show strong GFP fluorescence signals. (B1) Bright field picture of RKO-OE-EPLIN model. (B2) Fluorescence image of RKO-OE-EPLIN model that expressed clear GFP fluorescence signal. Photos were taken at 800ms using LEICA DFC3000 G microscope with Kubler CODIX system (Leica DMB, Milton Keynes, UK).

In addition to checking the fluorescence signals, transcript and protein expression levels of EPLIN in RKO cellular models were investigated to determine the efficiency of the transfections. To achieve this, qPCR and Western blotting were carried out (Figure 4.5).

As a representative qPCR data set shown in Figure 4.5 A, the expression of total EPLIN of RKO EPLIN α overexpression cell lines (RKO-OE-EPLIN) was higher than its in stuffer control group significantly ($p=0.0072$).

Western blot was also carried out to detect the expression of EPLIN α and EPLIN β in RKO stuffer control and RKO-OE-EPLIN cells at the protein level and to support the transcript verification experiments. Three different sets of samples were run and a representative replicate shown in Figure 4.5 B1. The bands of EPLIN β were almost absent and the band of EPLIN α in the RKO-OE-EPLIN sample was greatly enhanced compared to that in stuffer control cells. A column table was drafted after data was quantified in Image J, normalised by GAPDH and analysed by Excel and GraphPad (Figure 4.5 B2). A similar trend was shown as in the qPCR analyses and it could be observed that the expression of EPLIN α was stronger in the EPLIN α overexpression samples compared to control group significantly ($p=0.0064$). Therefore, a transfected model which stably overexpressed EPLIN α had been established for use in the coming stage of this study.

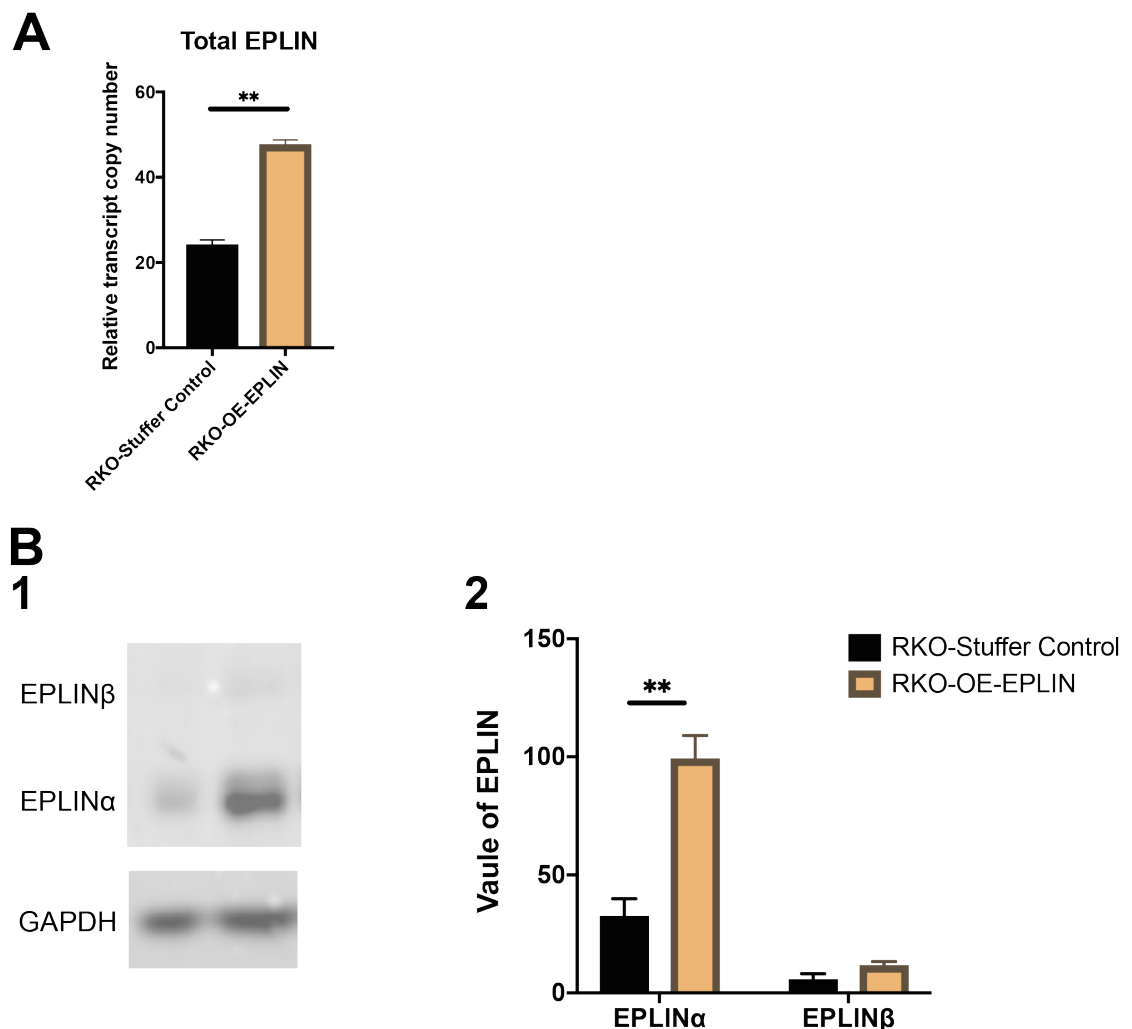


Figure 4.5 qPCR and western blot screening of EPLIN in RKO EPLIN-Overexpression (OE-EPLIN) Cells compared to RKO Stuffer control Cells. (A) Selected qPCR screening of total EPLIN's expression in RKO stuffer control and OE-EPLIN cells. (B) 1. Representative screening image from 3 independent sets of samples. 2. Three sets of data were extracted by image J and taken together for analysis by GraphPad. Data was shown at mean+SEM. ** represents $p<0.01$.

4.3.2.3 Confirmation of knockdown of EPLIN in HRT-18 cell lines

qPCR was carried out to examine transcript level of total EPLIN in HRT18 control and knocked down EPLIN (HRT18-KD-EPLIN) cells. A representative set of data was shown in Figure 4.6 and demonstrated a significant lower transcript level of total EPLIN in HRT18-KD-EPLIN group when compared to control group ($p=0.0087$).

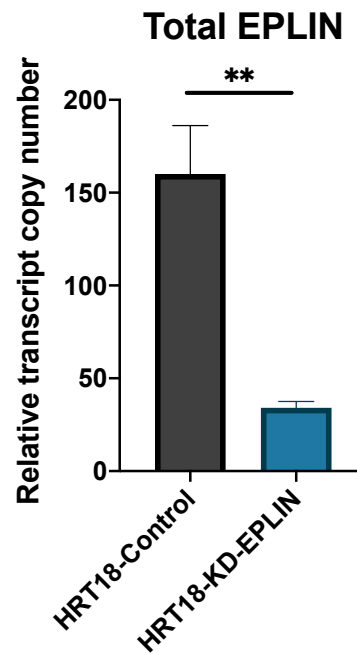


Figure 4.6 qPCR screening of total EPLIN in HRT18 transfected models. A representative data was shown with mean+SEM. **represents $p < 0.01$.

At the meantime, three individual sets of protein samples from these cell models were tested. A representative set is presented in Figure 4.7A1. It is obvious that both the EPLIN α and EPLIN β bands in the shRNA cells were weaker than those in control group. Images were then analysed using Image J and column graphs drafted after normalising by GAPDH (Figure 4.7A2). The expression of both isoforms of EPLIN were downregulated in HRT-18-shRNA cells compared with the control cells. As shown in Figure 4.7B, which combined all three independent sets, both EPLIN α and EPLIN β isoform expression was significantly lower by approximately 80% ($p < 0.001$) and 70% ($p < 0.01$), respectively. In conclusion, a stable knockdown model of EPLIN was established and verified for use in further experiments.

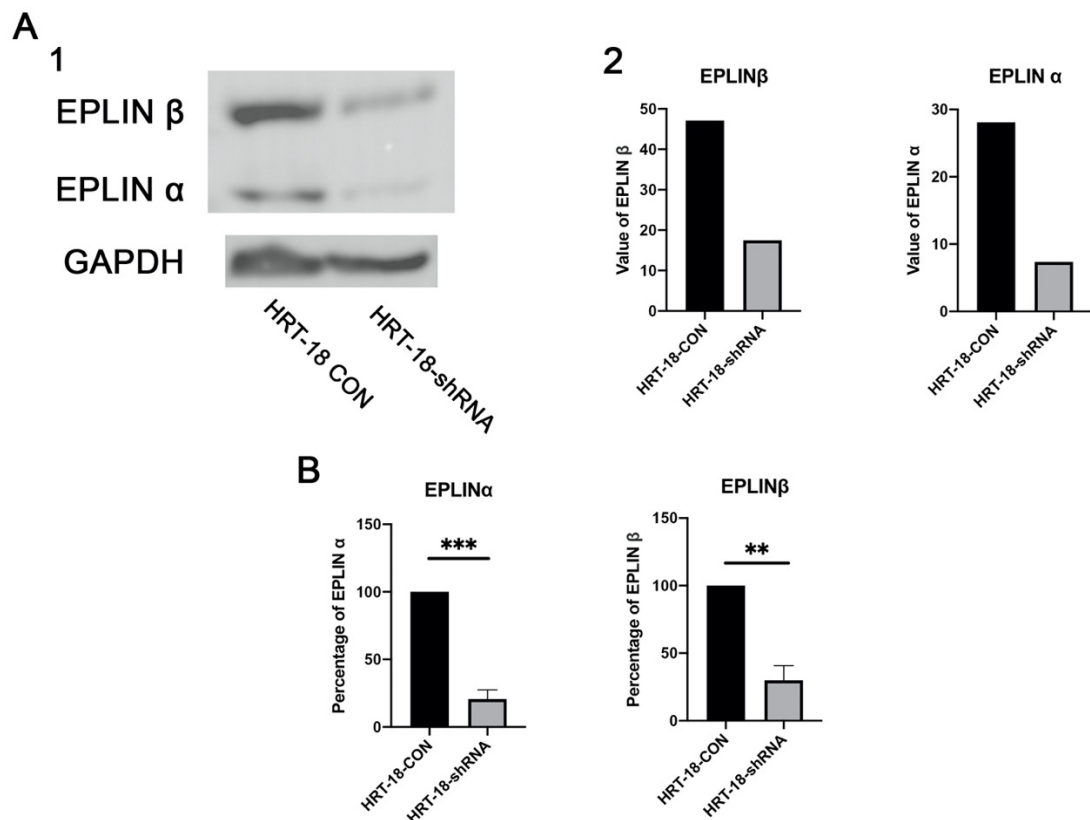


Figure 4.7 Western Blot analysis of EPLIN expression in HRT-18 Knockdown and Control Cells. (A) 1. Representative screening image of EPLIN expression in HRT-18 shRNA-EPLIN and control groups. The bands of EPLIN α and EPLIN β were weaker in HRT-18-shRNA than those in control group. 2. Two column tables were drafted by GraphPad based on GAPDH normalization. The expression of two isoforms of EPLIN in HRT-18-shRNA were obviously lower than those in control group. (B) Three sets of data were taken together and the expressions in control group were set as 100% while the rest was taken as a percentage of the control, mean + SEM shown, $n=3$, *** represents $p < 0.001$, ** represents $p < 0.01$. The expression of EPLIN α in HRT-18-shRNA was nearly 80% less compared to control group, while the expression of EPLIN β in knockdown cells was approximately 70% less than it in control group.

4.3.3 Implication of EPLIN expression on cell growth

In order to explore the impact of altered EPLIN expression, by way of genetic modifications, on CRC cells growth, established cell models were tested with the MTT growth assay for a period of 5 days. Firstly, RKO cell models (RKO-Stuffer Control and RKO-OE-EPLIN) were examined. A representative set of data of RKO cell models (n=8) is shown below (Figure 4.8). Cell density on Day1 was taken as the reference for comparison with Day3 and Day5. As Figure 4.8 demonstrates, on Day 3, cells in the RKO-Stuffer Control group (n=6, mean=337.0 percent vs Day1) grew faster than cells in the RKO-OE-EPLIN group (n=6, mean=279.3 percent vs Day1), accounting for 20 percent difference between groups (p=0.0395). A more obvious difference was noted on Day5, where the RKO-Stuffer Control group (n=6, mean=1069.2 percent vs Day1) displayed enhanced growth rates compared to the RKO-OE-EPLIN (n=6, mean=826.3 percent vs Day1), with a significant, 29.4 percent, difference (p=0.0011), indicating a repressive role played by EPLIN in cell growth in RKO cell lines.

Secondly, EPLIN's influence on cell growth was also investigated in HRT18 cell models. Cell growth rates between control HRT18 cells, transfected with a control plasmid, and those demonstrating EPLIN knockdown following transfection with a shRNA EPLIN plasmid, was investigated using MTT assays over a 5-day period. A representative set of data is demonstrated here (n=4) (Figure 4.9). Similar to the MTT assays conducted on RKO models, cell density on Day1 was set as reference for calculating percentage of growth changes on Day 3 and Day5. On Day3, the mean value of accumulation in the HRT18-Control group against Day 1 counted at 62.8 percent (n=6), while HRT18-KD-EPLIN group accumulated to 79.2 percent (n=6) more than Day 1. Although the HRT18-KD-EPLIN group displayed 26.2 percent more growth than the HRT18-Control group, it did not reach statistical significance (p=0.129). Interestingly, a significant difference of growth between two groups was observed on Day 5, in which the HRT18-KD-EPLIN group (n=6, mean=614.9percent vs Day 1) accumulated 34.9 percent faster than the HRT18-Control group (n=6, mean=455.7 percent vs Day 1) (p=0.0153). In line with the observation in RKO cell models, in which overexpression of EPLIN α lead to suppression of cell growth, knocking down total EPLIN in HRT18 cell lines resulted in enhanced cell growth on Day 5. This dataset, together with that of RKO cell models thus collectively indicate EPLIN's role as a growth suppressor in CRC.

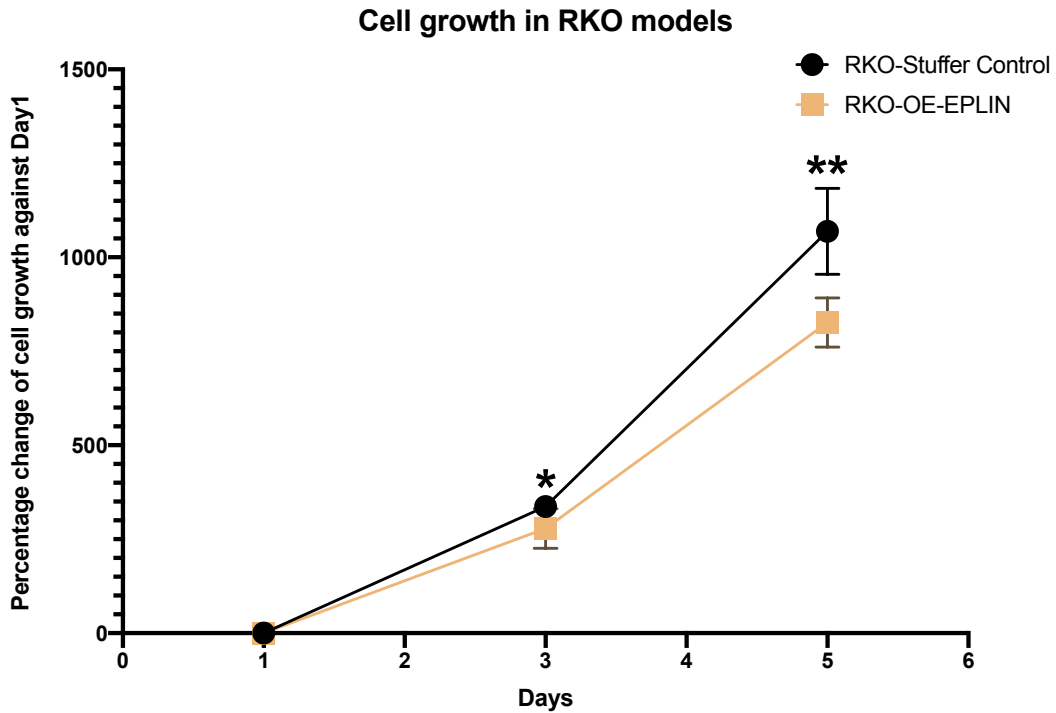


Figure 4.8 MTT growth assay on RKO cell models. Cell density of DAY1 was set as reference for DAY3 and DAY5 groups. While comparing each time point against Day1, RKO-OE-EPLIN group grew at a slower rate than RKO-Stuffer Control group, both at Day3 (For RKO-Stuffer Control group, mean=337.0; For RKO-OE-EPLIN group, mean=279.3) ($P=0.0395$) and Day5 (For RKO-Stuffer Control group, mean=1069.2; For RKO-OE-EPLIN group, mean=826.3) ($P=0.0011$). Representative set of data was presented ($n=8$), mean \pm SEM shown. * represents $p<0.05$, ** represents $p<0.01$.

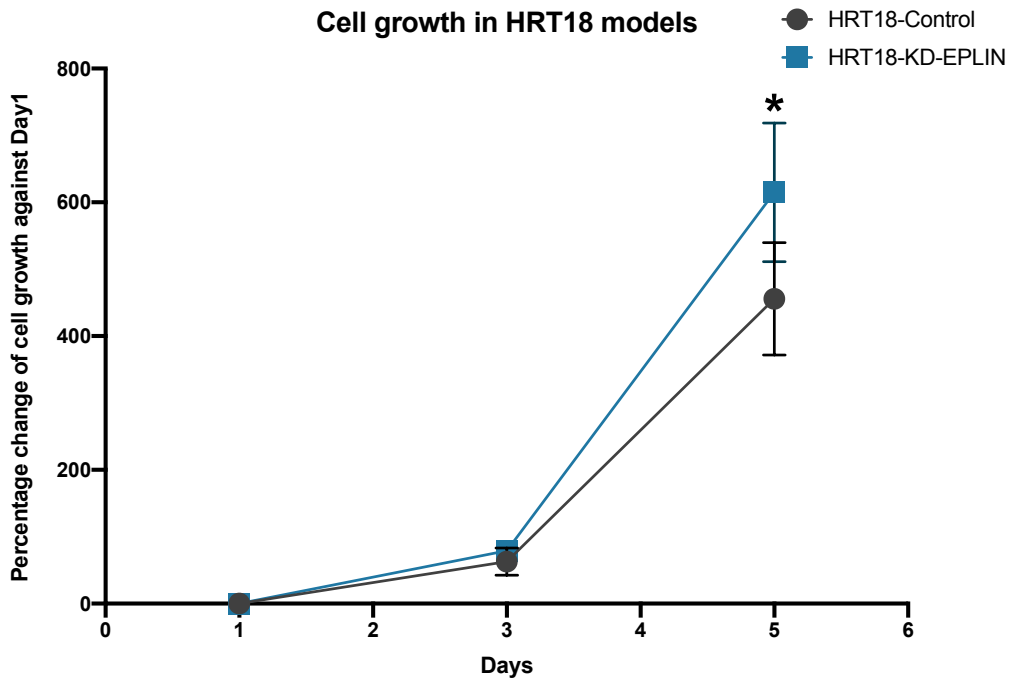


Figure 4.9 MTT growth assays on HRT18 cell models. Confluence of cells on Day1 was set as reference for calculating percentage changes of cell growth on Day 3 and Day5. On Day 3, for HRT18-Control group, mean=62.8; For HRT18-KD-EPLIN group, mean=79.2. On Day5, HRT18-KD-EPLIN group (mean=614.9) grows faster than HRT18-Control group (mean=455.7) ($p=0.0153$). Representative data was demonstrated ($n=4$) with mean \pm SEM, * represents $p<0.05$.

4.3.4 Implication of EPLIN expression on cell adhesion

The impact of EPLIN on CRC cells' adhesive ability was investigated by performing the Matrigel adhesion assays. In RKO cell models, a representative set of data from 3 independent sets is demonstrated here (Figure 4.10). As Figure 4.10A shows, the number of cells that attached to the Matrigel in the RKO-Stuffer Control group (n=5, mean=165.8) were significantly higher than in the RKO-OE-EPLIN group (n=6, mean=79.8) (p=0.0005), accounting for 51.8 percent fewer adhesive cells in the RKO-OE-EPLIN group than the control group (Figure 4.10 B). Representative photographs of each group are presented below (Figure 4.10 C). Therefore, overexpression of EPLIN in RKO cells reduces cell adhesion significantly.

Matrigel adhesion assays were also conducted utilising the HRT18 knock down EPLIN cell line and its respective control group. As the representative set of data (n=3) shows in Figure 4.11A, when EPLIN is downregulated in HRT18 cells, significantly more cells attached to the Matrigel (mean=229.6, n=6) than cells in the HRT18-Control group (mean=182.9, n=6) (p=0.0001). The number of attached cells in the HRT18-Control group was set as 100% for assessing the percentage changes of adhesive cells in the HRT18-KD-EPLIN group. HRT18-KD-EPLIN adhesive cells (mean=125.5, n=6) were 25.5 percent more than those in the HRT18-Control group. Representative photographs of each group (HRT18-Control group, n=20; HRT-KD-EPLIN group, n=24) are presented in Figure 4.11C 1&2 respectively to show the higher density of attached cells in the HRT18-KD-EPLIN group than in the HRT18-Control group. Hence, Downregulation of total EPLIN induced significant increased cell adhesion in HRT18 cells. EPLIN tends to act as a repressor of cells' adhesive ability.

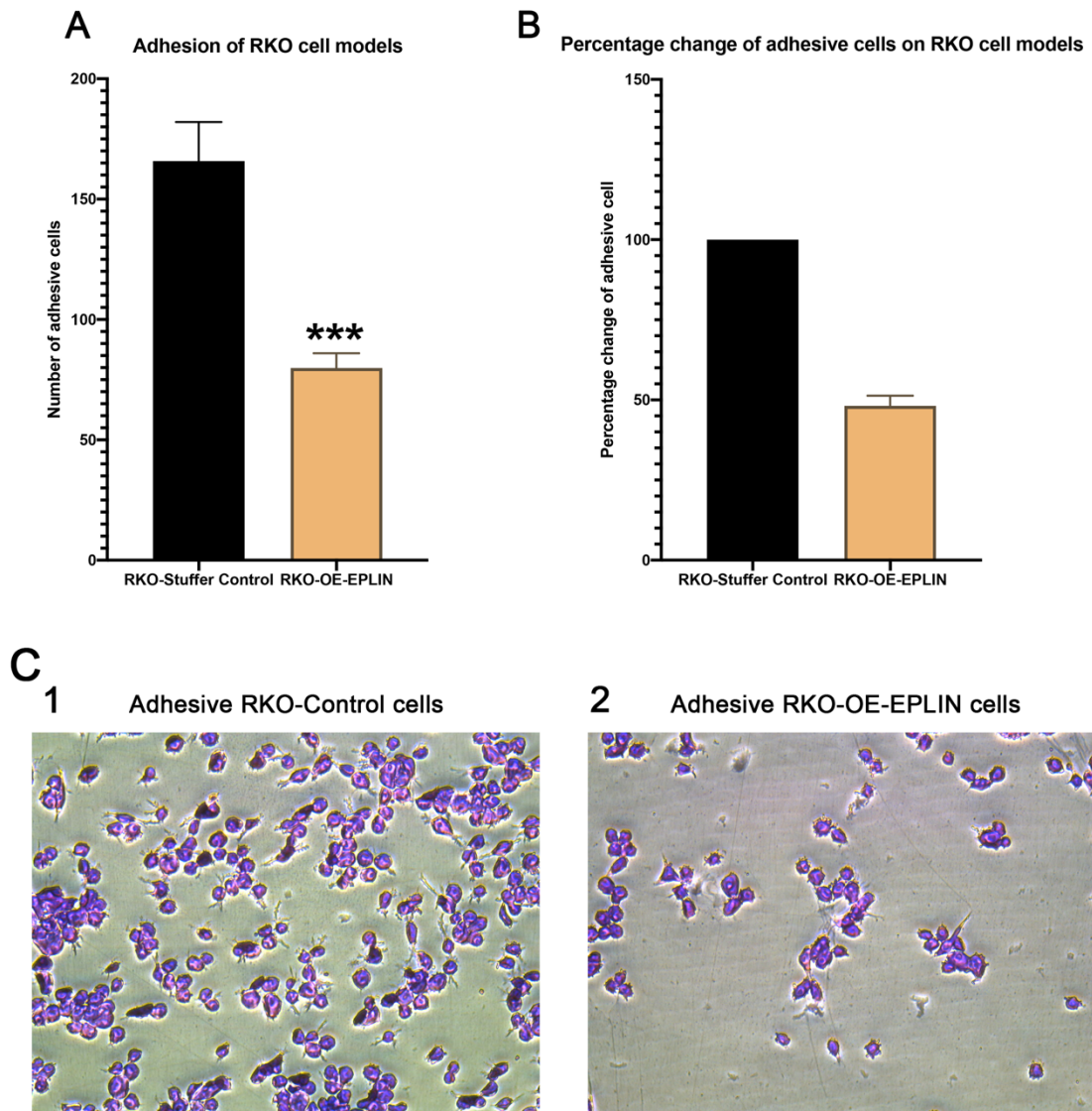


Figure 4.10 Matrigel adhesion assay on RKO cell models. (A) RKO-Stuffer Control group demonstrated an increase in adhesive cells (n=5, mean=165.8) compared to RKO-OE-EPLIN group (n=6, mean=79.8) (p=0.0005). (B) Number of adhesive RKO-Stuffer Control cells was set as 100% to calculate the percentage changes of RKO-OE-EPLIN group. Cells from RKO-OE-EPLIN attached 51.8 percent less than those from RKO-Stuffer-Control group (mean of RKO-OE-EPLIN group is 48.2). (C) 1. Representative photo of adhesive RKO-Control cells (n=20). 2. Representative photo of adhesive RKO-OE-EPLIN cells (n=24). Data was represented with mean + SEM, *** represents p<0.001. Cells were observed under a Leica DM IRB microscope (Leica GmbH, Bristol, UK) (X20) and photos of each field were captured using a Leica LAS EZ (Leica Microsystems (UK) Ltd, England, UK).

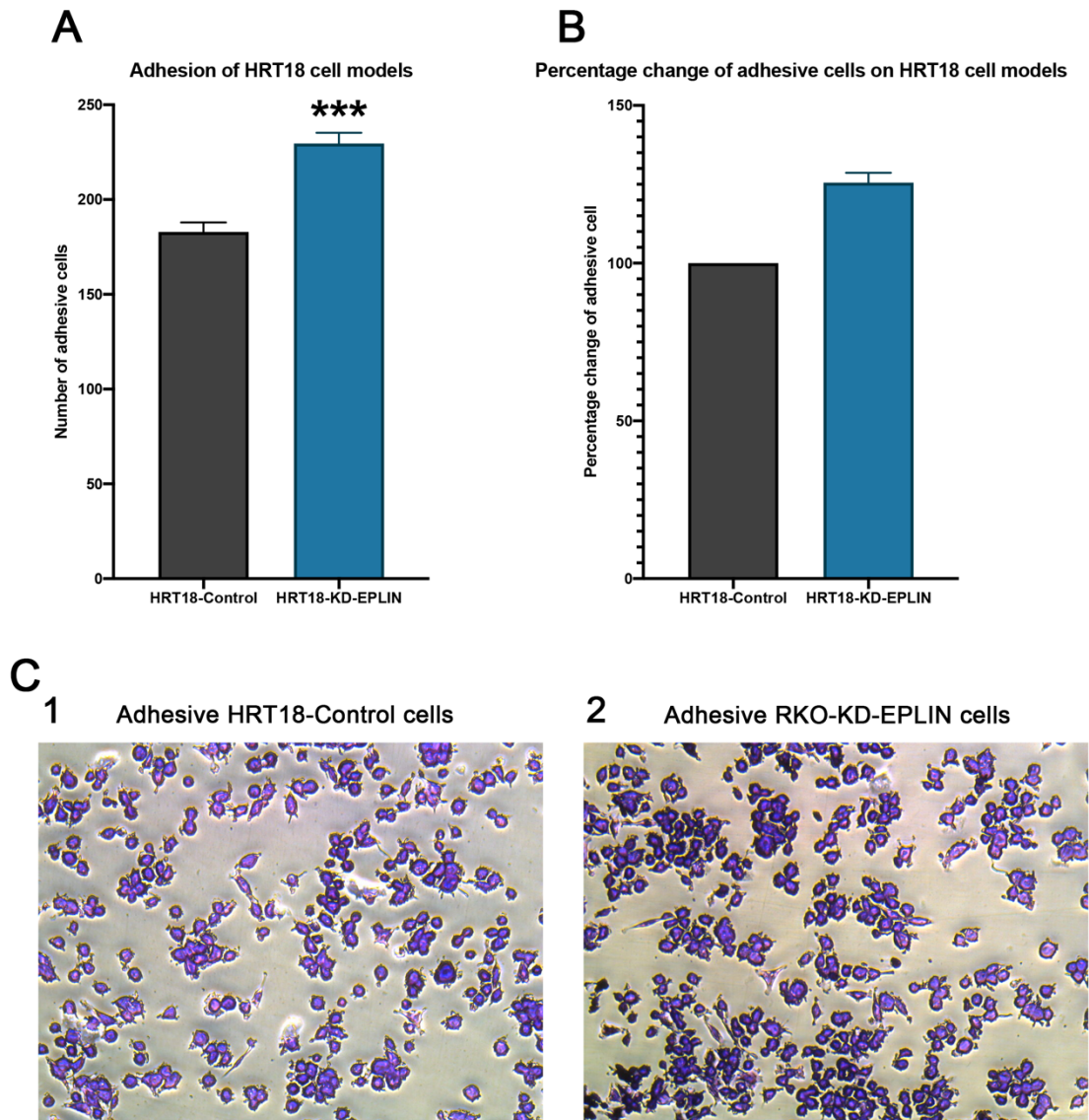


Figure 4.11 Matrigel adhesion assay on HRT18 cell models. (A) Knocking down total EPLIN in HRT18 cells leads to enhancement of cells' adhesion (mean=229.6, n=6) when compared to HRT18-Control group (mean=182.9, n=6) ($p=0.0001$). (B) In the same dataset, the number of adhesive cells in HRT18-Control group is determined as the reference (100%) to calculate the percentage changes of HRT18-KD-EPLIN group (mean=125.5, n=6). Compared to HRT18-Control group, HRT18-KD-EPLIN has 25.5 percent more cells attached to the Matrigel (C) 1. Representative image of adhesive cells from HRT18-Control group (n=20). 2. Representative image of adhesive cells from HRT18-KD-EPLIN group (n=24). Data is presented with mean + SEM, *** represents $p<0.001$. Cells were observed under a Leica DM IRB microscope (Leica GmbH, Bristol, UK) (X20) and photos of each field was captured using a Leica LAS EZ (Leica Microsystems (UK) Ltd, England, UK).

4.3.5 Implication of EPLIN expression on cell migration

EPLIN has been widely indicated as an essential factor to alter cell migration (Collins et al. 2015; Collins et al. 2018), which is largely attributed to its close connection to the cadherin-catenin complex and actin filaments (Maul et al. 2003; Han et al. 2007; Abe and Takeichi 2008). Thus, our attention is drawn to explore if EPLIN has a similar impact on migration in CRC cells. To achieve our goal, ECIS based cell migration assay was carried out to measure the impedance of different paired cell models after wounds were created by electrical wounding, to further evaluate the ability of migration in our established cell models.

For RKO cell models, 20,000 cells from the RKO-Stuffer Control and RKO-OE-EPLIN groups were seeded on the electrode array in 6 repeats and incubated for 5 hours at 37°C, followed by wounding electrically and recording impedance of each well continuously at 7 different frequencies (1000, 2000, 4000, 8000, 16,000, 32,000 and 64,000 Hz), using the ECIS system (Figure 4.12). As Figure 4.12A shows, normalised impedance recordings (8000 Hz), which are based on the starting point of wounding, implicated that RKO-OE-EPLIN cells migrated at a slower pace than RKO-Stuffer Control cells after wounding (n=6, mean ± SD). Observation of three-dimensional models of each group (Figure 4.12B & C) also indicated that overexpression of EPLIN decreased cell migration in RKO cells across 7 different frequencies, when compared to the control group.

Similarly, migration rates in the HRT18 cell models were investigated using the ECIS based cell migration assay (Figure 4.13). Twenty thousand cells per well from each group were seeded on the electrode array in 6 repeats. After incubating at 37°C for 5 hours, an electrical wound was created by the ECIS system in each well and impedance was recorded continuously for another 10 hours. As Figure 4.13A shows, the HRT18-KD-EPLIN group demonstrated a faster rate of migration compared with the control group, as indicated through the impedance data at 8000 Hz (n=6, mean ± SD). A more obvious difference was noted after the 11-hour time point. Three-dimensional models of each tested group were also constructed to provide a clearer indication at 7 different frequencies (1000, 2000, 4000, 8000, 16,000, 32,000 and 64,000 Hz), which showed higher normalised impedance value after the 11-hour time point in the HRT18-KD-EPLIN group compared with the HRT-Control group. Therefore, knocking down EPLIN lead to an increase in migration in HRT18 cells, when compared to its control group. Our results agree with other studies in which EPLIN, as a tumour suppressor and an actin binding protein, regulates cell migration in a number of cancer types (Collins et al. 2015; Collins et al. 2018), including CRC.

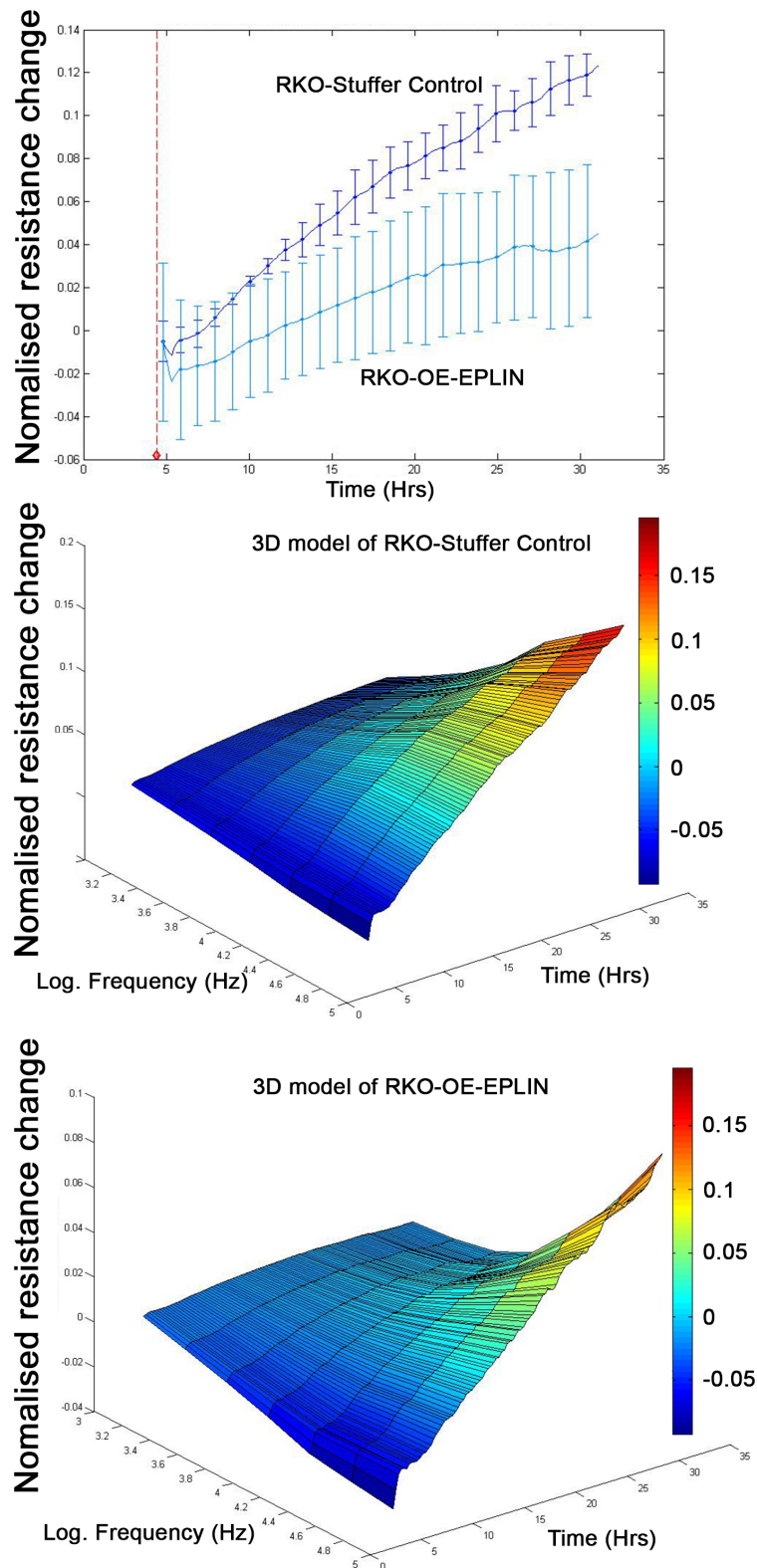


Figure 4.12 ECIS based migration assay on RKO cell models. (A) After wounding electrically, RKO-OE-EPLIN cells migrated slower than cells from the RKO-Stuffer Control group. Impedance data was recorded for 30 hours at 7 frequencies (1000, 2000, 4000, 8000, 16,000, 32,000 and 64,000 Hz). Data was normalised based on the starting points of electrical wounds by the ECIS system and shown at 8000Hz (n=6, mean \pm SD). (B) The three-dimensional model of the RKO-Stuffer Control group provided a clear observation of migration at different frequencies. (C) A three-dimensional model of the RKO-OE-EPLIN group, by comparing two three-dimensional models, overexpression of EPLIN downregulated cell migration. X-axis: frequencies; y-axis: normalised impedance resistance; z-axis: Hours.

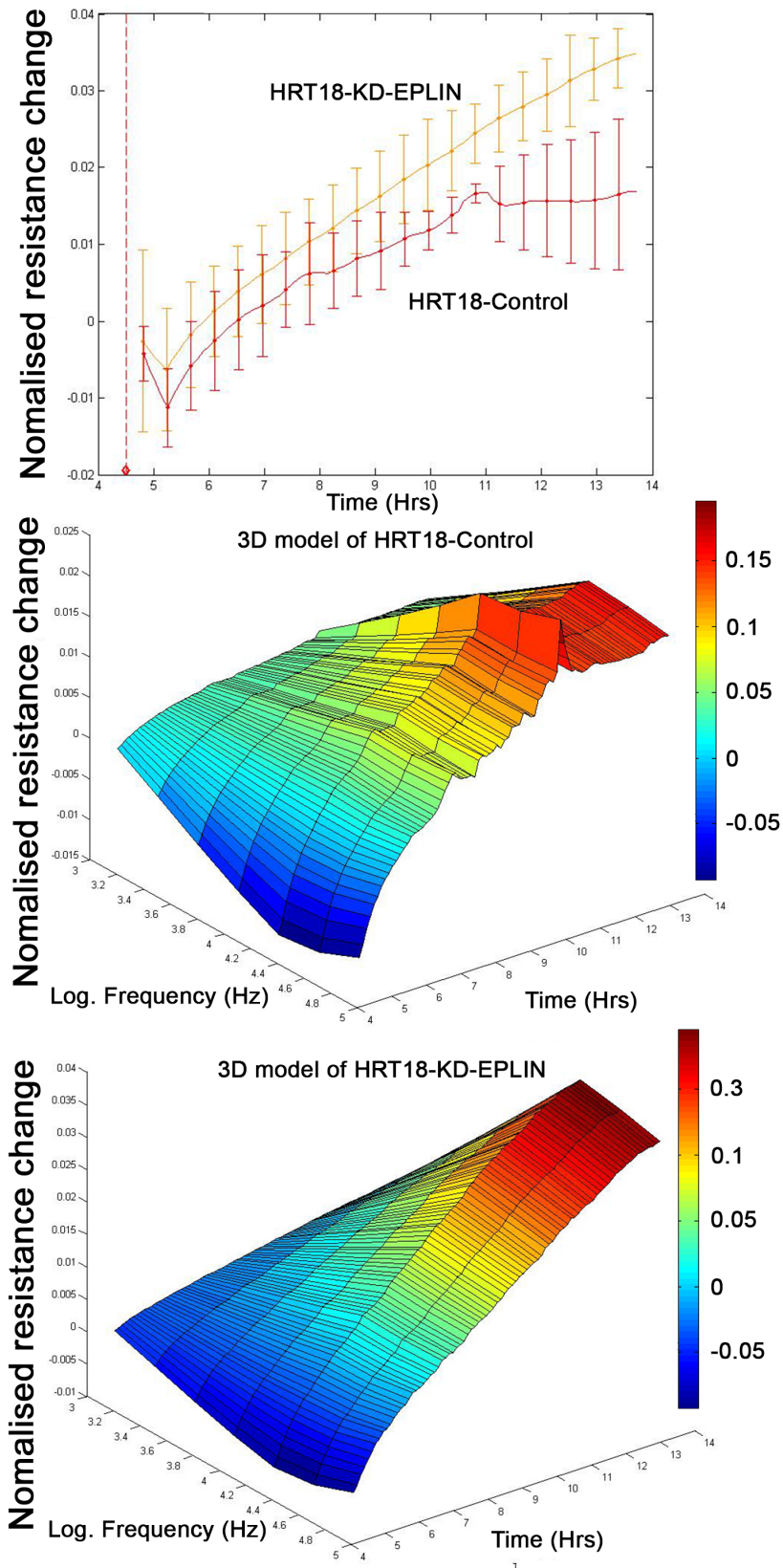


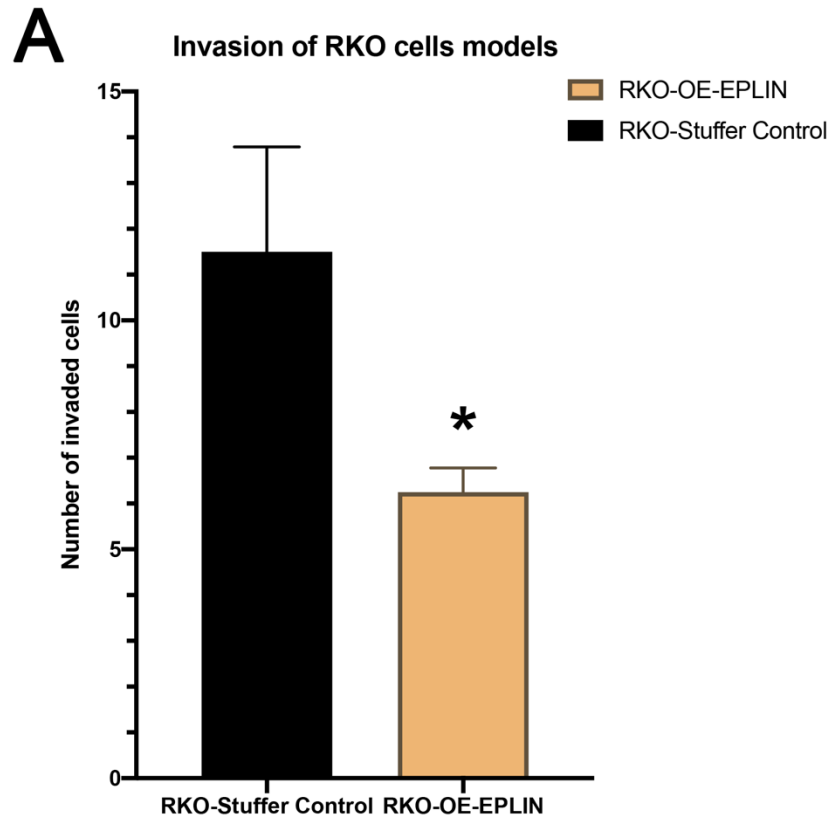
Figure 4.13 ECIS cell migration assay on HRT18 cell models. (A) The HRT18-KD-EPLIN group migrates faster than the HRT18-Control group following electrical wounding, especially after the 11-hour time point. Impedance data was recorded at 7 different frequencies (1000, 2000, 4000, 8000, 16,000, 32,000 and 64,000 Hz) for 10 hours after wounding. Shown data (8000 Hz) is normalised based on the starting point of wounding by the ECIS system (n=6, mean \pm SD). (B) Three-dimensional model of the HRT18-Control group. The 3D model allows observation across all 7 frequencies. (C) Three-dimensional model of the HRT18-KD-EPLIN group. By comparing with the model of the HRT18-Control group, faster migration in the HRT18-KD-EPLIN group was observed after 11-hour time point. X-axis: frequencies; y-axis: normalised impedance resistance; z-axis: Hours.

4.3.6 Implication of EPLIN expression on the *in vitro* invasiveness of colorectal cancer cells

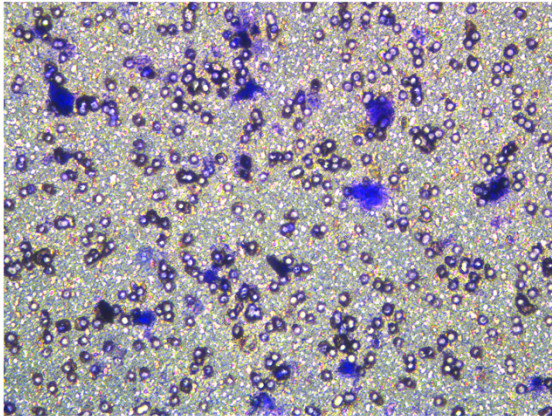
Invasiveness of cancer cells is one of the key factors that facilitate tumour invasion and metastasis (Zhang et al. 2011; Zhang et al. 2013). As EPLIN has been illustrated to be a potential regulator of EMT and represses cell invasion (Sanders et al. 2011; Liu et al. 2012a,b; Collins et al. 2018), the established cell models subject to investigation using a Matrigel cell invasion assays to explore EPLIN's role in the invasion of CRC cells.

Forty thousand cells from each RKO model were seeded in a transwell insert, precoated with 0.5mg/ml Matrigel in duplicate. After incubating for 72 hours, at 37 °C with 5% CO₂, the number of cells that invade through 8µm pores was counted and compared between groups to investigate the invasive ability. A representative set of data (n=3) is presented here (Figure 4.14). As Figure 4.14A shows, 45.7 percent less cells invaded through the Matrigel and 8µm pores in the RKO-OE-EPLIN group (n=8, mean=6.25) than in the RKO-Stuffer Control group (n=8, mean=11.5). This was found to be statistically significant (p=0.0424).

Similarly, 40,000 cells from HRT18 models were applied to the assay, with the same protocol. As the representative data indicates (Figure 4.15), 157.4 percent more HRT18-KD-EPLIN cells invaded through the pores (n=8, mean=17.75) than HRT18-Control cells (n=8, mean=17.375) and this was found to be significant (p=0.000428). In conclusion, upregulation of EPLIN could suppress cell RKO cell invasiveness, while downregulation of EPLIN enhanced cells invasion in HRT18 cells.



B1



B2

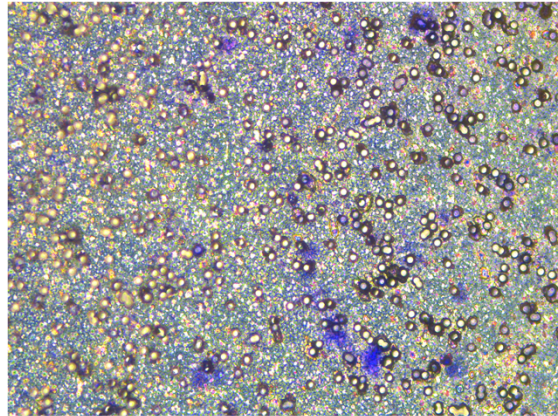
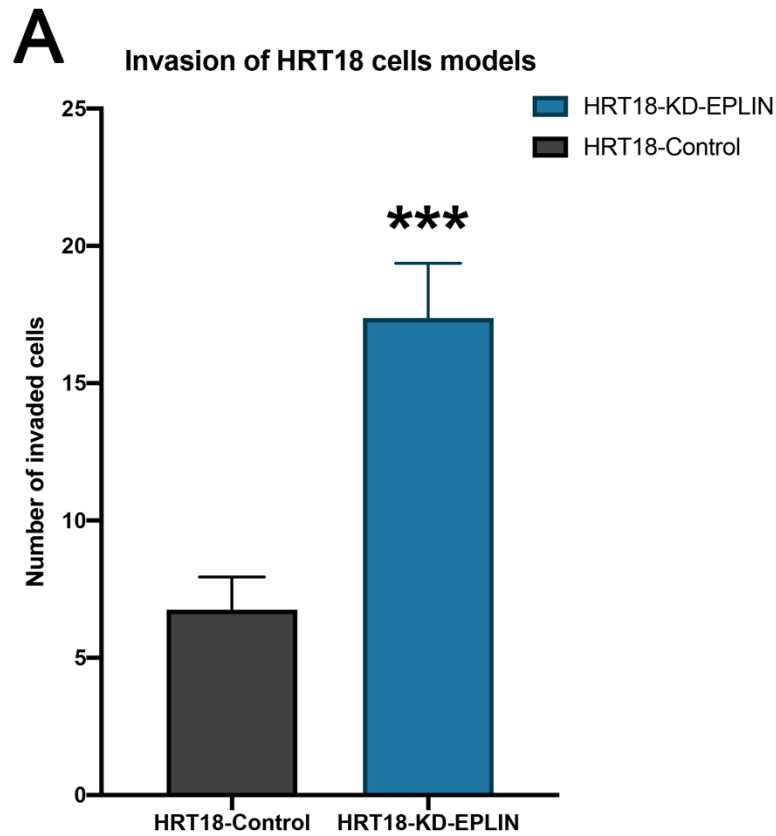
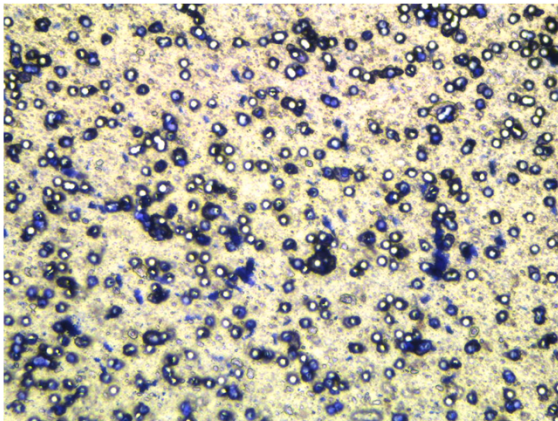


Figure 4.14 Matrigel invasion assays of RKO cell models. (A) Representative data of the invasion assays in RKO cell models (n=3). 40,000 cells from each model were seeded in duplicate into the upper chamber of 8µm pores-transwell inserts which were precoated with 50µg Matrigel. After incubating for 72 hours at 37 °C with 5% CO₂, fewer RKO-OE-EPLIN cells (n=8, mean=6.25) invaded through the pores than RKO-Stuffer Control cells (n=8, mean=11.5) (p=0.0424). Data was presented in mean +SEM, * represents p<0.05. (B) 1. Representative image of invaded cells in RKO-Stuffer Control group (n=8). 2. Representative image of invaded cells in the RKO-OE-EPLIN group (n=8). Cells were observed under a Leica DM IRB microscope (Leica GmbH, Bristol, UK) (X20) and images of each field were captured using a Leica LAS EZ (Leica Microsystems (UK) Ltd, England, UK).



B1



B2

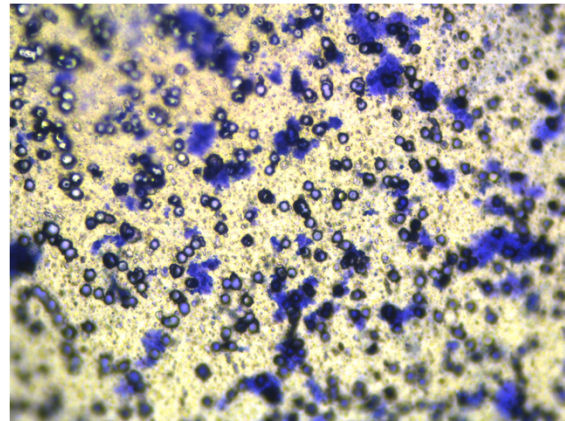


Figure 4.15 Matrigel invasion assay in HRT18 cell models. (A) Representative data of the invasion assays in HRT18 cell models (n=3). 40,000 cells from each model were seeded in duplicate into the upper chamber of 8µm pores-transwell inserts which were precoated with 50µg Matrigel. After incubating for 72 hours at 37 °C with 5% CO₂, more cells from the HRT18-KD-EPLIN group (n=8, mean=17.375) invaded through the pores than cells from the HRT18-Control group (n=8, mean=6.75) (p=0.000428). data was presented in mean +SEM, *** represents p<0.001. (B) 1. Representative image of invaded cells in HRT18-Control group (n=8). 2. Representative image of invaded cells in HRT18-KD-EPLIN group (n=8). Cells were observed under a Leica DM IRB microscope (Leica GmbH, Bristol, UK) (X20) and photos of each field was captured using a Leica LAS EZ (Leica Microsystems (UK) Ltd, England, UK).

4.4 Discussion

The abilities to attach, grow, migrate and invade are essential for cancer cells to establish, develop and disseminate/metastasise to secondary locations. Reported research which has investigated EPLIN and its cellular partners and interacting network, has implicated its potential to affect cellular functions. EPLIN, as an actin binding protein and a regulator of actin dynamics, bundles actin filaments directly, due to its two actin-binding sites (Maul and Chang 1999; Maul et al. 2003; Han et al. 2007), as well as inhibiting branching nucleation of F-actin by interacting with Arp2/3 (Abe and Takeichi 2008). EPLIN has also been shown to be essential for actin accumulation at the cleavage furrow (Chircop et al. 2009).

Furthermore, EPLIN connects to the cadherin-catenin complex, a crucial component of AJs, by binding to α -catenin, and its downregulation leads to disorganisation of AJs (Abe and Takeichi 2008). Similarly, phosphorylation of EPLIN caused by ERK resulted in disassembly of actin filaments (Han et al. 2007; Zhang et al. 2013). Apart from AJs and actin dynamics, EPLIN is also deeply involved in EMT by interactions with an array of proteins and pathways, such as ERK (Zhang et al. 2013). EPLIN is also reported to be involved in a number of signalling pathways that regulate cellular functions, such as β -catenin/Wnt (Zhang et al. 2011; Zhang et al. 2013), ERK2/3 (Zhang et al. 2013), AKT/STAT3 (Steder et al. 2013) and p53 (Ohashi et al. 2017).

Hence, as discussed in Chapter 1.3.5, researchers have been exploring the effects of EPLIN on cellular functions in multiple cancer types including breast (Jiang et al. 2008; Zhang et al. 2011), prostate cancer (Sanders et al. 2011; Collins et al. 2018), melanoma (Steder et al. 2013), oesophageal (Liu et al. 2012a), ovarian cancer (Liu et al. 2016) and pulmonary cancer (Liu et al. 2012b). However, the effects of EPLIN on cellular functions has not been fully investigated in CRC, in which low levels of EPLIN have been noted (Lee et al. 2006; Chen et al. 2017; Ohashi et al. 2017) and implicated to be involved in metastasis (Zhang et al. 2011; Steder et al. 2013). Thus, we decided to probe its influence on cellular functions in CRC. To achieve this goal, firstly, we manipulated EPLIN expression in two CRC cell lines. The RKO cell line was chosen as a EPLIN α overexpression model and HRT18 as a knockdown model, due to their respective and relative weak and modest EPLIN expression. Such models, combined with respective control lines were established for further experiments.

By comparing to the density of Day 1, RKO-Stuffer Control cells were increased by 337.0 percent on Day 3 while RKO-OE-EPLIN cells were increased by 279.3 percent, indicating RKO-Stuffer Control cells grow significantly more (57.7 percent) than RKO-OE-EPLIN cells,

under these experimental conditions ($p=0.0395$). More obvious differences between the two groups were observed on Day 5 (RKO-Stuffer Control: $n=6$, mean=1069.2; RKO-OE-EPLIN: $n=6$, mean=826.3; $p=0.0011$). Similar effects of EPLIN were detected in HRT18 cell models. Although no significant difference was found between HRT18-Control and HRT18-KD-EPLIN groups on Day 3, cells in the HRT18-KD-EPLIN group grew significantly faster than in the HRT18-Control group on Day5 ($p=0.0153$). Hence, our data strongly indicates that the presence of EPLIN leads to repressed cells growth in CRC. This observation is keeping in line with other research on breast (Jiang et al. 2008), prostate (Sanders et al. 2011; Collins et al. 2018), oesophageal (Liu et al. 2012a), ovarian (Liu et al. 2016) and pulmonary (Liu et al. 2012b) cancers and further establishes EPLIN's role in regulating cancer cell growth.

Meanwhile, to examine the impact of EPLIN on CRC cell adhesion, the two established cell models were subjected to analysis using Matrigel adhesion assays. This demonstrated that fewer RKO-OE-EPLIN cells attached (51.8 percent fewer) than RKO-Stuffer Control cells ($p=0.0005$). In keeping with this observation, HRT18-KD-EPLIN cells were found to be 25.5 percent more adherent than those in the control group ($p=0.0001$). Thus, EPLIN inhibits cellular adhesion in CRC. Similar observations have also been seen in oesophageal (Liu et al. 2012a) and ovarian tumour cells (Liu et al. 2016).

In order to study cellular migration, one of the key functions that EPLIN has been illustrated to regulate, we adopted an automated, high throughput and human interphase free method, namely a ECIS (electric cell-substrate impedance sensing) based wound assay. These demonstrated that RKO-OE-EPLIN cells tended to have a slower pace of migration than the RKO-Stuffer Control cells, while cells in the HRT18-KD-EPLIN model tended to migrate faster than cells in its control group. These observations agree with other studies in breast (Jiang et al. 2008), prostate (Zhang et al. 2011; Collins et al. 2018), pulmonary (Liu et al. 2012b) and ovarian cancers (Liu et al. 2016). And suggest that, as in these other cancers, EPLIN is a key regulator of CRC cell migration.

Finally, EPLIN's impact on cellular invasion was also investigated by performing Matrigel invasion assays. As our data shows, 45.7 percent less cells invaded through pores with Matrigel in the RKO-OE-EPLIN group than cells in the RKO-Stuffer Control group ($p=0.0424$), whilst 157.4 percent more cells invaded through the Matrigel in the HRT18-KD-EPLIN group when compared to the HRT18-Control group ($p=0.000428$). Such implication was also reported in breast(Jiang et al. 2008), prostate(Sanders et al. 2011; Zhang et al. 2011; Collins et al. 2018), pulmonary(Liu et al. 2012b), oesophageal(Liu et al. 2012a), ovarian cancer(Liu et al. 2016) and melanoma cancer(Steder et al. 2013).

In conclusion, by establishing successful cell models to manipulate the expression levels of EPLIN in CRC cell models, we have aided in the elucidation of EPLINs role and functional significance in CRC.

Implicated as a tumour and metastasis suppressor in a number of cancers, EPLIN has been observed to inhibit cellular growth, migration, adhesion and invasion, characteristics essential for cancer development and metastasis. The findings of this chapter strongly suggest that EPLIN plays a similar suppressive role in CRC. Such findings have furthered our understanding of EPLINs role in various cancers and represent interesting implications for understanding mechanisms underlying CRC metastasis. Further chapters will focus on identifying the wider cellular network connected with EPLIN and the range and significance of potential interaction partners together with their implication in CRC progression.

Chapter-5

Identification of key signalling pathways involving EPLIN in colorectal cancer

5.1 Introduction

EPLIN and its interactive protein partners including signalling molecules are poorly understood. As presented in Chapter-1 (Table-1.4, Figure-1.12), there are some reports on the potential interactive proteins in the literature including those studies from the host laboratory. Some of the interesting partner proteins and signalling proteins include paxillin, protein tyrosine phosphatases (for example PTPLAP) which are known regulators of cell migration. Others include E-cadherin, CTNN family (CTNN/A1/B1/D1), which are cell adhesion molecule and cell adhesion regulators. These discoveries tend to be from sporadic and isolated studies. A wide ranging study of the mechanisms of EPLIN in cancer cells is otherwise not available in the literature. However, there has been a recent project to explore the signalling events was from one of the fellow researchers in my host laboratory (Michal Uherick, MD thesis 2021) (<https://orca.cardiff.ac.uk/view/cardiffauthors/A2189793Q.html>). Uherick et al investigated the impact of EPLIN on the progression of breast cancer and have found that some of the cell-matrix interacting regulators, namely FAK and Paxillin are associated with EPLIN in breast cancer cells, so as a member of the Heat Shock Protein family member HSP90 (Uherick, 2021, unpublished).

Given the significance of EPLIN in clinical colorectal cancer and colorectal cancer cells as respectively presented in Chapter-3 and Chapter-4, a comprehensive and in depth analysis of the interactive proteins and signalling proteins associated with EPLIN in colorectal cancer cells has been provoked. This would also allow interrogation of the mechanistic events underlying the biological effects of EPLIN in this cancer type.

Firstly, EPLIN's interacting networks were explored by utilising Kinexus protein microarray platform. By doing so, we hoped to discover in a comprehensive matter the potential interacting network of EPLIN. Additional methods were employed to validate the key partners and investigate the impact of such potential interaction and the underlying mechanism.

5.2 Methods

5.2.1 Kinex™ antibody protein microarray

Interaction of EPLIN was investigated by applying EPLIN precipitated proteins from clinical cohort on Kinex™ antibody-based KAM-880 protein microarray (Kinexus Bioinformatics Ltd., Vancouver, BC, Canada). For details, please refer to Chapter 2.7.

5.2.2 Cell culture

Colorectal cancer cell lines, RKO, HRT18, HT115 and Caco2 were cultured in appropriate culture medium and conditions in line with protocol by the manufacturer, please refer to Chapter 2.2.

5.2.3 Protein extraction and quantification

Protein samples that were prepared for immunoprecipitation assay were extracted following the methods described in Chapter 2.4.1 and they were quantified following methods in Chapter 2.4.2.

5.2.4 Immunoprecipitation

Potential interacting partners of EPLIN were further investigated on colorectal cancer cell lines by carrying out immunoprecipitation assays. For details, please refer to Chapter 2.4.6.

5.2.5 Western blotting

Protein samples (precipitated and control) were applied to SDS-PAGE to be separated and were transferred to PVDF. Immunoblotting was carried out to probed target protein with antibodies. For details, please refer to Chapter 2.4.3-2.4.5.

5.3 Results

5.3.1 Searching for EPLIN interacting proteins and protein kinases in colorectal tissues

Here, we employed a protein kinase array platform technology from Kinexus Bioinformatics Corporation, Vancouver, Canada. From pairs of human colorectal tissues in our Cardiff cohort (paired fresh frozen normal and tumour tissues from the same patients), proteins were extracted following homogenisation and standardised to the same concentration. Proteins interacted with EPLIN was immunoprecipitated by using an anti-EPLIN antibody. The precipitated samples were subsequently applied to the KinexTMKAM-880 Array platform (Kinexus Bioinformatics Ltd., Vancouver, BC, Canada) (Figure 5.1), following labelling proteins with a fluorophore. As part of the Kinexus microarray service, quantitative reports of each tested sample are generated. Here, I combined the findings of the two datasets (ID128 vs ID129 and ID126 vs ID127), and demonstrate the top 52 protein kinases reported to potentially interact with EPLIN and which may be dysregulated due to the modification of EPLIN (Table 5.1).

Among these reported proteins with priority, Cyclin B1, Eukaryotic Translation Initiation Factor 4E (eIF4E) and Epidermal Growth Factor Receptor 2 (ErbB2/Her2) in tumour tissues have the highest positive correlation with EPLIN when compared to normal tissues (for Cyclin B1, Z-ratio from tumour to normal tissue is 4.72; For eIF4E, Z-ratio from tumour to normal tissue is 4.15; For Her2, Z-ratio from tumour to normal tissue is 3.96). Interestingly, some of these potential partners participate in regulating several carcinogenic events or signalling pathways together. For instance, Cyclin B1, prepro-retinoblastoma-associated protein (RB), Cyclin D1 and Cyclin Dependent Kinase 6 (CDK6) is involved in regulation of cell cycle (Lew et al. 1991; Harbour et al. 1999; Xie et al. 2019). Furthermore, Mitogen-Activated Protein (MAP) kinase family members and their downstream kinases were also observed to be aberrant, namely MAPK9 (JNK2), MAPK7 (ERK5), MAPK8 (JNK1), MAPK3 (ERK1) and MAPK Interacting Serine/Threonine Kinase 2 (MKNK2). Intensity of protein kinases that relate to MAPK/ERK pathways were observed to be dysregulated, such as B-Raf, PDGFRa, PDGFRb and Krs2. ERK1 and STAT3, two elements that EPLIN interacts with to regulate the EMT process (Steder et al. 2013; Zhang et al. 2013), were also observed to be aberrant.

One of the most interesting protein families that was highlighted to be associated with EPLIN in colon tissues is the Heat Shock Protein (HSP) family. Dysregulation of a few members of Heat shock protein (HSP) family were also detected, namely HSP60, HSP90b, HSP70 binding protein 1 (HSPBP1) and HSP70 Member 8 (HSC70).



Figure 5.1. Images from the Kinexus arrays, in which ID 126 and 128 were precipitated from normal colon mucosa tissues and 127 and 128 from the colorectal tissues of the respective patients. Each protein sample was applied to the Kinexus Microarrays chips to incubate with 878 different dye-labelled antibodies of proteins. Strongest signal is visible as red colour, following by orange, yellow, green and blue.

Table 5.1. Quantitative report of proteins that interact with EPLIN (All tests combined). Globally normalised intensity, intensity of each tested antibody was normalised by all the net signal median values from a samples. %CFC, percentage changes of normalised intensity from normal samples compared with tumour samples. Z-ratio, Z score differences were separated by standard deviation for the comparison. Priority leads were selected as %CFC \geq 50; SUM of %Error Ranges $< 0.75 \times$ %CFC value; At least one Globally Normalized intensity value \geq 1500.

Target Protein Name	Antibody Codes	Globally Normalized - Normal	Globally Normalized - Tumour	%CFC (Tumour from Normal)	Z-ratio (Tumour, normal)	Best Leads
Cyclin B1	PN190	747	1751	135	4.72	Priority
eIF4E	PN030-1	11990	36587	204	4.15	Priority
ErbB2	NK054-2	1076	3148	192	3.96	Priority
Kit	PK038	1422	4136	190	3.94	Priority
B-Raf	NK156-4	18354	36112	97	3.44	Priority
STAT5B	NN106	1523	3849	152	3.43	Priority
Rb	PN071	9750	21175	117	2.89	Priority
KAP	NP004	1591	3426	115	2.84	Priority
Hsp90b	NN165	3604	5987	67	2.73	Priority
JNK2	NK088-2	2265	4632	104	2.65	Priority
Lck	PK040	11772	23233	97	2.54	Priority
CDK6	NK029	23352	44824	92	2.45	Priority
Jun	PN048-2	9074	17405	91	2.44	Priority
Bcl-XL	NN007	15543	29299	88	2.38	Priority
Mnk2	NK111	2409	4530	88	2.34	Priority
HO1	NN052	9056	16911	86	2.34	Priority
Ros	NK163-3	9619	15068	57	2.31	Priority
CREB1	PN023	1007	1877	86	2.30	Priority
KDEL Receptor (KR10)	NN153	1962	3643	85	2.29	Priority
ERK5	NK206-3	3371	5149	53	2.29	Priority
Mnk2	NK111	1155	1710	49	2.25	Priority
PDK1	NK126-2	1997	3624	81	2.21	Priority
Epcam	NN173	1226	2166	76	2.11	Priority
PDI	NN141-1	7637	13248	73	2.06	Priority
Hsc70	NN054-2	8506	14370	69	1.97	Priority
Bid	NN009	6619	11136	68	1.95	Priority
Syk	PK821	8058	13400	66	1.91	Priority
Krs-2	NK113-3	4563	7545	65	1.88	Priority
PDGFRa	PK758	3078	4976	61	1.79	Priority
Hsp60	NN059-2	15137	24097	59	1.76	Priority
GFAP	PN034	1420	2239	57	1.69	Priority
Hsp60	NN059-3	1266	1977	56	1.65	Priority
PDGFRb	NK243-3	5131	7989	55	1.66	Priority
CSF1R	PK587	2940	4540	54	1.62	Priority
PKA Ca/b	PK067	17981	27421	52	1.60	Priority
Bcl-xS/L	NN008	2168	3263	50	1.52	Priority
GRK2	PK025	24141	12540	-48	-2.36	Priority
JNK1	NK217	425	220	-48	-2.42	Priority
ATF2	PN006-1	18012	8845	-51	-2.57	Priority
FRS2	PN146	3466	1686	-51	-2.63	Priority
STAT3	PN082-1	2689	1220	-55	-2.89	Priority
JAK3	NK086-4	22311	7690	-66	-3.87	Priority
Tau	PN122	287	1007	250	4.61	Possible

eIF4G	PN193	519	1163	124	2.97	Possible
Jun	PN163	890	1921	115	2.84	Possible
STAT6	NN107	714	1246	74	2.05	Possible
B23 (NPM)	PN008	602	1045	73	2.03	Possible
PRAS40	PN062	1172	556	-53	-2.74	Possible
BRCA1	PN014	2324	6509	181	5.53	Possible
HspBP1	NN063	558	1169	110	4.16	Possible
ERK1	NK055-2	16878	32201	91	3.29	Possible
MKK4	NK103-4	12720	21384	69	2.65	Possible
Cyclin D1	NN030-1	31906	17106	-46	-3.47	Possible

Priority candidates (both raised/activated and decreased/inhibited) were applied to an online protein-protein interaction database, STRING database, to predict potential interaction (Szklarczyk et al. 2021). By taking advantage of the STRING platform which analyses data across published datasets to predict protein connective strength, we showed that these potential interacting partners knitted interacting networks among themselves (Figure 5.2).

As Figure 5.2A demonstrates, among priority candidates that upregulated when EPLIN expression is inhibited, several upregulated/activated candidates hold a central role in its own networks. These include STAT5B, Lymphocyte Cell-Specific Protein-Tyrosine Kinase (LCK), Jun Proto-Oncogene, AP-1 Transcription Factor Subunit (JUN) and HSP90b (HSP90AB1).

As Figure 5.2B demonstrates, among priority candidates that were downregulated/inhibited due to the modification of EPLIN, Mitogen-Activated Protein Kinase 8 (MAPK8), Signal Transducer and Activator of Transcription 3 (STAT3) and kinases that are involved in their networks seem to play an important role.

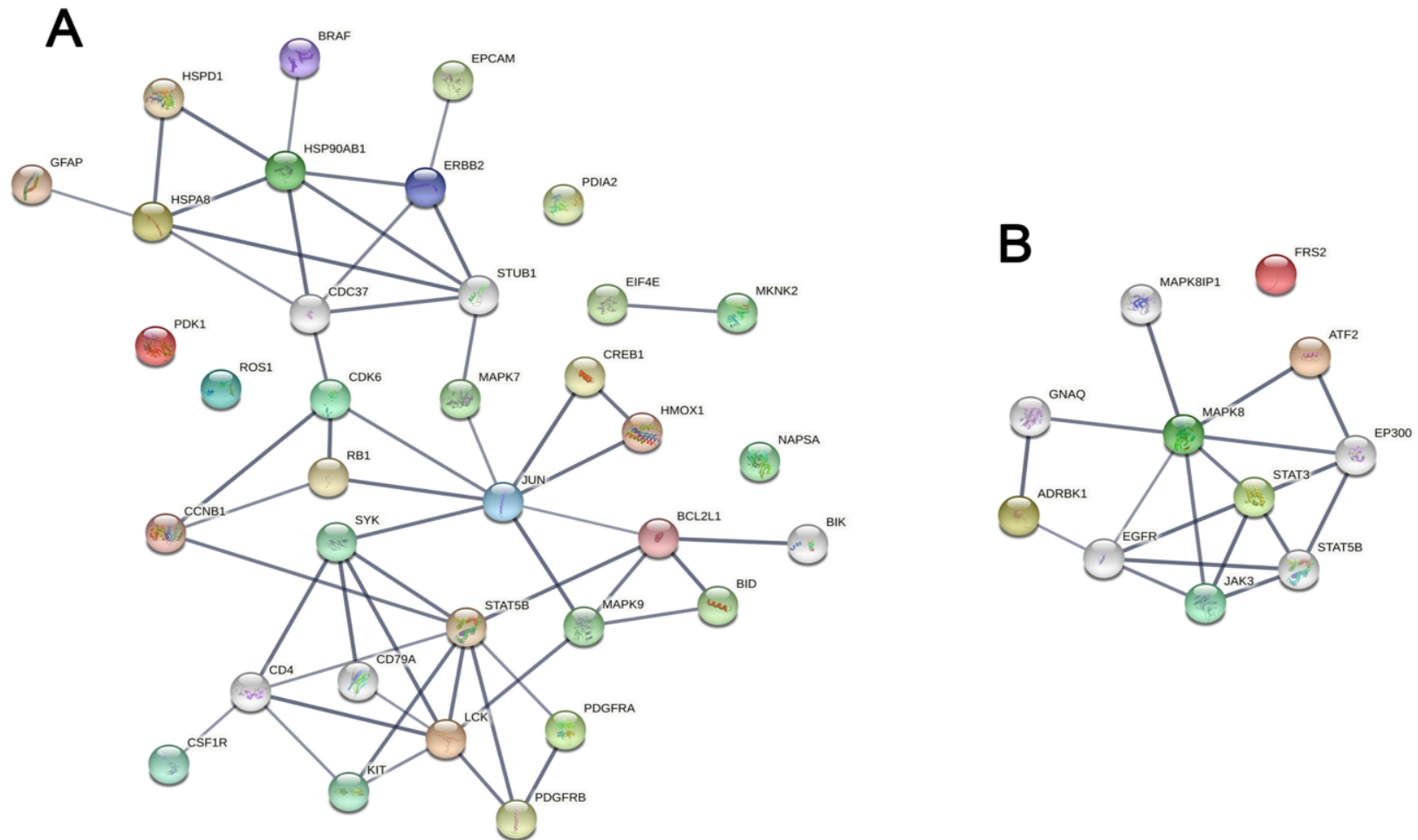


Figure 5.2 Raised or inhibited protein kinases due to modification of EPLIN in colorectal cancer. Priority candidates from reports of Kinexus microarray was further analysed by STRING database. A. Raised/activated protein kinases in colorectal cancer tissues over normal tissues (confidence 0.700). B. Reduced/inhibited protein kinases in colorectal cancer tissues over normal tissues (confidence 0.700). Colour dots: Input priority candidates. White dots: interacting partners of priority candidates provided by STRING database

5.3.2. Comprehensive analysis of signalling pathways from the most prominent priority EPLIN interacting proteins in colon tissues by way of Reactome analysis

We demonstrated most correlative proteins that might interact with EPLIN above by analysing our protein samples on Kinexus microarray, and highlighted a list of potential interacting targets of EPLIN for our further study. Reactome analysis, an online pathway analysing tool (Fabregat et al. 2018; Jassal et al. 2020), offers us a view of potential key pathways that EPLIN and its potential interacting partners may be involved in. Initially, by taking advantage of Reactome analysis platform, we explored which biological events that key pathways of EPLIN may participate (Figure 5.3). This allowed us to have a first glance of pathways in which EPLIN was involved in. As the figure implicates, EPLIN takes part in pathways that are related to signal transduction, disease and immune system.

After gaining this first glance of pathways that EPLIN may participates in, we continued to analyse the signalling pathways that its potential interacting partners may take part in (Table 5.2). After inputting all potential interacting partners of EPLIN that were identified from the Kinexus microarrays, as listed in the Table 5.2, further analyses using Reactome offered us an opportunity to identify key pathways that are involved. These interacting partners are significantly involved in interleukin-21, 4, 13, 17 and 2 pathways, MAP kinase activation pathways, PI3K/AKT signalling pathways and a few others.

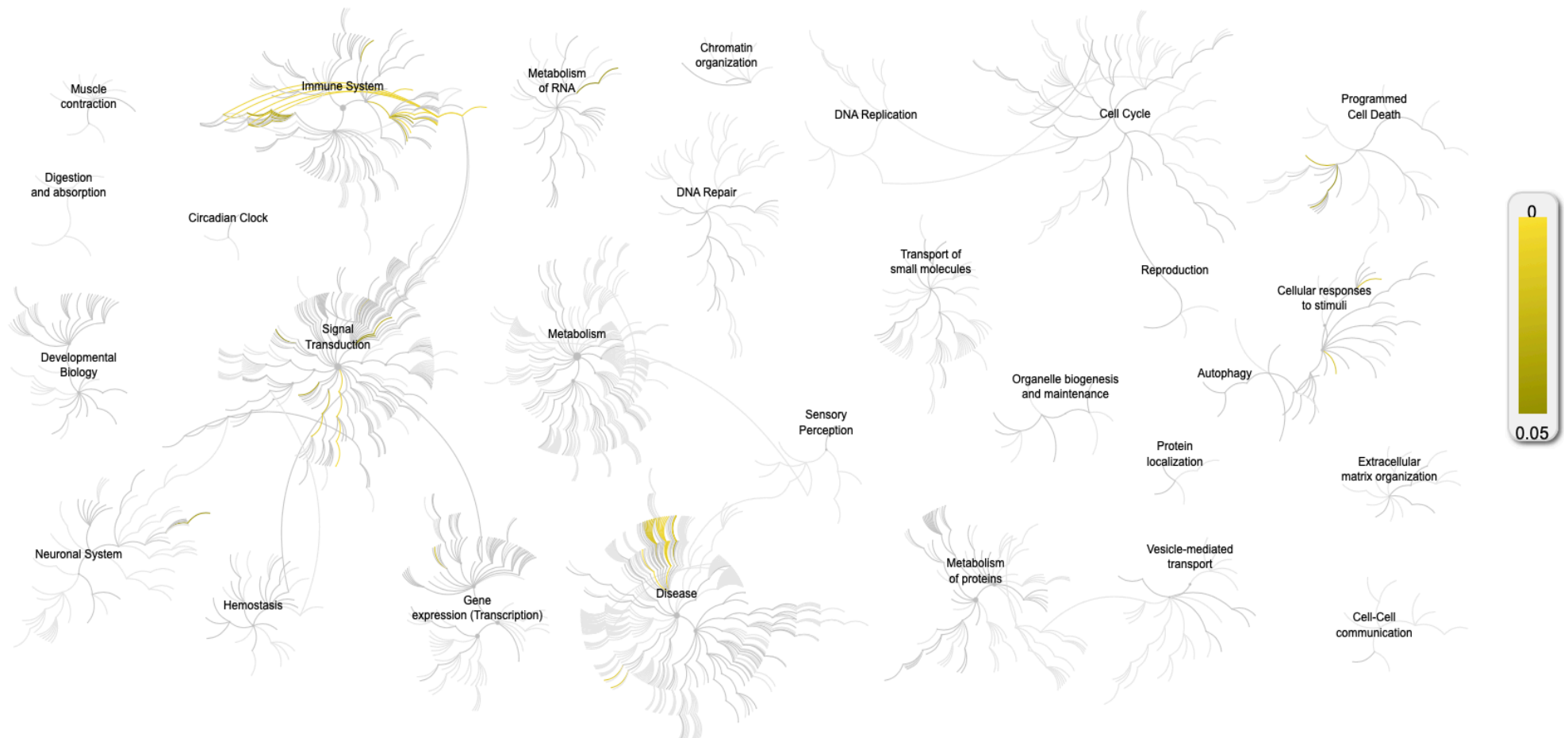


Figure 5.3 Key signalling pathways that involve EPLIN in the context of the biological system. Data is analysed using Reactome Pathway Browser (Fabregat et al. 2018). Each cluster includes signalling pathways that take part in such biological event, p value is marked by colour, brighter colour represents more statistical significance.

Table 5.2 Top signalling pathways that EPLIN priority protein partners participate in. Reported potential interacting proteins inputted, and significant signalling pathways are marked as $p < 0.05$. Data is analysed using Reactome signalling pathways platform (Jassal et al. 2020). Entities found: the number of input molecules found in pathways vs total number of molecules within pathways. Entities ratio: the proportion of Reactome pathway molecules represented by this pathway. False discovery rate (FDR): Corrected over-representation probability. Reaction found: the number of reactions in the pathways that are represented by input molecules vs total number of the reactions in the pathways. Reaction ratio: the proportion of Reactome reactions represented by this pathway.

Pathway name	Entities				Reactions	
	Found	Ratio	p-value	FDR*	Found	Ratio
Interleukin-21 signalling	4/13	5.9e-04	8.16e-07	0.001	4/5	3.70e-04
Interleukin-4 and Interleukin-13 signalling	11/351	0.016	1.07e-04	0.013	33/47	0.003
Interleukin-2 signalling	7/92	0.004	1.37e-04	0.013	17/19	0.001
MAP kinase activation	12/291	0.013	1.64e-04	0.013	21/32	0.002
Interleukin-17 signalling	12/300	0.014	2.01e-04	0.013	21/35	0.003
MAPK targets/Nuclear events mediated by MAP kinase	10/233	0.011	2.49e-04	0.013	15/16	0.001
JNK phosphorylation and activation mediated by activated human TAK1	3/26	0.001	3.75e-04	0.013	3/3	2.22e-04
PI3K/AKT signalling in Cancer	17/424	0.02	4.27e-04	0.015	19/21	0.002
Constitutive Signalling by Aberrant PI3K in Cancer	7/186	0.009	4.81e-04	0.016	2/2	1.48e-04
Senescence-Associated Secretory Phenotype (SASP)	5/137	0.0016	8.34e-04	0.028	9/22	0.002
PI5P, PP2A and IER3 Regulate PI3K/AKT Signalling	12/295	0.014	9.97e-04	0.032	5/7	5.18e-04
Erythropoietin activates STAT5	2/9	4.15e-04	0.001	0.033	3/3	2.22e-04
STAT5 Activation	2/9	4.15e-04	0.001	0.033	3/3	2.22e-04
Nuclear events stimulated by ALK signalling in cancer	6/87	0.001	0.001	0.036	9/9	6.66e-04
Signalling by KIT in disease	6/154	0.007	0.001	0.04	25/25	0.002
Signalling by phosphorylated juxtamembrane, extracellular and kinase domain KIT mutants	6/154	0.007	0.001	0.04	11/11	8.14e-04
RSK activation	2/11	5.07e-04	0.002	0.043	2/4	2.96e-04
Negative regulation of the PI3K/AKT network	12/324	0.015	0.002	0.043	6/10	7.40e-04
Activation of the AP-1 family of transcription factors	8/166	0.008	0.002	0.043	5/5	3.70e-04
ERKs are inactivated	2/15	6.91e-04	0.003	0.053	2/2	1.48e-04
TRAF6 mediated induction of NFkB and MAP kinase upon TLR7/8 or 9 activation	14/474	0.022	0.004	0.063	24/48	0.004
Defective binding of RB1 mutants to E2F1, (E2F2, E2F3)	2/17	7.84e-04	0.004	0.063	1/1	7.40e-05

5.3.3 Interaction of EPLIN with the Heat Shock Protein (HSP) family proteins

As we demonstrated in 5.3.1, HSP family proteins are reported to be potential interacting partners of EPLIN with priority. Hence, we extracted the HSP family proteins' data in the Kinexus dataset (Figure 5.3). There are some marked changes from normal to tumour tissue in the interaction between EPLIN and the HSP protein family. As the figure showed, the tested family members demonstrated changes between normal and tumour samples at different degrees. It is noteworthy that when EPLIN's expression was suppressed, all signal intensities of three HSP60 probe with different antibodies showed a trend of upregulation in tumour samples when compared with normal samples. While two antibodies that probed with HSP60 (NN059-2 and NN059-3) demonstrated obvious %CFC between tumour and normal samples (NN059-2, 59; NN059-3, 56) and were labelled as priority potential interaction.

While further investigating signalling pathways that such HSP family members may involve using the Reactome platform, a predicted signalling pathway that involves HSP60 was highlighted (R-HSA-8869496) (Figure 5.4). In this predicted pathway, Transcription Factor AP-2 Alpha (TFAP2A) binds with nucleophosmin (NPM1) to inhibit transcript expression of HSP60, p120 (NOP2) and b-Myb (MYBL2) via recruitment of histone deacetylases (HDAC1 & HDCA2) (Saville and Watson 1998; Liu et al. 2007).

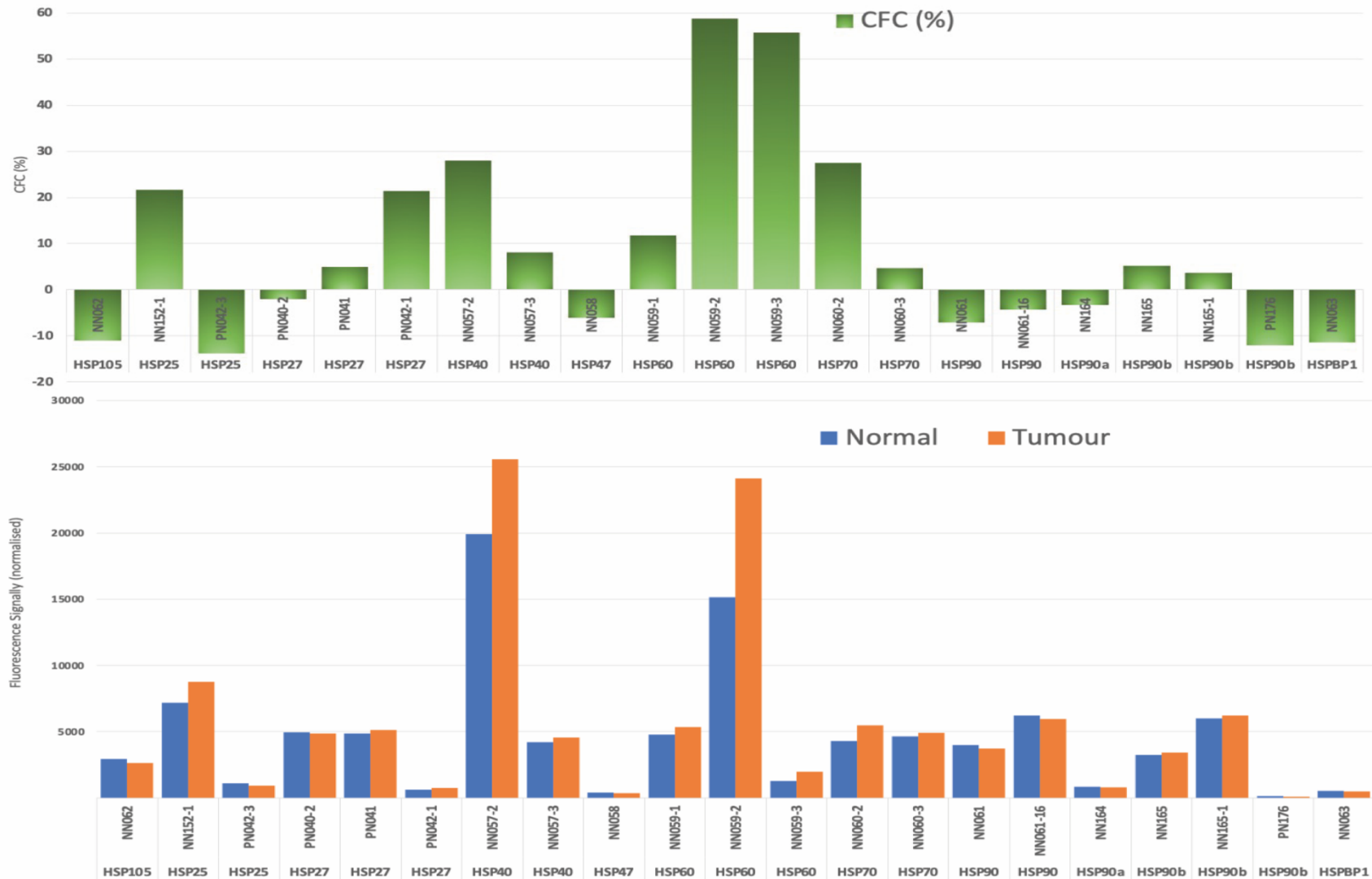


Figure 5.3 Relationship between EPLIN and HSP family based on Kinexus's report. Top. Percentage changes of signal intensity of each tested HSP family members. Below. Signal intensity of each tested samples in normal samples and tumour samples. Some HSP family members were probed with different antibodies.

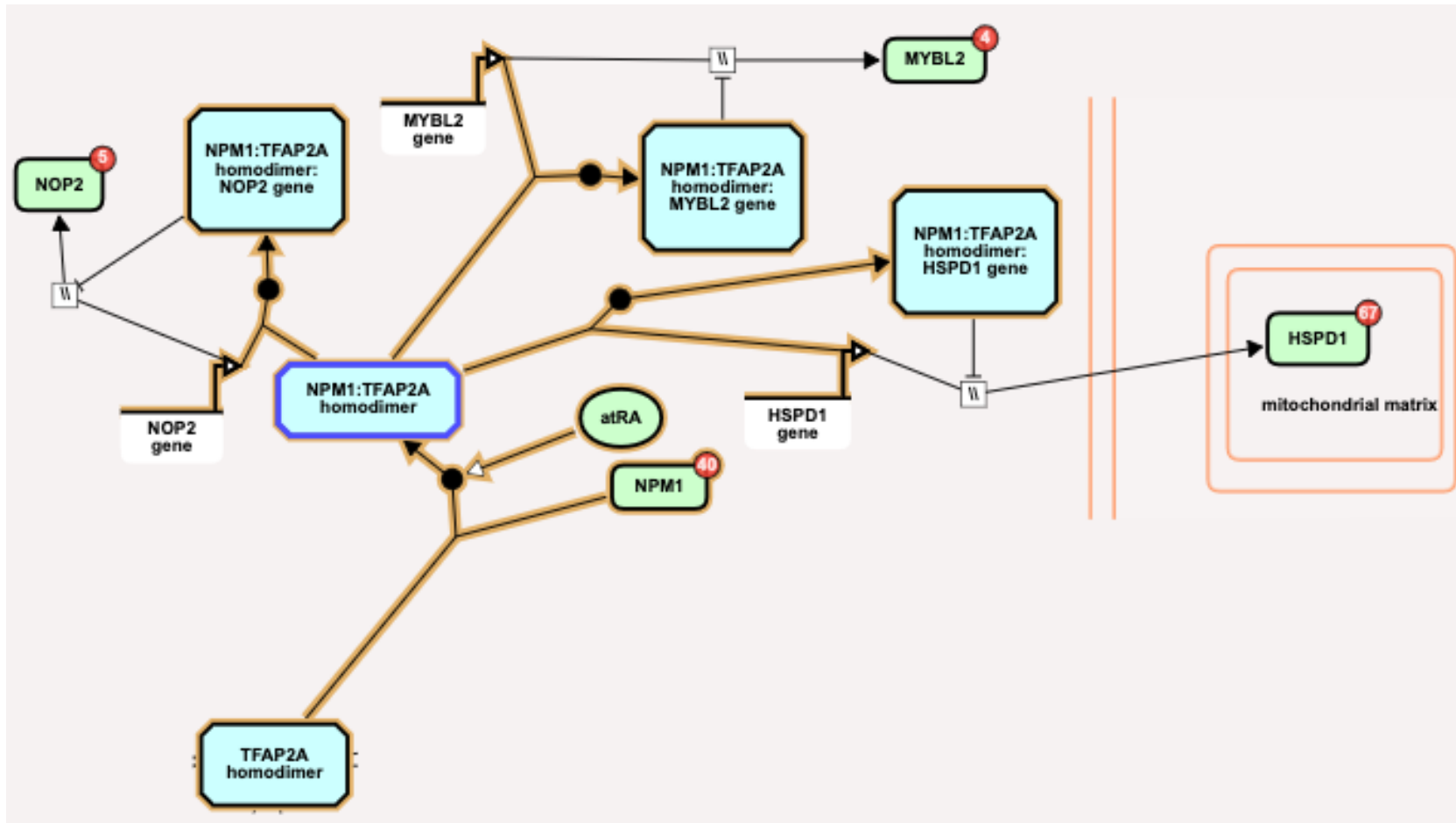


Figure 5.4 Predicted TFAP2A-NPM1 signalling pathway. According to Reactome signalling pathway platform, HSP60 is involved in TFAP2A-NPM1 signalling pathway where TFAP2A-NPM1 complex could suppress transcript expression of HSP60.

5.3.4 Interaction of EPLIN with the EGFR family proteins

The other most notable finding in the comparative study was that EGFR family members also showed potential to interact with EPLIN (Figure 5.5). The highlight finding is that ERBB2 (Her2) is amongst the most important pathway element that interacted with EPLIN and changed between normal and tumour. Of all 4 members, Her2 stands out as the most targeted protein by EPLIN. Three different antibodies were probed with pan-specific Her2 (NK054-2, NK054-4 and NK054-5), and showed a trend of enhanced signal intensity between normal samples and tumour samples. NK054-2 also demonstrated a 192% CFC changes and labelled as a priority target of EPLIN. Two phosphorylation sites of Her2 were also probed (PK134: T686 and PK013-1: Y1248), no outstanding difference between normal and tumour samples was noted.

A further key pathway in which Her2 plays a central role (Q00535) was identified in the Kinexus signalling profile report (Figure 5.6). Within this pathway, cyclin-dependent protein-serine kinase 5 (CDK5) was predicted to phosphorylate Her2 on S1174.

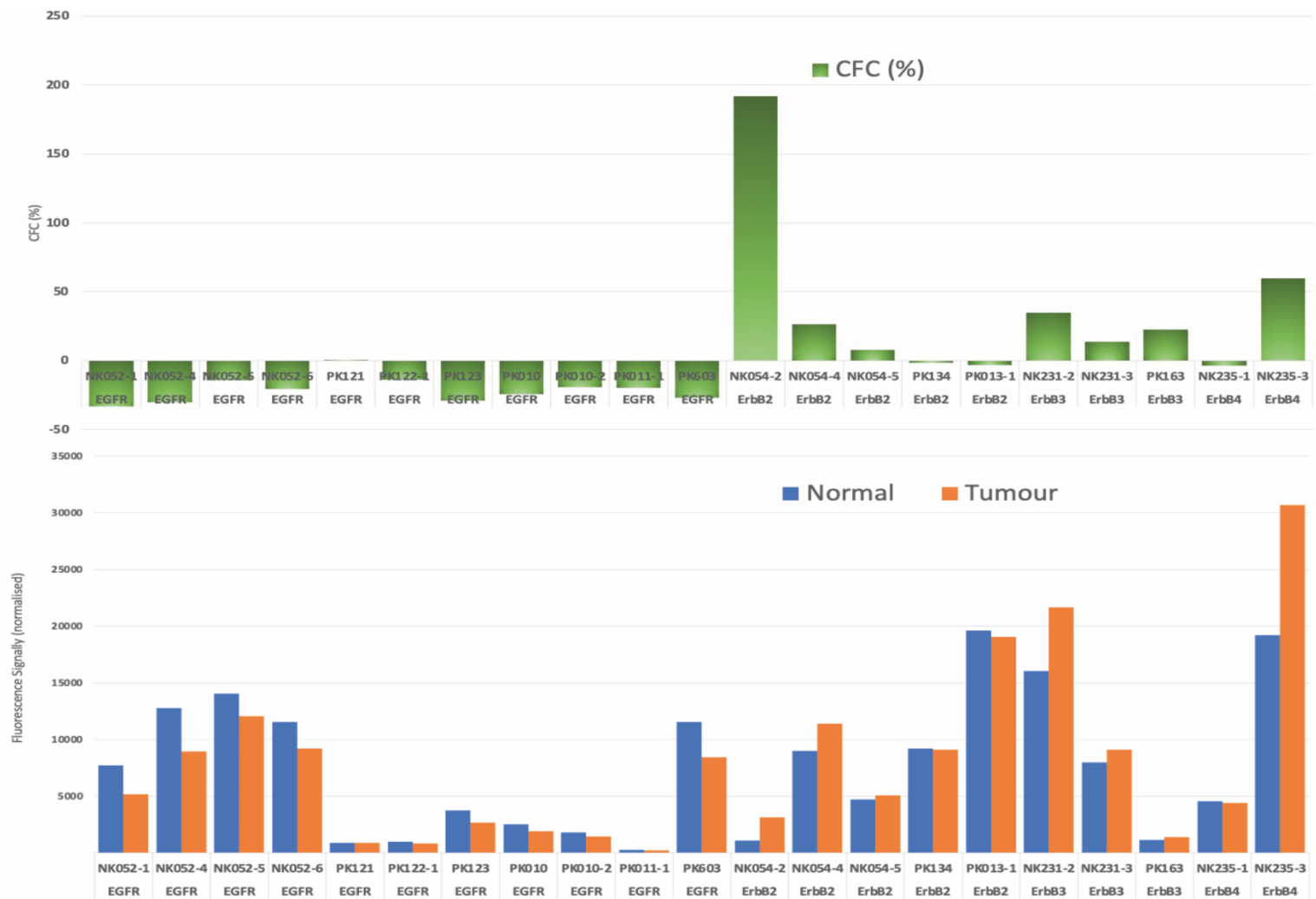


Figure 5.5 Interacting relationship between EPLIN and EGFR family members. Top. Percentage changes of signal intensity (%CFC) of tested EGFR family members between normal samples and tumour samples. Below. Normalised signal intensity of EGFR family members in normal samples and tumour samples. Different antibodies were utilised to probe with pan-specific proteins and phosphorylation sites.

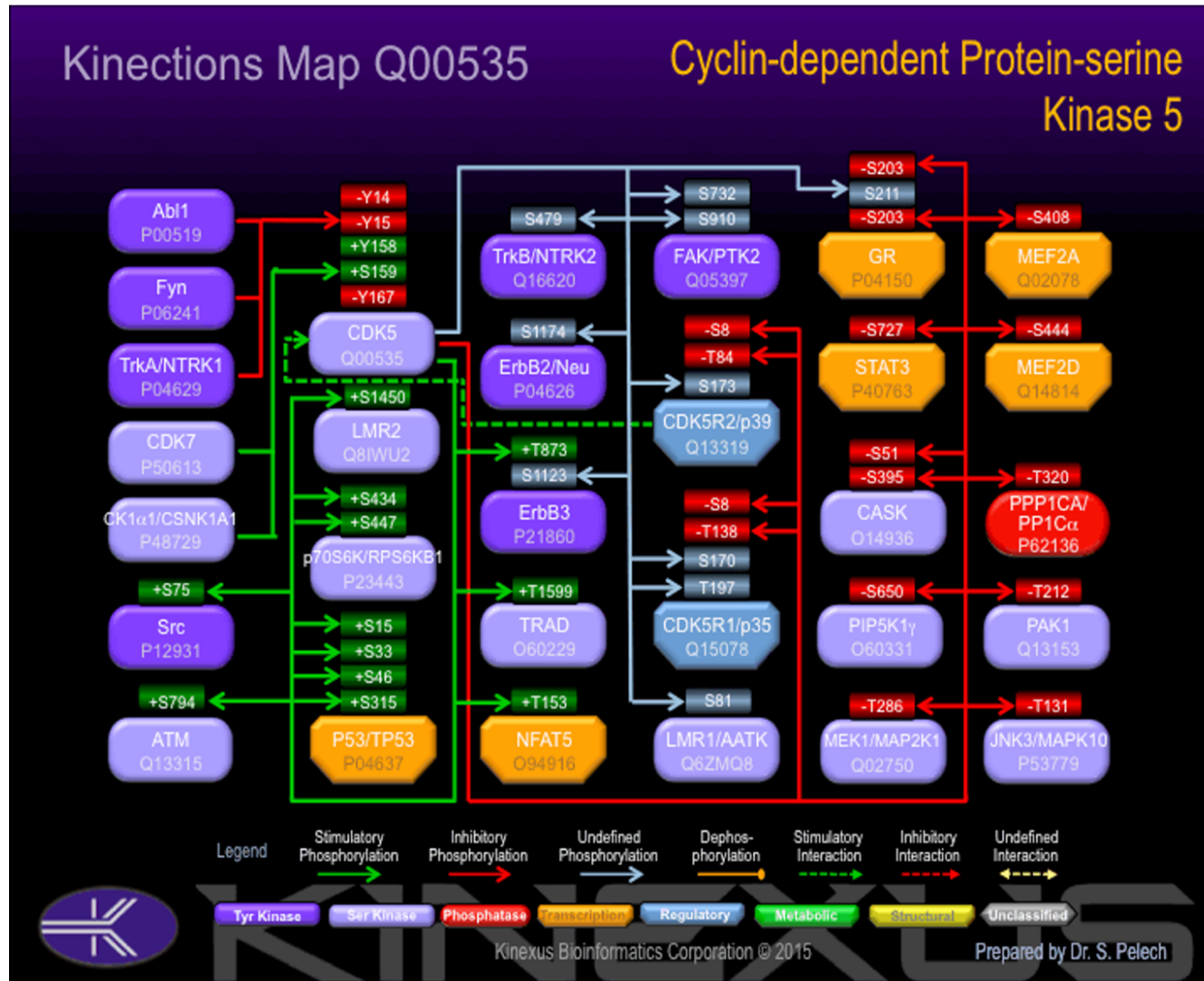


Figure 5.6 A Cyclin-dependent Protein-serine Kinase pathway that Her2 may involve. CDK5 was predicted to phosphorylate Her2 on S1174. Data was analysed by Kinexus (Kinexus Bioinformatics Ltd., Vancouver, BC, Canada).

5.3.5 Potential signalling pathways involved by the EPLIN interacting candidates

We also tested the key changes of these proteins in the Reactome analysis by emphasising the impact of the top upregulated and downregulated priority targets as well as HSP family members, namely Cyclin B1, eIF4E, Her2, STAT3, JAK3, HSP60, HSP90 and HSP70. The following Table is the key pathways that were identified (Table 5.3). The Reactome platform provided the most significant pathways that these candidates involve and interestingly, both HSP60 and Her2 are involved in the signalling pathway named Transcriptional regulation by the AP-2 (TFAP2) family of transcription factors (R-HSA-8864260) where Her2 transcript expression could be regulated by the family members TFAP2A, TFAP2B and or by the interaction between YY1 transcriptional factor and TFAP2A in breast cancer (Turner et al. 1998; Eckert et al. 2005). JAK3 and STAT3 were reported to participate in Interleukin-9 signalling (R-HSA-8985947), Interleukin-21 signalling (R-HSA-9020958), Interleukin-15 signalling (R-HSA-8983432), Interleukin-20 family signalling (R-HSA-8854691), Interleukin-7 signalling (R-HSA-1266695), signalling by ALK (R-HSA-201556) and Interleukin-2 family signalling (R-HSA-451927). Her2 and STAT3 are reported to be involved in Signalling by Non-Receptor Tyrosine Kinases (R-HSA-9006927) and signalling by PTK6 (R-HSA-8848021). Multiple drugs resistant pathways were also indicated due to Her2 was utilised as an input.

Table 5.3 Most significant pathways that top priority candidates involve. Cyclin B1, eIF4E, Her2, STAT3, JAK3, HSP60, HSP90 and HSP70 were used as input. Entities found: the number of input molecules found in pathways vs total number of molecules within pathways. Entities ratio: the proportion of Reactome pathway molecules represented by this pathway. False discovery rate (FDR): Corrected over-representation probability. Reaction found: the number of reactions in the pathways that are represented by input molecules vs total number of the reactions in the pathways. Reaction ratio: the proportion of Reactome reactions represented by this pathway.

Pathway name	Entities				Reactions	
	Found	Ratio	p-value	FDR*	Found	Ratio
Transcriptional regulation by the AP-2 (TFAP2) family of transcription factors	4/52	0.003	6.80e-08	1.03e-05	4/44	0.003
TFAP2 acts as a transcriptional repressor during retinoic acid induced cell differentiation	2/9	5.96e-04	2.33e-05	0.002	2/7	5.07e-04
Interleukin-9 signalling	2/11	7.27e-04	3.48e-05	0.002	10/13	9.42e-04
Interleukin-21 signalling	2/12	7.94e-04	4.14e-05	0.002	4/5	3.62e-04
Interleukin-15 signalling	2/16	0.001	7.35e-05	0.002	16/17	0.001
POU5F1 (OCT4), SOX2, NANOG activate genes related to proliferation	2/21	0.001	1.26e-04	0.003	2/16	0.001
TFAP2 family regulates transcription of growth factors and their receptors	2/21	0.001	1.26e-04	0.003	2/18	0.001
Interleukin-20 family signalling	2/29	0.002	2.40e-04	0.004	28/56	0.004
Interleukin-7 signalling	2/31	0.002	2.74e-04	0.004	13/26	0.002
Signalling by ALK	2/43	0.003	5.25e-04	0.007	16/40	0.003
Transcriptional regulation of pluripotent stem cells	2/45	0.003	5.74e-04	0.007	4/35	0.003
Interleukin-2 family signalling	2/47	0.003	6.26e-04	0.008	48/59	0.004
Signalling by Non-Receptor Tyrosine Kinase	2/70	0.005	0.001	0.014	8/53	0.004
Signalling by PTK6	2/71	0.005	0.001	0.014	8/53	0.004
Drug resistance in ERBB2 KD mutants	1/4	2.65e-04	0.003	0.019	8/8	5.80e-04
Drug-mediated inhibition of ERBB2 signalling	1/4	2.65e-04	0.003	0.019	3/3	2.17e-04
Resistance of ERBB2 KD mutants to osimertinib	1/4	2.65e-04	0.003	0.019	1/1	7.25e-05
Resistance of ERBB2 KD mutants to sapitinib	1/4	2.65e-04	0.003	0.019	1/1	7.25e-05
Resistance of ERBB2 KD mutants to tesevatinib	1/4	2.65e-04	0.003	0.019	1/1	7.25e-05
Resistance of ERBB2 KD mutants to AEE788	1/4	2.65e-04	0.003	0.019	1/1	7.25e-05
Resistance of ERBB2 KD mutants to trastuzumab	1/4	2.65e-04	0.003	0.019	1/1	7.25e-05
Resistance of ERBB2 KD mutants to lapatinib	1/4	2.65e-04	0.003	0.019	1/1	7.25e-05
Resistance of ERBB2 KD mutants to afatinib	1/4	2.65e-04	0.003	0.019	1/1	7.25e-05
Resistance of ERBB2 KD mutants to neratinib	1/4	2.65e-04	0.003	0.019	1/1	7.25e-05
Drug resistance in ERBB2 TMD/JMD mutants	1/4	2.65e-04	0.003	0.019	1/1	7.25e-05

5.3.6 Investigation of interaction among EPLIN, HSP60 and Her2 in CRC cell lines

As we demonstrated above, by utilising paired normal and tumour protein samples from the clinical cohort that precipitated EPLIN, the Kinexus protein microarray suggested that HSP60 and Her2 are two of the most priority potential interacting partners. To further investigate such potential protein interactions, we carried out immunoprecipitation assays using Protein A/G PLUS-Agarose immunoprecipitation reagent (sc-2003, Santa Cruz Biotechnology, Inc., Dallas, Texas, USA) on CRC cell lines. After extracting protein samples from 4 independent colorectal cancer cell lines, namely RKO, HRT18, HT115 and CaCo2, samples were then quantified to 2mg/ml and a portion (600µg) was used to precipitate with three different immunoglobulin G (IgG) monoclonal antibodies that target either EPLIN (sc-136399, Santa Cruz Biotechnology Inc. Dallas, Texas, USA), Her2 (sc-33684, Santa Cruz Biotechnology Inc. Dallas, Texas, USA) or HSP60 (sc-59567, Santa Cruz Biotechnology Inc. Dallas, Texas, USA) and then cross probed with antibodies to HSP60, Her2 or EPLIN in the following western blot analyses. Another portion of protein samples from total cell lysis (30µg) was also carried out on Western blotting to probe with EPLIN, Her2, HSP60 and GAPDH (sc-32233, Santa Cruz Biotechnology Inc. Dallas, Texas, USA) respectively as control.

Firstly, EPLIN precipitation was undertaken in the outlined cell lines' protein samples (600µg) and probed with HSP60 and Her2 by performing western blotting respectively. Total cell lysis from same the protein samples were utilised as controls (Figure 5.7). As shown in Figure 5.7A, following precipitation with EPLIN and probing with HSP60, two bands were visible which did not appear to related to HSP60 (60kDa) as clearly seen in the control samples. Given IgG monoclonal antibodies were used to perform immunoprecipitation assays and western blotting, these two identical bands could represent the heavy chain (around 50kDa) and light chain (25kDa) (Janeway CA Jr et al. 2001). Similarly, IP samples that were precipitated with EPLIN and probed with Her2 also show two bands that could similarly be identified as heavy (around 50kDa) and light polypeptide chains (25kDa) but not Her2 itself as the control samples indicated (Figure 5.7B).

Secondly, 600µg of protein samples was also utilised to precipitate either HSP60 or Her2. For samples that precipitated with HSP60, IgG monoclonal antibodies of EPLIN and Her2 were probed in 48µg IP samples respectively by performing western blotting. Similarly, the same amount of IP samples that precipitated with Her2 were carried out on western blotting to probe EPLIN and HSP60 (Figure 5.8). As shown in Figure 5.8A&B, no visible bands that

could indicate EPLIN or Her2 in all IP-HSP60 samples were seen. The only observable bands were seen between 48 and 63kDa and around 25kDa, which could represent IgG heavy or light polypeptide chains respectively. Hence, according to our observation, no direct protein-protein interactions between EPLIN, HSP60 and Her2 were identified in 4 different colorectal cancer cell lines.

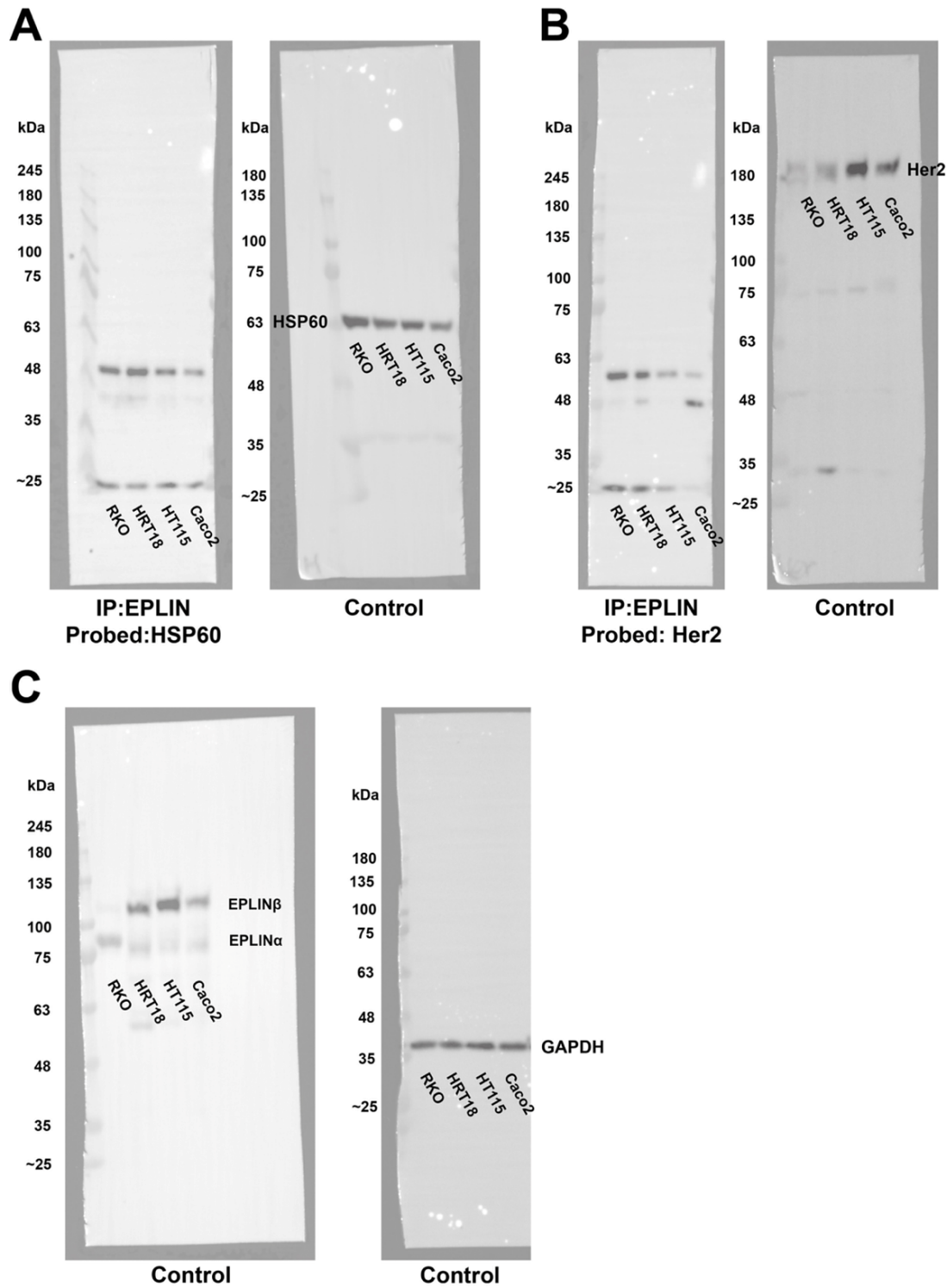


Figure 5.7 Immunoprecipitation of EPLIN in CRC cell lines. A. Left. 600 μ g Protein samples from four CRC cell lines were precipitated with EPLIN and 48 μ g was probed with HSP60 by western blotting. Right. 30 μ g of total cell lysis was used to probe HSP60 (as bands showed at around 60kDa) as control. B. Left. 600 μ g Protein samples were precipitated with EPLIN and 48 μ g of the IP samples was probed with Her2. Two identical bands of two IP samples possibly indicated heavy (50kDa) and light polypeptide chains (25kDa). Right. 30 μ g of total lysis protein samples was used to probe Her2 (185kDa, as band indicated). C. 30 μ g of protein samples from total cell lysis was used to probe EPLIN (α isoform: 90kDa; β isoform: 110kDa) and GAPDH (37kDa).

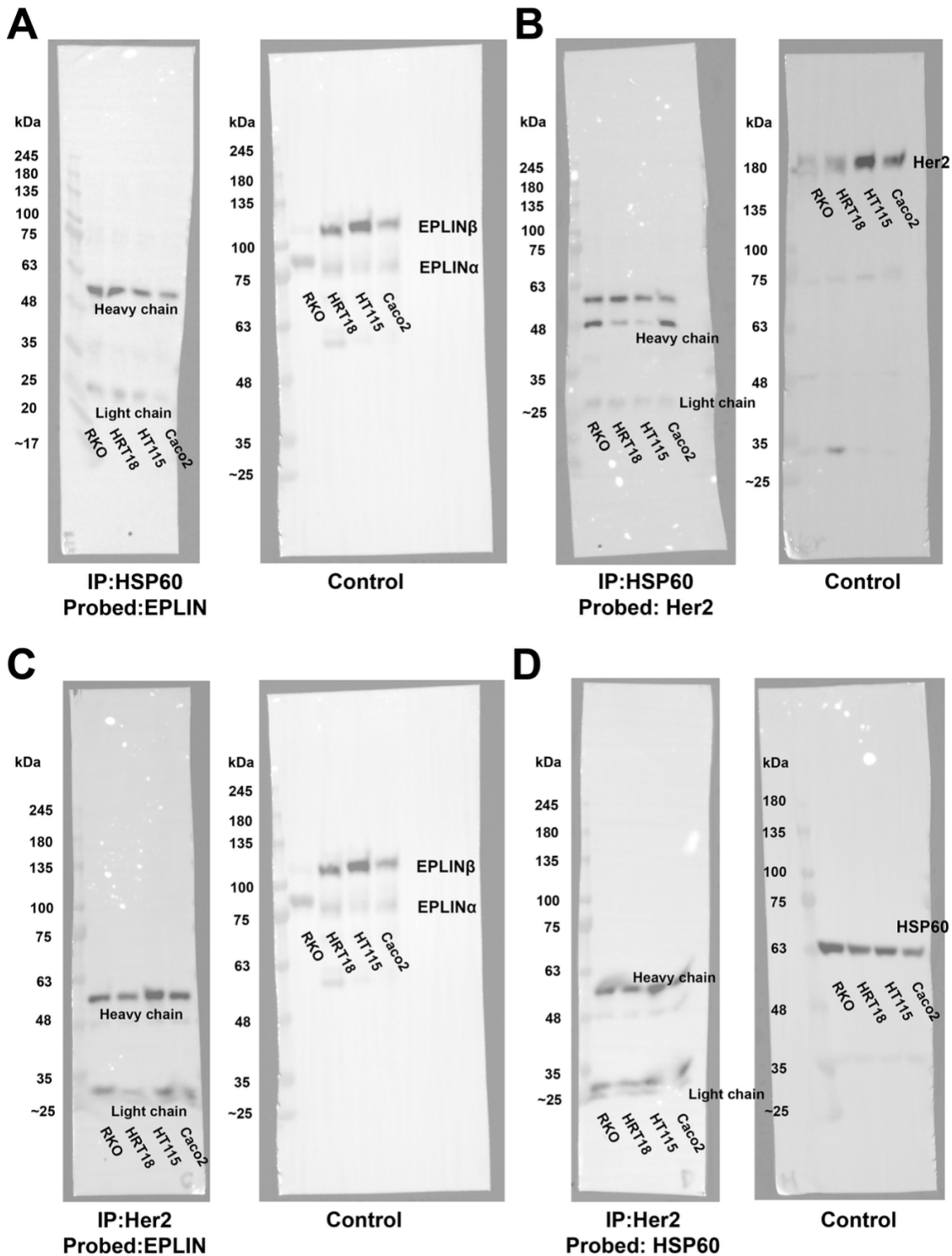


Figure 5.8 Immunoprecipitation of HSP60/Her2 on CRC cell lines. A. Left. 600 μ g protein samples from total cell lysis of 4 different CRC cell lines was used to precipitate HSP60 and 48 μ g was utilised to probe EPLIN by western blotting. A visible band between 48-63kDa might be identified as IgG heavy chain while a band showed around 25kDa might be IgG light chain. Right. 30 μ g protein samples of total cell lysis was used to probe EPLIN by western blotting as control. B. Left. 48 μ g HSP60 precipitated protein samples were used to probe Her2. Two visible bands between 48-63kDa were observed as well as one band around 25kDa which might be non-specific binding and could identified as heavy and light chains respectively. Right. 30 μ g of total cell lysis protein samples was used to probe Her2 as control. C. Left. 600 μ g protein samples was precipitated with Her2 and 48 μ g of it was used to probe EPLIN. Only possible IgG heavy chain (around 50kDa) and IgG light chain (25kDa) were identified. Right. 30 μ g samples from total cell lysis was used to probe EPLIN as control. D. Left. 48 μ g IP-Her2 samples was applied to probe HSP60, again, only non-specific binding bands (IgG heavy chain and light chain) could be seen. Right. 30 μ g total cell lysis samples was used to probe HSP60 as control.

5.3.7 Investigation into potential regulatory relationships between EPLIN, HSP60 and Her2 in colorectal cancer cell lines

In addition to carrying out immunoprecipitation assays on colorectal cancer wild type cell lines to investigate protein-protein interaction between EPLIN, HSP60 and Her2. We were also interested in exploring if these potential interacting partners have regulatory relationship between each other at either transcript or protein level.

Firstly, we established cellular models in RKO and HRT18 cell lines by knocking down EPLIN using shRNA EPLIN (RKO-KD-EPLIN, HRT18-KD-EPLIN). siRNA HSP60 was also used to create HSP60 inhibited cell lines (RKO-KD-HSP60, HRT18-KD-HSP60). Dual knocked down cell lines were established by carrying out shRNA EPLIN and siRNA HSP60 at the same time (RKO-KD-EPLIN/HSP60, HRT18-KD-EPLIN/HSP60). After RNA was extracted and used as a template to reverse transcribe cDNA, samples were subject to qPCR analysis to investigate transcript expression level of EPLIN, HSP60, GAPDH and Her2. Copy numbers of genes of interest was calculated according to the PDPL standard curve, that was amplified simultaneously, followed by normalisation against GAPDH. Normalised copy number of genes in RKO-WT and HRT18-WT was designated as 100% and used for comparison with other cellular models (Figure 5.9). As shown in Figure 5.9A &B, compared to RKO-WT and HRT18-WT, total EPLIN was successfully knocked down in RKO-KD-EPLIN ($p=0.046$), RKO-KD-EPLIN/HSP60 ($p=0.0051$), HRT18-KD-EPLIN ($p=0.0055$) and HRT18-KD-EPLIN/HSP60 ($p=0.0037$) cell lines, while HSP60 transcript expression was inhibited significantly in RKO-KD-HSP60 ($p=0.0039$), RKO-KD-EPLIN/HSP60 ($p=0.0049$), HRT18-KD-HSP60 ($p=0.00040$) and HRT18-KD-EPLIN/HSP60 ($p=0.0022$) cell lines. Following HSP60 suppression, although EPLIN transcript expression tended to be downregulated, no statistical significance was noted. Likewise, no significant changes of HSP60 transcript expression were observed following the inhibition of EPLIN expression in either RKO or HRT18 cell lines. Interestingly, as demonstrated in Figure 5.9C, a trend of Her2 transcript upregulation was noted when EPLIN or HSP60 expression was suppressed alone in RKO cell line, but it did not reach statistical significance. When EPLIN and HSP60 expressions were knocked down together in the RKO cell line, a significant 10-fold upregulation of Her2 transcript expression was noted (RKO-WT vs RKO-KD-EPLIN/HSP60: 100% VS 1085.3%, $p=0.043$). In the HRT18 cell lines, knocking down EPLIN alone led to a trend of upregulation of Her2 transcript expression but no significance was noted. While inhibition of HSP60 led to a significant upregulation of Her2 transcript expression (HRT18-WT vs HRT18-KD-HSP60: 100% vs 973.5%, $p=0.00016$). Increased transcript level of Her2 was also observed when EPLIN and HSP60 were knocked down

together in the HRT18 cell line (HRT18-WT vs HRT18-KD-EPLIN/HSP60: 100% vs 1657.8%, $p=0.00057$). Therefore, no significant regulatory relation was noted between HSP60 and EPLIN in RKO and HRT18 cell lines. Notably, knocking down EPLIN or HSP60 in RKO and HRT18 could result in an upregulation of Her2 transcript level, such upregulation was enhanced when both EPLIN and HSP60 were inhibited at the same time in RKO and HRT18 cell line.

Secondly, Protein samples were extracted from RKO-KD-EPLIN and control RKO-WT and subject to Western blot analysis to probe EPLIN, HSP60, Her2 and GAPDH (Figure 5.10 Left). As Figure 5.10A indicated, EPLIN expression was suppressed in RKO-KD-EPLIN when compared to the control. Following inhibition of EPLIN expression, no outstanding changes in HSP60 expression were observed (Figure 5.10C). Intriguingly, Her2 protein expression was upregulated when EPLIN expression was inhibited in the RKO cell line. Hence, our data suggested that downregulation of EPLIN could result in an upregulation of Her2 protein level.

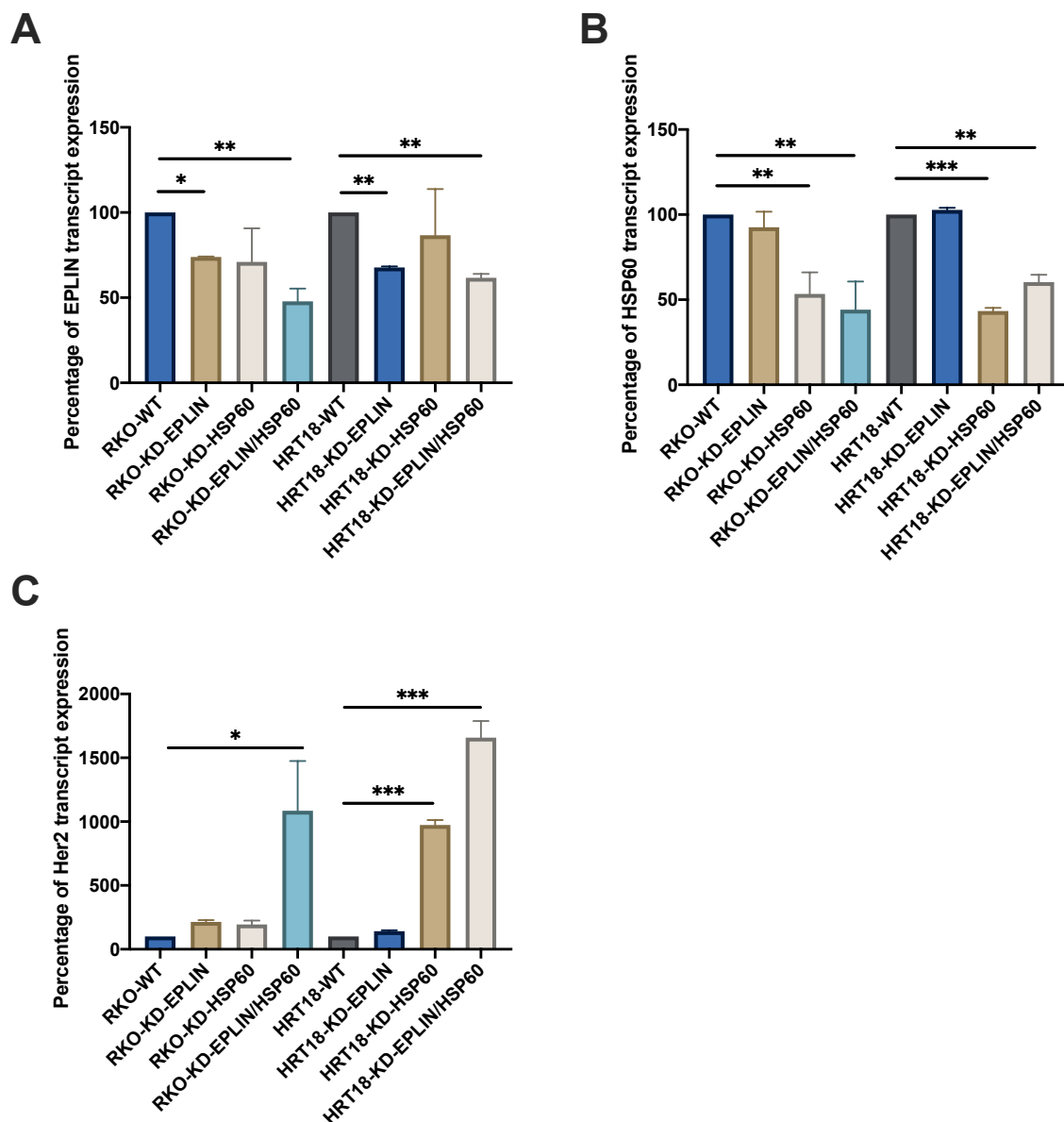


Figure 5.9 Regulatory relationship between EPLIN, HSP60 and Her2 transcript expression in colorectal cancer cellular models. A. EPLIN expression was inhibited in RKO and HRT18 cell lines successfully, although a trend of downregulation of EPLIN transcript level was noted when HSP60 was inhibited, it did not reach statistical significance. B. cellular models with knocked down HSP60 expression were established, but no significant changes of HSP60 transcript level was noted when EPLIN expression was suppressed. C. Upregulation of Her2 transcript expression could be observed when EPLIN and HSP60 expression was knocked down, significant upregulation was noted when HSP60 and EPLIN was suppressed together in RKO cell line (1085.3%) compared to RKO-WT (100%) ($p=0.043$) and in HRT18 cell line (1657.8%) when compared to HRT18-WT (100%) ($p=0.00057$). When HSP60 was inhibited alone in HRT18, Her2 transcript level was increased significantly (973.5%) when compared to HRT18-WT (100%) ($p=0.00016$). Copy number Data was quantified by PDPL standard, normalised by GAPDH. Data of WT was set as 100% and used to compare with other cellular models. $n=3$, * represents $p<0.05$, ** represents $p<0.01$, *** represents $p<0.001$.

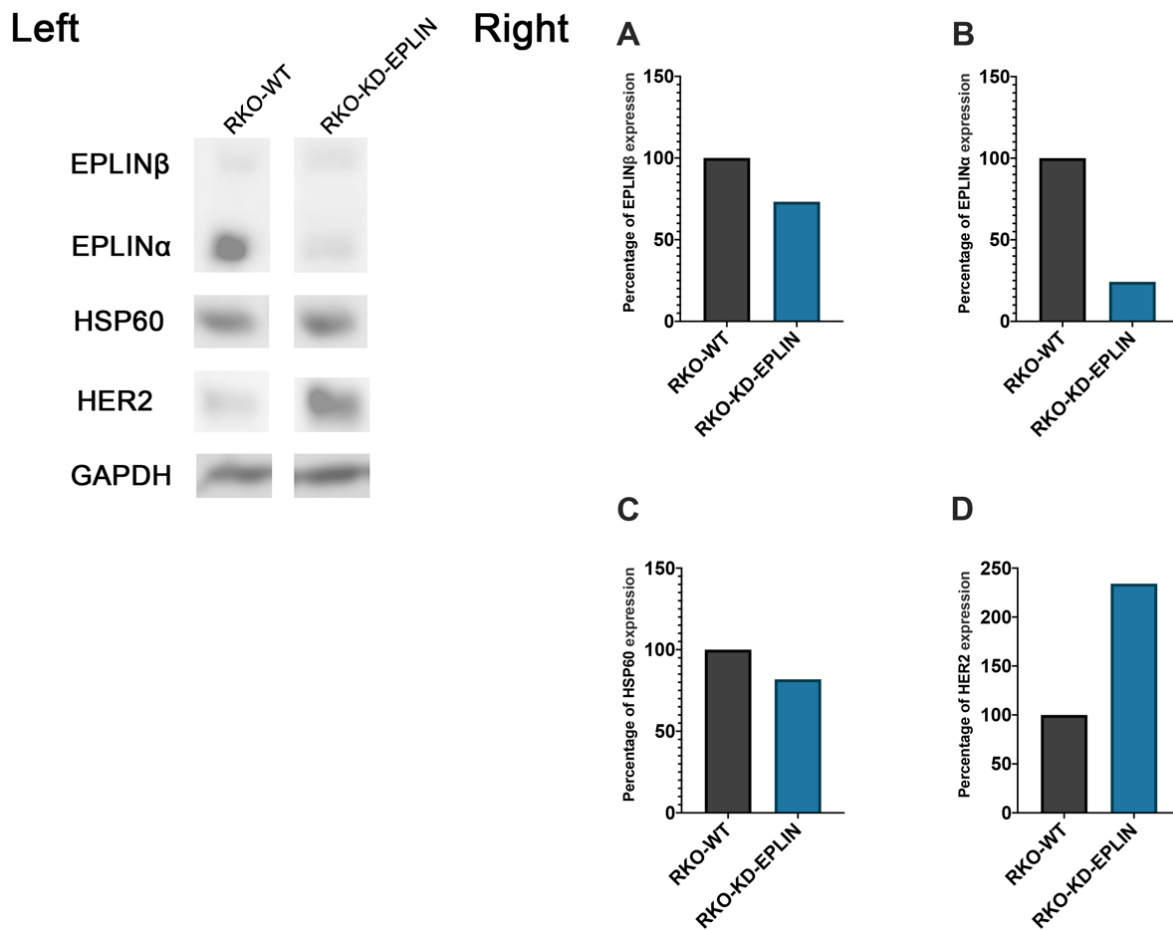


Figure 5.10 Regulatory relationship between EPLIN, HSP60 and Her2 protein expression in RKO cellular models. Left. Screening of western blot of RKO-WT and RKO-KD-EPLIN cell lines and probed with EPLIN, HSP60, Her2 and GAPDH. Right. A&B indicated a successful suppression of EPLIN isoforms in RKO-KD-EPLIN when compared to RKO-WT. C. No outstanding changes of HSP60 protein level was noted after knocking down EPLIN. D. Inhibition of EPLIN resulted in upregulation of Her2 protein level in the RKO cell line. Intensity of bands was quantified using ImageJ, then normalised by GAPDH. Data of RKO-WT was set as 100% and used for comparison with data of RKO-KD-EPLIN. n=3.

5.4 Discussion

This chapter aimed to explore EPLIN protein interactions and deduce a possible mechanism(s) underlying the biological function of EPLIN in colorectal cancer cells. Our previous protein microarray assays on EPLIN precipitated protein samples from colon cancer patients have suggested that EPLIN widely interacts with a number of protein kinases potentially and is involved in multiple signalling events in colon cancer. Apart from eIF4E, JAK3, a number of priority interacting candidates are involved in cyclins and MAPK related events. Some of these, for example, ERK1 and STAT3, have been reported to interact with EPLIN and regulate EMT process in prostate cancer (Steder et al. 2013; Zhang et al. 2013). Furthermore, we also noticed that EGFR family members, especially Her2 and HSP family members, were also on the list of leading priority candidates and related signalling events were also implicated, namely TFAP2 regulation signalling and drug

resistance signalling events due to Her2 and PKA Ca/b. Signalling events that related to Interleukins family were also suggested. From previous studies done in the host laboratory, CCMRC, we decided to focus on two key events related to EPLIN in colon cancer, namely Her2 and the HSP60 related events.

To further investigate their interacting relationship, we applied immunoprecipitation assays on colorectal cancer cell lines which indicated no interaction between EPLIN, HSP60 and Her2. Such disagreement with our protein microarray's data could be attributed to several reasons. Firstly, protein samples used for protein microarray assays were directly extracted from patient tissues, either normal tissues or tumour tissues. Such tissues not only include epithelial cells from colon cancer, but also other cells from microenvironments such as stromal cells, stem cells, etc. While immunoprecipitation was carried out on colorectal cancer epithelial cells, such outstanding interacting events might be occurring outside colorectal cancer epithelial cells, but not in the epithelial cells themselves. Apart from this, immunoprecipitation assays on colorectal cancer cells came back with strong bands of IgG non-specific bindings, namely IgG heavy chain and light chain. Because of the presence of these, weak interaction could be interfered with the image acquisition on the gel developer. The protein size of HSP60 is 60kDa, which is close to the size of the IgG heavy chain, around 50kDa, such interaction could also be affected. Last but not least, protein concentration could also be one of the impact factors, although we quantified samples to a reasonable concentration, weak interactions might not be observed. Interestingly, although no potential interaction between such candidates and EPLIN was noted, we did observe regulatory relation between them. Downregulation of HSP60 might lead to downregulation of EPLIN in RKO and HRT18, although no statistical significance was noted which might be due to the distribution of data. Downregulation of HSP60 resulted in upregulation of Her2 transcript level in HRT18. While inhibition of EPLIN might lead to upregulation of Her2 transcript level in RKO and HRT18, it did not have an impact on HSP60 in RKO at protein level. Notably, inhibition of EPLIN upregulated Her2 protein expression in RKO, and suppression of EPLIN and HSP60 together in RKO and HRT18 resulted in a more outstanding upregulation of Her2 transcript level. Such interesting findings highlighted an interesting and important line of investigation related to the relationship between EPLIN, HSP60 and Her2 and its wider implications in cancer progression and therapy response/resistance.

Chapter 6

Clinical significance of Her2 HSP60 and EPLIN interactions in colorectal cancer (CRC)

6.1 Introduction

EPLIN, a tumour suppressor, has been reported to be downregulated in a range of cancers including oral cancer (Chang et al. 1998; Maul and Chang 1999), breast cancer (Jiang et al. 2008), prostate cancer (Zhang et al. 2011), SCCHN (Zhang et al. 2013), lung cancer (Liu et al. 2012b), oesophageal cancer (Liu et al. 2012a), ovarian cancer (Liu et al. 2016), gastric cancer (Gong 2021) and CRC (Song et al. 2002; Lee et al. 2006). EPLIN has also been demonstrated to be related to clinical outcomes in multiple cancers such as breast cancer (Jiang et al. 2008), oesophageal cancer (Liu et al. 2012a) and gastric cancer (Gong 2021). In such studies, higher level of EPLIN have been associated with prolonged patient survival compared to those patients who expressed lower levels of EPLIN. Similar, by analysing our Cardiff clinical cohort and online databases in Chapter 3, we highlighted that patients with higher level of EPLIN had longer OS and RFS in comparison with those with lower levels of EPLIN in CRC. Hence, EPLIN has been implicated to be involved in carcinogenesis as well as prognosis.

Her2 is a member of the EGFR family and its activation, due to possibly add related ligand binding and receptor dimerization within the family leads to triggering of MAPK and AKT/PI3K signalling pathways which contribute to promotion of tumour developments (Greally et al. 2018). Overexpression of Her2 has been observed in a number of cancer types such as breast cancer, lung cancer, gastric cancer and CRC (Greally et al. 2018; Oh and Bang 2020). Attributing to its approximate 20% overexpression rates in breast cancer and multiple clinical traits, Her2 targeted therapies along with other EGFR targeted agents or adjuvant therapies have been well established in breast cancer. These therapeutic strategies have been indicated to have positive impact on patients' clinical outcomes (Isakoff and Baselga 2011; Oh and Bang 2020).

Although Her2 overexpression rates in CRC only accounts for around 7% (El-Deiry et al. 2015), it draws significant scientific attention to investigate its potential clinical implication in CRC. The pattern and expression profile of Her2 in CRC has been reported to be controversial (Schuell et al. 2006). However, a few studies have reported its upregulation, at the protein level, in aggressive CRC or CRC with wild type KRAS by conducting IHC (Osako et al. 1998; Siena et al. 2018). Moreover, a number of studies have implicated that high level of Her2 led to worse OS, RFS and PFS in patients with colorectal cancer (Osako et al. 1998; Yonesaka et al. 2011; Sartore-Bianchi et al. 2019).

Meanwhile, a few clinical trials investigating Her2 targeted therapies in CRC suggest that targeting Her2 might benefit CRC patients, especially those with positive EGFR and those with more aggressive pathological stages (Clark et al. 2003; Ramanathan et al. 2004; Hurwitz et al. 2016; Sartore-Bianchi et al. 2016; Meric-Bernstam et al. 2019). Therefore, Her2 has been indicated to be a potential marker associated with patients' survival in CRC.

Another molecule that has been placed in the spot light in CRC studies and indicated as a protein of interest in the present study is HSP60. HSP60 is a chaperonin protein that belongs to heat shock protein family (Gupta 1995). In the past, HSP60 was more considered as an intramitochondrial protein and researchers were more focused on its role in post-translational modification for client proteins in alliance with Hsp10 (Cappello et al. 2011; Caruso Bavisotto et al. 2020). Recently, growing scientific interest has focused on its role in carcinogenesis and cancer development.

Cappello *et al.* conducted IHC on colorectal cancer tissues and observed an upregulation of HSP60 in carcinoma tissues when compared to normal tissues. Further screening by western blotting also revealed an elevation of HSP60 in CRC cell lines (Cappello et al. 2003). Another study by He *et al.* also reported a relationship between HSP60 and clinical outcome in CRC by performing IHC and ELISA analysis on clinical tissue and serum samples (He et al. 2007). Similarly, by analysing serum samples from CRC patients and drawing comparisons with normal healthy samples, Vocka et al. (2019) reported an increased level in the CRC group when compared with the normal group and also reported an upregulation in lung metastatic samples (Vocka et al. 2019). Additionally, upregulation of HSP60 was observed at transcript and protein level in CRC by Campanella et al. In this study the authors highlighted that HSP60 expression levels decreased, in comparison to pre-surgery, in patients following ablative surgery (Campanella et al. 2015). Moreover, HSP60 has been demonstrated to be related with CRC patients' survival. Vocka *et al.* (2019) showed that high serum levels of HSP60 had a shorter OS in CRC patients compared to the negative group (Vocka et al. 2019). Therefore, HSP60 has also been implicated to participate in CRC carcinogenesis, development and prognosis.

Thus, similar to EPLIN, HSP60 and Her2 have been indicated to play a role in not only CRC carcinogenesis, but also cancer development and clinical outcomes. In this chapter, I have evaluated the clinical implication of these molecules, individually and in combination, in CRC clinical cohorts and online databases to verify if such interactions, highlighted in chapter 5 would affect clinical outcomes in CRC patients.

6.2 Methods

6.2.1 Tissue collection and processing

Please refer to chapter 2.5.

6.2.2 RNA extraction

Please refer to chapter 2.3.2.

6.2.3 Reverse transcription of RNA

Please refer to chapter 2.3.3.

6.2.4 qPCR

Please refer to chapter 2.3.6

6.2.5 IHC and TMA

A colorectal TMA (CO2161a) slide was utilised for IHC analysis to probe HSP60 at the protein level. For IHC assay protocol, please refer to Chapter 2.6. For detail information of the CRC TMA slide, please refer to Supplement-1.

6.2.5 Statistical analysis

SPSS (IBM, Armonk, New York, USA) and Minitab (Minitab Ltd. Coventry, UK) were used to analyse qPCR data from the clinical cohort.

6.3 Results

6.3.1 Transcript expressions of HSP60 in clinical CRC cohort.

Here, the Cardiff CRC clinical cohort, utilised in the analysis of EPLIN transcript expression in Chapter 3, was used in the qPCR analysis of HSP60 and Her2 transcript expression. The data was then analysed in comparison to clinical pathological information (Table 6.1 & Table 6.2).

As shown in Table 6.1, median transcript expression of HSP60 in tumour samples (n=94) is significantly higher than in normal samples (n=80) (0.45 vs 0.05, p=0.0097). Kruskal Wallis ANOVA on RANKS test revealed significant differences in TNM stages (p=0.045), T stages (0.033). When samples were divided based on TNM stages, median transcript expression in TNM1 group (n=9, median=53.9) was upregulated when compared with its expression in TNM 2, 3, 4, 2&3 and 3&4 groups. Similarly, samples were separated according to T-stages.

The T1 group was found to have the highest median transcript expression (n=2, median=152), while samples in T2 (n=10, median=54.3), T3 T3 (n=40, median=0.09) and T4 (n=18, median=0.4) presented with lower median transcript expression levels. No statistical significance was noted in comparison of other pathological information.

Table 6.1 Transcript expression profile of HSP60 in comparison to clinical pathological information of Cardiff CRC cohort.
a Mann Whitney; b Kruskal Wallis ANOVA on RANKS.

Characteristic	Sample number (n)	Median transcript expression	Q1	Q3	p - value
Tumour	94	0.45	0	39.5	
Normal	80	0.05	0.01	9.10	0.0097 ^a
Differentiation					0.562 ^b
High	2	27	*	*	
Moderate	54	0.1	0	29.8	
Low	14	1.6	0.1	54.3	
Moderate & low	67	0.2	0	32.6	
TNM stage					0.045 ^b
TNM1	9	53.9	13.5	255.4	
TNM2	30	0.1	0	5.3	0.0124 ^a
TNM3	26	0.1	0	4.3	0.0201 ^a
TNM4	6	32.9	13.3	93.1	0.5169 ^a
TNM2&3	56	0.1	0	4.5	0.0091 ^a
TNM3&4	32	0.2	0	32.6	0.0338 ^a
TNM2&3&4	62	0.2	0	21.1	0.0133 ^a
T stage					0.033 ^b
T1	2	152	*	*	
T2	10	54.3	0.1	275.7	
T3	40	0.09	0.01	6.38	
T4	18	0.4	0	19.6	
Dukes stage					0.235 ^b
Dukes A	7	36.2	0.1	242.6	
Dukes B	33	0.2	0	16	
Dukes C	32	0.2	0	32.6	
Nodal involvement					
Negative	39	0.5	0	38.8	
N1	16	0.3	0	48.8	0.9114 ^a
N2	15	0.1	0	11.2	0.6354 ^a
All node positive	0.2	0.2	0	27.3	0.8369 ^a
Metastasis					
No metastasis	50	0.2	0	37	
Distant metastasis	19	0.17	0.01	2.13	0.3634 ^a
Incidence					
Disease free	35	1	0	53.9	
With incidence	23	0.11	0.01	1.16	0.0845 ^a
Recurrence					
No Recurrence	58	0.2	0	31.6	
Local Recurrence	7	0.459	0.106	1.165	0.8888 ^a
Survival					
Alive	36	0.2	0	38.1	
Died	22	0.09	0.01	2.73	0.1914 ^a
Non invasive	50	0.2	0	25.1	
Invasive	26	0.2	0	43.4	0.8927 ^a

6.3.2 Transcript expressions of HER2 in clinical CRC cohorts.

The transcript expression of Her2 in the Cardiff clinical cohort was analysed in comparison to pathological information (Table 6.2). Tumour samples were found to express significantly higher level of Her2 (median=0.4103) compared with normal samples (median=0.0043) ($p < 0.001$). A trend of increasing median transcript expressions of Her2 along T-stages with was also observed, which may indicate that Her2 is related to invasiveness, although this observation did not reach statistical significance ($p = 0.571$). Intriguingly, median transcript expression of Her2 in CRC patients with distant metastasis (0.176), incidence (1.153), local recurrence (1.248), or who died (1.141) was found to be elevated when compared to relative counterpart groups (no metastasis median=0.413, disease free median=0.843, no recurrence median=0.431, alive median=0.902 respectively). Once again, no statistical significance was reported ($p > 0.05$), which may be due to the limitation of the sample size.

Table 6.2 Transcript expression profile of Her2 in comparison to clinical pathological information of Cardiff CRC cohort. a
Mann Whitney; b Kruskal Wallis ANOVA on RANKS.

Characteristic	Sample number (n)	Median transcript expression	Q1	Q3	p - value
Tumour	94	0.4103	0.066	1.352	
Normal	80	0.0043	0.0002	0.02	<0.001 ^a
Differentiation					0.379 ^b
High	2	0.553	*	*	
Moderate	54	0.810	0.186	1.591	
Low	14	0.302	0.055	1.284	
Moderate and low	67	0.553	0.149	1.560	
TNM stage					0.492 ^b
TNM1	9	0.29	0.05	1.52	
TNM2	30	0.874	0.224	1.561	
TNM3	26	0.393	0.114	1.616	
TNM4	6	0.118	0.003	1.211	
TNM2&3	56	0.720	0.197	1.616	
TNM3&4	32	0.363	0.048	1.503	
TNM2&3&4	62	0.553	0.144	1.503	
T stage					0.571 ^b
T1	2	0.1217	*	*	
T2	10	0.35	0.19	1.31	
T3	40	0.72	0.139	1.42	
T4	18	1.046	0.122	1.887	
Dukes stage					0.548 ^b
Dukes A	7	0.77	0	1.94	
Dukes B	33	0.846	0.224	1.309	
Dukes C	32	0.363	0.048	1.503	
Nodal involvement					
N0	39	0.784	0.178	1.477	
N1	16	0.298	0.144	1.591	0.5942 ^a
N2	15	0.413	0.009	1.355	0.6065 ^a
N1&2	0.2	0.373	0.073	1.544	0.5100 ^a
Metastasis					
No metastasis	50	0.413	0.0688	1.313	
Distant metastasis	19	1.123	0.176	2.088	0.1767 ^a
Incidence					
Disease free	35	0.843	0.243	1.616	
With incidence	23	1.153	0.17	2.088	0.6385 ^a
Recurrence					
No Recurrence	58	0.431	0.142	1.37	
Local Recurrence	7	1.248	0.95	2.643	0.1649 ^a
Survival					
Alive	36	0.902	0.226	1.645	
Died	22	1.141	0.208	1.898	0.666 ^a
Non invasive	50	0.879	0.16	1.55	
Invasive	26	0.376	0.032	1.402	0.8927 ^a

6.3.3 Correlation of Hers, HSP60 and EPLIN in clinical CRC cohort

To explore a possible relation in clinical samples between EPLIN and the key targets of interest discovered in the previous chapter, I examined the correlation between EPLIN and the Hers family members (EGFR, Her2, Her3 and Her4) and HSP60.

Firstly, we performed the analysis in normal samples (Table 6.3). EPLIN is positively correlative with Her2 (Spearman's correlation: 0.419) and HSP60 (Spearman's correlation: 0.713) significantly ($p < 0.01$). Her2 also holds a significant positive correlation with HSP60 (Spearman's correlation: 0.438; $p < 0.01$). Interestingly, these three molecules, all significant correlate with Her1 (EGFR) in a positive manner (EPLIN vs Her1: 0.233, $p = 0.046$; Her2 vs Her1: 0.347, $p = 0.02$; HSP60 vs Her1: 0.296, $p = 0.008$). These observations implicate a correlation and possible interaction/regulatory relationship between these three molecules in normal tissues. Moreover, they are all indicated to be involved in the EGFR signalling pathway network.

Table 6.3 Spearman's correlation between EPLIN, Hers and HSP60 in normal samples from the Cardiff clinical cohort. * represents p value (two-tailed) < 0.05 , ** represents p value (two-tailed) < 0.01 .

Name		EPLIN (Normal)	Her1 (Normal)	Her2 (Normal)	Her3 (Normal)	Her4 (Normal)	HSP60 (Normal)
EPLIN (Normal)	Correlation	1	0.223*	0.419**	0.136	-0.155	0.713**
	Number	80	80	79	73	80	80
	P value	*	0.046	< 0.01	0.253	0.169	< 0.01
Her1 (Normal)	Correlation	0.223*	1	0.347**	0.312**	0.116	0.296**
	Number	80	80	79	73	80	80
	P value	0.046	*	0.002	0.007	0.304	0.008
Her2 (Normal)	Correlation	0.419**	0.347**	1	0.134	0.03	0.438**
	Number	80	80	79	72	79	79
	P value	< 0.01	0.002	*	0.261	0.794	< 0.01
Her3 (Normal)	Correlation	0.136	0.312**	0.134	1	0.004	0.283*
	Number	80	80	72	73	73	73
	P value	0.253	0.007	0.261	*	0.971	0.015
Her4 (Normal)	Correlation	-0.155	0.116	0.03	-0.172	1	-0.355**
	Number	80	80	79	68	80	75
	P value	0.169	0.304	0.794	0.16	*	0.002
HSP60 (Normal)	Correlation	0.713**	0.296**	0.438**	.283*	-0.047	1
	Number	80	80	79	73	80	80
	P value	< 0.01	0.008	< 0.01	0.015	0.679	*

Secondly, we analysed the correlation of these molecules in the tumour samples (Table 6.4). Unlike the correlation between EPLIN and Her2 in normal samples, their correlation was not found to be significant in tumour samples. While HSP60 and EPLIN still displayed a significant positive correlations (EPLIN vs HSP60: 0.488, $p < 0.01$). Additionally, the observed significant relationship between EPLIN and Her1 in normal samples was no longer noted in the tumour samples. Interestingly, EPLIN and Her3 have a negative correlation in tumour samples (EPLIN vs Her3: -0.272, $p = 0.018$). Meanwhile, Her2 appeared not to correlate with either EPLIN nor HSP60, but Her3 (Her2 vs Her3: 0.248, $p = 0.034$). In addition to correlating positively with EPLIN, Her1 as well as Her4 are indicated to correlate with HSP60 positively and significantly (HSP60 vs Her1: 0.406, $p < 0.01$; HSP60 vs Her4: 0.248, $p = 0.017$). The Spearman's analysis conducted in tumour samples highlights that EPLIN has a significant positive correlation with HSP60, but not Her2.

Table 6.4 Spearman's correlation between EPLIN, Hers and HSP60 in tumour samples from the Cardiff clinical cohort. * represents p value (two-tailed) < 0.05 , ** represents p value (two-tailed) < 0.01 .

Name		Her1 (Tumour)	Her2 (Tumour)	Her3 (Tumour)	Her4 (Tumour)	HSP60 (Tumour)
EPLIN (Tumour)	Correlation	0.09	-0.152	-0.272*	0.191	0.488**
	Number	91	92	75	94	93
	P value	0.394	0.148	0.018	0.065	< 0.01
Her1 (Tumour)	Correlation	1	0.179	-0.078	0.220*	0.406**
	Number	91	89	75	91	90
	P value	*	0.093	0.507	0.036	< 0.01
Her2 (Tumour)	Correlation	0.179	1	0.248*	-0.029	0.012
	Number	89	92	73	92	91
	P value	0.093	*	0.034	0.784	0.909
Her3 (Tumour)	Correlation	-0.078	0.248*	1	-0.230*	-0.179
	Number	75	73	75	75	74
	P value	0.507	0.034	*	0.047	0.127
Her4 (Tumour)	Correlation	0.220*	-0.029	-0.230*	1	0.248*
	Number	91	92	75	94	93
	P value	0.036	0.784	0.047	*	0.017
HSP60 (Tumour)	Correlation	0.406**	0.012	-0.179	0.248*	1
	Number	90	91	74	93	93
	P value	< 0.01	0.909	0.127	0.017	*

Finally, I also investigated the correlation in the cohort as a whole (Table 6.5). In this analysis EPLIN was found to correlate with HSP60 positively (EPLIN vs HSP60: 0.477,

p<0.01), which remains in line the observations of the normal and tumour sample analyses. Her2 was not found to have a significant correlation with EPLIN, as it did in normal samples. Regarding HSP60, the analysis still shows a significant positive correlation with Her2 (HSP60 vs Her2: 0.295, p<0.01). Apart from the relationships between these two potential interacting partners, we also observed that Her1 and Her3 hold a negative correlated relationship with EPLIN (EPLIN vs Her1: -0.232, p=0.02; EPLIN vs Her3: -0.175, p=0.033). Moreover, HSP60 also correlates with Her1 positively (HSP60 vs Her1: 0.342, p<0.01).

Table 6.5 Spearman's correlation between EPLIN, Hers and HSP60 in all samples from the Cardiff clinical cohort. * represents p value (two-tailed) < 0.05, ** represents p value (two-tailed) < 0.01.

Name		Her1 (All)	Her2 (All)	Her3 (All)	Her4 (All)	HSP60 (All)
EPLIN (All)	Correlation	-0.232**	-0.0137	-0.175*	0.023	0.477**
	Number	171	171	148	174	173
	P value	0.002	0.075	0.033	0.766	<0.01
Her1 (All)	Correlation	1	0.605**	0.276**	0.023	0.342**
	Number	171	168	148	174	170
	P value	*	<0.01	0.001	0.766	<0.01
Her2 (All)	Correlation	0.605**	1	0.289**	0.011	0.295**
	Number	168	171	145	171	170
	P value	<0.01	*	<0.01	0.883	<0.01
Her3 (All)	Correlation	0.276**	0.289**	1	-0.11	0.051
	Number	148	145	148	148	147
	P value	0.001	<0.01	*	0.181	0.543
Her4 (All)	Correlation	0.023	0.011	-0.11	1	0.129
	Number	174	171	148	174	173
	P value	0.766	0.883	0.181	*	0.091
HSP60 (All)	Correlation	0.342**	0.295**	0.051	0.129	1
	Number	170	170	147	173	173
	P value	<0.01	<0.01	0.543	0.091	*

6.3.4 Implications of Her2, HSP60 and EPLIN on patients' overall survival.

The above analysis has indicated the possible relationships between EPLIN, HSP60 and Her2 family and that EPLIN may be involved in their networks. Additionally, aberrant expression of EPLIN, HSP60 and Her2 are implicated to relate to oncogenesis and tumour development in CRC. Here, I carried out survival analysis to further investigate their clinical implications in CRC. Firstly, we generated survival curves to analyse patients' overall survival (OS) in the Cardiff clinical cohort.

As Figure 6.1A shows, in the Cardiff clinical cohort, patients with tumours presenting with high levels of HSP60 (n=14) have significantly better OS (mean=167.231 months) than those with lower levels of HSP60 (n=59) (mean=113.758 months) (p=0.025). Analysis of the implication of Her2 expression on OS (Figure 6.1B) demonstrated that patients who expressed higher level of Her2 (n=40) had significantly worse OS than those who expressed lower level of Her2 (n=19) (mean: 101.319 months vs 149.386 months) (p=0.003).

We also explored patients' OS in the clinical cohort in combination with the expression of EPLIN, HSP60 and Her2 by performing the Kaplan-Meier method. As we demonstrated in Figure 6.1C, patients with no aberrant expression of either HSP60 or Her2 (n=13) hold a significant longer OS (mean=167.231 months) than those with abnormal expression of either HSP60 or Her2 (n=33) (mean=136.34 months) (p=0.004), while patients who express both aberrant HSP60 and Her2 (n=28) have the worst OS compared to the rest two groups (mean=96.854 months) (p=0.004). Interestingly, when we include expression of EPLIN into the analysis (Figure 6.1 D), the aberrant expression of these molecules have a significant impact on patients' OS (p<0.001). Patients with aberrant expressions of EPLIN, HSP60 and Her2 (n=10) have the worst OS (mean=35.05 months) compared to those with either abnormal expression of EPLIN, HSP60 or Her2 (n=52) (mean=129.44months) and those without any (n=12) (mean=166.417 months). Therefore, patients who express aberrant EPLIN, HSP60 and Her2 have the worst clinical outcome compared with other groups.

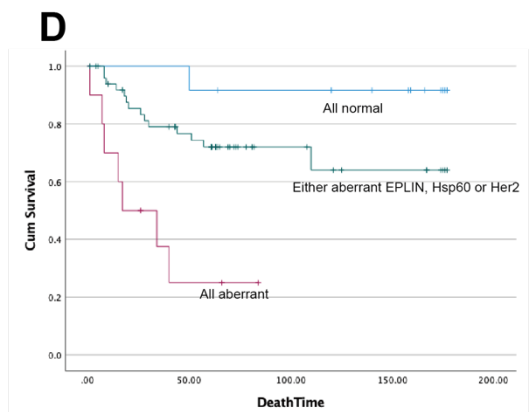
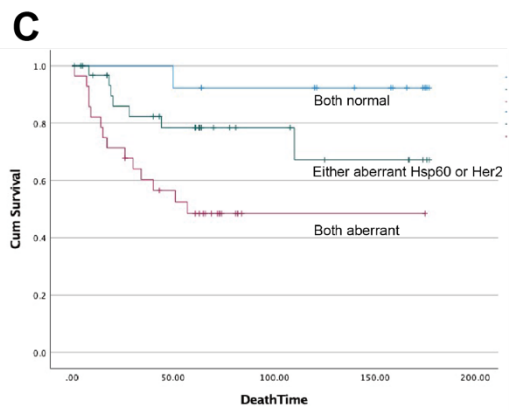
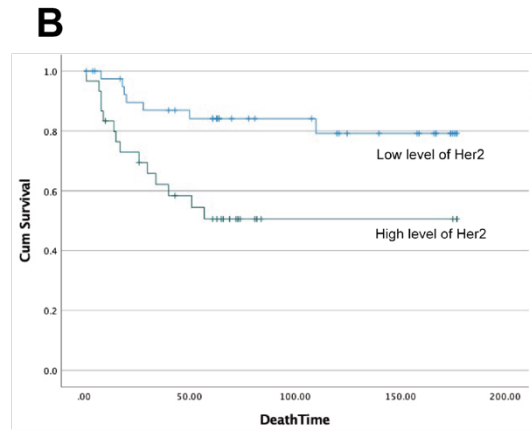
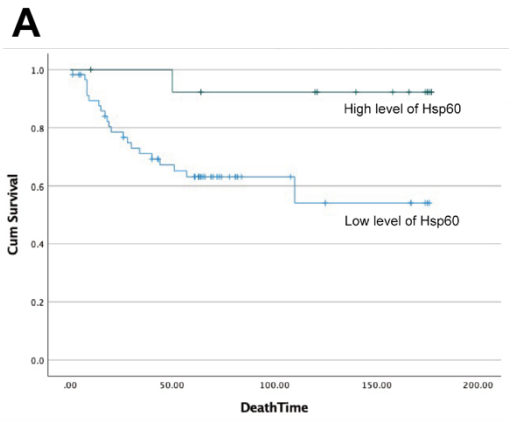


Figure 6.1 Survival Curve showing the impact of EPLIN, HSP60 and Her2 expression on patients' overall survival in the Cardiff clinical cohort. *A.* Patients with low levels of HSP60 have the worst OS. *B.* Patients with high levels of Her2 have the worst OS. *C.* Patients with aberrant levels of HSP60 and Her2 have the worst OS compared to those with either abnormal expression of HSP60 or Her2 and those without aberrant expression of neither of them. *D.* Patients with abnormal expressions of EPLIN, Her2 and HSP60 have the worst OS compared to those who express aberrant expression of either of them and those without any abnormal expression of neither.

Apart from analysing our available clinical cohort, we were also interested in exploring other independent cohorts to authenticate our own findings. Therefore, we accessed the Kaplan-Meier Plotter (www.kmplot.com) site, which includes a rectum adenocarcinoma dataset from TCGA, to investigate the impact of HSP60 and Her2 on OS (Figure 6.2). Patients were grouped according to the expression of HSP60 or Her2 using the best cutoff value identified with the online survival analysis, KMplot platform. Surprisingly, non-significant impact of expressions of HSP60 or Her2 on patients' OS was noted in this dataset ($p=0.058$, $p=0.077$ representatively). However, some outstanding trends could be observed. For example, patients with high level of HSP60 tended to have longer OS, especially after 60 months (Figure 6.2A). While patients with high level of Her2 tended to have longer OS before 60 months, which dropped rapidly after 60 months and lead to a shorter OS when compared to the patients with weaker expression of Her2 (Figure 6.2B). These intriguing findings support our results to a certain degree, but the non-significance might be due to the limited number of samples.

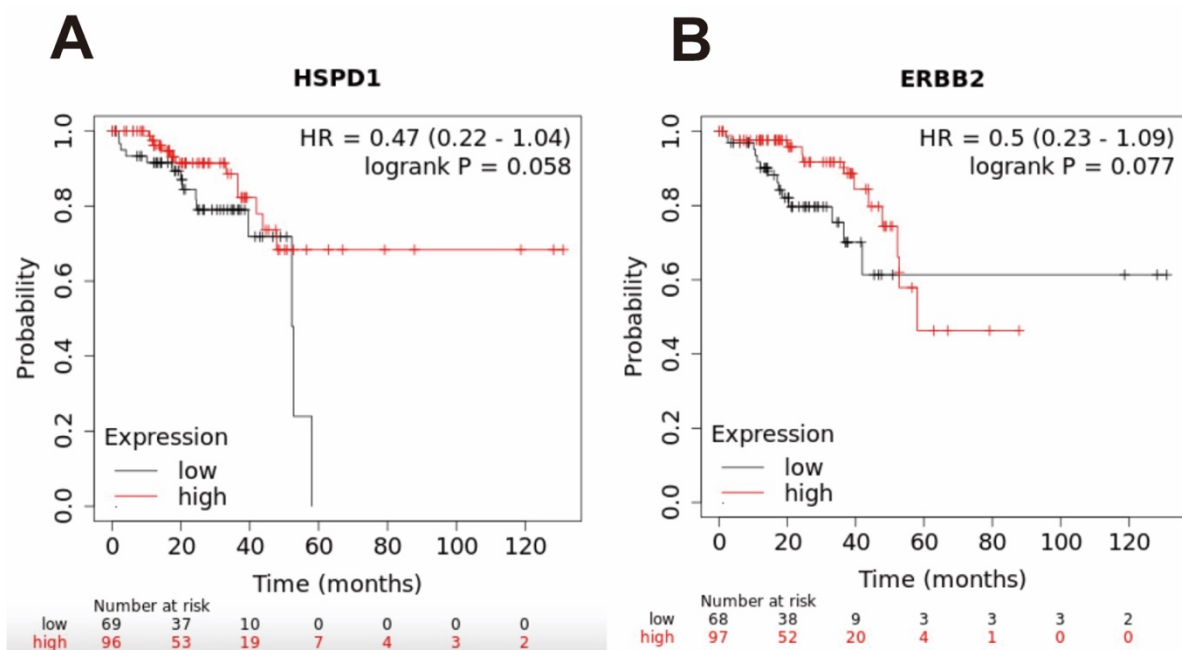


Figure 6.2 Survival Curve showing the impact of HSP60 and Her2 expressions on overall survival in rectum adenocarcinoma patients from TCGA-CRC dataset. (Left) Expression levels of HSP60 do not have a significant impact on rectum adenocarcinoma patients' OS, $p=0.058$. (Right) Expression levels of Her2 do not affect rectum adenocarcinoma patients' OS significantly, $P=0.077$. Data was accessed and collected from Kaplan-Meier Plotter (kmplot.com).

Moreover, to further investigate the impact of these molecules on patients' OS, we carried out a multivariate analysis using the Cox regression model in the Cardiff clinical cohort to examine if EPLIN, HSP60 and Her2 would be a reliable predictor for patients' OS (Table 6.6). As the table showed, none of the pathological and clinical indicators presented a significant predicative value. Interestingly, the combination of EPLIN, HSP60 and Her2 was shown as a significant predictor for OS on patients (Harzard Ratio 5.461, $p=0.024$). Hence, this supports our findings that EPLIN, HSP60 and Her2 could have an impact on OS on CRC patients.

Table 6.6 Cox regression multivariate analysis on Cardiff clinical cohort. Combination of EPLIN, HSP60 and Her2 were identified to be a significant predictor affecting OS on CRC patients.

	B	SE	Wald	df	significance	Hazard Ratio
Invasion	.988	.796	1.541	1	.215	2.685
Treatment	.237	.429	.305	1	.581	1.267
Location	-.615	.372	2.732	1	.098	.540
Dukes	-2.344	1.259	3.467	1	.063	.096
Stage	.810	.677	1.432	1	.231	2.249
TNM	.768	.977	.618	1	.432	2.155
Node	-.455	1.451	.099	1	.754	.634
Differentiation	-.717	.819	.766	1	.381	.488
EPLIN, HSP60&Her2	1.698	.753	5.085	1	.024	5.461

6.3.5 Implications of Her2, HSP60 and EPLIN on patients' relapse-free survival.

Likewise, we investigate the influence of EPLIN, Her2 and HSP60 on RFS of CRC patients simultaneously.

Initially, we conducted survival curve analysis using the Kaplan-Meier method on the Cardiff clinical CRC cohort. As Figure 6.3A shows, Patients with higher level of HSP60 was found to have better RFS (n=14, mean=164.43) than those with lower level of HSP60 (n=59, mean=106.44) ($p=0.022$), while Figure 6.3B indicated that patients who had higher level of Her2 (n=30, mean=93.42) was found to have worse RFS than those had lower level of Her2 (n=42, mean=143.55) ($p=0.008$). Besides, As Figure 6.3 C&D shows, HSP60 and Her2 have a significant impact on RFS ($p=0.009$). The EPLIN/HSP60/Her2 combination was found to be a far more powerful indicator of RFS of CRC patients (Figure 6.3B, $p<0.001$).

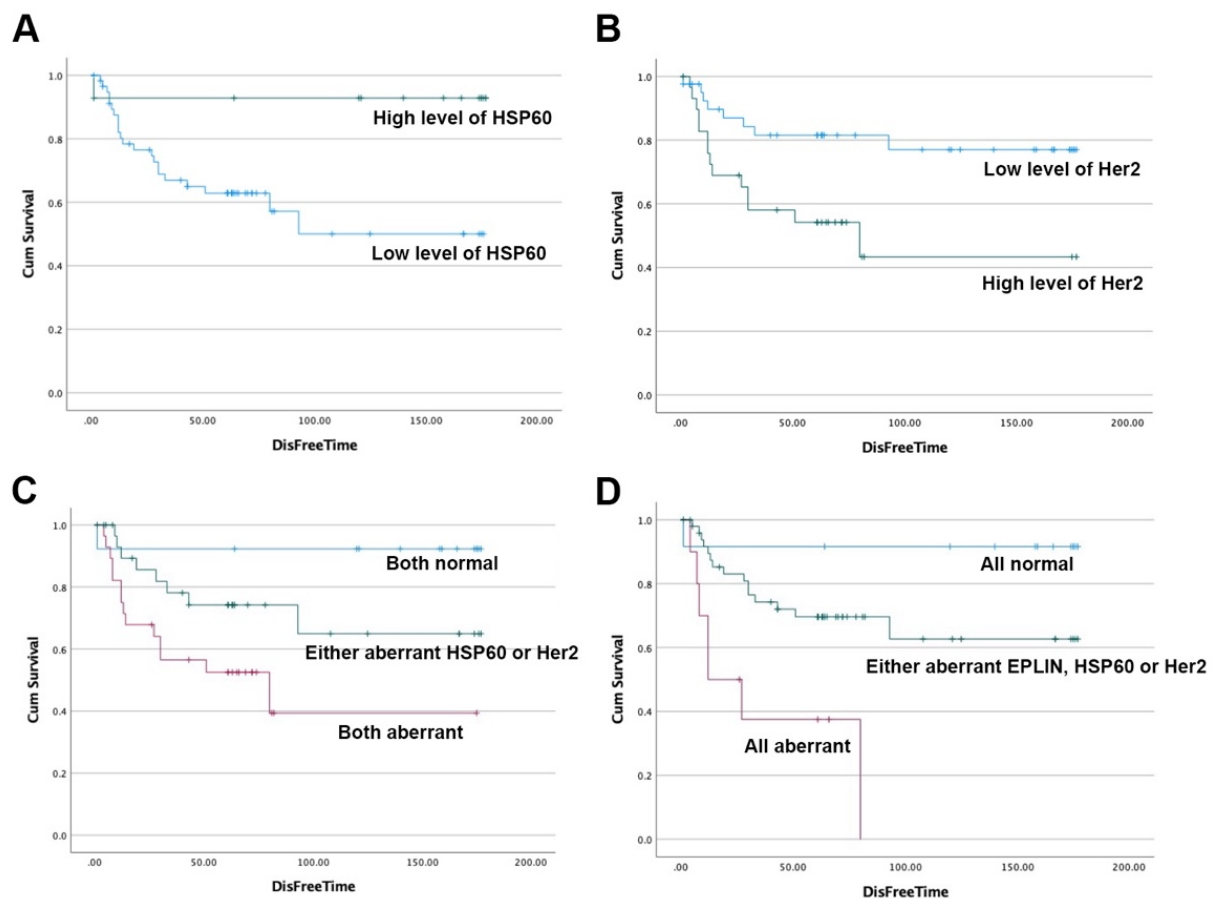


Figure 6.3 Survival Curve showing impact of EPLIN, HSP60 and Her2 expressions on patients' relapse-free survival in the Cardiff clinical cohort. (A) Patients with high level of HSP60 had longer RFS than those with low level of HSP60 ($p=0.022$). (B) Patients with high level of Her2 was found to have worse RFS than those with lower level of Her2 ($p=0.008$). (C) Patients without any abnormal expression of neither Her2 nor HSP60 have a longer RFS than those with abnormal expression. While patients have the aberrant expressions of all HSP60 and Her2 have the worst RFS ($p=0.009$). (D) CRC patients with abnormal expressions of EPLIN, HSP60 and Her2 have the worst RFS among three groups, while patients express non-abnormal expression of neither EPLIN, HSP60 nor Her2 have the shorter RFS than other groups ($p<0.001$).

In addition, we explored the impact of HSP60 and Her2 on RFS of rectum adenocarcinoma patients in the Kaplan-Meier Plotter (www.kmplot.com) database (Figure 6.4). Patients were divided to two groups based on expression levels of HSP60 or Her2 according to the best cutoff value provided by Kaplan-Meier Plotter. As Figure 6.4A shows, patients with higher level of HSP60 tend to have a longer RFS than those who have lower expression of HSP60. While in Figure 6.4B, patients with high level of Her2 tended to have a shorter RFS compared to patients with low level of Her2. However, both analyses, did not reach statistical significance ($p=0.074$ and $p=0.15$ respectively). Again, these observations support our findings to a certain degree and the limitation of sample numbers might be the cause of non-significance.

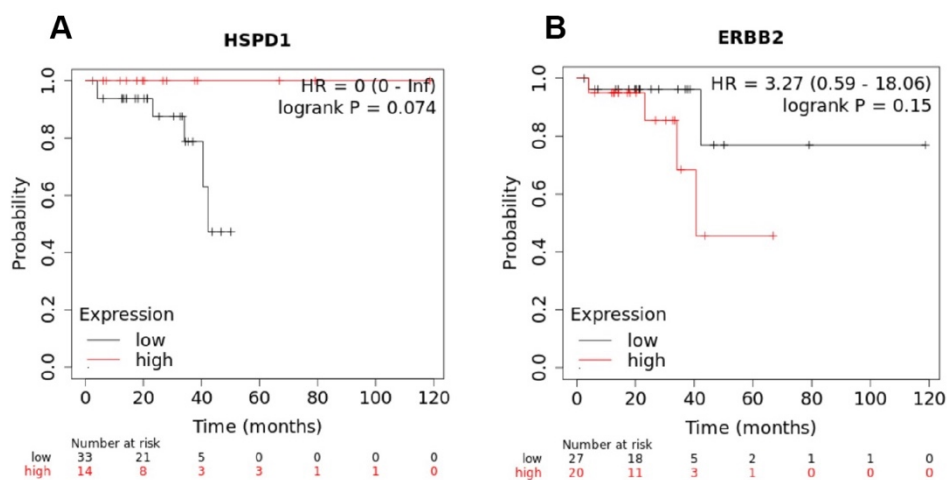


Figure 6.4 Survival Curves showing the impact of HSP60 and Her2 expression on relapse-free survival in rectum adenocarcinoma patients from TCGA-CRC dataset. (A) Patients with higher level of HSP60 tend to have a better RFS ($p=0.075$). (B) Patients with lower level of Her2 tend to have a worse RFS ($p=0.15$).

Additionally, I conducted an analysis on the power of the combination of the three molecules in predicting RFS in the Cardiff clinical cohort using a multivariate Cox regression model (Table 6.7). Both Dukes staging and TNM stage were found to be significant predictors of RFS of CRC patients ($p=0.021$ and $p=0.04$ respectively). Additionally, the combination of EPLIN, HSP60 and Her2 was also found to be a significant predictor of RFS ($p=0.049$ with a hazard ratio of 2.929), which similarly, indicates the essential impact of these three molecules on CRC patients RFS.

Table 6.7 Cox regression multivariate analysis of RFS of CRC patients in the Cardiff clinical cohort. Dukes stage was found to be a significant predictor ($p=0.021$) as well as TNM stage ($p=0.04$). Additionally, the combination of EPLIN, HSP60 and Her2 expression was also found to be a significant predictor to affect CRC patients' RFS ($p=0.049$).

	B	SE	Wald	df	significance	Hazard Ratio
Invasion	1.076	.731	2.166	1	.141	2.933
Treatment	.216	.395	.298	1	.585	1.241
Location	-.391	.339	1.328	1	.249	.676
Dukes	-2.728	1.183	5.319	1	.021	.065
Stage	.237	.611	.150	1	.698	1.267
TNM	1.788	.869	4.232	1	.040	5.980
Node	-1.583	1.264	1.569	1	.210	.205
Differentiation	-1.285	.768	2.803	1	.094	.277
EPLIN, HSP60&Her2	1.075	.545	3.883	1	.049	2.929

6.3.6 HSP60 protein expression profile in CRC tissues

In order to further investigate the protein expression profile of HSP60 in CRC tissues we performed IHC assay to probe HSP60 in a commercial CRC TMA (CO2161a) (US Biomax, supplied through Insight Biotechnologies, Middlesex, UK) (Appendix-1). Scoring analysis and representative pictures of this analysis are shown in Table 6.8 and Figure 6.5 respectively.

HSP60 protein expression in tumour tissues is generally stronger than in normal tissues and the staining was mainly located within the cytoplasm (Figure 6.5). Overall, the staining of HSP60 in normal tissues was rated as negative to weak (n=8), while 47.4% of adenocarcinoma tissues was rated moderate to strong of HSP60 (83 of 175) (Table 6.8). Interestingly, only 4 of 26 tissues of mucinous adenocarcinoma was rated as moderate to strong intensity of HSP60. Chi-Square test revealed significance between the adenocarcinoma group and the mucinous adenocarcinoma group ($p=0.0005$). Figure 6.5 also shows some representative images of HSP60 staining in tumours with different grade. For instance, B12 (Stage I, Grade-1) and J15 (Stage I, Grade-3) both showed stronger staining of HSP60 than L14 (normal tissue).

Furthermore, a trend of stronger HSP60 staining was observed in more aggressive stages. Over 38.9% of tissues in Stage I (7 of 18) was considered moderately to strongly stained with HSP60, while it was 40.9% in Stage II (47 of 115) and 45.7% in Stage III. However, no statistical significance was noted when Stage II group and Stage III group were compared with Stage I group (both $p>0.05$). Surprisingly, 3 of 4 tissues in Stage IV were rated as negative to weak staining of HSP60, but due to the limitation of sample number, it was not significantly different from other groups ($p>0.05$). A larger tissue cohorts needed in a future study in order to confirm this finding. Figure 6.5 shows representative images indicating the trend of stronger HSP60 staining intensity in stage IIA, IIB, IIIB and IIIC than in stage I. For example, in D9 (Stage IIA, Grade-2), D1 (Stage IIB, Grade-2), E6 (Stage IIIB, Grade-2) and E17 (Stage IIIC, Grade-2), HSP60 staining was observed to be stronger than in B12 (Stage I, Grade-1) and B7 (Stage I, Grade-2).

We also assessed staining against the differentiation status (Grade-1: well differentiated, Grade-2: moderately differentiated and Grade-3: poorly differentiated). Moderate to strong staining of HSP60 accounted of 42.4% of Grade-1 group (14 of 33), 53.1% of Grade-2 group (52 of 98) and 30.9% of Grade-3 group (17 of 55) ($p=0.0291$) (Table 6.8). This trend can also be seen from the representative images given in Figure 6.5. For instance, B12 (Grade-1), G10 (Grade-1) and C15 (Grade-1) tended to have weaker staining of HSP60 than D9

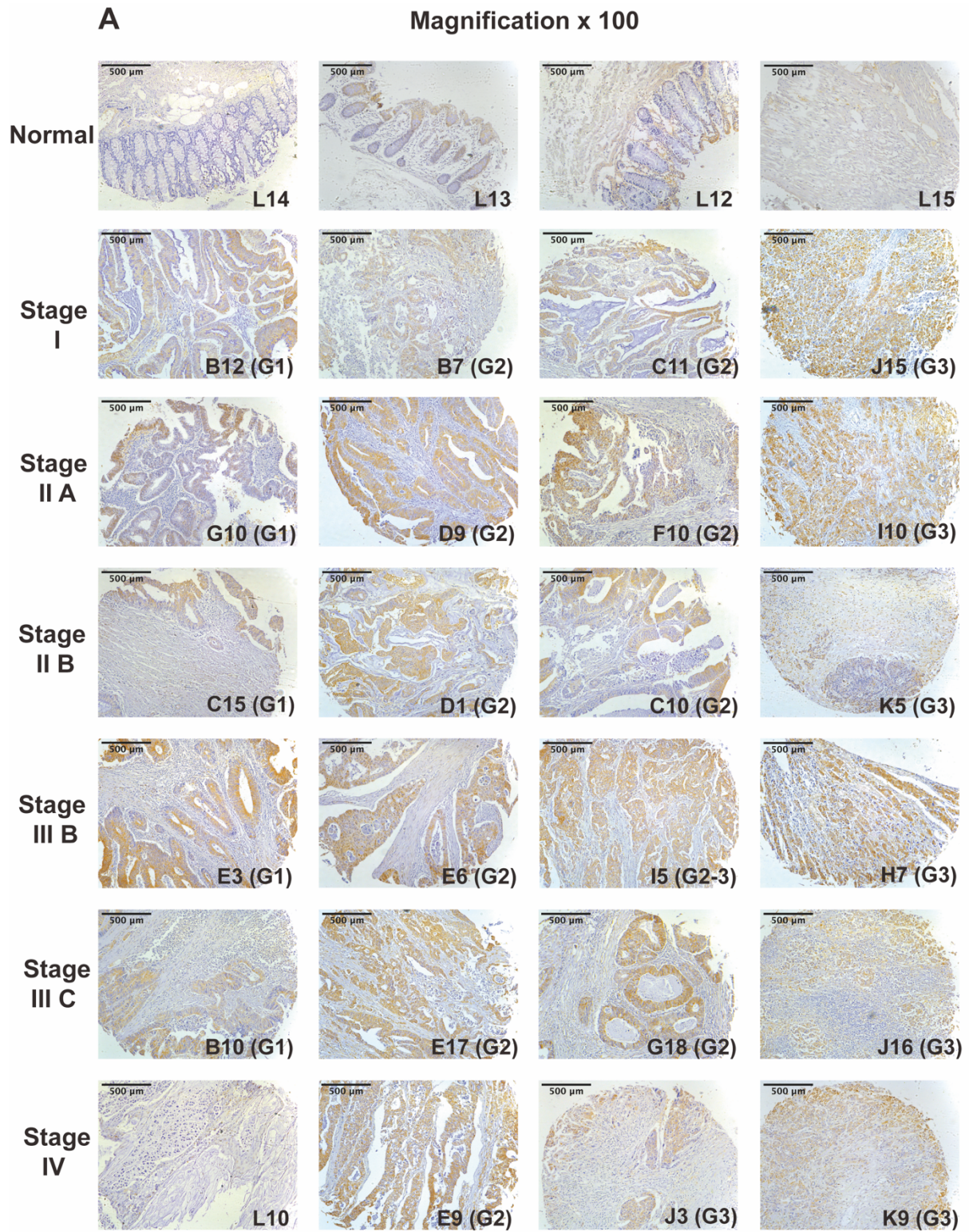
(Grade-2), I5 (Grad-2/3) and E17 (Grade-2). Intriguingly, only 30.9% of tissues in Grade3 group was rated as moderate to strong, an interesting finding warrant further investigation and validation.

Hence, by analysing the TMA slide, we suggest that HSP60 is upregulated in tumour tissues at the protein level when compared to normal tissues and higher protein expression of HSP60 might be related to more aggressive CRC, a larger tissue cohort was needed in the future to fully understand the relationship between HSP60, aggressiveness and differentiation of colorectal cancer, as well as its expression profile in mucinous adenocarcinoma.

Table 6.8 Scoring analysis of HSP60 in colorectal cancer TMA (CO2161a)

	Total Number	Intensity		Statistical significance	
		Negative to weak (0-1)	Moderate to strong (2-3)	Chi value	p
Pathology					
Normal tissue	8	8	0		
Adenocarcinoma	175	92	83		
Mucinous adenocarcinoma	30	26	4	12.19	0.0005 ^a
Signet ring cell carcinoma	3	3	0		
Stage					
I	18	11	7		
II	115	68	47	0.1591	0.8736 ^b
III	70	38	32	0.2703	0.6031 ^b
IV	4	3	1	0.2728	0.6014 ^b
Differentiation Code					
Grade1	33	19	14	7.074	0.0291 ^c
Grade2	98	46	52		
Grade3	55	38	17		

Note: ^aCompared with adenocarcinoma group; ^bCompared with Stage I group; ^cOverall chi-square analysis among differentiation groups.



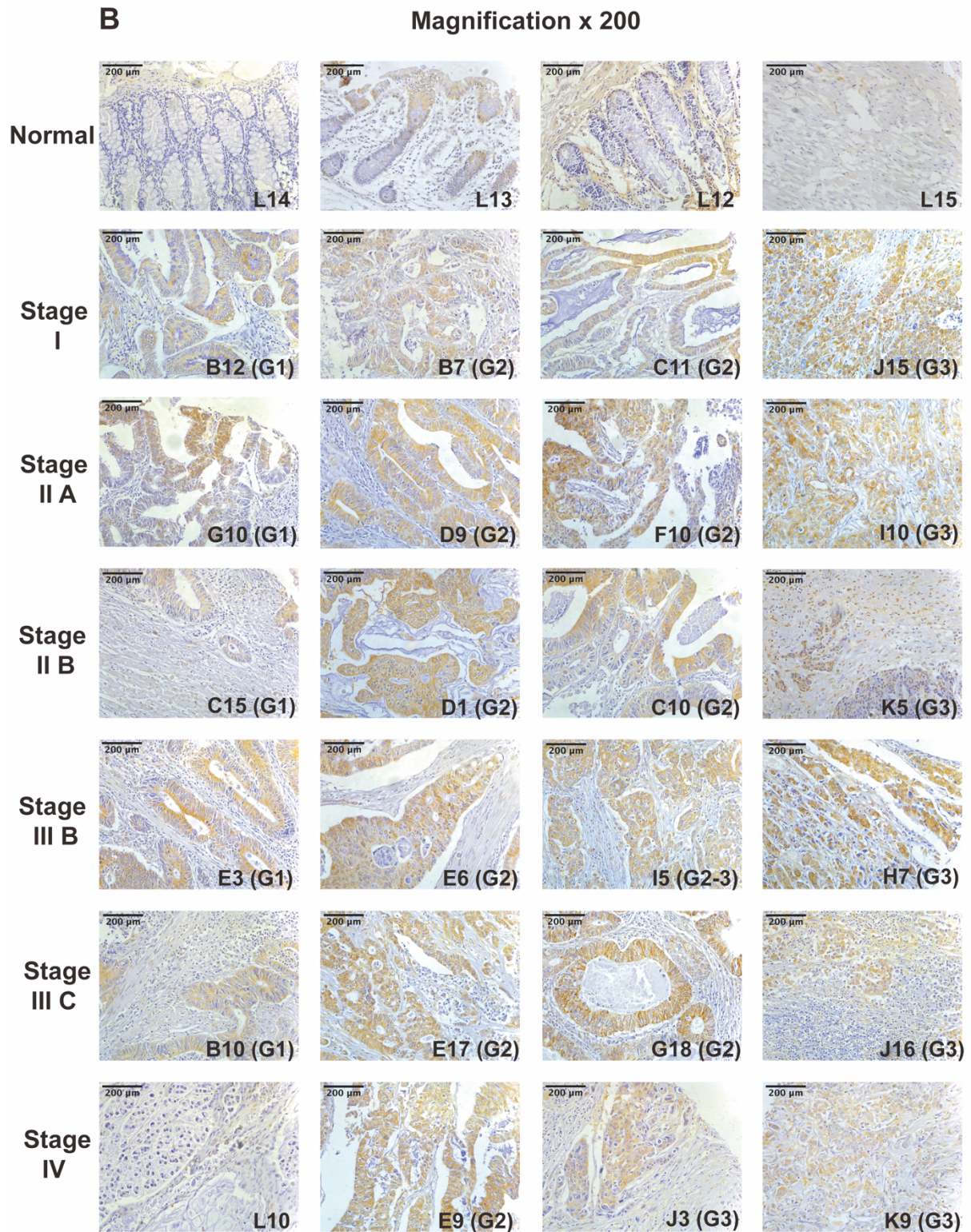


Figure 6.5 Expression profile of HSP60 at the protein level in CRC TMA (CO2161a). A. Photos were taken under a Leica DM IRB Microscope (Leica GmbH, Bristol, UK) at X100 objective magnification. B. Photos were taken under a Leica DM IRB Microscope (Leica GmbH, Bristol, UK) at X200 objective magnification. G1-3 stands for histological grade of CRC tissues.

6.4 Discussion

As demonstrated in Chapter 3 through analysis of online databases and our available clinical cohorts, the downregulation of EPLIN transcript and protein is related to CRC oncogenesis and furthermore has a negative impact on OS and RFS in CRC patients. Our Kinexus protein platform study (Chapter 5) has identified that Her2 and HSP60 may represent two essential missing pieces of the puzzle in the interacting network of EPLIN. In this chapter, we aimed to investigate the implication of such potential interacting partners on the clinical outcomes of CRC.

In order to achieve this, we scrutinised transcript levels of HSP60 and Her2 in the Cardiff CRC clinical cohort in comparison with pathological information. In the HSP60 analysis, one of the highlighted findings was that median transcript expression of HSP60 in tumour samples was significantly greater than it in normal samples ($p=0.0097$). In addition, the analysis of the colorectal TMA slide demonstrated that HSP60 is upregulated in tumour samples compared to normal tissues at the protein level. These findings are in line with reported observation at protein levels (Cappello et al. 2003; He et al. 2007; Cappello et al. 2011; Vocka et al. 2019), which indicates HSP60, might act as a tumour supporter in CRC carcinogenesis.

Another significant observation we noted was a significant trend in TNM stages, namely, HSP60 median transcript expression in TNM1 stage is upregulated when compared to other TNM stages. This is in conflict with the report from Vocka *et al.*, in which protein expression of HSP60 in CRC lung metastatic serum samples is significantly upregulated compared to those without metastasis ($p=0.01$) (Vocka et al. 2019). This difference might be due to the differences of samples types between serum samples and RNA samples. There may be a whole range of post transcriptional/translational regulatory pathways as well as regulation of secretion or shedding that may also account for these differences. Besides, the limitation of our sample number might also contribute to the difference. We also noted a significance difference in the T stages, a finding in support of our observation that HSP60 expression is higher in less aggressive CRC samples at transcript level. However, the analysis of colorectal TMA slides show a possible trend of abundant HSP60 protein expression in aggressive stages, hence, these two findings warrant further investigation to confirm the connection between HSP60 and CRC aggressiveness.

Analysis of Her2 expression highlighted that median transcript expression of Her2 was significantly higher in tumour samples when compared to the normal healthy group

($p < 0.001$). Upregulated trends of Her2 expression were also observed in patients with distant metastases, local recurrence, and those who died of colorectal cancer. However, due to the sample sizes, none of these trends were statistically significant ($p > 0.05$). These findings partly match other studies (Osako et al. 1998; Siena et al. 2018). Taken together, Her2 expression is aberrant in CRC, and it might be involved in metastasis and clinical prognosis.

We identified Her2 and HSP60 as novel interacting partners of EPLIN by conducting the Kinexus microarray assay in chapter 5. Here, by utilising the Cardiff clinical cohort, we carried out Spearman's correlation analysis to reveal the correlation of EPLIN, HSP60 and Her family members at the transcript level. EPLIN only correlated with Her2 positively at transcript level in normal samples, while it had a positive correlation with HSP60 in normal samples, tumour samples and a combined cohort of normal and tumour samples. We also noted that all of these molecules have correlation with other Her family members, especially Her1, namely EGFR. Interestingly, in clinical studies, Her2 targeted therapy is widely used in combination of EGFR targeted therapeutic agents and Her2 has been identified as a marker to improve clinical outcome and possible drug resistance of targeting EGFR (Isakoff and Baselga 2011; Oh and Bang 2020). It raises the question as to whether such possible correlations could lead to implication on clinical outcomes, drug resistance or cellular functions. These important questions represent key future areas for scientific investigation.

Furthermore, we investigated the implication of the expression of EPLIN, HSP60 and Her2 on CRC patients' survival by performing Kaplan-Meier survival curve analysis on the Cardiff clinical cohort and rectum adenocarcinoma datasets available on Kaplan-Meier Plotter (www.kmplot.com). Interestingly, in the Cardiff clinical cohort, patients with higher level of HSP60 ($n=14$) have a significantly longer OS than those with lower level of HSP60 ($p=0.025$). Analysis of KM Plotter revealed a similar trend on OS and RFS and such analysis showed near statistical significance ($p=0.074$). However, such observations do not agree with the findings by Vocka *et al.*, in which patients with higher serum levels of HSP60 had a significant shorter OS than those without (Vocka et al. 2019). Studies about HSP60's clinical significance on CRC is limited, and in the light of the present study, it would warrant a much large investigation.

Our analysis demonstrated that patients with higher transcript levels of Her2 had significantly worse OS than those with lower levels of Her2 ($p=0.003$) in the Cardiff clinical cohort. Although non-significance was noted when we analysed the impact Her2 might have on rectum adenocarcinoma patients in KM Plotter, we found a rapid drop of patients' OS after

60 months in patients with higher level of Her2 ($p=0.077$). While rectum adenocarcinoma patients with higher levels of Her2 have shorter RFS than those with lower levels of Her2 in KM Plotter database, it did not reach statistical significance ($p=0.15$). Our findings are in line with others' (Osako et al. 1998; Yonesaka et al. 2011; Sartore-Bianchi et al. 2019), and collectively, the higher levels of Her2 are implicated to have a negative impact on survival in CRC patients.

The most interesting finding in this part of the study was the power of the combination of the three related molecules, EPLIN, HSP60 and Her2 in predicting the OS and RFS in CRC patients. It was very clear that the combination of EPLIN, HSP60 and Her2 had the most significant predictive value of OS, compared with other molecules individually, and appears to be the only independent prognostic factors when all the other available clinical and pathological factors were considered together in a multivariate analysis. These observations implicate that patients with aberrant expression of EPLIN/HSP60/Her2 conferred a possible mechanism that impacts on the clinical progress of the disease.

In conclusion, we revealed that high transcript levels of HSP60 and Her2 are related to carcinogenesis in CRC and they might result in more aggressive CRC and poor prognosis. Interestingly, we reported that high transcript expression of HSP60 leads to shorter OS and RFS which does not agree to others' research (Vocka et al. 2019). High transcript expression of Her2 results in poor OS and RFS. EPLIN, HSP60, Her2 and Her1 expression is correlated at the transcript levels, but such correlations need further confirmation by exploring other databases. The combination of aberrant expression of EPLIN, Her2 and HSP60 leads to worse clinical outcome than the presence of only either of them in CRC. Moreover, such combination has been implicated to be an independent factor to predict CRC patients' OS and RFS.

Her2 and HSP60 have been explored as novel players in the interacting network of EPLIN. All three molecules have been reported to be potential factors to affect drugs resistance. It is interesting to consider whether the interaction of these three molecules may have an impact on drug resistance, which could contribute to the clinical course. This possibility will be further investigated in the following chapter (Chapter-7), which explored the link between these three molecules and drug sensitivity/resistance in colorectal cancer.

Chapter 7

Implication of EPLIN, HSP60 and Her2 on drug sensitivity in colorectal cancer

7.1 Introduction

In the previous chapters we highlighted HSP60 and Her2 as EPLIN's potential interacting candidates. Although immunoprecipitation assays ruled out the possibility of close interaction between these molecules in colorectal cancer cell lines, we revealed downregulation of EPLIN or HSP60 led to an upregulation of Her2 at transcript or protein level and such regulatory relationships were observed to be enhanced due to the inhibition of HSP60 and EPLIN at the same time. Further investigation of the clinical implication of these proteins in colorectal cancer cohorts demonstrated that patients with aberrant expression of EPLIN, HSP60 and Her2 would result in worse clinical outcomes. Such findings motivated us to explore more of the implication of these proteins on colorectal cancer and the potential mechanisms behind them.

Treatment of colorectal cancer broadly involves surgery, radiotherapy, immunotherapy, chemotherapy and targeted therapy. EPLIN, a potential tumour suppressor in multiple cancer types, has been investigated for its possible role in chemotherapeutic resistance in prostate cancer (Zhang et al. 2011) and gastric cancer (Gong et al. 2021). Indeed, resistance to chemotherapeutic agents is also an urgent issue in colorectal cancer. For example, resistance to 5-FU due to mutation of PIK3CA (Wang et al. 2018) or dysregulation of miR-34a (Liu et al. 2020) have been reported. Similarly, resistance to EGFR targeted therapy has also been observed in colorectal cancer (Van der Jeught et al. 2018). Apart from traditional chemotherapy and EGFR targeted therapy, Her2 targeted therapy has been reported to be an emerging novel therapeutic strategy in CRC (Clark et al. 2003; Ramanathan et al. 2004; Hurwitz et al. 2016; Sartore-Bianchi et al. 2016; Meric-Bernstam et al. 2019).

Additionally, HSP60, a potential oncogene, has also been implicated to be involved in chemotherapeutic resistance to cisplatin and oxaliplatin in ovarian cancer cells (Abu-Hadid et al. 1997), as well as 5-FU in colorectal cancer cells (Wong et al. 2008). Whereas Her2 has been implicated to mediate EGFR targeted therapy resistance by overexpressing itself to bypass EGFR inhibitor signalling (Greally et al. 2018; Yonesaka 2021).

Our observations in the previous chapters have raised some additional questions related to the role of EPLIN in CRC. This include, would EPLIN and HSP0 be potential mediators of chemotherapeutic resistance in colorectal cancer? Would the implicated regulatory relationship between EPLIN, HSP0 and Her2 have impact on EGFR or Her2 targeted therapies? And, if so, what would be the mechanism behind it? To answers such questions,

firstly, I analysed public databases in ROC Plotter containing information on drug resistant colorectal cancers in an attempt to explore such a relationship in a clinical settings; Secondly, I attempted to establish cellular models by knocking down EPLIN and HSP60 alone or together in colorectal cancer cell lines and carry out cytotoxicity assays on several classic colorectal cancer chemotherapeutic agents and EGFR or Her2 inhibitors. Finally, I examined if and how mitochondrial metabolism may play a role here, with the knowledge that HSP60 is a key mitochondrial element.

7.2 Methods

7.2.1 Cell culture and transfection

Colorectal cancer cell lines, RKO and HRT18 were cultured as described in chapter 2.2.2. Transfection protocols, used to manipulate EPLIN and HSP60 expression, in above cell lines were performed as described in chapter 2.24.

7.2.2 RNA extraction, reverse transcription and qPCR

RNA samples from cellular models were extracted then quantified and used as a template to reverse transcribe cDNA as outlined in chapter 2.3.2 & 2.3.3. Real time quantitative PCR (qPCR) was performed to verify transfection efficiency and screen transcript expression of Hers family members as outlined in chapter 2.3.6.

7.2.3 Cytotoxicity assays

Cytotoxicity assays were carried out as described in chapter 2.2.12.

7.2.4 Griess Reagent System

Griess Reagent System was performed to monitor NO₂- level as described in chapter 2.2.13.1.

7.2.5 NAD(P)H-Glo™ Detection System

NAD(P)H-Glo™ Detection System was performed as outlined in chapter 2.2.13.2.

7.2.6 Statistics

GraphPad was utilised to create column charts. Microsoft Excel and GraphPad were used for analysing raw data and analysing statistical significance via two tailed t test.

7.3 Results

7.3.1 Implication of EPLIN, HSP60 and Her2 on chemotherapeutic resistance in the TCGA colorectal cancer cohort

In order to investigate these molecules' impact on chemotherapeutic resistance in colorectal cancer, we accessed ROC plotter (<http://www.rocplot.org/>), an analysis platform includes an online TCGA colorectal cancer database (n=440). The dataset contained patients' information of responsiveness to chemotherapeutic agents, including all chemotherapy combined (non-responders: n=234; responders: n=206), bevacizumab (non-responders: n=26; responders: n=28), 5-FU (non-responders: n=169; responders: n=159), irinotecan (non-responders: n=69; responders: n=60), oxaliplatin (non-responders: n=91; responders: n=108) and capecitabine (non-responders: n=41; responders: n=16). The response to such agents were calculated based on Response Evaluation Criteria in Solid Tumours (RECIST). Data was represented as a box and whisker plot and analysed by Mann-Whitney U test. Receiver Operating Characteristic (ROC) analysis was also carried out to investigate if a molecule had clinical potential to impact on chemotherapeutic resistance (Fekete and Gyorffy 2019).

7.3.1.1 All chemotherapies combined

Firstly, EPLIN (217892_s_at), HSP60 (200806_s_at) and Her2 (210930_s_at) were probed to investigate their impact on chemotherapeutic resistance to any chemotherapy in the colorectal cancer database (non-responders: n=234; responders: n=206) (Figure 7.1). As Figure 7.1A showed, patients who responded to chemotherapies had a median expression of EPLIN of 3288 (q1=2595, q3=4375), while median expression of EPLIN in non-responders was 3429 (q1=2636, q3=4712). Regarding HSP60 (Figure 7.1B), patients who responded to chemotherapies had a median expression of HSP60 of 7915 (q1=5974, q3=10168) while the median expression of HSP60 in non-responders was 8515 (q1=6396, q3=10906). Figure 7.1C demonstrates the relationship between Her2 and chemotherapy response. The median expression of Her2 in responders was 63 (q1=27.25, q3=116.3) while in non-responders, the median expression of Her2 was 59.5 (q1=21, q3=114.8). Although a trend of patients with high median expression of HSP60 tended to response to any chemotherapy was observed, none of these observations reached statistical significance (EPLIN, p=0.1419, HSP60, p=0.1097, Her2, p=0.3733).

ROC plotter was also used to analyse the dataset with ROC curve analysis (Figure 7.1 bottom). The Area Under ROC Curve (AUC) of EPLIN (Figure 7.1A bottom) was 0.543

($p=0.07$). AUC of HSP60 (Figure 7.1B bottom) was 0.547 ($p=0.054$). While AUC of Her2 (Figure 7.1C bottom) was 0.526 ($p=0.19$). No statistical significance was noted in each group and AUC did not indicate any of these molecules to have strong potential to have impact on resistance to any chemotherapeutic methods.

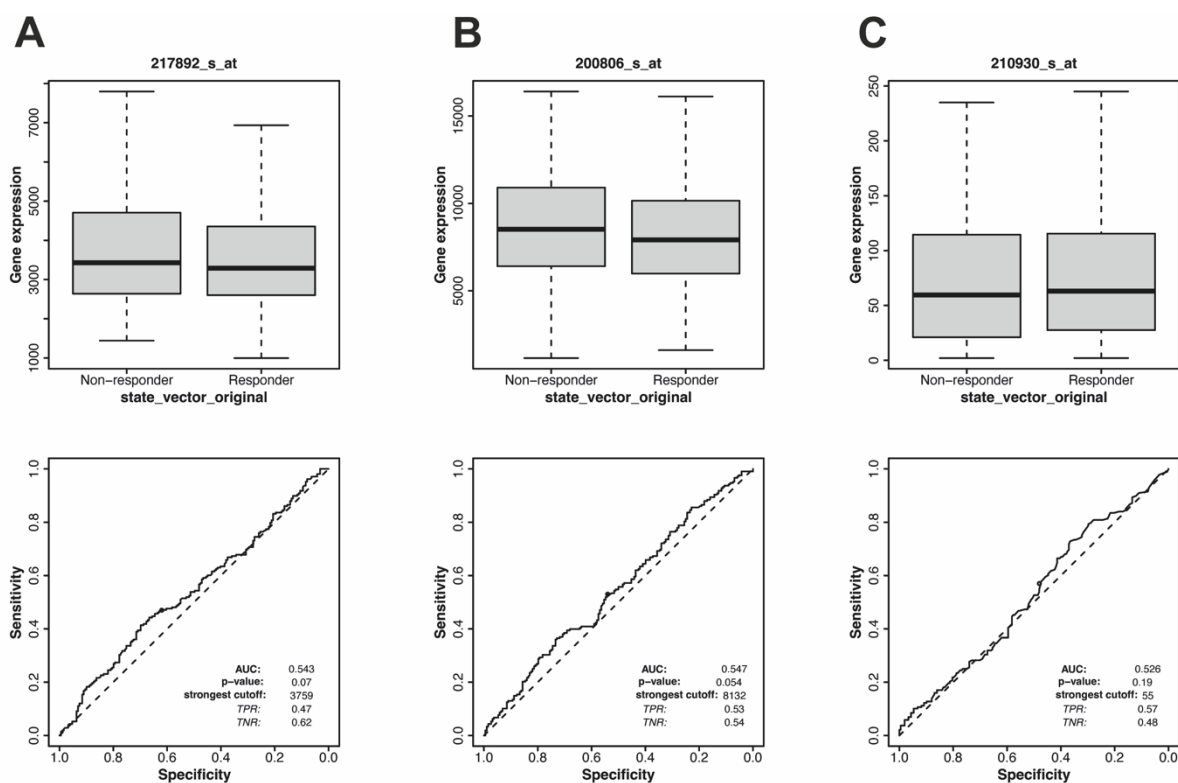


Figure 7.1 Implication of EPLIN, HSP60 and Her2 on resistance to any chemotherapy in TCGA colorectal cancer dataset. A. EPLIN (217892_s_at) was probed. B. HSP60 (200806_s_at) was probed. C. Her2 (210930_s_at) was probed. Non-responders: $n=234$, responders: $n=206$. TPR: true positive rate/Sensitivity. TNR: true negative rate/Specificity. Raw data, box plots and ROC curves were analysed and obtained from ROC plotter (<http://www.rocplot.org/>, accessed in April, 2022). Data was analysed by Graphpad and Mann-Whitney U test was applied. Whiskers represents maximum and minimum.

7.3.1.2 Bevacizumab

Apart from investigating responsiveness to any type of chemotherapy, several target agents were also tested individually. EPLIN, HSP60 and Her2 were probed to investigate their impact on resistance to Bevacizumab (non-responders: $n=26$; responders: $n=28$) (Figure 7.2). Median EPLIN expression levels of patients who responded to bevacizumab was 3731 ($q_1=2794$, $q_3=6036$), while it was 4179 ($q_1=2875$, $q_3=4887$) for those who did not respond. Although those who did not respond had a higher median expression of EPLIN compared to those who did, no significant changes between the two group were noted ($p=0.49$) (Figure 7.2A top). Similarly, no significant changes were observed when HSP60 was probed (responders: median expression= 7149 , $q_1=2896$, $q_3=12143$; non-responders: median expression= 8610 , $q_1=7605$, $q_3=11771$; $p=0.8352$) (Figure 7.2B top). However, significant

differences were observed in relation to Her2 (Figure 7.2C top), where, median expression of non-responders (median expression=59, q1=19.5, q3=102) was found to be lower than that in those who responded to bevacizumab (median expression=105, q1=65.5, q3=189.5) ($p=0.0319$). ROC analysis revealed similar trends (Figure 7.2 bottom). Interestingly, an AUC of 0.678 was observed for Her2 and reached statistical significance ($p=0.012$). Hence, no obvious potential impact of EPLIN and HSP60 in relation to response to bevacizumab could be noted, but patients with higher level of Her2 seemed to respond better to bevacizumab.

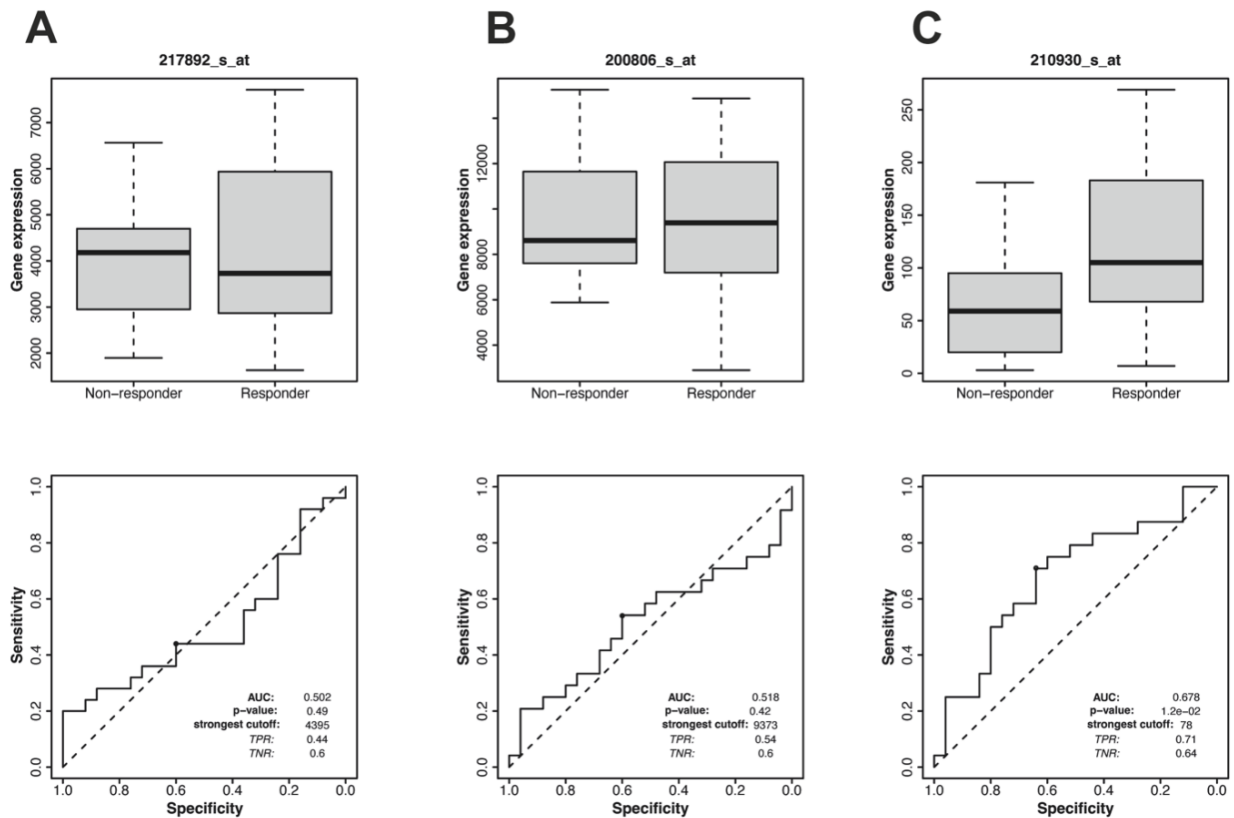


Figure 7.2 Implication of EPLIN, HSP60 and Her2 on colorectal cancer patients' response to bevacizumab in TCGA dataset. A. EPLIN (217892_s_at) was probed. B. HSP60 (200806_s_at) was probed. C. Her2 (210930_s_at) was probed. Non-responders: n=26, responders: n=28. TPR: true positive rate/Sensitivity. TNR: true negative rate/Specificity. Raw data, box plots and ROC curves were analysed and obtained from ROC plotter (<http://www.rocplot.org/>, accessed in April, 2022). Data was analysed by Graphpad and Mann-Whitney U test was applied. Whiskers represents maximum and minimum.

7.3.1.3 Capecitabine

The impact of the three molecules on patients' response to capecitabine (non-responders: n=41; responders: n=16) were also investigated (Figure 7.3). No significant difference was seen with EPLIN or Her2 between patients who did and did not respond to capecitabine. For EPLIN (Figure 7.3A top), median expression for non-responders=4589 (q1=2821, q3=5698), while for responders, median=4956 (q1=3809, q3=5795), p=0.498. For Her2 (Figure 7.3B top), median expression for non-responders=52 (q1=10.5, q3=115), while median for responders was 56.5 (q1=13.25, q3=92.25), p=0.3903. Regarding HSP60 (Figure 7.3C top), patients who responded to capecitabine tended to have lower median levels of HSP60 (median=6574, q1=3920, q3=8098) compared to those who did not respond (median=7752, q1=4778, q3=11532), though it was not found to be significant (p=0.1126). As Figure 7.3 bottom indicated, ROC curve analysis did not suggest EPLIN or Her2 had a significant impact on response to capecitabine. Interestingly, ROC curve analysis indicated HSP60 could represent a potential impact factor for responding to capecitabine, as AUC=0.607, p=0.032.

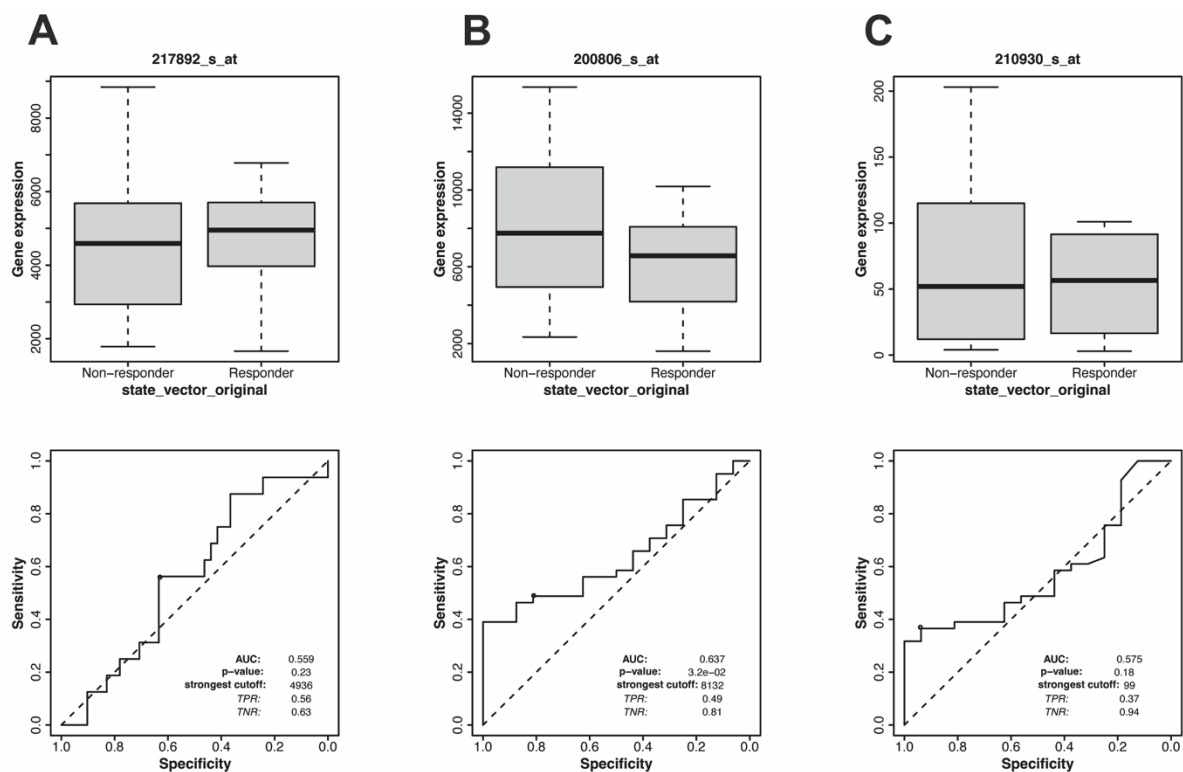


Figure 7.3 Implication of EPLIN, HSP60 and Her2 on patients' response to capecitabine in TCGA colorectal cancer dataset. A. EPLIN (217892_s_at) was probed. B. HSP60 (200806_s_at) was probed. C. Her2 (210930_s_at) was probed. Non-responders: n=41, responders: n=16. TPR: true positive rate/Sensitivity. TNR: true negative rate/Specificity. Raw data, box plots and ROC curves were analysed and obtained from ROC plotter (<http://www.rocplot.org/>, accessed in April, 2022). Data was analysed by Graphpad and Mann-Whitney U test was applied. Whiskers represents maximum and minimum.

7.3.1.4 Irinotecan

Response to Irinotecan was also analysed by the ROC plotter platform by probing EPLIN, HSP60 and Her2 expression in non-responders: n=69 and responders: n=60 (Figure 7.4). As Figure 7.4A,B&C top showed, no significant changes in median expressions could be observed for EPLIN (non-responders: median=3199, q1=2555, q3=4250; responders: median=3472, q1=2685, q3=4373; p=0.7401), HSP60 (non-responders: median=8610, q1=6813, q3=10617; responders: median=7915, q1=6035, q3=10617; p=0.1707) or Her2 (non-responders: median=90, q1=23, q3=156.5; responders: median=80, q1=24, q3=132.5; p=0.4778). ROC curve analysis also suggested that none of these molecules have a potential for influencing the respond to irinotecan (Figure 7.4A, B&C bottom).

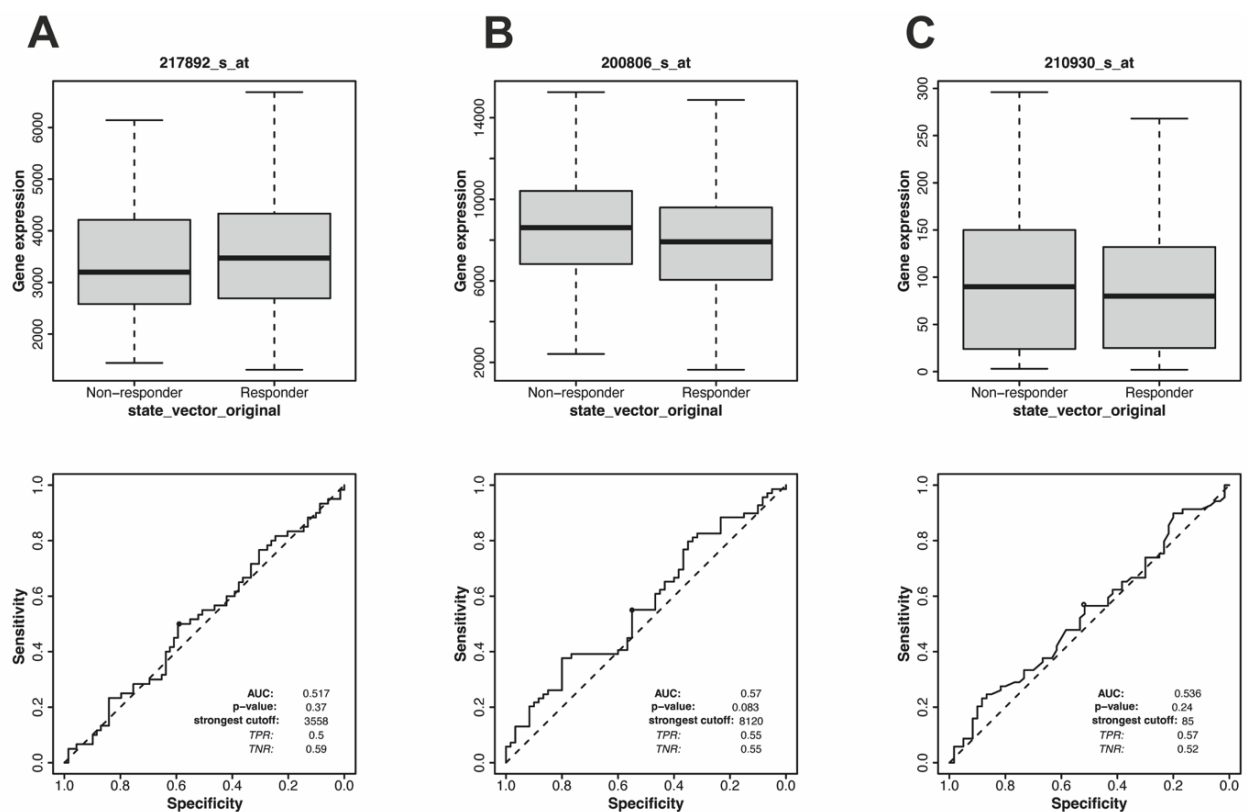


Figure 7.4 Implication of EPLIN, HSP60 and Her2 on patients' response to Irinotecan in TCGA colorectal cancer dataset. A. EPLIN (217892_s_at) was probed. B. HSP60 (200806_s_at) was probed. C. Her2 (210930_s_at) was probed. Non-responders: n=69, responders: n=60. TPR: true positive rate/Sensitivity. TNR: true negative rate/Specificity. Raw data, box plots and ROC curves were analysed and obtained from ROC plotter (<http://www.rocplot.org/>, accessed in April, 2022). Data was analysed by Graphpad and Mann-Whitney U test was applied. Whiskers represents maximum and minimum.

7.3.1.5 5-fluorouracil (5-FU)

5-FU, one of the most classic and frequently used chemotherapeutic agents in colorectal cancer was also analysed (non-responders: n=169, responders: n=159) (Figure 7.5). No obvious changes of median expression of EPLIN (non-responders: median=3324, q1=2529, q3=4395; responders: median=3222, q1=2642, q3=4190; p=0.646), HSP60 (non-responders: median=8679, q1=6822, q3=10852; responders: median=8257, q1=6078, q3=10350; p=0.181) or Her2 (non-responders: median=67, q1=22, q3=120; responders: median=64, q1=34, q3=122; p=0.795) could be seen between patients who responded to 5-FU and those did not. ROC curve analysis also suggested that none of these molecules has an impact on responding to 5-FU.

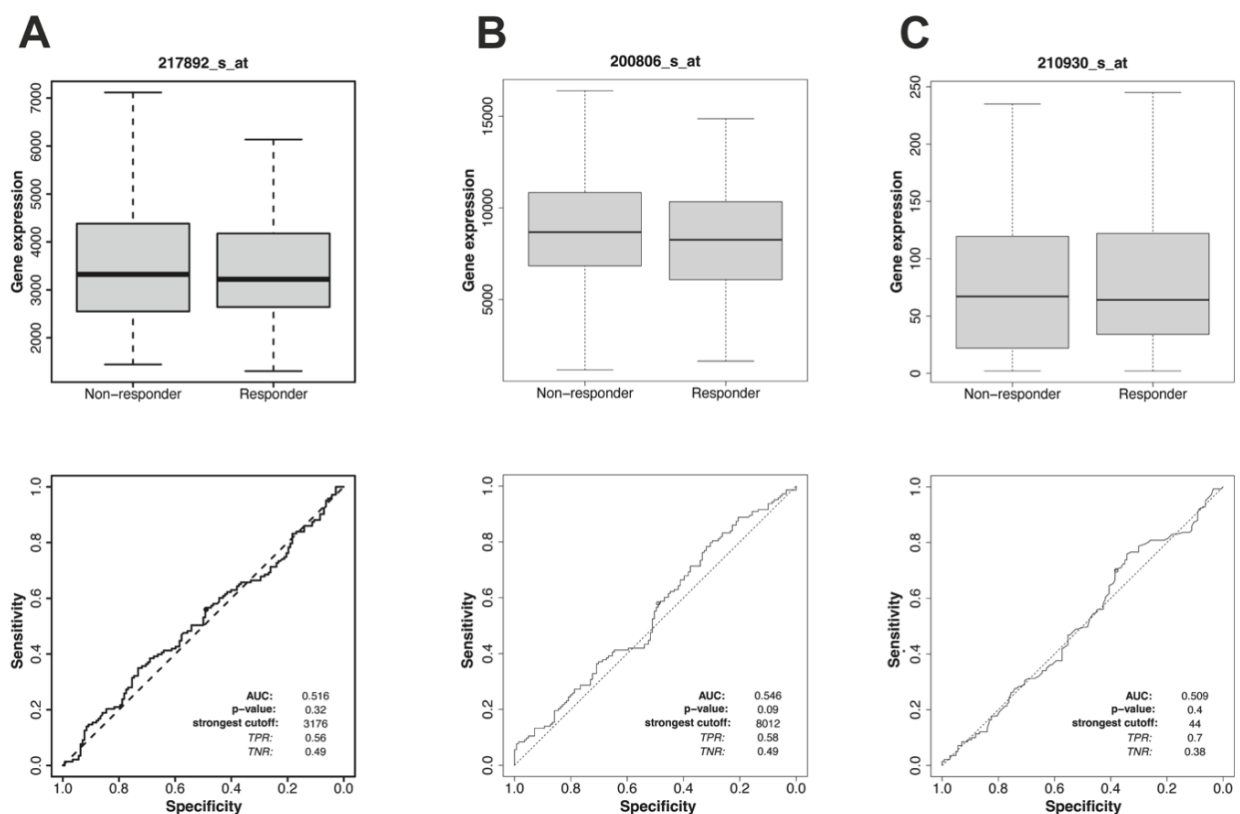


Figure 7.5 Implication of EPLIN, HSP60 and Her2 on patients' response to 5FU in TCGA colorectal cancer dataset. A. EPLIN (217892_s_at) was probed. B. HSP60 (200806_s_at) was probed. C. Her2 (210930_s_at) was probed. Non-responders: n=169, responders: n=159. TPR: true positive rate/Sensitivity. TNR: true negative rate/Specificity. Raw data, box plots and ROC curves were analysed and obtained from ROC plotter (<http://www.rocplot.org/>, accessed in April, 2022). Data was analysed by Graphpad and Mann-Whitney U test was applied. Whiskers represents maximum and minimum.

7.3.1.6 Oxaliplatin

Finally, another classic and important agent, oxaliplatin, was tested by probing these three molecules on the ROC plotter platform (non-responders: n=91, responders: n=108) (Figure 7.6). As Figure 7.6A indicated, patients who did not respond to the therapy tended to have a higher median level of EPLIN (median=3621, q1=2678, q3=5520) when compared to those who did respond (median=3288, q1=2602, q3=4175), but it did not reach statistical significance (p=0.142). Additionally, no obvious change of Her2 was noted between the two groups (non-responders: median=47, q1=23.5, q3=94; responders: median=48.5, q1=26, q3=112.3; p=0.5404) (Figure 7.6C). ROC curve analysis did not suggest EPLIN or Her2 have an impact on responding to 5-FU. Notably, patients who did not respond to 5-FU (median=8960, q1=7022, q3=11194) had a significantly higher median level of HSP60 compared to those did (median=7802, q1=5457, q3=10357) (p=0.0469). ROC curve analysis also suggested that HSP60 could be an impact factor of oxaliplatin resistance in colorectal cancer (AUC=0.592, p=0.021).

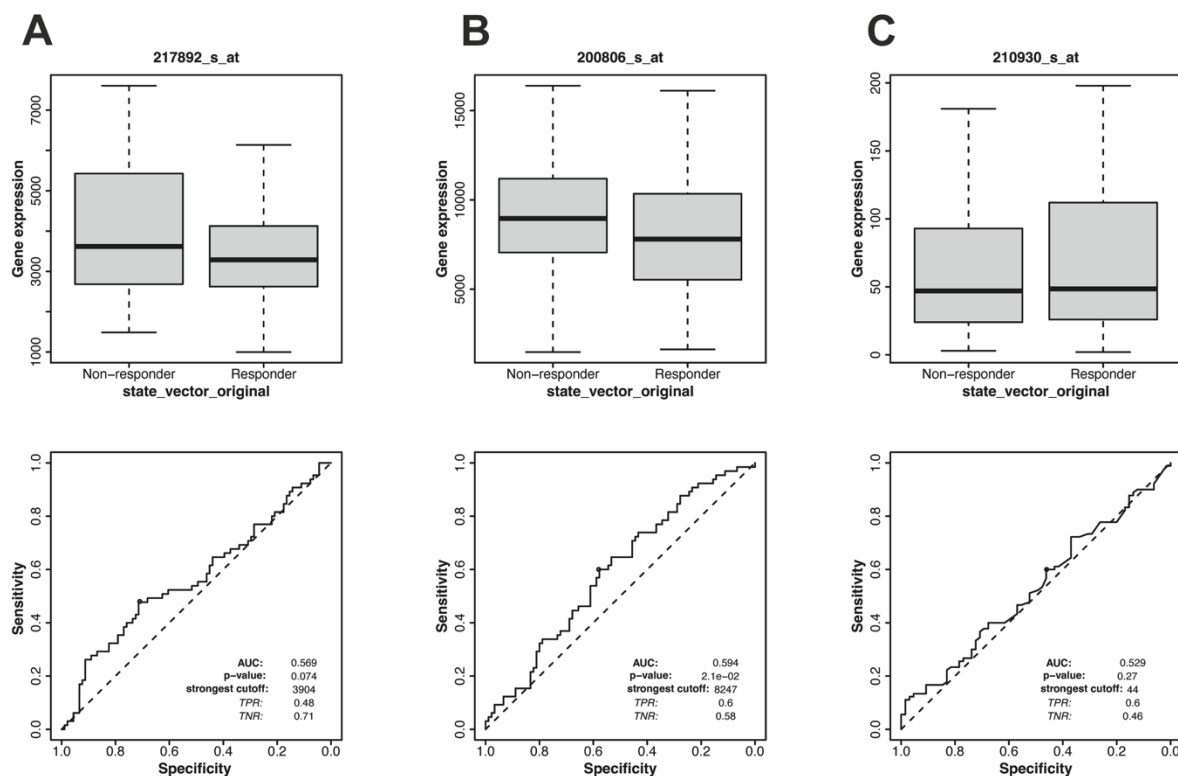


Figure 7.6 Implication of EPLIN, HSP60 and Her2 on patients' response to oxaliplatin in TCGA colorectal cancer dataset. A. EPLIN (217892_s_at) was probed. B. HSP60 (200806_s_at) was probed. C. Her2 (210930_s_at) was probed. TPR: true positive rate/Sensitivity. Non-responders: n=91, responders: n=108. TNR: true negative rate/Specificity. Raw data, box plots and ROC curves were analysed and obtained from ROC plotter (<http://www.rocplot.org/>, accessed in April, 2022). Data was analysed by Graphpad and Mann-Whitney U test was applied. Whiskers represents maximum and minimum.

7.3.2 Implication of EPLIN and HSP60 on response to chemotherapeutic agents in colorectal cancer cells.

Apart from exploring online datasets, we also investigated the impact of EPLIN and HSP60 on the response of colorectal cancer cell lines to therapeutics. To achieve this, we employed a number of RKO and HRT18 manipulated cellular models, including those displaying individual knock down of EPLIN or HSP60 as well as those displaying knock down of both molecules. Wild type cells were utilised as control groups and qPCR was carried out to verify if the manipulation of such molecules was successful (Figure 7.7). These models were subsequently applied to perform cytotoxicity assays by using several classic and heavily used chemotherapeutic agents for colorectal cancer that were available in the host lab, namely 5-FU, docetaxel and oxaliplatin.

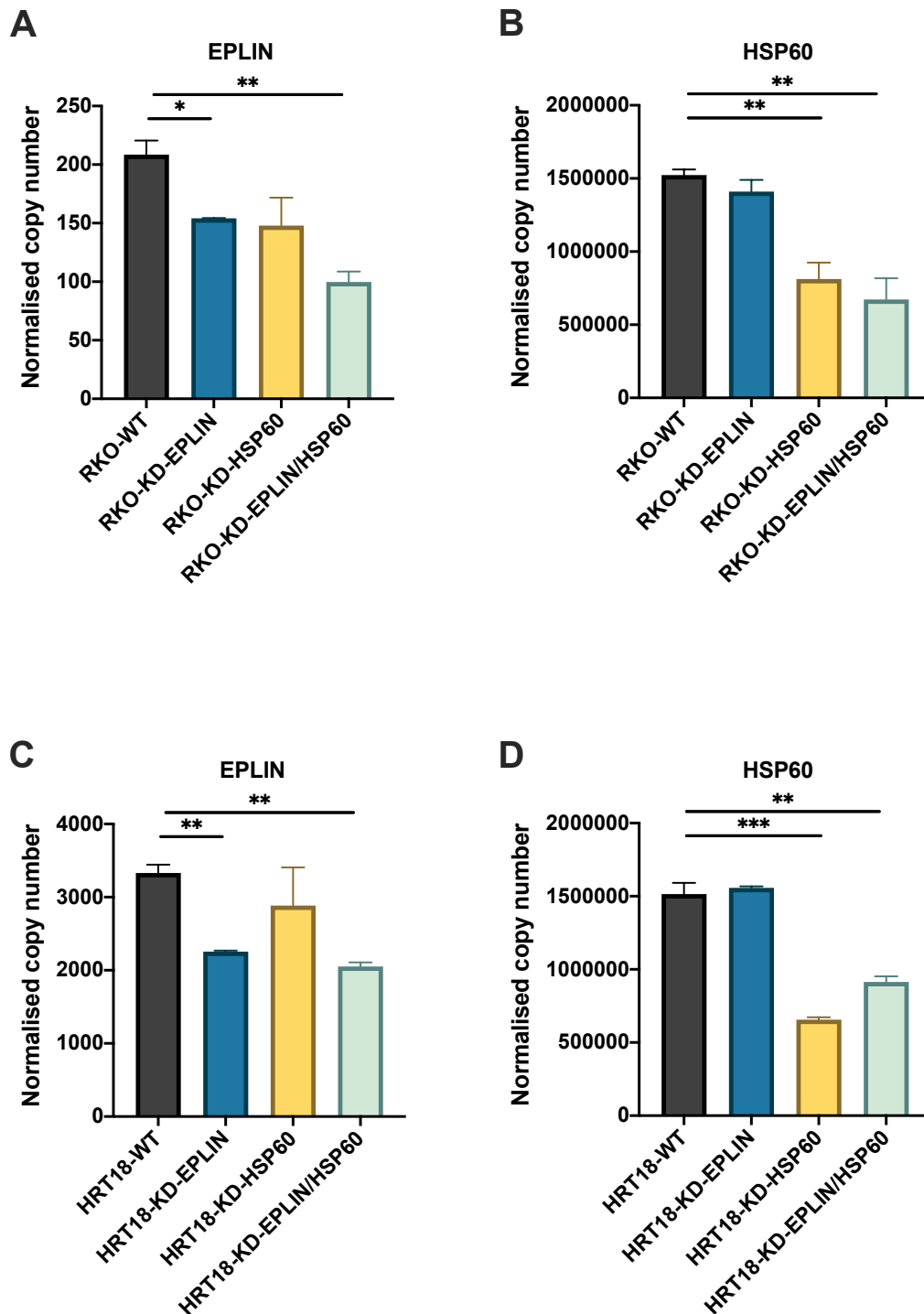


Figure 7.7 Confirmation of cellular models by qPCR. A. EPLIN normalised transcript expression in RKO cellular models. B. HSP60 normalised transcript expression in RKO cellular models. C. EPLIN normalised transcript expression in HRT18 cellular models. D. HSP60 normalised transcript expression in HRT18 cellular models. Data was shown as mean \pm SEM. Raw data was standardised to PDPL standard and normalised by GAPDH. N=3. Statistical significance was analysed by conducting two-tailed t test. * represents $p < 0.05$, ** represents $p < 0.01$, *** represents $p < 0.001$.

7.3.2.1 5-fluorouracil (5-FU)

Following the incubation of cellular models in serially diluted 5-FU for 72 hours (Figure 7.8) the IC₅₀ of RKO-WT group was calculated to be 10.66 μ M, while it was 23.44 μ M when EPLIN was knocked down alone. Knocking down HSP60 alone or with EPLIN did not result in any significant change in IC₅₀s (RKO-KD-HSP60=15.39 μ M, RKO-KD-EPLIN/HSP60=13.01 μ M) when compared to the RKO-WT group. A similar trend could be observed in HRT18 cellular models. Inhibition of EPLIN led to a decreased IC₅₀ when compared to HRT-18 wild type group (11.47 μ M vs 8.97 μ M), but the differences was not as obvious as that observed in the RKO cellular models. Decreased trends could also be noted when HSP60 was inhibited alone or with EPLIN (HRT18-KD-HSP60=13.73 μ M, HRT18-KD-EPLIN/HSP60=13.22 μ M). Hence, downregulation of EPLIN could lead to potential resistance to 5-FU in RKO cells.

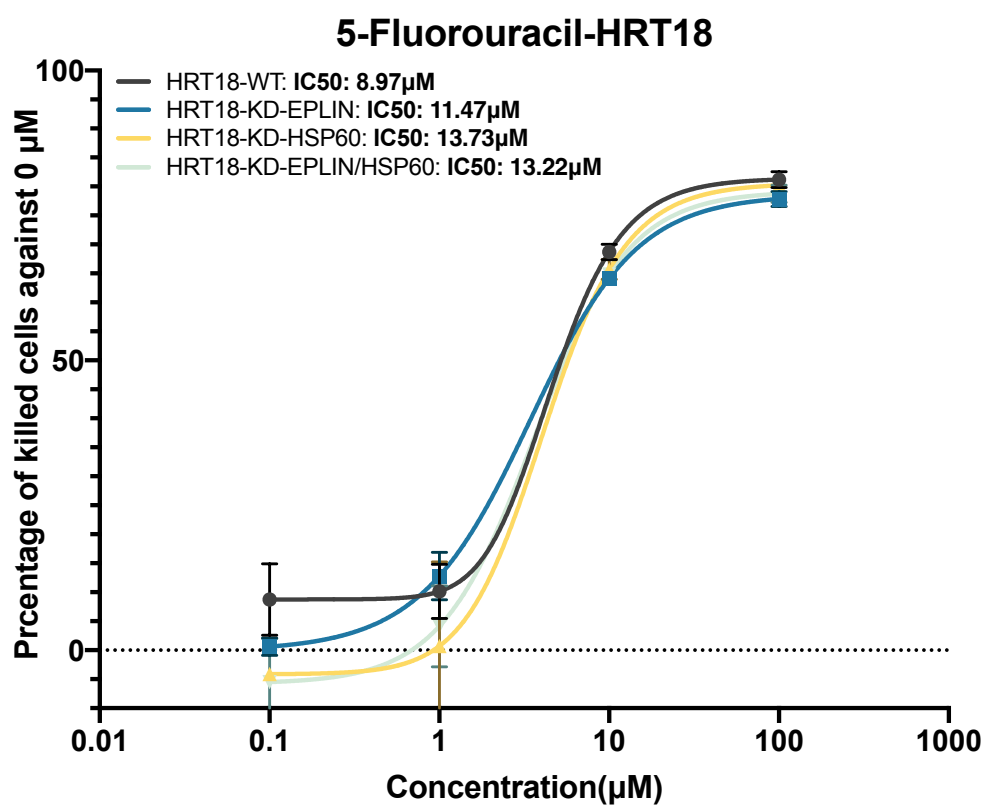
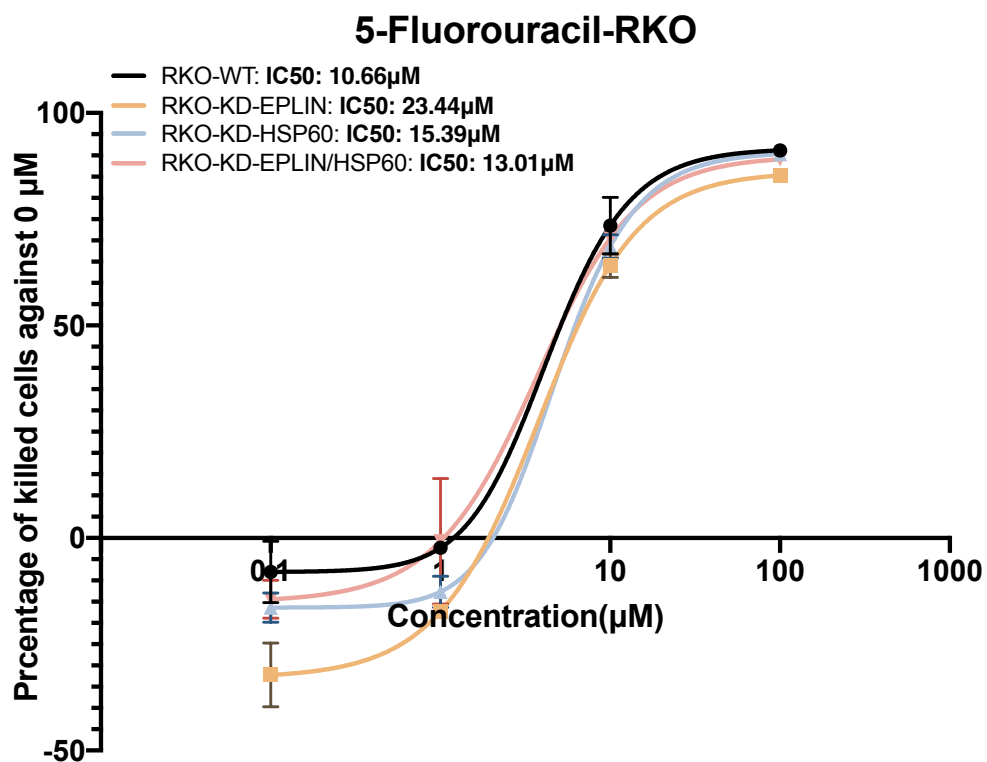


Figure 7.8 5-FU cytotoxicity assays. A. RKO cellular models were tested with serial diluted 5-FU (0-1000 μ M). B. HRT18 cellular models were tested with serial diluted 5-FU (0-1000 μ M). Representative set of data was shown (n=3). Data was shown as mean with \pm SD (n=3). IC50s were calculated based on logarithmic trend line.

7.3.2.2 Docetaxel

After incubating with serial diluted docetaxel (Figure 7.9A), no obvious changes in IC₅₀s were noted between each RKO cellular model (RKO-WT=0.27nM, RKO-KD-EPLIN=0.24nM, RKO-KD-HSP60=0.24nM, RKO-KD-EPLIN/HSP60=0.22nM). Additionally, in the HRT18 cellular models (Figure 7.9B), knocking down EPLIN did not make an obvious change to IC₅₀ compared to HRT18-WT group (0.15nM vs 0.26nM). Interestingly, inhibition of HSP60 led to a marked change of IC₅₀s compared with HRT18-WT group (0.047nM vs 0.15nM), while inhibition of EPLIN and HSP60 at the same time in HRT18 cells led to a similar result, but at a lesser degree (HRT18-WT=0.15nM, HRT18-KD-EPLIN/HSP60=0.098nM). Therefore, although manipulation of EPLIN and HSP60 did not affect the response to docetaxel in RKO cells, inhibition of HSP60 in HRT18 cells increased the responsive efficiency to docetaxel. This effect seems to be interfered with by suppressing EPLIN in HRT18 cells.

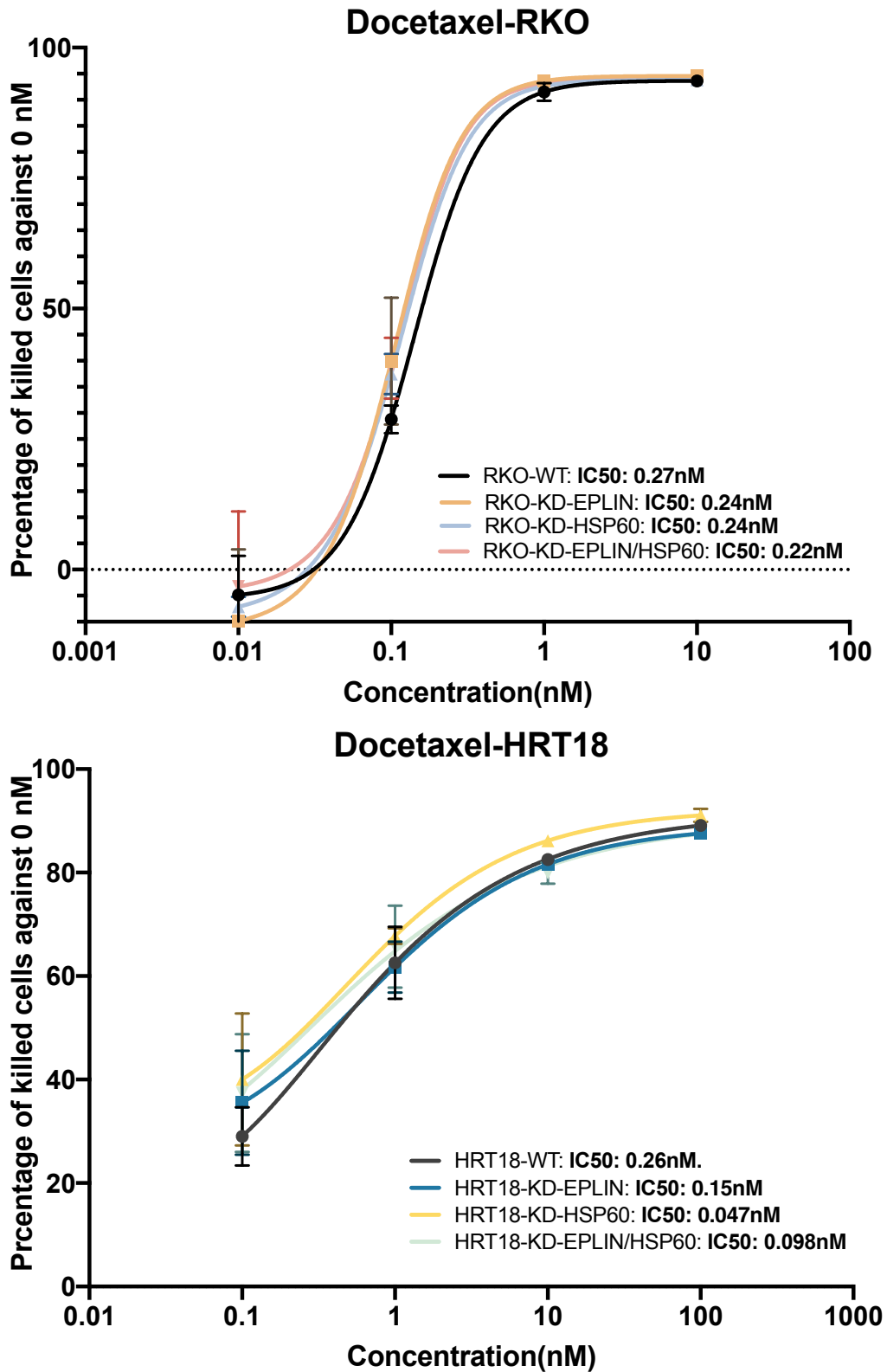


Figure 7.9 Docetaxel (DTX) cytotoxicity assays. A. RKO cellular models were tested with serial diluted docetaxel (0-1 μ M). B. HRT18 cellular models were tested with serial diluted docetaxel (0-10 μ M). Representative set of data was shown (n=3). Data was shown as mean with \pm SD (n=3). IC₅₀s was calculated based on logarithmic trend line.

7.3.2.3 Oxaliplatin

After 72 hours of incubation (Figure 7.10), inhibition of EPLIN or HSP60 alone did not substantially change the IC₅₀s of oxaliplatin treatment in RKO cells (RKO-WT=4.01 μ M, RKO-KD-EPLIN=3.28 μ M, RKO-HSP60=3.68 μ M). However, in HRT18 cells, suppression of EPLIN/HSP60 appeared to impact IC₅₀ values of oxaliplatin (HRT18-WT=4.51 μ M, HRT18-KD-EPLIN=0.31 μ M, HRT18-KD-HSP60=0.54 μ M). Interestingly, when EPLIN and HSP60 were inhibited at the same time, RKO cells seemed to become more resistant to oxaliplatin (RKO-WT=4.01 μ M, RKO-KD-EPLIN/HSP60=7.89). A greater effect was observed in HRT18 cellular models (HRT18-WT=4.51 μ M, HRT18-KD-EPLIN/HSP60=64.04 μ M). Hence, inhibition of EPLIN and HSP60 together in RKO cells seemed to decrease cell's response to oxaliplatin. Regarding the HRT18 cellular models, knocking down either EPLIN or HSP60 led to increased response to oxaliplatin while HRT18 cells became more resistance to oxaliplatin if the two molecules were inhibited at the same time.

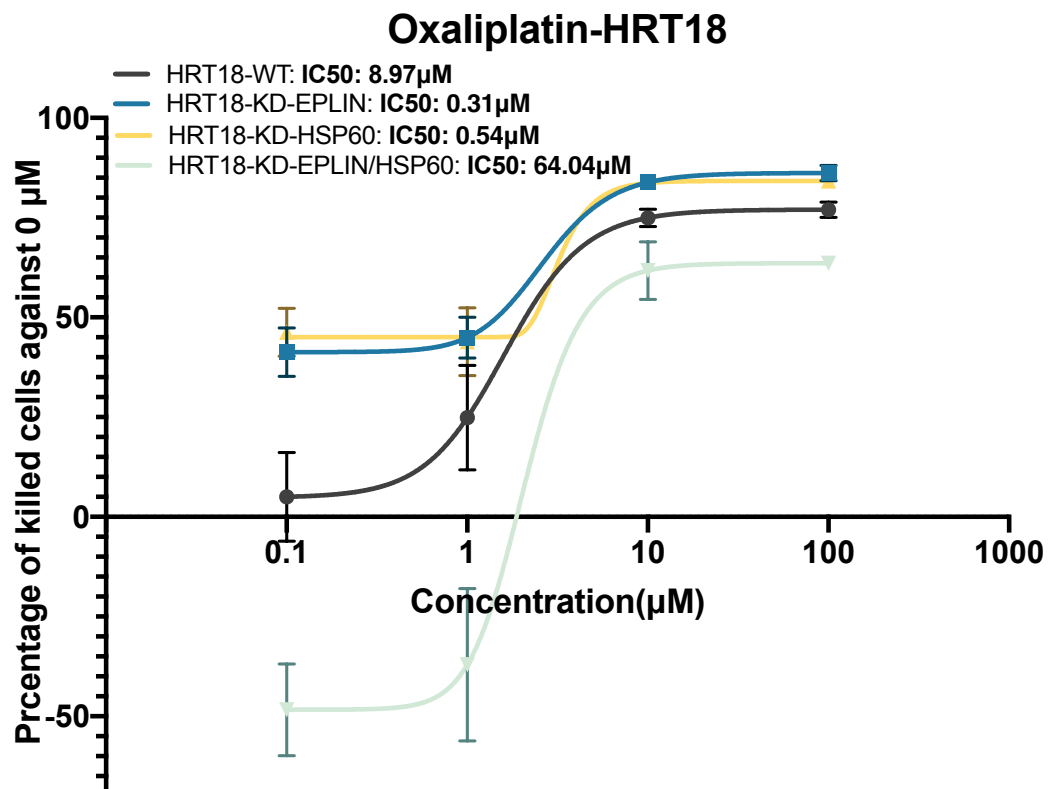
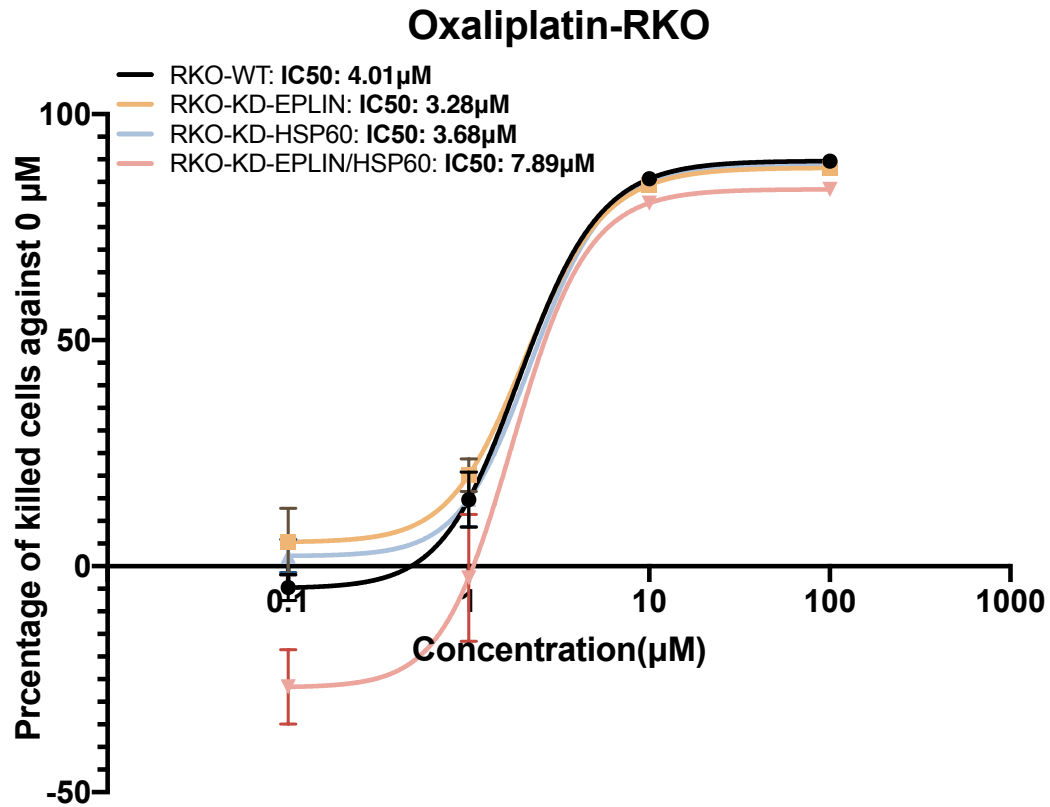


Figure 7.10 Oxaliplatin cytotoxicity assays. A. RKO cellular models were tested with serial diluted oxaliplatin (0-100 μ M). B. HRT18 cellular models were tested with serial diluted oxaliplatin (0-1000 μ M). Representative set of data was shown (n=3). Data was shown as mean with \pm SD (n=3). IC50s was calculated based on logarithmic trend line.

7.3.3 Implication of EPLIN and HSP60 on EGFR/Her2 targeted therapy in colorectal cancer cells

Several broad spectrum Her targeted therapeutic agents including Afatinib and Neratinib, known to inhibit EGFR and primarily Her2, were tested. A selective Her2 inhibitor, AG825, which inhibits tyrosine phosphorylation was also chosen to investigate if EPLIN or HSP60 would affect Her-2 therapies.

7.3.3.1 AG825

After incubating for 72 hours with AG825, as Figure 7.11 demonstrated, either knocking down EPLIN or HSP60 alone or knocking down both molecules together in RKO or HRT18 cell lines resulted in increased response to AG825 compared to their control group respectively.

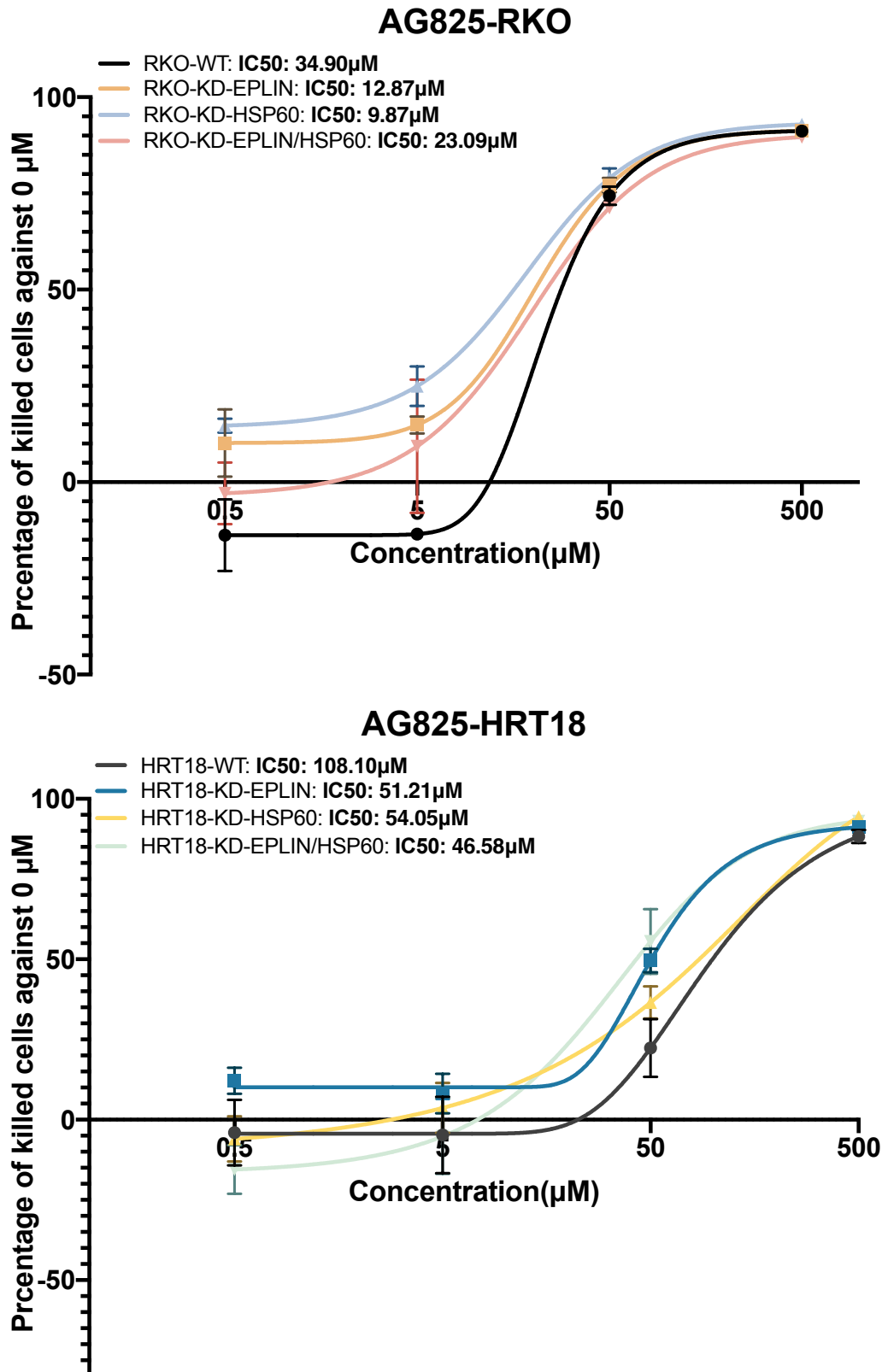
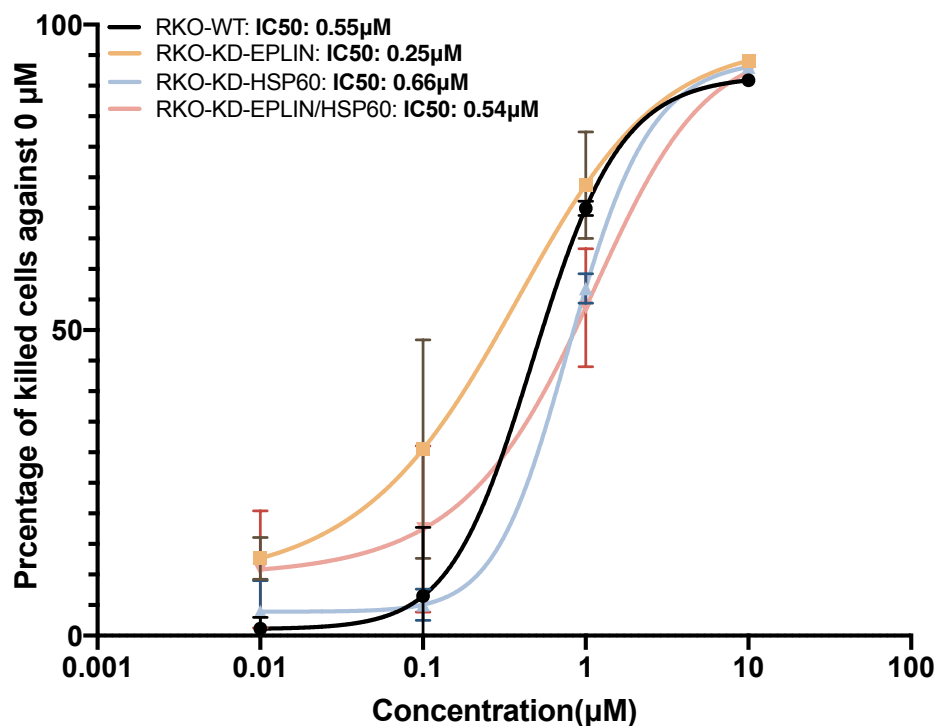


Figure 7.11 AG825 cytotoxicity assays. A. RKO cellular models were tested with serial diluted AG825 (0-500 μ M). B. HRT18 cellular models were tested with serial diluted AG825 (0-500 μ M). Representative set of data was shown (n=3). Data was shown as mean with \pm SD (n=3). IC₅₀s was calculated based on logarithmic trend line.

7.3.3.2 *Neratinib*

As Figure 7.12 showed, knocking down EPLIN in RKO or HRT18 cells alone led to increased response to neratinib when compared to RKO-WT or HRT18-WT respectively (RKO-WT=0.55 μ M, RKO-KD-EPLIN=0.25 μ M; HRT18-WT=0.34 μ M, HRT18-KD-EPLIN=0.05 μ M). No significant changes of IC50s were noted in RKO-KD-HSP60, RKO-KD-EPLIN/HSP60 group. Interestingly, inhibition of HSP60 increased responsiveness to neratinib (0.03 μ M), indicating a similar effect as inhibition of EPLIN alone. Suppression of both molecules in HRT18 cells also had a similar effect, but to a lesser degree (0.096 μ M).

Neratinib-RKO



Neratinib-HRT18

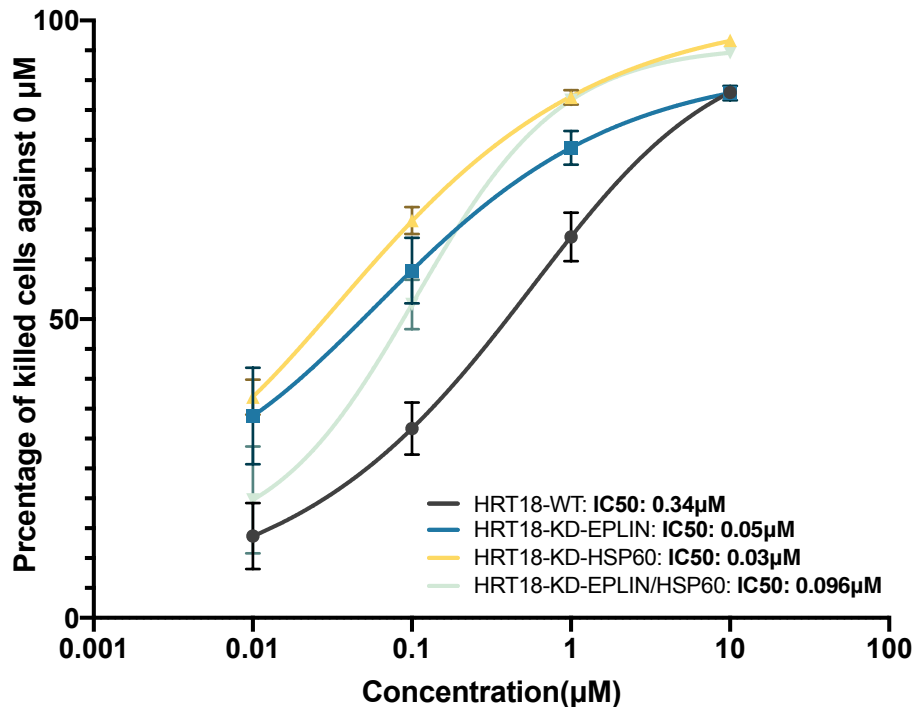
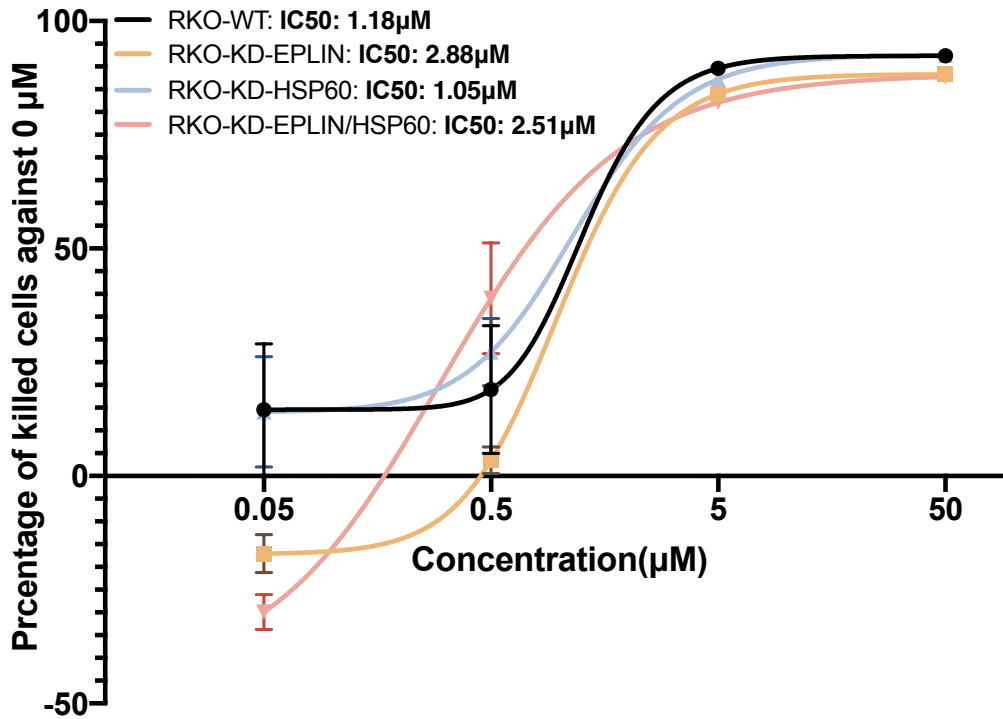


Figure 7.12 Neratinib Cytotoxicity assays. A. RKO cellular models were tested with serial diluted Neratinib (0-10 μM). B. HRT18 cellular models were tested with serial diluted Neratinib (0-100 μM). Representative set of data was shown (n=3). Data was shown as mean with \pm SD (n=3). IC₅₀s was calculated based on logarithmic trend line.

7.3.3.3 Afatinib

Following the incubation and comparing to RKO-WT (IC₅₀=1.18μM) or HRT18-WT (IC₅₀=0.36μM), inhibition of EPLIN in both cell lines lead to decreased response to afatinib (RKO-KD-EPLIN=2.88μM, HRT18-KD-EPLIN=0.85μM). No significant changes of IC₅₀s were observed when HSP60 was inhibited alone. Interestingly, when EPLIN and HSP60 were inhibited together in both cell lines, responsiveness was decreased (RKO-KD-EPLIN/HSP60=2.15μM, HRT18-KD-EPLIN/HSP60=0.54μM).

Afatinib-RKO



Afatinib-HRT18

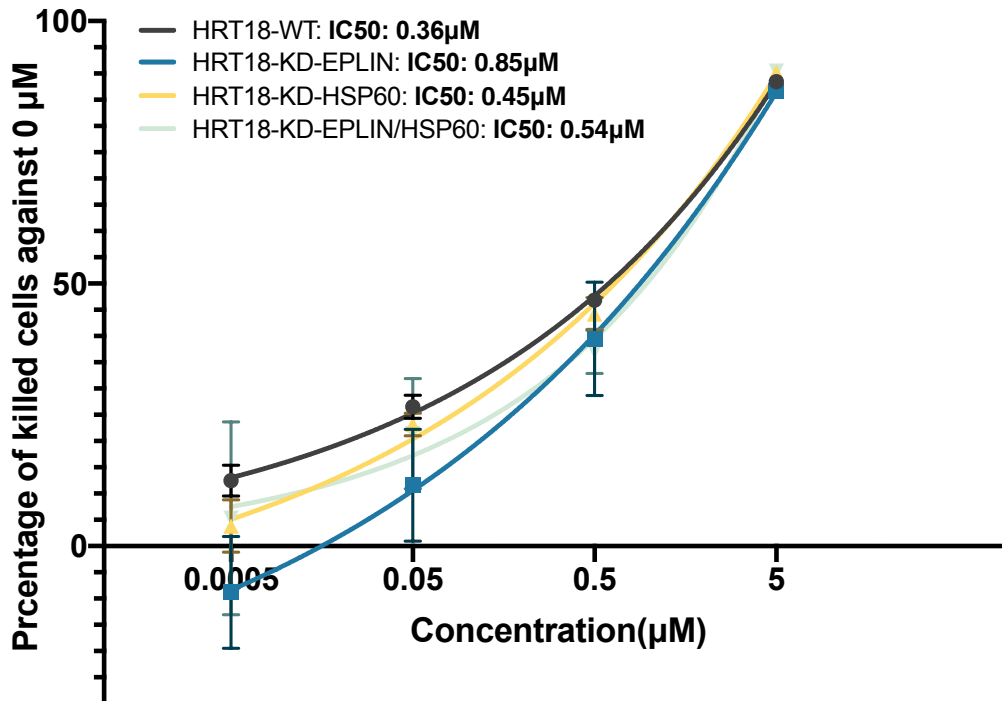
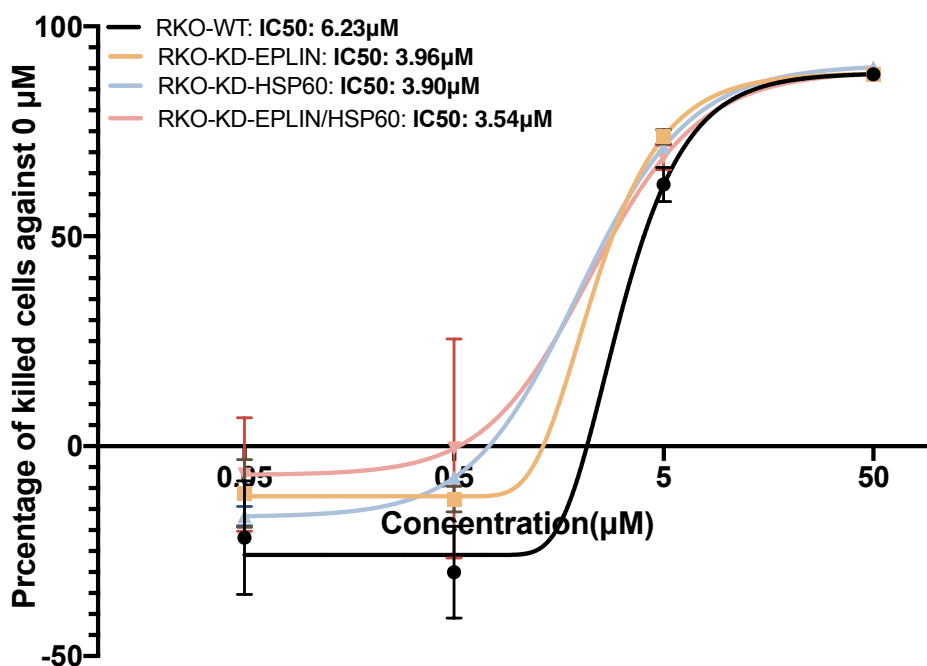


Figure 7.13 Afatinib cytotoxicity assays. A. RKO cellular models were tested with serial diluted afatinib (0-50 μM). B. HRT18 cellular models were tested with serial diluted afatinib (0-50 μM). Representative set of data was shown (n=3). Data was shown as mean with ± SD (n=3). IC₅₀s was calculated based on logarithmic trend line.

7.3.3.4 *Lapatinib*

After the incubation period, knocking down EPLIN and HSP60 alone or together resulted in decreased IC50s of lapatinib in RKO cells compared to the control group (Figure 7.14A). Opposite results were observed in HRT18 cellular models, where such manipulation led to increased IC50s of lapatinib when compared to the control group. The differences were nonetheless not significant (Figure 7.14B).

Lapatinib-RKO



Lapatinib-HRT18

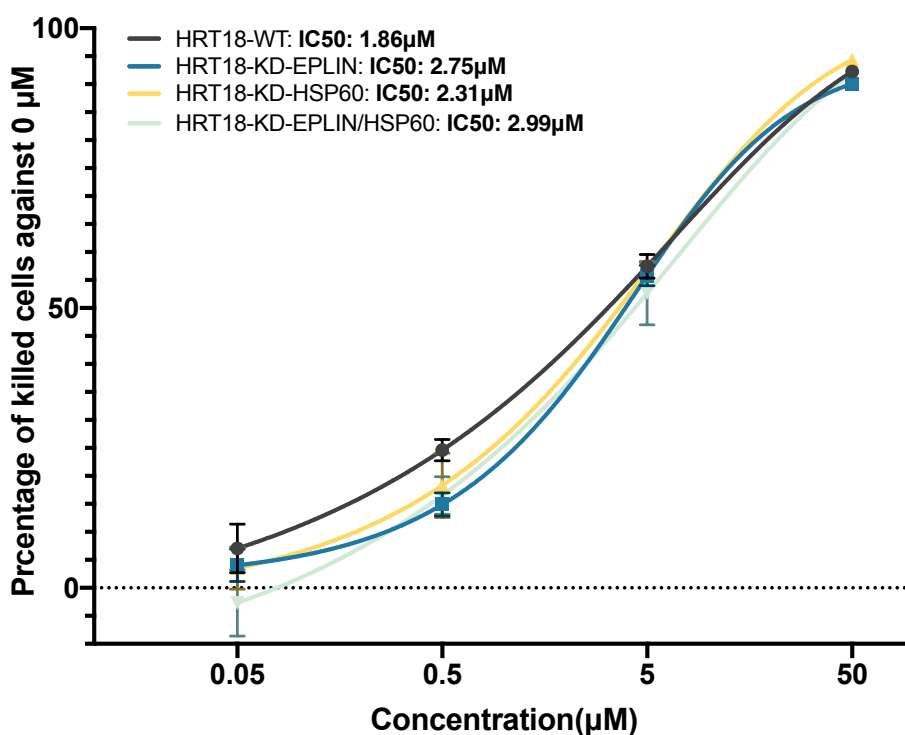


Figure 7.14 Lapatinib cytotoxicity assays on lapatinib. A. RKO cellular models were tested with serial diluted lapatinib (0-50 μ M). B. HRT18 cellular models were tested with serial diluted lapatinib (0-50 μ M). Representative set of data was shown (n=3). Data was shown as mean with \pm SD (n=3). IC50s was calculated based on logarithmic trend line.

7.3.3.5 Regulatory relationship between EPLIN, HSP60 and Her family

We have demonstrated the different impact EPLIN and HSP60 might have on Her2 and EGFR/Her2 inhibitors. Here, we also attempted to screen transcript expressions of other Her family members (Figures 7.15 & 7.16). As Figure 7.15 indicated, manipulation of EPLIN and HSP60 did not lead to significant changes of EGFR and Her3 transcript level. However, knocking down EPLIN and HSP60 resulted in significant downregulation of Her4 transcript expression (RKO-WT: mean=8.70±1.001; RKO-KD-EPLIN: mean=1.64±0.79, p=0.003; RKO-KD-HSP60: mean=1.55±0.79, p=0.003; RKO-KD-EPLIN/HSP60: mean=2.70±3.47, p>0.05).

In HRT18 cell models (Figure 7.16), knocking down EPLIN and HSP60 alone or together resulted in upregulation of EGFR (HRT18-KD-EPLIN: mean=4.11±1.25, p=0.031; HRT18-KD-HSP60: mean=5.37±0.01, p=0.002; HRT18-KD-EPLIN/HSP60: mean=9.85±4.24, p=0.028) and Her3 (HRT18-KD-EPLIN: mean=36.80±7.75, p=0.067; HRT18-KD-HSP60: mean=264.41±5.22, p<0.001; HRT18-KD-EPLIN/HSP60: mean=494.96±61.43, p<0.001) compared to their mean transcript level in wild type control (HRT18-WT: Her1 mean transcript=1.59±0.47; Her3 mean transcript=21.09±7.62). No significant impacts on Her4 transcript expression were observed (p value>0.05 in all groups)

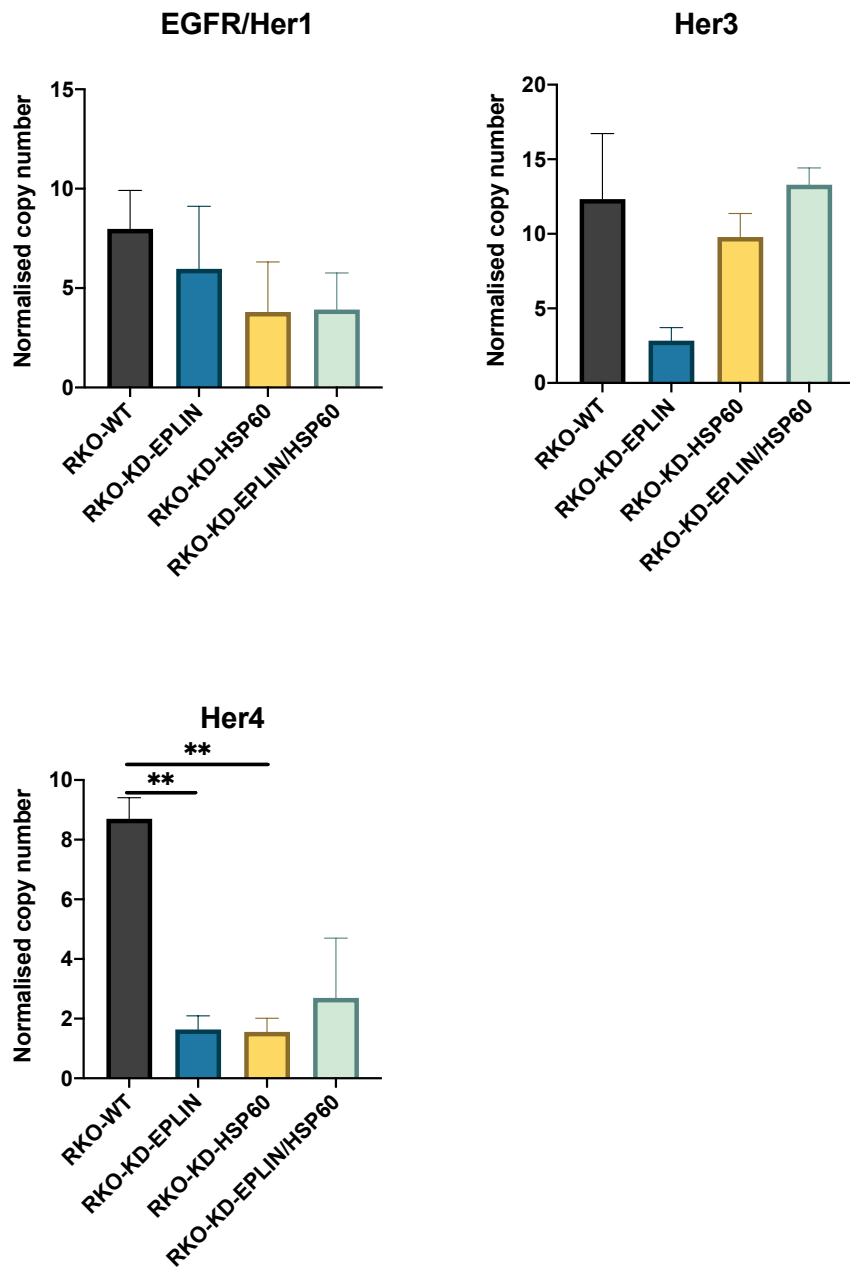


Figure 7.15 Transcript expression of HERS family members in RKO cellular models. Data was shown in mean \pm SEM. Raw data was standardised to PDPL standard and normalised by GAPDH. N=3. Statistical significance was analysed by conducting two-tailed t test. ** represents $p < 0.01$.

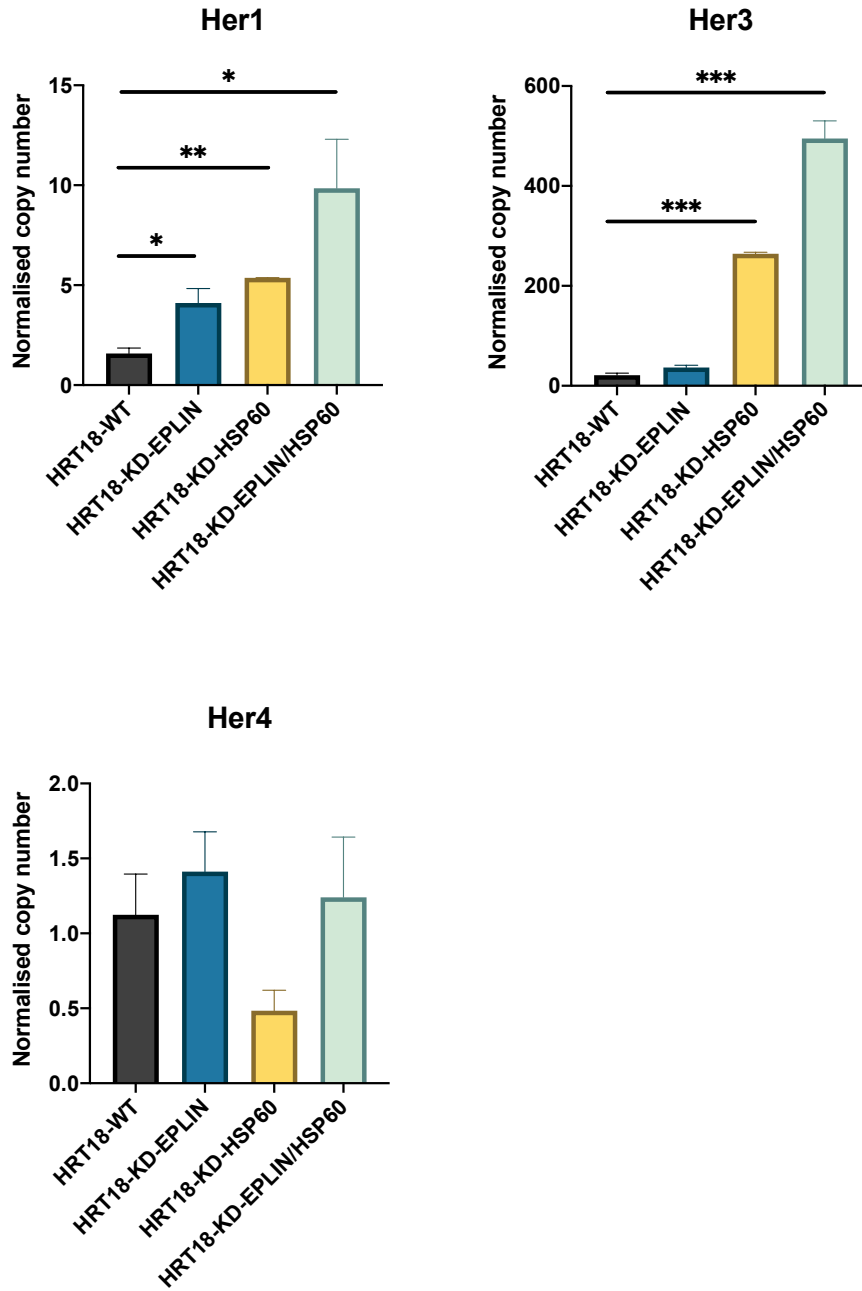


Figure 7.16. Transcript expression of Hers family members in HRT18 cellular models. Data was shown in mean \pm SEM. Raw data was standardised to PDPL standard and normalised by GAPDH. N=3. Statistical significance was analysed by conducting two-tailed t test. * represents $p < 0.05$, **represents $p < 0.01$, ***represents $p < 0.001$.

7.3.4 Implication of manipulating EPLIN/HSP60 on mitochondrial metabolism

After accessing what role EPLIN and HSP60 might play in chemotherapeutic and targeted therapeutic resistance, as well as activation of Her2, we attempted to shed light on the possible mechanism behind such implications. Since HSP60 is known to be deeply involved in mitochondrial metabolic pathways and metabolism is one of key mechanism behind chemotherapy and targeted therapy, we decided to utilise limited resources in the host lab to undertake initial investigate to explore if manipulation of such molecules would have an impact on NAD(P)H and NO₂⁻. To achieve this, Griess Reagent System (Promega, Southampton, UK) and NAD(P)H-Glo™ Detection System (Promega, Southampton, UK) assays were carried out.

7.3.4.1 Implication of manipulation of EPLIN/HSP60 on NAD(P)H

NAD(P)H-Glo™ Detection System (Promega, Southampton, UK) was performed to monitor the level of reduced nicotinamide adenine dinucleotide (NADH) or nicotinamide adenine dinucleotide phosphate (NADPH) that cells produced or released into the extracellular matrix (Figure 7.17). As Figure 7.17A demonstrated, after incubating overnight, NAD(P)H luminescent levels were significantly downregulated when EPLIN alone was suppressed (mean=29851.4±5141.35; p=0.0035) or when knockdown of EPLIN and HSP60 were conducted at the same time (mean=36558.1±1780.58; p=0.0046) in HRT18 cells, compared to the control group (mean=64124.2±8125.74). A trend of increased luminescent signal was observed after suppressing HSP60, but it did not reach statistical significance (p=0.102). No significant changes of luminescent signal of NAD(P)H, secreted into the extracellular matrix were observed in RKO cellular models (Figure 7.17B, all p>0.05). Notably, knocking down EPLIN in HRT18 cells led to significant upregulation of NAD(P)H's luminescent level (mean=2552.1±28.4) compared to the wild type cells (mean=2306.4±13.0) (p=0.008). Hence, our results suggested that knocking down EPLIN alone in HRT18 cells led to downregulation of production of NAD(P)H in cells, but it resulted in upregulated secretion of NAD(P)H into extracellular matrix. Additionally, inhibition of EPLIN and HSP60 together also led to downregulation of NAD(P)H in HRT18 cells.

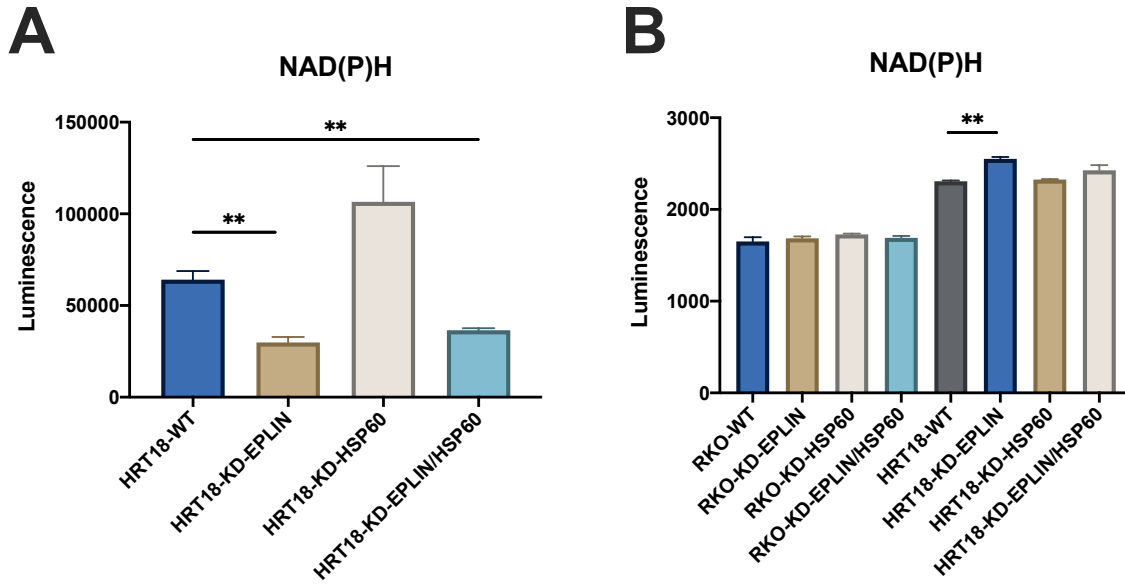


Figure 7.17 Detection of NAD(P)H level based on luminescent signals. A. luminescent signals of NAD(P)H in HRT18 cellular models. B. luminescent signals of NAD(P)H in culture medium of HRT18 cellular models. Data was shown with mean \pm SEM, two tailed t test was performed, ** represents $p < 0.01$.

7.3.4.2 Implication of manipulation of EPLIN/HSP60 on nitrite production in cells

Griess Reagent System (Promega, Southampton, UK) was carried out to access produced level of nitrite (NO_2^-) in total cells and in culture medium. After incubation overnight, as Figure 7.18A&B demonstrated, manipulation of EPLIN and HSP60 alone or together in HRT18 cells, did not lead to obvious or significant changes of nitrite level in cells or extracellular nitrite levels (all p value > 0.05). Similarly, such manipulation in RKO cells did not show significant or obvious changes of extracellular nitrite level (all p value > 0.05). Hence, our results suggested that manipulation of EPLIN/HSP60 did not have an impact on producing nitrite in these cell models.

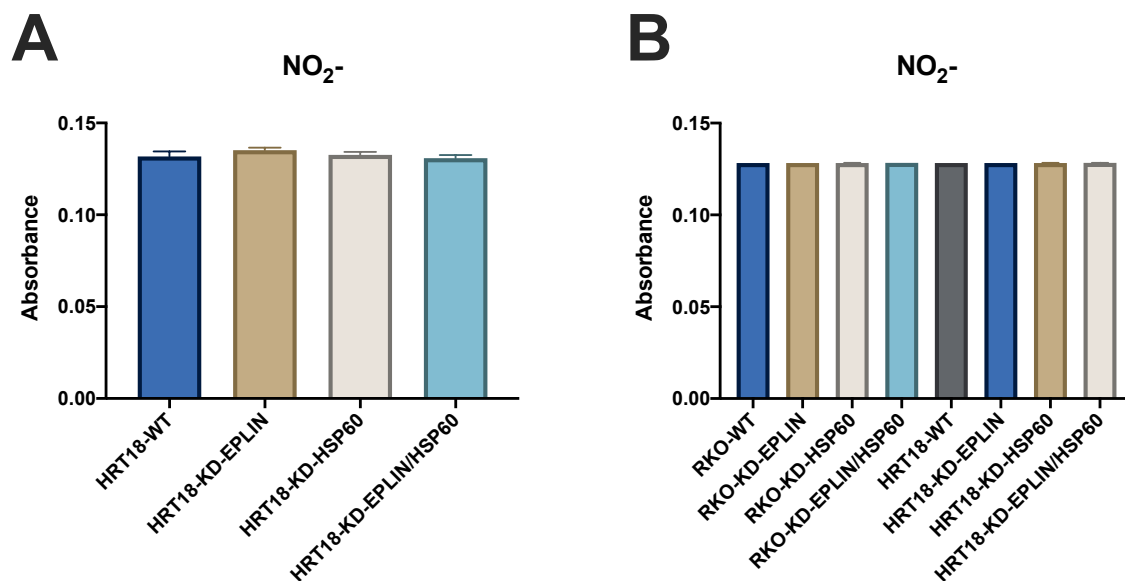


Figure 7.18 Detection of nitrite (NO_2^-) level based on absorbance. A. Nitrite level in HRT18 cellular models in absorbance. B. extracellular nitrite level in RKO & HRT18 cellular models. Absorbance was detected at 540nm wavelength.

7.4 Discussion

This chapter investigated the possibility that EPLIN and HSP60 may have implications on chemotherapeutic resistance/response and targeted therapeutic resistance/response related to Her2. In the first instance, we explored a public database which provides the clinical information of patients response to chemotherapies (TCGA dataset). The database allows analysis of the relationship between EPLIN gene transcript expression and patients sensitivity/resistance to individual chemotherapeutic agents. From the online databases, it seems as though the widely studied tumour suppressor, EPLIN seemed to play a different role in mediating responsive efficiency to chemotherapeutic agents. An upregulation trend related to median transcript expression of EPLIN was observed in patients who did not respond to oxaliplatin and bevacizumab, whilst downregulation of EPLIN seemed to be related to non-responders to capecitabine and irinotecan. Upregulation of HSP60 seemed to link to chemotherapeutic resistance expect for bevacizumab. Downregulation of Her2 was also implicated in the resistance to bevacizumab. None of these analyses provide a concrete link between the three molecules and treatment responses, arguing for a larger datasets and more intensive scientific investigation.

Further cytotoxicity assays, applying established EPLIN/HSP60 manipulated cellular models on several classic chemotherapeutic agents in colorectal cancer revealed some more interesting findings. Knocking down EPLIN led to increased resistance to 5FU in RKO and

HRT18 cells, as did knocking down HSP60 alone or knocking down both molecules at the same time. Interestingly, inhibition of EPLIN and HSP60 alone or together in HRT18 cells resulted in a more sensitive response to docetaxel and a similar effect was observed for oxaliplatin when EPLIN or HSP60 were suppressed alone in RKO and HRT18 cells. However, RKO and HRT18 cells became more resistant to oxaliplatin if EPLIN and HSP60 were inhibited at the same time.

Attempting to seek possible explanation and answer to these rather cluttered findings, mitochondrial metabolic assays were carried out and showed that knocking down EPLIN alone or with HSP60 in HRT18 cells resulted in significant reduction of NAD(P)H, while an enhanced, but non-significant, trend could be seen when HSP60 was inhibited. Indeed, upregulation of NADPH and NADPH mediated reactive oxygen species (ROS) pathway have been reported to be related to not only tumour development (Ju et al. 2020; Rather et al. 2021), but also resistances to 5-FU (Feng et al. 2017; Yang et al. 2021), docetaxel (Hung et al. 2015) and oxaliplatin (Wang et al. 2020). Hence, downregulation of NAD(P)H when EPLIN was knocked down in HRT18 cells could be a potential mechanism behind such manipulation leading to a more sensitive response to oxaliplatin and docetaxel. EPLIN mediated resistance to 5-FU unlikely via this route.

Another interesting finding related to enhanced NAD(P)H levels being observed when HSP60 was inhibited alone and this has not been reported by other researchers. The HSP60 molecule is deeply involved in mitochondrial metabolism and was reported to downregulate NADPH in myeloma cells when it was inhibited (Wu et al. 2020). What would be the mechanism behind the upregulated pattern we observed? Would it be one of the mechanisms behind HSP60 mediated resistance to 5FU in RKO and HRT18? The observation that knocking down EPLIN and HSP60 leading to different effects on oxaliplatin and docetaxel response is rather fascinating, and raises the question as to whether the more sensitive response may also be attributed to downregulation of NAD(P)H? Further questions remain regarding the observed pattern of enhanced resistance to oxaliplatin? The mechanisms of action behind these drugs are different. After getting access to intracellular domains, 5-FU is converted into fluorodeoxyuridine monophosphate (FdUMP), fluorodeoxyuridine triphosphate (FdUTP) and fluorouridine triphosphate (FUTP), further disturbs functions of DNA and RNA synthesis by placing its metabolites into RNA and DNA, as well as inhibiting thymidylate synthase (Longley et al. 2003). While docetaxel acts as an anti-microtubule agent to suppress microtubule function by increasing polymerization (Verweij et al. 1994). Oxaliplatin, a platinum-based agent, acts to suppress DNA synthesis by inducing DNA intrastrand cross-links (Espinosa et al. 2005). Collectively, the database

interrogation and *in vitro* cell model tests have revealed some interesting leads in the relationship between EPLIN/HSP60/Her2 and therapeutic responses. These leads have provided initial insight but further extensive and robust studies, both at a cell level and utilising clinical cohorts are required to fully understand these complex relationships, interactions and implications in therapy response. Due to the COVID-19 pandemic, associated restrictions and with the limitations to our clinical resources, more in depth and larger scale experiments to hunt for possible answers were not possible within this early study. It is hoped that future investigations can take these leads forward.

In chapter 6, I demonstrated that downregulation of EPLIN and HSP60 resulted in upregulation of Her2 at both transcript and protein levels. Here, I showed that knocking down EPLIN and HSP60 alone or together in RKO and HRT18 cells led to a more sensitive response to a Her2 selective inhibitor, AG825. Hence, upregulation of Her2 due to manipulation of EPLIN and HSP60 lead to a more sensitive respond to AG825. Inhibition of EPLIN in RKO and HRT18 cells led to a more sensitive response to neratinib. Interestingly, more dramatically decreased IC50s of neratinib were observed when HSP60 was inhibited alone or with EPLIN in HRT18 cells, but not in RKO cells. Neratinib is an irreversible inhibitor for EGFR and Her2 (Kavuri et al. 2015; Roskoski 2019), and has been reported to be more sensitive to Her2 mutated colorectal cancer cells (Kavuri et al. 2015). HRT18 cellular models displayed a significant upregulation of EGFR when EPLIN and HSP60 were inhibited alone or together. Taken together, it is suggested that the changes of Her family members in response to EPLIN manipulation may be one reason behind more sensitive respond in HRT18 cellular models.

When it comes to afatinib, another irreversible inhibitor for the family members EGFR, Her2 and Her4 (Moosavi and Polineni 2022). Manipulation of EPLIN in both RKO and HRT18 cells resulted in decreased responsive efficiency, while inhibition of HSP60 did not have obvious impact. It seems that when HSP60 and EPLIN were inhibited together, the response due to EPLIN was weakened as a result of HSP60 suppression. This impact EPLIN had on afatinib is the opposite of neratinib based on our observation. Downregulation of EPLIN and HSP60 resulted in significant downregulation of Her4 in RKO cell lines. This intriguing and interesting finding deserves further investigation.

In conclusion, we reported EPLIN and HSP60 have potential in regulating chemotherapeutic resistance as well as EGFR/Her2 targeted therapeutic resistance. But such regulations appear to be drug independent and cell line independent. Due to the serious impact of the COVID-19 pandemic, we were not able to carry more experiments to further explore the

newly derived hypothesis. Our findings are rather fascinating and EPLIN might not be the traditional tumour suppressor as established, at least not in colorectal cancer. Such relationship between Her2, EPLIN and HSP60 might lead to a novel pathway for acquired resistance. Again, further investigation is needed to extend our understanding of these molecules.

Chapter 8

EPLIN expression profile in pancreatic cancer and its clinical implication

8.1 Introduction

Derived from endocrine pancreas or exocrine pancreas (Shih et al. 2013), pancreatic cancer is ranked 10th most common cancer type and 6th most common cause of cancer death in the UK. Most patients (79%) are diagnosed in more aggressive stages. There has been virtually no improvement in 5-year survival rates since 1970s (Cancer Research UK, 2022). Apart from surgical resection, chemotherapy is one the most widely used treatments in pancreatic cancer, for example 5FU, oxaliplatin, paclitaxel, gemcitabine and their combinations (Ansari et al. 2016). As well as limited choice of therapeutic agent, chemotherapeutic resistances, especially gemcitabine, have resulted in poorer responses and poor clinical outcomes (Zeng et al. 2019).

In previous chapters, we have established the importance of EPLIN in colorectal cancer. EPLIN is less well investigated in other gastrointestinal (GI) cancers. Our host laboratories have recently reported the clinical relevance of EPLIN in gastric cancer (Gong et al. 2021) and esophageal cancer (Liu et al. 2012a), while its implication in other GI cancers such as pancreatic cancer remains unknown. Naturally, the question was asked, does EPLIN play a common role as a tumour suppressor in gastrointestinal cancers including pancreatic cancer, or it has a contrasting role based on specific cancer type in the GI system, such as seen in other cancer types? To further advance our knowledge on the clinical importance of EPLIN in colorectal cancers during the COVID lockdown period had become extremely challenging as mentioned in preceding chapters. Fortunately, an available resource of pancreatic cancer specimens in the host laboratories aided the development of the study. In this chapter, I present for the expression profile of EPLIN in pancreatic cancer at transcript and protein level as well as its clinical implications to provide additional evidence for the diverse role of EPLIN in malignancies of the gastrointestinal system.

8.2 Methods

8.2.1 Pancreatic cancer clinical cohort

The pancreatic ductal cancer clinical cohort is a resource from the collaboration with Peking University Cancer Hospital. Tissues and pathological information were collected following the Ethics Research Committee of Peking University Cancer Hospital and is fully in accordance with the Helsinki declarations. For details, please refers to Chapter 2.5.2.

8.2.2 QPCR

Quantitative PCR was performed to probe EPLIN transcript expression in the pancreatic cancer clinical cohort. For details, please refer to Chapter 2.3.6.

8.2.3 IHC and TMA

A tissue microarray contains normal and tumour pancreatic tissues (PA2081a) underwent IHC to probe protein expression of EPLIN. For details of TMA and IHC, please refer to Chapter 2.6 and Supplement-2.

8.2.4 Statistics

SPSS (IBM, Armonk, New York, USA) and Minitab (Minitab Ltd. Coventry, UK) were used to analyse data from qPCR for the clinical cohort, GraphPad (GraphPad Software, San Diego, CA, USA) was used to generate figures for TCGA dataset.

8.3 Results

8.3.1. Expression profile of EPLIN gene transcript in pancreatic ductal cancer clinical cohort

As shown in Table 8.1, no significant change of EPLIN transcript expression was noted between tumour samples and normal tumours ($p > 0.05$).

Furthermore, an increasing transcript level of EPLIN was found to be related to the invasiveness of pancreatic cancer. Firstly, upregulation of EPLIN transcript expression was significantly related to differentiation, in which EPLIN was upregulated in moderate and low differentiated tumour samples ($n=68$, $\text{mean}=6.5 \pm 2.1$) when compared to high and moderate tumour samples ($n=16$, $\text{mean}=1.42 \pm 0.79$; $p=0.025$). Secondly, EPLIN expression was significantly upregulated in TNM2 group ($n=20$) when compared to TNM1 group ($n=126$) (3.7 ± 1.1 vs 0.93 ± 0.59 ; $p=0.031$). Although higher EPLIN expression was also observed in TNM3 ($n=18$, $\text{mean}=5.3 \pm 4.7$) & TNM4 groups ($n=11$, $\text{mean}=3.4 \pm 3.4$) compared to TNM1 group, there was no statistical significance ($p > 0.05$). Thirdly, EPLIN expression in T3&4 group ($n=133$, $\text{mean}=4.3 \pm 1.2$) was also upregulated in comparison with T1&2 ($n=32$, $\text{mean}=1.53 \pm 0.84$), but lacked statistical significance ($p=0.064$). Although EPLIN was observed to upregulate in metastatic tumour samples ($n=15$, $\text{mean}=4.2 \pm 2.9$) compared to no metastatic samples ($n=184$, $\text{mean}=3.6 \pm 0.94$), no significance was noted ($p=0.84$). Intriguingly, relatively higher expression of EPLIN was detected in tumour samples located in the head of pancreas ($n=65$, $\text{mean}=3.9 \pm 1.7$) compared to those located in the body ($n=14$,

mean=2.6±1.8; p=0.59), the tail (n=5, mean=1.7508E-09±1.7217E-09; p=0.024) and other locations (N=7, mean=0.0443±0.044; p=0.025). No statistical significance was observed in comparison to patients' survival, vascular embolic status, nodal involvement, and gender.

Table 8.1 Transcript expression profile of EPLIN in comparison to clinical pathological information of the pancreatic cancer cohort. Data was presented in mean ± SD, statistical significance was investigated by performing two-tailed T test.

Characteristic	Sample number (n)	Relative transcript expression (mean ± SD)	p - value
Tissue type			
Tumour	199	3.633 ± 0.898	
Normal	146	53960404 ± 49210036	0.27
Gender			
Male	120	3.59 ± 1.24	
Female	79	3.70 ± 1.27	0.95
Differentiation			
High	12	1.79 ± 1.77	
Moderate	68	1.99 ± 1.06	0.93
Low	12	1.88 ± 1.47	0.97
High & Moderate	16	1.42 ± 0.79	
Moderate & low	68	6.5 ± 2.1	0.025
TNM stage			
TNM1	20	0.93 ± 0.59	
TNM2	126	3.7 ± 1.1	0.031
TNM3	18	5.3 ± 4.7	0.37
TNM4	11	3.4 ± 3.4	0.49
TNM1&2	32	3.3 ± 0.96	
TNM3&4	133	4.6 ± 3.1	0.70
Anatomical location			
Head	65	3.9 ± 1.7	
Body	14	2.6 ± 1.8	0.59
Tail	5	1.7508E-09 ± 1.7217E-09	0.024
Other location	7	0.0443 ± 0.044	0.025
T stage			
T1	5	5.6 ± 4.8	
T2	27	0.77 ± 0.45	0.37
T3	111	4.3 ± 1.3	0.80
T4	22	4.3 ± 3.8	0.84
T1&2	32	1.53 ± 0.84	
T3&4	133	4.3 ± 1.2	0.064
Nodal involvement			
Negative	80	3.4 ± 1.3	
Positive	99	3.9 ± 1.4	0.79
Presence of Metastases			
No metastasis	184	3.6 ± 0.94	
Distant metastasis	15	4.2 ± 2.9	0.84
Vascular embolism			
Negative	114	3.3 ± 1.1	
Positive	55	3.4 ± 1.7	0.94
Survival			
Alive	44	4.1 ± 2.3	
Died	139	3.8 ± 1.1	0.91

8.3.2 Expression profile of EPLIN in pancreatic adenocarcinoma from TCGA database

In the interest of gaining a wider picture of EPLIN's expression profile in pancreatic cancer, a pancreatic adenocarcinoma dataset, with total sample number of 182, that is available in TCGA database, was analysed by accessing UALCAN platform (Chandrashekar et al. 2017). Data was obtained from UALCAN platform and demonstrated in Figure 8.1.

As Figure 8.1A shows, primary tumour samples have higher median transcript expression level of EPLIN (n=178, median=73.458, q1=54.101, q3=102) than normal samples (n=4, median=52.335, q1=42.79, q3=57.172), but this was not statistically significant which may be due to limitation of sample numbers (p=0.227). EPLIN median transcript expression appears to be upregulated as differentiation status develops (Figure 8.1B). Moderately differentiated group presents significantly higher EPLIN median transcript expression (n=95, median=73.138, q1=55.521, q3=102.441) than well differentiated group (n=31, median=54.941, q1=7.592, q3=75.151) (p=0.0232). Similarly, EPLIN expression in poorly differentiated group is upregulated significantly (n=48, median=86.127, q1=57.107, q3=112.053) when compared with well differentiated group (p=0.0333). No significance was noted in the comparison between moderately differentiated group and poorly differentiated group (p=0.882). This observation agrees with our analysis of the pancreatic cancer clinical cohort.

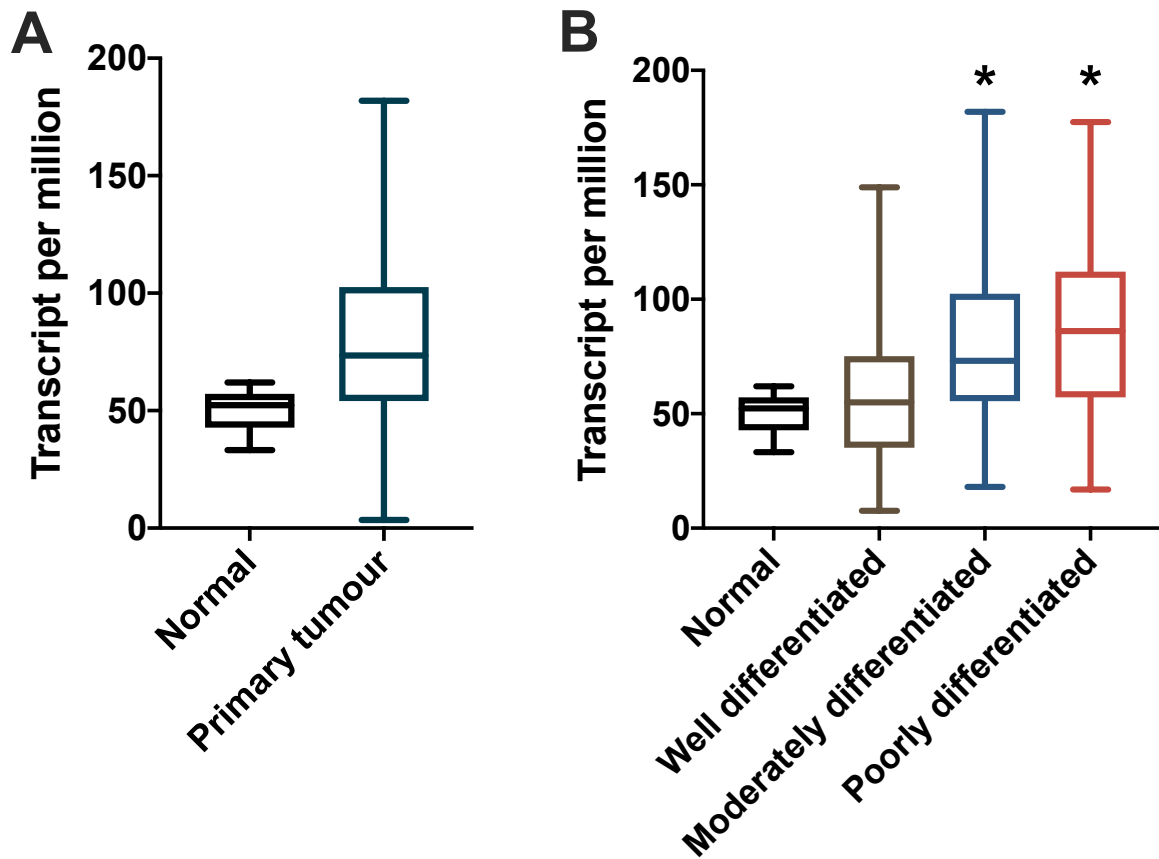


Figure 8.1 TCGA Profile data set of EPLIN in pancreatic adenocarcinoma. A. A trend of upregulation of EPLIN median transcript expression in primary tumour samples (n=178, median=73.458, q1=3.478, q3=102.586) was observed when compared to normal samples (n=4, median=52.335, q1=33.245, q3=57.172) (p=0.227). B. EPLIN median transcript level was increased as the tumours become more poorly differentiated. Well differentiated group (n=31, median=54.941, q1=7.592, q3=75.151). Moderately differentiated group (n=95, median=73.138, q1=55.521, q3=102.441). Poorly differentiated group (n=48, median=86.127, q1=57.107, q3=112.053). Moderately differentiated group vs well differentiated group, p=0.0232. Poorly differentiated group vs well differentiated group, p=0.0333. TCGA Data was obtained from UALCAN platform (Chandrashekar et al. 2017), * represents p<0.05.

8.3.3 Implication of EPLIN on patients' overall survival in the pancreatic cancer clinical cohort

Next, we investigated the influence of EPLIN transcript expression on pancreatic cancer patients' overall survival by performing Kaplan-Meier analysis on the pancreatic cancer clinical cohort. As Figure 8.2 demonstrates, patients are divided into two groups - high level of EPLIN (n=101) and low level of EPLIN (n=73). Surprisingly, patients with higher level of EPLIN had a significantly shorter mean overall survival (mean=20.015 months, 95% CI: 14.141-25.890) than those with lower level of EPLIN (mean=22.630 months, 95% CI: 17.562-27.698) and this was found to be statistically significantly (p=0.045), which suggests a contrasting trend to its implication on CRC patient's survival.

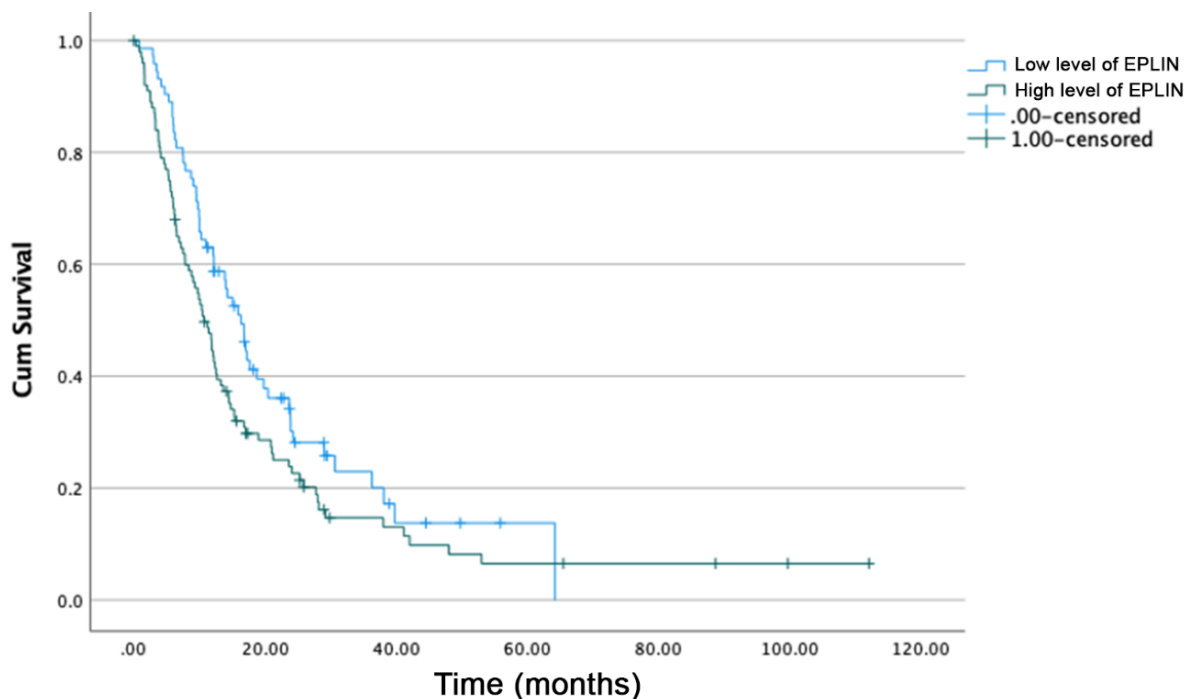


Figure 8.2 Implication of EPLIN transcript level on patient's overall survival in the pancreatic cancer cohort. Patients who expressed higher transcript expression of EPLIN had worse overall survival (n=101, mean=20.015 months, 95% CI: 14.141-25.890) than those with lower level of EPLIN (n=73, mean=22.630 months, 95% CI: 17.562-27.698) (p=0.046). Data was divided into higher EPLIN level group and lower EPLIN level group and analysed using Kaplan-Meier method, p value was estimated by using log rank method.

8.3.4 Implication of EPLIN expression on patients' survival in TCGA pancreatic ductal adenocarcinoma data set

To further explore EPLIN's impact on patients' survival. Kaplan-Meier Plotter was accessed to analyse a TCGA pancreatic ductal adenocarcinoma RNA sequence data set by Kaplan-Meier method (Nagy et al. 2021).

As Figure 8.3 shows, patient samples were divided into two groups based on best cut off value calculated by Kaplan-Meier Plotter - high expression of EPLIN (OS, n=45; RFS, n=24) and low expression of EPLIN (OS, n=132; RFS, n=45). Patients with high expression of EPLIN (median=16.17 months) had significantly shorter OS than those with low expression of EPLIN (median=23.17 months) ($p=0.0047$). Similarly, patients who expressed high levels of EPLIN had significantly shorter RFS than those who expressed low levels of EPLIN (median=16.4 months vs median=50.37 months, $p=0.017$). Again, these observations keep in line with our finding in the pancreatic clinical cohort that a high level of EPLIN led to poorer clinical outcomes.

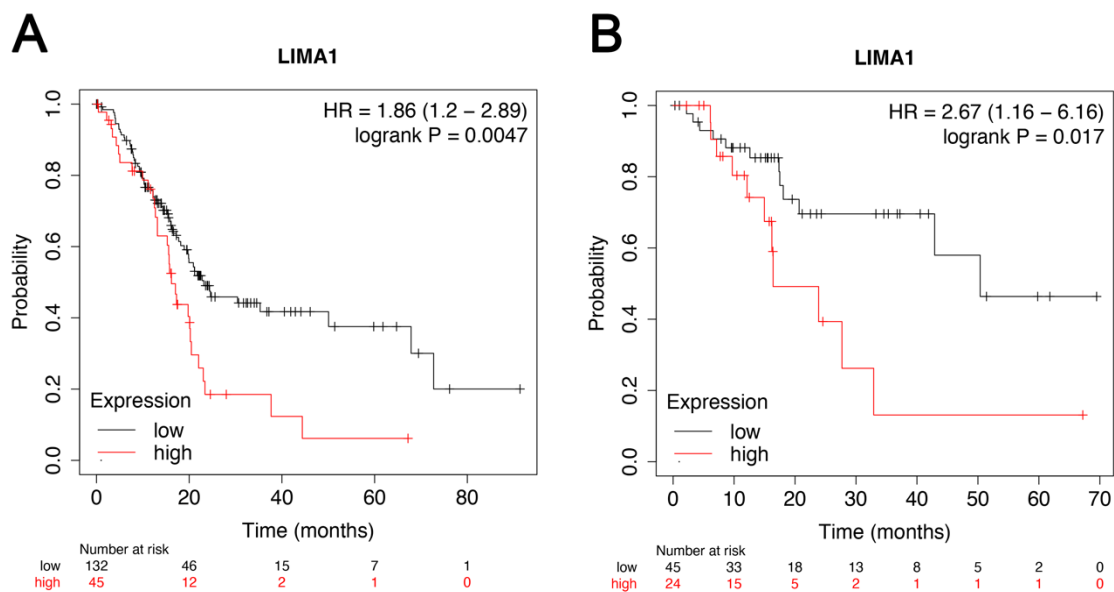


Figure 8.3 Implication of EPLIN on patient's overall survival and relapse-free survival in TCGA pancreatic cancer data set. A. High level of EPLIN leads to worse overall survival in pancreatic cancer patients (n=45, median=16.17 months) when compared to patients with low level of EPLIN (n=132, median=23.17) ($p=0.0047$). B. Patients with high expression of EPLIN result in worse RFS (n=24, median=16.4 months) compared to those with low expression of EPLIN (n=45, median=50.37 months) ($p=0.017$). Data was analysed and obtained by accessing Kaplan-Meier Plotter.

8.3.5 Protein expression profile of EPLIN in pancreatic cancer tissues.

As demonstrated above, we discovered an interesting finding that higher EPLIN transcript expression might be related to the development of pancreatic cancer and poorer clinical outcomes. A TMA from US Biomax (Insight Biotechnologies, Middlesex, UK) (Supplement-2) was purchased to investigate EPLIN expression in pancreatic cancer at the protein level. The TMA slide (PA2081a) includes 103 cases and 208 cores, in which 42 tissues are pancreatic ductal adenocarcinoma, 3 tissues are pancreatic adenosquamous carcinoma, 1 tissue is islet cell carcinoma, 6 tissues are pancreatic metastatic carcinoma, 10 tissues are pancreatic islet cell tumour, 11 tissues are pancreatic inflammation, 21 tissues are adjacent normal pancreatic samples and 10 tissues are pancreatic tissues (Detail information is listed in Supplement-2). EPLIN protein was probed with an anti-EPLIN antibody by IHC assay and the staining intensity was scored and presented in Table 8.2 & Figure 8.4.

As Table 8.2 shows, 50% of the normal tissues (10 of 10) and 38.1% of the adjacent normal tissues (16 of 42) had moderate to strong staining of EPLIN, while the moderate to strong staining was seen in 83.3% in adenosquamous carcinoma tissues (5 of 6), 67.9% in ductal adenocarcinoma groups (57 of 84) and 95.5% in islet cell carcinoma tissues (21 of 22). Chi-square analysis returned a statistical significance among them ($p < 0.001$). Additionally, in the representative pictures (Figure 8.4), the staining of EPLIN is generally stronger in tumour samples when compared to normal samples. For instance, EPLIN mainly stains in cytoplasm in adjacent normal tissue (J13), as well as in stage I adenocarcinoma tissue (D10), and EPLIN expression in D10 is stronger than J13. In addition, islet cancer (pancreatic endocrine cancer) samples expressed strong EPLIN expression (F11 & F12), and this was seen to be stronger than adenocarcinoma samples.

When the staining was assessed against tumour stage, 65.9% of the tissues in Stage I (29 of 44) was rated as moderate to strong, while it was 70% in Stage II (21 of 30), 83.3% in Stage III (10 of 12) and 50% in Stage IV (2 of 4). This was not statistically different ($p = 0.5654$). Stage IV group ($n = 4$) had weaker staining than other groups, largely due to the limitation of sample numbers (Figure 8.4 and Table 8.2), a larger tissue cohort of pancreatic cancer would be necessary to strengthen these findings.

We also classified tumour samples by differentiation grades - well differentiation (G1), moderate differentiation (G2) and poor differentiation (G3). As Table 8.2 demonstrates, 12 of 14 tissues in Grade-1, 13 of 25 tissues in Grade-2 and 21 of 34 in Grade-3 tumour tissues were rated as moderate to strong. Statistical significance was found when Grade-1 compared with Grade-2 ($p = 0.0353$). Upregulated trend could also be observed in Grade3

group when compared with Grade-2 Group. Although it did not reach significance (p=0.1037). Overall chi-square test among groups did not return a statistical significance either (p=0.1097).

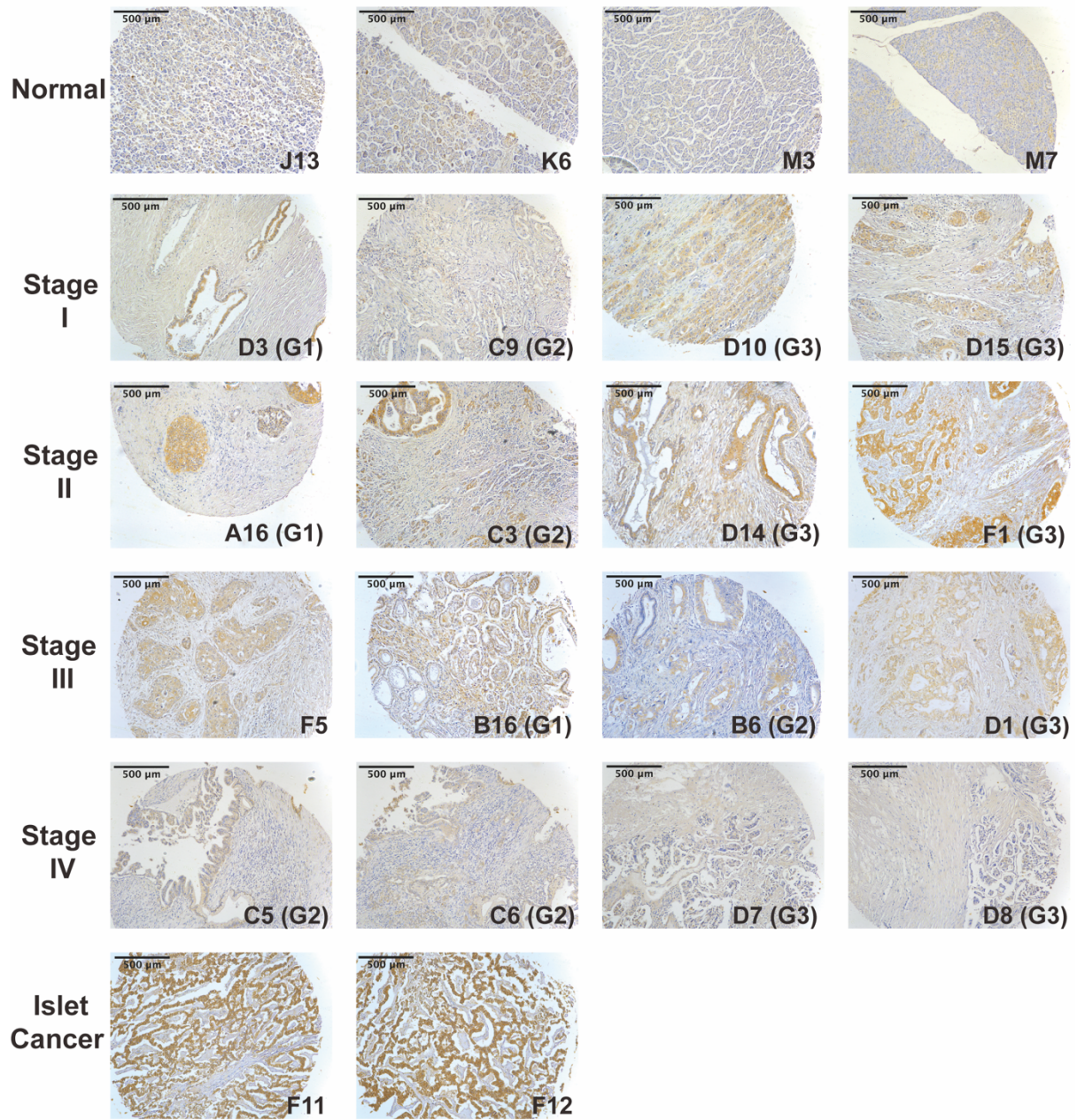
Table 8.2 Scoring analysis of pancreatic cancer TMA (PA2081a)

	Total Number	Intensity		Statistical significance	
		Negative to weak (0-1)	Moderate to strong (2-3)	Chi value	p
Pathology				24.38	<0.001 ^a
Normal tissue	20	10	10		
Cancer adjacent normal tissue	42	26	16		
Adenosquamous carcinoma	6	1	5		
Ductal adenocarcinoma	84	27	57		
Islet cell carcinoma	22	1	21		
Stage				2.034	0.5654 ^b
I	44	15	29		
II	30	9	21		
III	12	2	10		
IV	4	2	2		
Differentiation Code				4.419	0.1097 ^c
Grade1	14	2	12		
Grade2	25	12	13	4.433	0.0353 ^d
Grade3	34	13	21	2.648	0.1037 ^d
Metastatic Site					
Omentum	1	1	0		
Liver	6	2	4		
Abdominal cavity	2	0	2		
Lymph node	2	1	1	0.1778	0.6733 ^e

Note: ^aOverall chi-square test among pathology groups; ^bOverall chi-square test among stage groups; ^cOverall chi-square test among differentiation groups; ^dCompared with Grade1 group; ^eCompared with liver group.

A

Magnification x 100



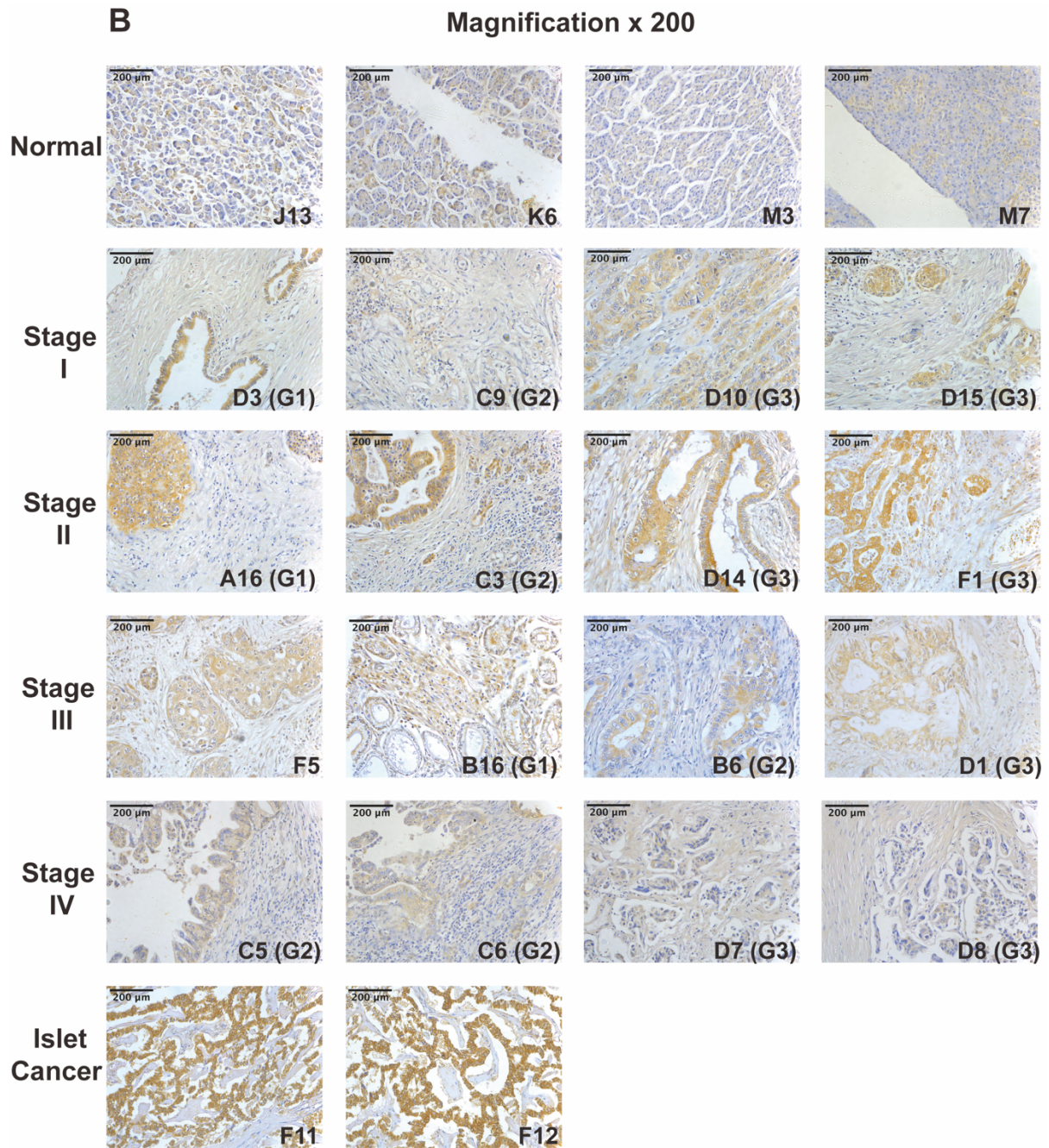


Figure 8.4 Representative pictures of pancreatic TMA (PA2081a). A. Photos were taken under a Leica DM IRB Microscope (Leica GmbH, Bristol, UK) at X100 objective magnification. B. Photos were taken under a Leica DM IRB Microscope (Leica GmbH, Bristol, UK) at X200 objective magnification. G1-3 stands for histological grade of pancreatic cancer tissues.

Metastatic tumour samples that migrate from primary pancreatic cancer were also probed with EPLIN to investigate its protein expression. After migrating to abdominal cavity, lymph node and omentum, both tissues of abdominal cavity had moderate staining of EPLIN but it was in limited area. Interestingly, weak staining of EPLIN could be seen in the omentum tissue and 1 of the lymph node tissues. While 4 of 6 liver tissues had moderate to strong staining of EPLIN (Table 8.2 & Figure 8.5).

Hence, EPLIN protein expression in pancreatic ductal adenocarcinoma, as well as islet cancer, is generally stronger than it in normal tissues, and its expression tended to increase as tumour got more aggressive. Furthermore, EPLIN profile in pancreatic cancer might differ from other cancer types.

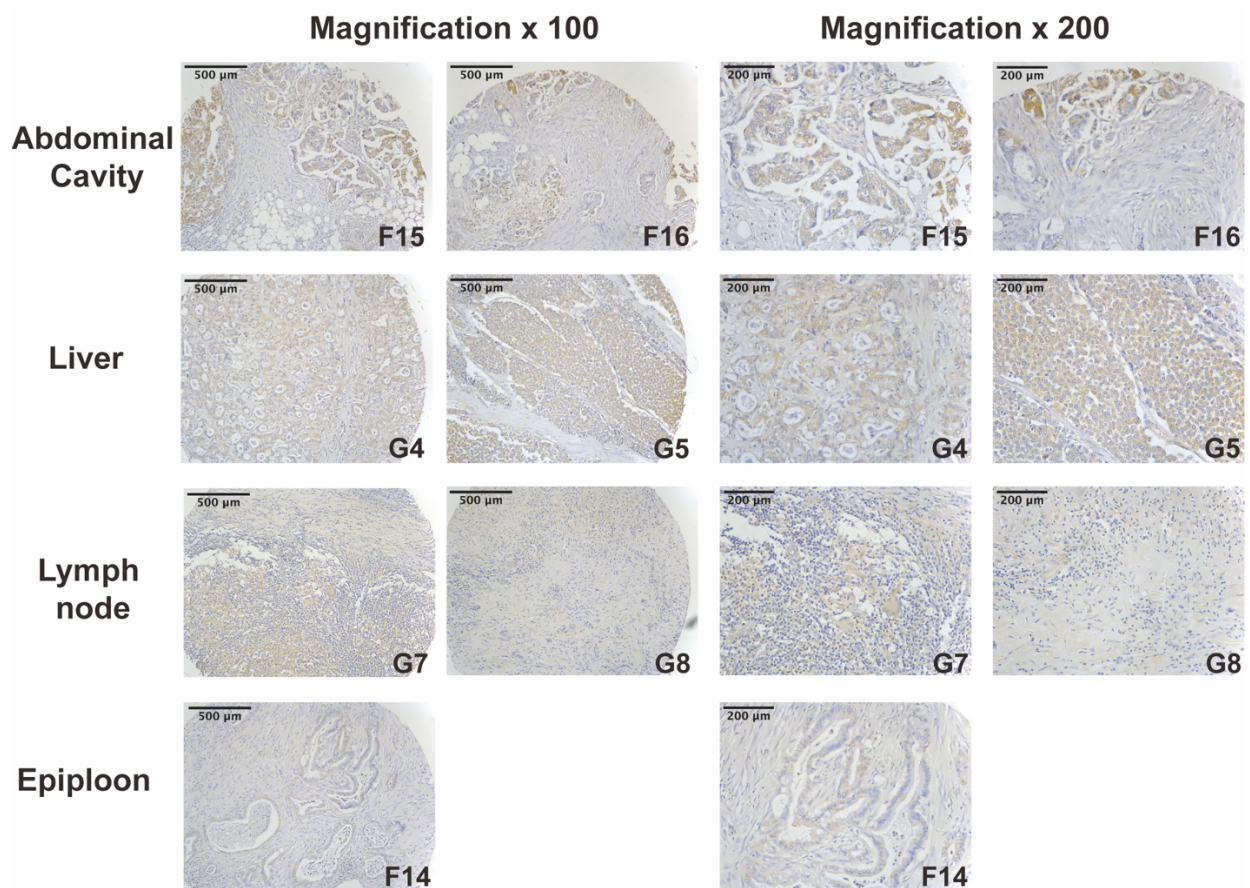


Figure 8.5 Representative pictures of tumour tissues migrate from pancreatic tumour in TMA (PA2081a). Photos were taken under a Leica DM IRB Microscope (Leica GmbH, Bristol, UK) at X100/X200 objective magnification.

8.4 Discussion

Over the last two decades, researchers have implicated that EPLIN acts as a tumour suppressor in multiple epithelial cancer types. Studies in our laboratory have also previously suggested EPLIN plays a similar role in various gastrointestinal cancers including CRC, gastric and oesophageal cancer. In this chapter, we observed an exciting different expression profile of EPLIN in pancreatic cancer at transcript and protein level.

Firstly, our pancreatic cancer clinical cohort was carried out to demonstrate that higher transcript expression of EPLIN is related to invasiveness in pancreatic cancer, as EPLIN transcript expression was upregulated significantly in moderately and poorly differentiated samples when compared to well and moderately samples, and significant upregulation was noted in the TNM2 group when compared to the TNM1 group. Although higher transcript expression of EPLIN was observed in the TNM3 and the TNM4 group when compared with the TNM1 group, EPLIN transcript expression was higher in the T3&4 group than in the T1&2 group, but this did not reach statistical significance. Our analysis also suggested that EPLIN expression profile in primary pancreatic cancer is related to its location, as tumours in the head of pancreas were found to have significantly higher levels of EPLIN transcript than those in the body and tail. Secondly, although there were no significant changes of EPLIN transcript expression between normal and tumour samples in the Beijing clinical cohort, the analysis of pancreatic adenocarcinoma dataset in the TCGA database shows a trend of upregulation of EPLIN transcript expression in primary tumour samples when compared to normal samples but again this was not statistically significant. By analysing the TCGA dataset, we also noted that EPLIN expression in moderately differentiated and poorly differentiated group was higher than its expression in well differentiated group significantly. This was in keeping with our finding in the Beijing clinical cohort and implicating that high level of EPLIN transcript expression might lead to more aggressive development of pancreatic cancer. Further investigation by applying Kaplan-Meier method to analyse the Beijing clinical cohort and pancreatic ductal adenocarcinoma TCGA dataset on Kaplan-Meier Plotter showed that patients with high level of EPLIN had worse OS and RFS when compared to those with low levels of EPLIN.

IHC analysis of TMA was also carried out to probe EPLIN and investigate its profile in pancreatic cancer at the protein level. Stronger EPLIN expression was not only observed in ductal adenocarcinoma tissues and islet cancer tissues compared to normal tissues, but also in tumour tissues with more aggressive stages (Stage II & III). Interestingly, we discovered that EPLIN expression is generally weak in tumour tissues in abdominal cavity,

lymph node and omentum following dissemination of cells away from the primary tumour and establishment of metastatic tumours in these sites. However, its expression in tumour samples from liver metastases is the strongest among these investigated metastatic sites. Pancreas and liver share similar embryonic development and form a functionally linked tissue organisation. Moreover, subtypes of pancreatic cancer and liver cancer share some degree of similarities (Ghurburrun et al. 2018).

One of the possible mechanisms behind the contrast in levels of expression of EPLIN between colon cancer and pancreatic cancer could be due to the hyper-methylation status of the *LIMA1* (EPLIN coding gene) gene promoter, an aspect that was not part of the current study. Indeed, when exploring the TCGA datasets of both human colon adenocarcinoma and human pancreatic adenocarcinoma on UALCAN platform (<http://ualcan.path.uab.edu/cgi-bin/TCGA-methyl-Result.pl?genenam=LIMA1&ctype=COAD>), this argument can find its support. The methylation dataset indeed showed there was no difference in the hypermethylation of the *LIMA1* gene promoter in pancreatic cancer when compared with normal pancreatic tissues ($p=0.9411$, tumour versus normal; <http://ualcan.path.uab.edu/cgi-bin/TCGA-methyl-Result.pl?genenam=LIMA1&ctype=PAAD>). However, the *LIMA1* gene promoter was significantly hypermethylated in colorectal cancer when compared with normal colon tissues ($p=0.0222$) (<http://ualcan.path.uab.edu/cgi-bin/TCGA-methyl-Result.pl?genenam=LIMA1&ctype=COAD>). This additional information from the TCGA database does indicate that upregulation of promoter methylation of the *LIMA1* gene is at least one of the most possible contributing factors to the difference of the levels EPLIN gene transcript and protein in certain tumour types, colon cancer in this case. This is also the most plausible reason for the contrast expression pattern of EPLIN between pancreatic cancer and colorectal cancer. Therefore, such findings suggest that high EPLIN expression profile might be one of the exclusive features for pancreatic cancer, one of few cancer types with this feature. The other cancer type has a similar link to pancreatic cancer is head and neck squamous cell carcinoma (HNSCC), in which the *LIMA1* promoter methylation was significantly reduced ($p<0.0000001$) (<http://ualcan.path.uab.edu/cgi-bin/TCGA-methyl-Result.pl?genenam=LIMA1&ctype=HNSC>) together with a markedly increased expression of the EPLIN transcript ($p<0.000001$) (<http://ualcan.path.uab.edu/cgi-bin/TCGAExResultNew2.pl?genenam=LIMA1&ctype=HNSC>). This finding was also reported recently in the HNSCC (Ma et al. 2022).

In conclusion, we demonstrated that EPLIN has diverse and contrasting roles in malignancies of the gastrointestinal system. Whilst it appears to be acting as a tumour

suppressor in colorectal, oesophageal and gastric cancers, it clearly elicits the opposite effect in pancreatic cancer. This new information is an exciting addition to the studies of EPLIN in human cancers and would undoubtedly raise more interest in the future.

Chapter 9

General Discussion

Colorectal cancer is the 4th most common cancer type and the 2nd most common cause of cancer death in the UK. Thanks to the development of screening methods and treatments, especially chemotherapy, targeted therapy and immunotherapy, survival rates of colorectal cancer are improving in recent years. However, low 5-year survival rates for the more aggressive stages, along with increasing incidence rates in the younger 25-49 age group and the phenomenon of acquired resistance to chemotherapeutic and targeted therapeutic agents, remind us that colorectal cancer is still a heavy health burden in the Western society.

Pancreatic cancer, also belongs to the gastrointestinal cancers, and is one of the most deadly. It ranks as 10th most common cancer type and 5th most common cause of cancer death in the UK. Unsurprisingly, and in similarity to colorectal cancer, acquired resistance to chemotherapeutic and targeted therapeutic agents has become a more serious problem, despite the positive effects of newer agents.

In order to improve clinical outcomes of such cancers, researchers are continuously working to develop new strategies. One of the important approaches is hunting biomarkers for such cancers, to understand their implication on cellular functions and related mechanisms, further shed light on developing novel therapeutic strategies. In this study, we focused on a widely studied tumour suppressor, EPLIN. Since it was discovered to be downregulated in oral cancer at the end of last century (Chang et al. 1998), its role in multiple cancer types has been revealed, and several signalling pathways that in which EPLIN participates have been revealed. To our surprise, little research on the role EPLIN may play has been done on gastrointestinal cancers, especially colorectal cancer and pancreatic cancer. In this project, I revealed clinical and functional implications of EPLIN in colorectal cancer. I also identified potential novel regulating partners of EPLIN in colorectal cancer. Such partners were demonstrated to impact efficiency of responding to chemotherapeutic and Her2 targeted therapeutic agents. Moreover, I also shed light on a different role EPLIN might play in pancreatic cancer.

9.1 Clinical implication of EPLIN in colorectal cancer

By accessing EPLIN expression in online public databases, clinical cohorts and TMA slides, we highlighted that EPLIN transcript expression and protein expression was downregulated in tumour samples when compared to normal samples. Such findings keep in line with related researches in other cancer types (Lee et al. 2006; Jiang et al. 2008; Sanders et al. 2011; Zhang et al. 2011; Liu et al. 2012b,a; Steder et al. 2013; Ohashi et al. 2017; Collins et

al. 2018). Researchers also reported such downregulation of EPLIN in tumour samples was related to metastasis in breast cancer (Jiang et al. 2008; Zhang et al. 2011), prostate cancer (Sanders et al. 2011; Collins et al. 2018), oesophageal cancer (Liu et al. 2012a) and lung cancer (Liu et al. 2012b), SCCHN and melanoma cancer (Steder et al. 2013). Decreasing trend of EPLIN was observed in TMA slides at protein level, which implicates a potential correlation between EPLIN expression and colorectal metastatic progression. Such deduction was also supported by trawling public database to reveal EPLIN was correlated with players involved in the EMT process at transcript level. Another highlight finding was that colorectal cancer patients with lower transcript expression of EPLIN had worse overall and disease-free survival compared to those with higher expression. This was also in line with other researchers' findings in other cancer types (Jiang et al. 2008; Liu et al. 2012a,b; Liu et al. 2016; Collins et al. 2018). Our findings further reveal EPLIN might play an essential role in carcinogenesis and development of colorectal cancer.

9.2 EPLIN regulates cellular functions in colorectal cancer

Functionally, EPLIN regulates actin dynamic and adherens junctions due to it bundles and cross links actin filament (Maul and Chang 1999; Zhang et al. 2011; Zhang et al. 2013) and β -catenin (Abe and Takeichi 2008). Besides, EPLIN acts as a negative regulator of cellular growth in breast cancer (Jiang et al. 2008), prostate cancer (Sanders et al. 2011; Collins et al. 2018), oesophageal cancer (Liu et al. 2012a), pulmonary cancer (Liu et al. 2012b) and ovarian cancer (Liu et al. 2016)), and of cellular migration in breast cancer (Jiang et al. 2008), prostate cancer (Zhang et al. 2011; Collins et al. 2018), pulmonary cancer (Liu et al. 2012b) and ovarian cancer (Liu et al. 2016). It is also a negative regulator of cellular invasion in breast cancer (Jiang et al. 2008), prostate cancer (Sanders et al. 2011; Zhang et al. 2011; Collins et al. 2018), malignant melanoma (Steder et al. 2013), oesophageal cancer (Liu et al. 2012a) and ovarian cancer (Liu et al. 2016). In this study, EPLIN expression was manipulated in colorectal cancer cell lines and by carrying out MTT growth assays, ECIS migration assays and Matrigel invasion assays it was demonstrated that EPLIN plays a similar role in colorectal cancer. Downregulation of EPLIN in colorectal cell lines led to increased cellular growth, migration and invasion. Similarly, overexpression of EPLIN brought about the opposite effects, strongly implicating EPLIN in these processes. The ability to impact cellular function in colorectal cancer further implicated EPLIN's involvement and importance in colorectal cancer development.

9.3 Potential novel interacting partners and signalling pathways of EPLIN in colorectal cancer

By utilising data from a foregoing Kinexus protein microarray on colorectal cancer patient samples, a number of potential interacting partners and signalling events were identified. Apart from MAPK related events, in which some of them were already reported by other researchers (Steder et al. 2013; Zhang et al. 2013), EGFR family and HSP family members were also listed as priority targets, especially Her2 and HSP60. From previous studies done in the host laboratory, Her2 and HSP60 related events were chosen for the further investigation. However, such potential interaction of EPLIN, HSP60 and Her2 were not found in epithelial colorectal cancer cell lines when we performed co-IP assays. Protein microarrays were performed on clinical patient's tissues, which contain not only epithelial cells but also other components from microenvironments such as stem cells and stromal cells. Also tumours themselves represent a heterogenous population of cancer cells, hence may be different to that seen in basic cell line models. Hence, such interactions might be detected from non-epithelial cells which are not the cause of the cancer, but not from the cancerous epithelial cells. One possible solution for this was to carry out the protein microarrays on protein samples from colorectal cancer cell lines. Cell lines are guaranteed to provide homogenous cells types, but these may carry various unrelated genetic mutations compared to cancer cells derived from primary tumours. Due to the limitations in laboratory access and other negative impacts of the COVID-19 pandemic, this was not possible and hence this available Kinexus data was utilised to provide an indication of novel candidates for further in vitro investigation to explore wider implications between these molecules and EPLIN. By accessing transcript and protein levels of Her2 and HSP60 on EPLIN manipulated cell lines, Her2 was found to be upregulated when EPLIN and HSP60 were repressed. Such upregulation seemed to be enhanced when EPLIN and HSP60 were inhibited at the same time. Hence, we suggest that EPLIN and HSP60 regulate Her2 expression level at transcript and protein levels. Although no direct protein-protein interaction relationships were discovered between them in epithelial colorectal cancer cells, the mechanism behind the observed regulatory relationships might be worth further investigation in the future. Moreover, data from protein microarray suggested Eukaryotic translation initiation factor 4E (EIF4E) as a priority target. EIF4E has been reported to be involved in not only cellular invasion and the EMT process (Robichaud et al. 2015), but also downstream of EGFR/Her2 signalling (Evans et al. 2018). By manipulating EPLIN and HSP60 expression, we also observed dysregulation of EIF4E at transcript level (data not shown). Whether eIF4E is also involved in the EPLIN/HSP60/Her2 interacting network remains an important question for the focus of future scientific investigation. However, due to

the pandemic it was not possible to fully explore this exciting lead in the current study. Further questions have also been raised by the current study. For example, could Her2/HSP60 related signalling events (TFAP2 regulation signalling) identified by online databases be the missing puzzle? Or could it be the MAPK related signalling events? Or the regulation is an independent event? Further investigations are needed.

9.4 Clinical implication of Her2, HSP60 and EPLIN on colorectal cancer

I demonstrated high transcript and protein levels of HSP60 was associated with colorectal cancer by analysing CRC clinical cohort and TMA. However, higher transcript level was detected in less aggressive stages in clinical colorectal cancer and seems to be associated with better OS and RFS. Such findings are contradictory to research by Vocka et al. (Vocka et al. 2019), given the study of HSP60's clinical significance on colorectal cancer was limited, a much larger investigation is warranted. While high transcript level of Her2 is observed in clinical colorectal cancer tumour samples, and is associated with worse clinical outcomes.

Another highlight finding is that the combination of EPLIN, HSP60 and Her2 is a significant predictive factor of OS, and patients with aberrant level of three molecules had worst OS and RFS. Analysis of the clinical cohort also revealed EPLIN, HSP60 and EGFR family members, especially Her2, had regulatory relationships at the transcript level, which is partly in line with the correlation found in the cellular models. Hence, the three molecules are found to have potential to have impact on clinical outcomes in colorectal cancer, although future studies are again warranted to confirm and further explore these initial findings.

9.5 EPLIN and HSP60 have the potential to regulate responsive efficiency of chemotherapeutic and EGFR/Her2 targeted therapeutic agents

In the light of my findings regarding EPLIN, HSP60 and Her2, I further attempted to investigate if they have impact on chemotherapeutic or targeted therapeutic resistance. The analysis of colorectal cancer clinical resistance online database had shown such molecules have potential to affect responsive efficiency to chemotherapeutic agents, but it did not lead a clear way to show such molecules are involved in regulating response to chemotherapy. Analysis of a larger cohort was required for a clearer understanding. To explore this at potential implication at a cellular level, cytotoxicity assays were utilised *in vitro* in conjunction with manipulated models. Interestingly, by knocking down EPLIN or HSP60 alone or together in RKO and HRT18 cell lines, interestingly, different impacts were observed when

5FU, oxaliplatin and docetaxel were applied. Inhibition of EPLN and HSP60 alone or together resulted in less sensitive response to 5FU, but more sensitive response to docetaxel. Surprisingly, inhibition of EPLIN and HSP60 alone led to more sensitive response to oxaliplatin, but less sensitive response to the agent if the two molecules were inhibited together. Such observations may be in line with the downregulation of NAD(P)H when EPLIN was knocked down in HRT18 cells. Hence, this could be a potential mechanism behind such manipulation led to more sensitive response to oxaliplatin and docetaxel. Upregulation of NAD(P)H could be the potential mechanism behind less sensitive response to 5FU in RKO and HRT18 cells. However, it did not lead us to the destination where such observations could be explained clearly and the mechanisms of action behind these drugs are different. Therefore, more in depth investigation and analysis of a larger clinical cohort in the future could lead us forward.

While inhibition of EPLIN and HSP60 alone or together led to more sensitive response to AG825, a Her2 selective inhibitor. The trend of more sensitive response was also observed in lapatinib and neratinib, but the opposite effect was noted for afatinib. These agents utilised as EGFR/Her2 targeted treatment. I also reported inhibition of EPLIN and HSP60 alone or together upregulated Her2 at transcript and protein level, while it regulated EGFR and Her3 in HRT18 cell lines, and downregulated Her4 in RKO cell lines. Would such regulation of Her family be responsible for the dysregulation of sensitive efficiency of such agents? These intriguing and interesting findings deserve further investigation.

9.6 Potential novel signalling pathway of EPLIN in colorectal cancer

By investigating EPLIN and its potential partners in colorectal cancer, we demonstrated that EPLIN played a negative role in regulating cellular functions (growth, migration, adhesion and invasion) in colorectal cancer. HSP60 and Her2 were identified as potential partners involved in EPLINs regulatory and interaction network. We verified that inhibition of EPLIN regulated Her2, but not HSP60, while downregulation of HSP60 also upregulated Her2. Downregulation of EPLIN and HSP60 in colorectal cancer cell lines led to different dysregulation of responsive efficiency to chemotherapeutic and EGFR/Her2 targeted therapeutic agents. Hence, I proposed a novel signalling pathway of EPLIN/HSP60/Her2 in colorectal cancer (Figure 9.1). Although EPLIN seemed to work as a tumour suppresser in colorectal cancer when we analysed the clinical cohort and carried out functional assays, cytotoxicity assays on chemotherapeutic and EGFR/Her2 targeted therapeutic agents tended to tell a different story.

EPLIN was reported to be related to EGFR signalling events, where EGF could induce protein turnover of EPLIN via its downstream player, ERK 1/2 (Zhang et al. 2013). Our findings not only highlighted the regulatory relationships between EPLIN, HSP60 and Her2, but also EPLIN and other EGFR family members, especially EGFR. Hence, EGFR-EPLIN signalling would be one of the worthy path to follow in our future study. Once again, detailed mechanisms behind such interesting findings would be worth border investigation and study.

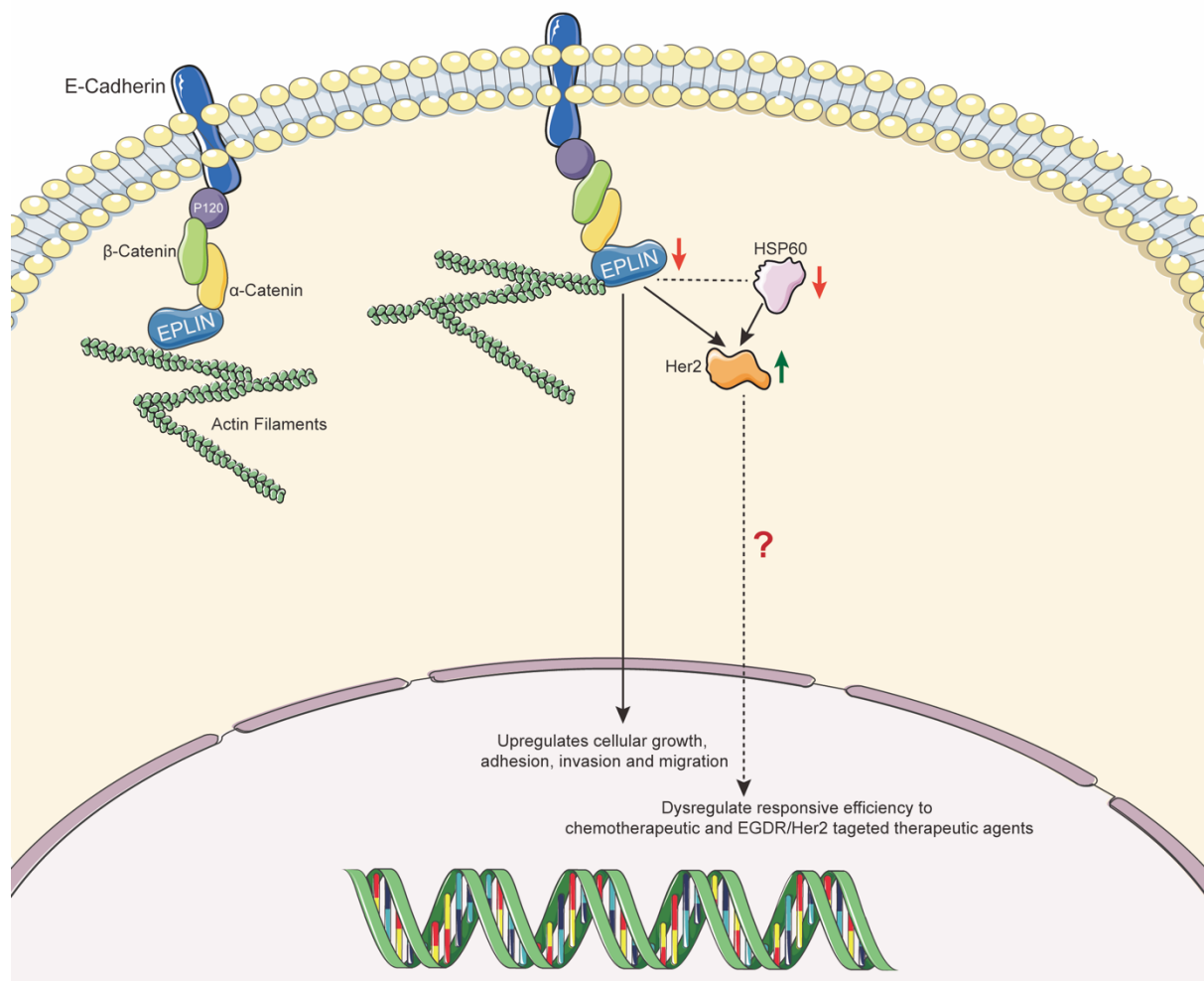


Figure 9.1 Hypothetical EPLIN/HSP60/Her2 signalling pathway.

9.7 EPLIN plays a different role in pancreatic cancer

Because of the negative impact given by the COVID-19 pandemic, further experiments planned for colorectal cancer could not be carried out. In order to minimise this negative impact and broaden my understanding of EPLIN in gastrointestinal cancers, I decided to investigate the possible role EPLIN might play in pancreatic cancer. To my surprise, EPLIN was upregulated in pancreatic cancer at transcript and protein levels, and such upregulating trend tended to be associated with more aggressive stages. Upregulation of EPLIN also

resulted in worse OS in pancreatic cancer patients. It is clear that EPLIN acts as a potential oncogenic protein in pancreatic cancer based on our findings. Besides, by analysing TMA, metastatic samples located in liver from primary pancreatic cancers maintained strong signals compared to metastases from the abdominal cavity, lymph nodes and omentum. Since pancreas and liver share some degree of similarities (Ghurburrun et al. 2018), this expression profile might be specific to pancreatic cancer and might be related to its embryonic development. Different expression pattern of EPLIN between pancreatic cancer and colorectal cancer might be due to the different status of hyper-methylation. Again, we could not go deeper into pancreatic cancer because of COVID, but I shed light on a novel area of EPLIN in pancreatic cancer. Further investigation is needed for reveal its functional impact and possible mechanism in pancreatic cancer.

9.8 Future work

Despite of the negative impact by the COVID-19 pandemic, my study proposed some novel and interesting findings of EPLIN in gastrointestinal cancers. However, whilst I have given an initial idea of the implications of EPLIN and its potential interacting/regulatory molecules, further work to fully elucidate such networks in depth is required. Firstly, the implication of EPLIN/HSP60/Her2 signalling on cellular functions require further in-depth mechanistic studies to explore the impact of such individual and co manipulated models on cancer cell function. Secondly, HSP60's role in clinical outcomes of colorectal cancer is rather fascinating but requires further clarification in larger clinical cohort. Thirdly, manipulation of EPLIN/HSP60 led to dysregulation of responsive efficiency to chemotherapeutic and EGFR/Her2 targeted agents. Although I attempted to establish the specific mechanism behind it, further work is required to fully elucidate such mechanisms. Whether EPLIN/HSP60/Her2 signalling or mitochondrial metabolism be significant factors here remains to be fully established and warrants further investigation. Additionally, in order to finalise fully EPLIN/HSP60/Her2 signalling, other important candidates are worthy of future investigations, namely EIF4E, TFAP2 and their related signalling events. Moreover, we demonstrated a differential role for EPLIN in pancreatic cancer. Full studies are now required in multiple pancreatic cell models to examine this relationship at a cellular level and investigate further potential interactions and regulatory relationships between Her2 and HSP60 in this cancer type. Last but not least, *in vivo* works were planned but could not be completed due to the pandemic, we are eager to expand our work further to reveal EPLIN's implications in *in vivo* models, and shed light on its potential of developing novel therapeutic agents.

References

- Aaltonen, L. A. et al. 1998. Incidence of hereditary nonpolyposis colorectal cancer and the feasibility of molecular screening for the disease. *N Engl J Med* 338(21), pp. 1481-1487. doi: 10.1056/NEJM199805213382101
- Abe, K. and Takeichi, M. 2008. EPLIN mediates linkage of the cadherin catenin complex to F-actin and stabilizes the circumferential actin belt. *Proc Natl Acad Sci U S A* 105(1), pp. 13-19. doi: 10.1073/pnas.0710504105
- Abu Taha, A. and Schnittler, H. J. 2014. Dynamics between actin and the VE-cadherin/catenin complex: novel aspects of the ARP2/3 complex in regulation of endothelial junctions. *Cell Adh Migr* 8(2), pp. 125-135. doi: 10.4161/cam.28243
- Abu-Hadid, M. et al. 1997. Relationship between heat shock protein 60 (HSP60) mRNA expression and resistance to platinum analogues in human ovarian and bladder carcinoma cell lines. *Cancer Lett* 119(1), pp. 63-70. doi: 10.1016/s0304-3835(97)00255-3
- Aghabozorgi, A. S. et al. 2019. Role of adenomatous polyposis coli (APC) gene mutations in the pathogenesis of colorectal cancer; current status and perspectives. *Biochimie* 157, pp. 64-71. doi: 10.1016/j.biochi.2018.11.003
- Ahmed, M. 2020. Colon Cancer: A Clinician's Perspective in 2019. *Gastroenterology Res* 13(1), pp. 1-10. doi: 10.14740/gr1239
- Aird, W. C. 2007. Phenotypic heterogeneity of the endothelium: II. Representative vascular beds. *Circ Res* 100(2), pp. 174-190. doi: 10.1161/01.RES.0000255690.03436.ae
- Aleksandrova, K. et al. 2017. Physical activity, mediating factors and risk of colon cancer: insights into adiposity and circulating biomarkers from the EPIC cohort. *Int J Epidemiol* 46(6), pp. 1823-1835. doi: 10.1093/ije/dyx174
- Altobelli, E. et al. 2019. Differences in colorectal cancer surveillance epidemiology and screening in the WHO European Region. *Oncol Lett* 17(2), pp. 2531-2542. doi: 10.3892/ol.2018.9851
- Ansari, D. et al. 2016. Pancreatic cancer: yesterday, today and tomorrow. *Future Oncol* 12(16), pp. 1929-1946. doi: 10.2217/fon-2016-0010
- Astler, V. B. and Coller, F. A. 1954. The prognostic significance of direct extension of carcinoma of the colon and rectum. *Ann Surg* 139(6), pp. 846-852. doi: 10.1097/00000658-195406000-00015
- Azzouz, L. L. and Sharma, S. 2020. Physiology, Large Intestine. *StatPearls*. Treasure Island (FL).

- Bardi, G. et al. 2004. Tumor karyotype predicts clinical outcome in colorectal cancer patients. *J Clin Oncol* 22(13), pp. 2623-2634. doi: 10.1200/JCO.2004.11.014
- Barresi, V. et al. 2015. Histological grading in colorectal cancer: new insights and perspectives. *Histol Histopathol* 30(9), pp. 1059-1067. doi: 10.14670/HH-11-633
- Beauchemin, N. and Huot, J. 2010. *Metastasis of colorectal cancer*. Dordrecht ; New York: Springer.
- Beerling, E. et al. 2016. Plasticity between Epithelial and Mesenchymal States Unlinks EMT from Metastasis-Enhancing Stem Cell Capacity. *Cell Rep* 14(10), pp. 2281-2288. doi: 10.1016/j.celrep.2016.02.034
- Biller, L. H. and Schrag, D. 2021. Diagnosis and Treatment of Metastatic Colorectal Cancer: A Review. *JAMA* 325(7), pp. 669-685. doi: 10.1001/jama.2021.0106
- Bosman, F. T. et al. 2010. *WHO classification of tumours of the digestive system*. World Health Organization.
- Brocardo, M. and Henderson, B. R. 2008. APC shuttling to the membrane, nucleus and beyond. *Trends Cell Biol* 18(12), pp. 587-596. doi: 10.1016/j.tcb.2008.09.002
- Brown, K. F. et al. 2018. The fraction of cancer attributable to modifiable risk factors in England, Wales, Scotland, Northern Ireland, and the United Kingdom in 2015. *Br J Cancer* 118(8), pp. 1130-1141. doi: 10.1038/s41416-018-0029-6
- Bruser, L. and Bogdan, S. 2017. Adherens Junctions on the Move-Membrane Trafficking of E-Cadherin. *Cold Spring Harb Perspect Biol* 9(3), doi: 10.1101/cshperspect.a029140
- Burn, J. et al. 2011. Long-term effect of aspirin on cancer risk in carriers of hereditary colorectal cancer: an analysis from the CAPP2 randomised controlled trial. *Lancet* 378(9809), pp. 2081-2087. doi: 10.1016/S0140-6736(11)61049-0
- Butterworth, A. S. et al. 2006. Relative and absolute risk of colorectal cancer for individuals with a family history: a meta-analysis. *Eur J Cancer* 42(2), pp. 216-227. doi: 10.1016/j.ejca.2005.09.023
- Campanella, C. et al. 2015. Heat shock protein 60 levels in tissue and circulating exosomes in human large bowel cancer before and after ablative surgery. *Cancer* 121(18), pp. 3230-3239. doi: 10.1002/cncr.29499
- Cao, H. et al. 2015. Epithelial-mesenchymal transition in colorectal cancer metastasis: A system review. *Pathol Res Pract* 211(8), pp. 557-569. doi: 10.1016/j.prp.2015.05.010
- Cao, J. and Schnittler, H. 2019. Putting VE-cadherin into JAIL for junction remodeling. *J Cell Sci* 132(1), doi: 10.1242/jcs.222893
- Cappello, F. et al. 2003. 60KDa chaperonin (HSP60) is over-expressed during colorectal carcinogenesis. *Eur J Histochem* 47(2), pp. 105-110. doi: 10.4081/814

- Cappello, F. et al. 2011. Hsp60: molecular anatomy and role in colorectal cancer diagnosis and treatment. *Front Biosci (Schol Ed)* 3, pp. 341-351. doi: 10.2741/s155
- Cardel, M. et al. 2014. Long-term use of metformin and colorectal cancer risk in type II diabetics: a population-based case-control study. *Cancer Med* 3(5), pp. 1458-1466. doi: 10.1002/cam4.306
- Carethers, J. M. and Jung, B. H. 2015. Genetics and Genetic Biomarkers in Sporadic Colorectal Cancer. *Gastroenterology* 149(5), pp. 1177-1190 e1173. doi: 10.1053/j.gastro.2015.06.047
- Caruso Bavisotto, C. et al. 2020. Hsp60 Post-translational Modifications: Functional and Pathological Consequences. *Front Mol Biosci* 7, p. 95. doi: 10.3389/fmolb.2020.00095
- Castellsague, E. et al. 2008. Detection of APC gene deletions using quantitative multiplex PCR of short fluorescent fragments. *Clin Chem* 54(7), pp. 1132-1140. doi: 10.1373/clinchem.2007.101006
- Chandrashekar, D. S. et al. 2017. UALCAN: A Portal for Facilitating Tumor Subgroup Gene Expression and Survival Analyses. *Neoplasia* 19(8), pp. 649-658. doi: 10.1016/j.neo.2017.05.002
- Chang, D. D. et al. 1998. Characterization of transformation related genes in oral cancer cells. *Oncogene* 16(15), pp. 1921-1930. doi: 10.1038/sj.onc.1201715
- Chen, J. et al. 2014. BRAF V600E mutation and KRAS codon 13 mutations predict poor survival in Chinese colorectal cancer patients. *BMC Cancer* 14, p. 802. doi: 10.1186/1471-2407-14-802
- Chen, N. P. et al. 2017. Human phosphatase CDC14A regulates actin organization through dephosphorylation of epithelial protein lost in neoplasm. *Proc Natl Acad Sci U S A* 114(20), pp. 5201-5206. doi: 10.1073/pnas.1619356114
- Chen, S. et al. 2000. Characterization of the human EPLIN (Epithelial Protein Lost in Neoplasm) gene reveals distinct promoters for the two EPLIN isoforms. *Gene* 248(1-2), pp. 69-76. doi: 10.1016/s0378-1119(00)00144-x
- Cheng, J. et al. 2015. Meta-analysis of prospective cohort studies of cigarette smoking and the incidence of colon and rectal cancers. *Eur J Cancer Prev* 24(1), pp. 6-15. doi: 10.1097/CEJ.0000000000000011
- Chervin-Petinot, A. et al. 2012. Epithelial protein lost in neoplasm (EPLIN) interacts with alpha-catenin and actin filaments in endothelial cells and stabilizes vascular capillary network in vitro. *J Biol Chem* 287(10), pp. 7556-7572. doi: 10.1074/jbc.M111.328682
- Chircop, M. et al. 2009. The actin-binding and bundling protein, EPLIN, is required for cytokinesis. *Cell Cycle* 8(5), pp. 757-764. doi: 10.4161/cc.8.5.7878
- Choi, Y. J. et al. 2018. Light Alcohol Drinking and Risk of Cancer: A Meta-Analysis of Cohort Studies. *Cancer Res Treat* 50(2), pp. 474-487. doi: 10.4143/crt.2017.094

Clark, J. et al. 2003. Phase-II trial of 5-fluorouracil (5-FU), leucovorin (LV), oxaliplatin (Ox), and trastuzumab (T) for patients with metastatic colorectal cancer (CRC) refractory to initial therapy: 3584. *Onkologie* 26,

Collins, R. J. et al. 2015. EPLIN: a fundamental actin regulator in cancer metastasis? *Cancer Metastasis Rev* 34(4), pp. 753-764. doi: 10.1007/s10555-015-9595-8

Collins, R. J. et al. 2018. Mechanistic insights of epithelial protein lost in neoplasm in prostate cancer metastasis. *Int J Cancer* 143(10), pp. 2537-2550. doi: 10.1002/ijc.31786

Collisson, E. A. et al. 2019. Molecular subtypes of pancreatic cancer. *Nat Rev Gastroenterol Hepatol* 16(4), pp. 207-220. doi: 10.1038/s41575-019-0109-y

Conteduca, V. et al. 2013. Precancerous colorectal lesions (Review). *Int J Oncol* 43(4), pp. 973-984. doi: 10.3892/ijo.2013.2041

Cunningham, C. et al. 2017. Association of Coloproctology of Great Britain & Ireland (ACPGBI): Guidelines for the Management of Cancer of the Colon, Rectum and Anus (2017) - Diagnosis, Investigations and Screening. *Colorectal Dis* 19 Suppl 1, pp. 9-17. doi: 10.1111/codi.13703

Dariya, B. et al. 2020. Colorectal Cancer Biology, Diagnosis, and Therapeutic Approaches. *Crit Rev Oncog* 25(2), pp. 71-94. doi: 10.1615/CritRevOncog.2020035067

Day, F. et al. 2015. A mutant BRAF V600E-specific immunohistochemical assay: correlation with molecular mutation status and clinical outcome in colorectal cancer. *Target Oncol* 10(1), pp. 99-109. doi: 10.1007/s11523-014-0319-8

de Cuba, E. M. et al. 2012. Understanding molecular mechanisms in peritoneal dissemination of colorectal cancer : future possibilities for personalised treatment by use of biomarkers. *Virchows Arch* 461(3), pp. 231-243. doi: 10.1007/s00428-012-1287-y

De Sousa, E. M. F. et al. 2013. Poor-prognosis colon cancer is defined by a molecularly distinct subtype and develops from serrated precursor lesions. *Nat Med* 19(5), pp. 614-618. doi: 10.1038/nm.3174

Deakin, N. O. and Turner, C. E. 2014. Paxillin inhibits HDAC6 to regulate microtubule acetylation, Golgi structure, and polarized migration. *J Cell Biol* 206(3), pp. 395-413. doi: 10.1083/jcb.201403039

Dimova, I. et al. 2014. Angiogenesis in cancer - general pathways and their therapeutic implications. *J BUON* 19(1), pp. 15-21.

Dukes, C. E. 1932. The classification of cancer of the rectum. *The Journal of Pathology and Bacteriology* 35(3), pp. 323-332. doi: <https://doi.org/10.1002/path.1700350303>

Eckert, D. et al. 2005. The AP-2 family of transcription factors. *Genome Biol* 6(13), p. 246. doi: 10.1186/gb-2005-6-13-246

- Eklof, V. et al. 2013. The prognostic role of KRAS, BRAF, PIK3CA and PTEN in colorectal cancer. *Br J Cancer* 108(10), pp. 2153-2163. doi: 10.1038/bjc.2013.212
- El-Deiry, W. S. et al. 2015. Molecular profiling of 6,892 colorectal cancer samples suggests different possible treatment options specific to metastatic sites. *Cancer Biol Ther* 16(12), pp. 1726-1737. doi: 10.1080/15384047.2015.1113356
- Espinosa, M. et al. 2005. Oxaliplatin activity in head and neck cancer cell lines. *Cancer Chemother Pharmacol* 55(3), pp. 301-305. doi: 10.1007/s00280-004-0847-5
- Evans, M. K. et al. 2018. XIAP Regulation by MNK Links MAPK and NFkappaB Signaling to Determine an Aggressive Breast Cancer Phenotype. *Cancer Res* 78(7), pp. 1726-1738. doi: 10.1158/0008-5472.CAN-17-1667
- Fabregat, A. et al. 2018. Reactome diagram viewer: data structures and strategies to boost performance. *Bioinformatics* 34(7), pp. 1208-1214. doi: 10.1093/bioinformatics/btx752
- Fearon, E. R. and Vogelstein, B. 1990. A genetic model for colorectal tumorigenesis. *Cell* 61(5), pp. 759-767. doi: 10.1016/0092-8674(90)90186-i
- Fedirko, V. et al. 2011. Alcohol drinking and colorectal cancer risk: an overall and dose-response meta-analysis of published studies. *Ann Oncol* 22(9), pp. 1958-1972. doi: 10.1093/annonc/mdq653
- Fekete, J. T. and Gyorffy, B. 2019. ROCplot.org: Validating predictive biomarkers of chemotherapy/hormonal therapy/anti-HER2 therapy using transcriptomic data of 3,104 breast cancer patients. *Int J Cancer* 145(11), pp. 3140-3151. doi: 10.1002/ijc.32369
- Feng, X. et al. 2017. The role of NLRP3 inflammasome in 5-fluorouracil resistance of oral squamous cell carcinoma. *J Exp Clin Cancer Res* 36(1), p. 81. doi: 10.1186/s13046-017-0553-x
- Fleming, M. et al. 2012. Colorectal carcinoma: Pathologic aspects. *J Gastrointest Oncol* 3(3), pp. 153-173. doi: 10.3978/j.issn.2078-6891.2012.030
- Gala, M. and Chung, D. C. 2011. Hereditary colon cancer syndromes. *Semin Oncol* 38(4), pp. 490-499. doi: 10.1053/j.seminoncol.2011.05.003
- Ganesh, K. et al. 2019. Immunotherapy in colorectal cancer: rationale, challenges and potential. *Nat Rev Gastroenterol Hepatol* 16(6), pp. 361-375. doi: 10.1038/s41575-019-0126-x
- Ghurburrun, E. et al. 2018. Liver and Pancreas: Do Similar Embryonic Development and Tissue Organization Lead to Similar Mechanisms of Tumorigenesis? *Gene Expr* 18(3), pp. 149-155. doi: 10.3727/105221618X15216414278706
- Goncalves, J. et al. 2020. LUZP1 and the tumor suppressor EPLIN modulate actin stability to restrict primary cilia formation. *J Cell Biol* 219(7), doi: 10.1083/jcb.201908132

- Gong, W. et al. 2021. EPLIN Expression in Gastric Cancer and Impact on Prognosis and Chemoresistance. *Biomolecules* 11(4), doi: 10.3390/biom11040547
- Gong, W. Z., J.; Ji, J.; Jia, Y.; Jia, S.; Sanders, A.J.; Jiang, W.G. 2021. EPLIN Expression in Gastric Cancer and Impact on Prognosis and Chemoresistance. *Biomolecules* 11(4),547, doi: <https://doi.org/10.3390/biom11040547>
- Goral, V. 2015. Pancreatic Cancer: Pathogenesis and Diagnosis. *Asian Pac J Cancer Prev* 16(14), pp. 5619-5624. doi: 10.7314/apjcp.2015.16.14.5619
- Grant, T. J. et al. 2016. Molecular Pathogenesis of Pancreatic Cancer. *Prog Mol Biol Transl Sci* 144, pp. 241-275. doi: 10.1016/bs.pmbts.2016.09.008
- Greally, M. et al. 2018. HER2: An emerging target in colorectal cancer. *Curr Probl Cancer* 42(6), pp. 560-571. doi: 10.1016/j.currprobcancer.2018.07.001
- Guo, Z. et al. 2018. Beta-elemene increases chemosensitivity to 5-fluorouracil through down-regulating microRNA-191 expression in colorectal carcinoma cells. *J Cell Biochem* 119(8), pp. 7032-7039. doi: 10.1002/jcb.26914
- Gupta, G. D. et al. 2015. A Dynamic Protein Interaction Landscape of the Human Centrosome-Cilium Interface. *Cell* 163(6), pp. 1484-1499. doi: 10.1016/j.cell.2015.10.065
- Gupta, R. S. 1995. Evolution of the chaperonin families (Hsp60, Hsp10 and Tcp-1) of proteins and the origin of eukaryotic cells. *Mol Microbiol* 15(1), pp. 1-11. doi: 10.1111/j.1365-2958.1995.tb02216.x
- Half, E. et al. 2009. Familial adenomatous polyposis. *Orphanet J Rare Dis* 4, p. 22. doi: 10.1186/1750-1172-4-22
- Han, M. Y. et al. 2007. Extracellular signal-regulated kinase/mitogen-activated protein kinase regulates actin organization and cell motility by phosphorylating the actin cross-linking protein EPLIN. *Mol Cell Biol* 27(23), pp. 8190-8204. doi: 10.1128/MCB.00661-07
- Hankey, W. et al. 2018. Functions of the APC tumor suppressor protein dependent and independent of canonical WNT signaling: implications for therapeutic targeting. *Cancer Metastasis Rev* 37(1), pp. 159-172. doi: 10.1007/s10555-017-9725-6
- Harada, S. and Morlote, D. 2020. Molecular Pathology of Colorectal Cancer. *Adv Anat Pathol* 27(1), pp. 20-26. doi: 10.1097/PAP.0000000000000247
- Harbour, J. W. et al. 1999. Cdk phosphorylation triggers sequential intramolecular interactions that progressively block Rb functions as cells move through G1. *Cell* 98(6), pp. 859-869. doi: 10.1016/s0092-8674(00)81519-6
- Hassan, C. et al. 2014. Systematic review with meta-analysis: the incidence of advanced neoplasia after polypectomy in patients with and without low-risk adenomas. *Aliment Pharmacol Ther* 39(9), pp. 905-912. doi: 10.1111/apt.12682

He, Y. et al. 2007. Proteomics-based identification of HSP60 as a tumor-associated antigen in colorectal cancer. *Proteomics Clin Appl* 1(3), pp. 336-342. doi: 10.1002/prca.200600718

Hirsh, V. 2018. Turning EGFR mutation-positive non-small-cell lung cancer into a chronic disease: optimal sequential therapy with EGFR tyrosine kinase inhibitors. *Ther Adv Med Oncol* 10, p. 1758834017753338. doi: 10.1177/1758834017753338

Hofer, I. et al. 2018. Advanced Methods for the Investigation of Cell Contact Dynamics in Endothelial Cells Using Fluorescence-Based Live Cell Imaging. *J Vasc Res* 55(6), pp. 350-364. doi: 10.1159/000494933

Holscher, H. D. 2017. Dietary fiber and prebiotics and the gastrointestinal microbiota. *Gut Microbes* 8(2), pp. 172-184. doi: 10.1080/19490976.2017.1290756

Hong, Y. et al. 2007. A susceptibility gene set for early onset colorectal cancer that integrates diverse signaling pathways: implication for tumorigenesis. *Clin Cancer Res* 13(4), pp. 1107-1114. doi: 10.1158/1078-0432.CCR-06-1633

Huang, C. et al. 2004. MAP kinases and cell migration. *J Cell Sci* 117(Pt 20), pp. 4619-4628. doi: 10.1242/jcs.01481

Huang, D. et al. 2018. Mutations of key driver genes in colorectal cancer progression and metastasis. *Cancer Metastasis Rev* 37(1), pp. 173-187. doi: 10.1007/s10555-017-9726-5

Hung, C. H. et al. 2015. Docetaxel Facilitates Endothelial Dysfunction through Oxidative Stress via Modulation of Protein Kinase C Beta: The Protective Effects of Sotrastaurin. *Toxicol Sci* 145(1), pp. 59-67. doi: 10.1093/toxsci/kfv017

Hurwitz, H. et al. 2016. Targeted therapy for gastrointestinal (GI) tumors based on molecular profiles: Early results from MyPathway, an open-label phase IIa basket study in patients with advanced solid tumors. *Journal of Clinical Oncology* 34(4_suppl), pp. 653-653. doi: 10.1200/jco.2016.34.4_suppl.653

Huxley, R. R. et al. 2009. The impact of dietary and lifestyle risk factors on risk of colorectal cancer: a quantitative overview of the epidemiological evidence. *Int J Cancer* 125(1), pp. 171-180. doi: 10.1002/ijc.24343

InternationalAgencyforResearchonCancer. 2020. *IARC MONOGRAPHS ON THE IDENTIFICATION OF CARCINOGENIC HAZARDS TO HUMANS*. International Agency for Research on Cancer: Available at: <https://monographs.iarc.fr/agents-classified-by-the-iarc/>

Ionov, Y. et al. 1993. Ubiquitous somatic mutations in simple repeated sequences reveal a new mechanism for colonic carcinogenesis. *Nature* 363(6429), pp. 558-561. doi: 10.1038/363558a0

Isakoff, S. J. and Baselga, J. 2011. Trastuzumab-DM1: building a chemotherapy-free road in the treatment of human epidermal growth factor receptor 2-positive breast cancer. *J Clin Oncol* 29(4), pp. 351-354. doi: 10.1200/JCO.2010.31.6679

- Itzkowitz, S. H. and Yio, X. 2004. Inflammation and cancer IV. Colorectal cancer in inflammatory bowel disease: the role of inflammation. *Am J Physiol Gastrointest Liver Physiol* 287(1), pp. G7-17. doi: 10.1152/ajpgi.00079.2004
- Janeway CA Jr et al. 2001. The structure of a typical antibody molecule. *immunobiology: The Immune System in Health and Disease. 5th edition*. New York: Garland Science.
- Jasperson, K. W. et al. 2010. Hereditary and familial colon cancer. *Gastroenterology* 138(6), pp. 2044-2058. doi: 10.1053/j.gastro.2010.01.054
- Jassal, B. et al. 2020. The reactome pathway knowledgebase. *Nucleic Acids Res* 48(D1), pp. D498-D503. doi: 10.1093/nar/gkz1031
- Jeong, W. J. et al. 2018. Interaction between Wnt/beta-catenin and RAS-ERK pathways and an anti-cancer strategy via degradations of beta-catenin and RAS by targeting the Wnt/beta-catenin pathway. *NPJ Precis Oncol* 2(1), p. 5. doi: 10.1038/s41698-018-0049-y
- Jiang, W. G. et al. 2008. Eplin-alpha expression in human breast cancer, the impact on cellular migration and clinical outcome. *Mol Cancer* 7, p. 71. doi: 10.1186/1476-4598-7-71
- Jiang, Y. et al. 2011. Diabetes mellitus and incidence and mortality of colorectal cancer: a systematic review and meta-analysis of cohort studies. *Eur J Epidemiol* 26(11), pp. 863-876. doi: 10.1007/s10654-011-9617-y
- Ju, H. Q. et al. 2020. NADPH homeostasis in cancer: functions, mechanisms and therapeutic implications. *Signal Transduct Target Ther* 5(1), p. 231. doi: 10.1038/s41392-020-00326-0
- Kadeer, A. et al. 2017. Plectin is a novel regulator for apical extrusion of RasV12-transformed cells. *Sci Rep* 7, p. 44328. doi: 10.1038/srep44328
- Kadmas, J. L. and Beckerle, M. C. 2004. The LIM domain: from the cytoskeleton to the nucleus. *Nat Rev Mol Cell Biol* 5(11), pp. 920-931. doi: 10.1038/nrm1499
- Kajita, M. et al. 2014. Filamin acts as a key regulator in epithelial defence against transformed cells. *Nat Commun* 5, p. 4428. doi: 10.1038/ncomms5428
- Karagiannis, G. S. et al. 2012. Cancer-associated fibroblasts drive the progression of metastasis through both paracrine and mechanical pressure on cancer tissue. *Mol Cancer Res* 10(11), pp. 1403-1418. doi: 10.1158/1541-7786.MCR-12-0307
- Kasai, N. et al. 2018. The paxillin-plectin-EPLIN complex promotes apical elimination of RasV12-transformed cells by modulating HDAC6-regulated tubulin acetylation. *Sci Rep* 8(1), p. 2097. doi: 10.1038/s41598-018-20146-1
- Kasprzak, A. 2021. The Role of Tumor Microenvironment Cells in Colorectal Cancer (CRC) Cachexia. *Int J Mol Sci* 22(4), doi: 10.3390/ijms22041565
- Kavuri, S. M. et al. 2015. HER2 activating mutations are targets for colorectal cancer treatment. *Cancer Discov* 5(8), pp. 832-841. doi: 10.1158/2159-8290.CD-14-1211

- Kedrin, D. and Gala, M. K. 2015. Genetics of the serrated pathway to colorectal cancer. *Clin Transl Gastroenterol* 6, p. e84. doi: 10.1038/ctg.2015.12
- Keum, N. and Giovannucci, E. 2019. Global burden of colorectal cancer: emerging trends, risk factors and prevention strategies. *Nat Rev Gastroenterol Hepatol* 16(12), pp. 713-732. doi: 10.1038/s41575-019-0189-8
- Khamas, A. et al. 2012. Screening for epigenetically masked genes in colorectal cancer Using 5-Aza-2'-deoxycytidine, microarray and gene expression profile. *Cancer Genomics Proteomics* 9(2), pp. 67-75.
- Kinoshita, M. 2003. The septins. *Genome Biol* 4(11), p. 236. doi: 10.1186/gb-2003-4-11-236
- Klaver, Y. L. et al. 2012. Peritoneal carcinomatosis of colorectal origin: Incidence, prognosis and treatment options. *World J Gastroenterol* 18(39), pp. 5489-5494. doi: 10.3748/wjg.v18.i39.5489
- Klein, A. P. 2013. Identifying people at a high risk of developing pancreatic cancer. *Nat Rev Cancer* 13(1), pp. 66-74. doi: 10.1038/nrc3420
- Kobiela, J. et al. 2018. Ablative stereotactic radiotherapy for oligometastatic colorectal cancer: Systematic review. *Crit Rev Oncol Hematol* 129, pp. 91-101. doi: 10.1016/j.critrevonc.2018.06.005
- Kojima, M. et al. 2014. Human subperitoneal fibroblast and cancer cell interaction creates microenvironment that enhances tumor progression and metastasis. *PLoS One* 9(2), p. e88018. doi: 10.1371/journal.pone.0088018
- Koveitypour, Z. et al. 2019. Signaling pathways involved in colorectal cancer progression. *Cell Biosci* 9, p. 97. doi: 10.1186/s13578-019-0361-4
- Kramer, H. U. et al. 2012. Type 2 diabetes mellitus and colorectal cancer: meta-analysis on sex-specific differences. *Eur J Cancer* 48(9), pp. 1269-1282. doi: 10.1016/j.ejca.2011.07.010
- Kyrgiou, M. et al. 2017. Adiposity and cancer at major anatomical sites: umbrella review of the literature. *BMJ* 356, p. j477. doi: 10.1136/bmj.j477
- Lakatos, P. L. and Lakatos, L. 2012. Challenges in calculating the risk for colorectal cancer in patients with ulcerative colitis. *Clin Gastroenterol Hepatol* 10(10), pp. 1179; author reply 1179-1180. doi: 10.1016/j.cgh.2012.04.021
- Lambert, A. W. et al. 2017. Emerging Biological Principles of Metastasis. *Cell* 168(4), pp. 670-691. doi: 10.1016/j.cell.2016.11.037
- Langman, G. et al. 2017. Association of Coloproctology of Great Britain & Ireland (ACPGBI): Guidelines for the Management of Cancer of the Colon, Rectum and Anus (2017) - Pathology Standards and Datasets. *Colorectal Dis* 19 Suppl 1, pp. 74-81. doi: 10.1111/codi.13708

- Larsson, S. C. et al. 2005. Diabetes mellitus and risk of colorectal cancer: a meta-analysis. *J Natl Cancer Inst* 97(22), pp. 1679-1687. doi: 10.1093/jnci/dji375
- Lauby-Secretan, B. et al. 2016. Body Fatness and Cancer--Viewpoint of the IARC Working Group. *N Engl J Med* 375(8), pp. 794-798. doi: 10.1056/NEJMSr1606602
- Lee, S. et al. 2006. Differential expression in normal-adenoma-carcinoma sequence suggests complex molecular carcinogenesis in colon. *Oncol Rep* 16(4), pp. 747-754.
- Lee, Y. S. et al. 2012. Oncologic Outcomes of Stage IIIA Colon Cancer for Different Chemotherapeutic Regimens. *J Korean Soc Coloproctol* 28(5), pp. 259-264. doi: 10.3393/jksc.2012.28.5.259
- Lemoine, L. et al. 2016. Pathophysiology of colorectal peritoneal carcinomatosis: Role of the peritoneum. *World J Gastroenterol* 22(34), pp. 7692-7707. doi: 10.3748/wjg.v22.i34.7692
- Levin, B. et al. 2008. Screening and surveillance for the early detection of colorectal cancer and adenomatous polyps, 2008: a joint guideline from the American Cancer Society, the US Multi-Society Task Force on Colorectal Cancer, and the American College of Radiology. *Gastroenterology* 134(5), pp. 1570-1595. doi: 10.1053/j.gastro.2008.02.002
- Lew, D. J. et al. 1991. Isolation of three novel human cyclins by rescue of G1 cyclin (Cln) function in yeast. *Cell* 66(6), pp. 1197-1206. doi: 10.1016/0092-8674(91)90042-w
- Li, D. et al. 2004. Pancreatic cancer. *Lancet* 363(9414), pp. 1049-1057. doi: 10.1016/S0140-6736(04)15841-8
- Li, J. C. and Zeng, Y. S. 2018. *Histology and Embryology*. China: People's Medical Publishing House Co., LTD.
- Li, W. et al. 2015a. Colorectal carcinomas with KRAS codon 12 mutation are associated with more advanced tumor stages. *BMC Cancer* 15, p. 340. doi: 10.1186/s12885-015-1345-3
- Li, X. L. et al. 2015b. P53 mutations in colorectal cancer - molecular pathogenesis and pharmacological reactivation. *World J Gastroenterol* 21(1), pp. 84-93. doi: 10.3748/wjg.v21.i1.84
- Liang, L. et al. 2017. MiR-93-5p enhances growth and angiogenesis capacity of HUVECs by down-regulating EPLIN. *Oncotarget* 8(63), pp. 107033-107043. doi: 10.18632/oncotarget.22300
- Liang, P. S. et al. 2009. Cigarette smoking and colorectal cancer incidence and mortality: systematic review and meta-analysis. *Int J Cancer* 124(10), pp. 2406-2415. doi: 10.1002/ijc.24191
- Liu, F. et al. 2020. LncRNA NEAT1 knockdown attenuates autophagy to elevate 5-FU sensitivity in colorectal cancer via targeting miR-34a. *Cancer Med* 9(3), pp. 1079-1091. doi: 10.1002/cam4.2746

- Liu, H. et al. 2007. Nucleophosmin acts as a novel AP2alpha-binding transcriptional corepressor during cell differentiation. *EMBO Rep* 8(4), pp. 394-400. doi: 10.1038/sj.embor.7400909
- Liu, R. et al. 2016. Epithelial protein lost in neoplasm-alpha (EPLIN-alpha) is a potential prognostic marker for the progression of epithelial ovarian cancer. *Int J Oncol* 48(6), pp. 2488-2496. doi: 10.3892/ijo.2016.3462
- Liu, T. et al. 2019. Exosome-transmitted miR-128-3p increase chemosensitivity of oxaliplatin-resistant colorectal cancer. *Mol Cancer* 18(1), p. 43. doi: 10.1186/s12943-019-0981-7
- Liu, Y. et al. 2012a. EPLIN-alpha expression in human oesophageal cancer and its impact on cellular aggressiveness and clinical outcome. *Anticancer Res* 32(4), pp. 1283-1289.
- Liu, Y. et al. 2012b. Expression Profile of Epithelial Protein Lost in Neoplasm-Alpha (EPLIN- α) in Human Pulmonary Cancer and Its Impact on SKMES-1 Cells in Vitro. *Journal of Cancer Therapy* 3, pp. 452-459.
- Lodish H, B. A., Zipursky SL. 2000. The Actin Cytoskeleton. *Molecular Cell Biology*. 4th edition. New York: W. H. Freeman.
- Longley, D. B. et al. 2003. 5-fluorouracil: mechanisms of action and clinical strategies. *Nat Rev Cancer* 3(5), pp. 330-338. doi: 10.1038/nrc1074
- Luo, W. et al. 2012. Diabetes mellitus and the incidence and mortality of colorectal cancer: a meta-analysis of 24 cohort studies. *Colorectal Dis* 14(11), pp. 1307-1312. doi: 10.1111/j.1463-1318.2012.02875.x
- Lutgens, M. W. et al. 2013. Declining risk of colorectal cancer in inflammatory bowel disease: an updated meta-analysis of population-based cohort studies. *Inflamm Bowel Dis* 19(4), pp. 789-799. doi: 10.1097/MIB.0b013e31828029c0
- Lynch, H. T. and Lynch, J. F. 2004. Lynch syndrome: history and current status. *Dis Markers* 20(4-5), pp. 181-198. doi: 10.1155/2004/460240
- Ma, P. C. et al. 2003. c-Met: structure, functions and potential for therapeutic inhibition. *Cancer Metastasis Rev* 22(4), pp. 309-325. doi: 10.1023/a:1023768811842
- Ma, W. et al. 2022. Overexpression of LIMA1 Indicates Poor Prognosis and Promotes Epithelial-Mesenchymal Transition in Head and Neck Squamous Cell Carcinoma. *Clin Med Insights Oncol* 16, p. 11795549221109493. doi: 10.1177/11795549221109493
- Ma, Y. et al. 2013. Obesity and risk of colorectal cancer: a systematic review of prospective studies. *PLoS One* 8(1), p. e53916. doi: 10.1371/journal.pone.0053916
- Maishi, N. and Hida, K. 2017. Tumor endothelial cells accelerate tumor metastasis. *Cancer Sci* 108(10), pp. 1921-1926. doi: 10.1111/cas.13336

- Marant-Micallef, C. et al. 2019. The risk of cancer attributable to diagnostic medical radiation: Estimation for France in 2015. *Int J Cancer* 144(12), pp. 2954-2963. doi: 10.1002/ijc.32048
- Marisa, L. et al. 2013. Gene expression classification of colon cancer into molecular subtypes: characterization, validation, and prognostic value. *PLoS Med* 10(5), p. e1001453. doi: 10.1371/journal.pmed.1001453
- Marmol, I. et al. 2017. Colorectal Carcinoma: A General Overview and Future Perspectives in Colorectal Cancer. *Int J Mol Sci* 18(1), doi: 10.3390/ijms18010197
- Martinez, M. E. et al. 2009. A pooled analysis of advanced colorectal neoplasia diagnoses after colonoscopic polypectomy. *Gastroenterology* 136(3), pp. 832-841. doi: 10.1053/j.gastro.2008.12.007
- Maul, R. S. and Chang, D. D. 1999. EPLIN, epithelial protein lost in neoplasm. *Oncogene* 18(54), pp. 7838-7841. doi: 10.1038/sj.onc.1203206
- Maul, R. S. et al. 2001. Characterization of mouse epithelial protein lost in neoplasm (EPLIN) and comparison of mammalian and zebrafish EPLIN. *Gene* 262(1-2), pp. 155-160. doi: 10.1016/s0378-1119(00)00540-0
- Maul, R. S. et al. 2003. EPLIN regulates actin dynamics by cross-linking and stabilizing filaments. *J Cell Biol* 160(3), pp. 399-407. doi: 10.1083/jcb.200212057
- Maupin, P. and Pollard, T. D. 1986. Arrangement of actin filaments and myosin-like filaments in the contractile ring and of actin-like filaments in the mitotic spindle of dividing HeLa cells. *J Ultrastruct Mol Struct Res* 94(1), pp. 92-103. doi: 10.1016/0889-1605(86)90055-8
- Meric-Bernstam, F. et al. 2019. Pertuzumab plus trastuzumab for HER2-amplified metastatic colorectal cancer (MyPathway): an updated report from a multicentre, open-label, phase 2a, multiple basket study. *Lancet Oncol* 20(4), pp. 518-530. doi: 10.1016/S1470-2045(18)30904-5
- Mikula-Pietrasik, J. et al. 2018. The peritoneal "soil" for a cancerous "seed": a comprehensive review of the pathogenesis of intraperitoneal cancer metastases. *Cell Mol Life Sci* 75(3), pp. 509-525. doi: 10.1007/s00018-017-2663-1
- Missiaglia, E. et al. 2014. Distal and proximal colon cancers differ in terms of molecular, pathological, and clinical features. *Ann Oncol* 25(10), pp. 1995-2001. doi: 10.1093/annonc/mdu275
- Mitchison, H. M. and Valente, E. M. 2017. Motile and non-motile cilia in human pathology: from function to phenotypes. *J Pathol* 241(2), pp. 294-309. doi: 10.1002/path.4843
- Mittal, V. 2018. Epithelial Mesenchymal Transition in Tumor Metastasis. *Annu Rev Pathol* 13, pp. 395-412. doi: 10.1146/annurev-pathol-020117-043854
- Moosavi, L. and Polineni, R. 2022. Afatinib. *StatPearls*. Treasure Island (FL).

Nagy, A. et al. 2021. Pancancer survival analysis of cancer hallmark genes. *Sci Rep* 11(1), p. 6047. doi: 10.1038/s41598-021-84787-5

NationalCancerInstitute. 2022. Colon Cancer Treatment (PDQ(R)): Patient Version. In: Institute, N.C. ed. *PDQ Cancer Information Summaries*. Bethesda (MD): National Cancer Institute.

Nojadeh, J. N. et al. 2018. Microsatellite instability in colorectal cancer. *EXCLI J* 17, pp. 159-168. doi: 10.17179/excli2017-948

Novellademunt, L. et al. 2015. Targeting Wnt signaling in colorectal cancer. A Review in the Theme: Cell Signaling: Proteins, Pathways and Mechanisms. *Am J Physiol Cell Physiol* 309(8), pp. C511-521. doi: 10.1152/ajpcell.00117.2015

Oh, D. Y. and Bang, Y. J. 2020. HER2-targeted therapies - a role beyond breast cancer. *Nat Rev Clin Oncol* 17(1), pp. 33-48. doi: 10.1038/s41571-019-0268-3

Ohashi, T. et al. 2017. p53 mediates the suppression of cancer cell invasion by inducing LIMA1/EPLIN. *Cancer Lett* 390, pp. 58-66. doi: 10.1016/j.canlet.2016.12.034

Ohoka, A. et al. 2015. EPLIN is a crucial regulator for extrusion of RasV12-transformed cells. *J Cell Sci* 128(4), pp. 781-789. doi: 10.1242/jcs.163113

Osako, T. et al. 1998. Immunohistochemical study of c-erbB-2 protein in colorectal cancer and the correlation with patient survival. *Oncology* 55(6), pp. 548-555. doi: 10.1159/000011911

Papadatos-Pastos, D. et al. 2015. The role of the PI3K pathway in colorectal cancer. *Crit Rev Oncol Hematol* 94(1), pp. 18-30. doi: 10.1016/j.critrevonc.2014.12.006

Patil, A. and Zhang, L. 2022. *Anatomy & histology*. PathologyOutlines.com Available at: <https://www.pathologyoutlines.com/topic/colonhistology.html>. [Accessed: 10].

Pawlik, T. M. et al. 2004. Colorectal carcinogenesis: MSI-H versus MSI-L. *Dis Markers* 20(4-5), pp. 199-206. doi: 10.1155/2004/368680

Pearlman, R. et al. 2017. Prevalence and Spectrum of Germline Cancer Susceptibility Gene Mutations Among Patients With Early-Onset Colorectal Cancer. *JAMA Oncol* 3(4), pp. 464-471. doi: 10.1001/jamaoncol.2016.5194

Petrelli, F. et al. 2018. Stereotactic body radiotherapy for colorectal cancer liver metastases: A systematic review. *Radiother Oncol* 129(3), pp. 427-434. doi: 10.1016/j.radonc.2018.06.035

Pino, M. S. and Chung, D. C. 2010. The chromosomal instability pathway in colon cancer. *Gastroenterology* 138(6), pp. 2059-2072. doi: 10.1053/j.gastro.2009.12.065

Powell, S. M. et al. 1992. APC mutations occur early during colorectal tumorigenesis. *Nature* 359(6392), pp. 235-237. doi: 10.1038/359235a0

- Pretzsch, E. et al. 2019. Mechanisms of Metastasis in Colorectal Cancer and Metastatic Organotropism: Hematogenous versus Peritoneal Spread. *J Oncol* 2019, p. 7407190. doi: 10.1155/2019/7407190
- Qiao, Y. et al. 2018. Associations between aspirin use and the risk of cancers: a meta-analysis of observational studies. *BMC Cancer* 18(1), p. 288. doi: 10.1186/s12885-018-4156-5
- Rajilic-Stojanovic, M. and de Vos, W. M. 2014. The first 1000 cultured species of the human gastrointestinal microbiota. *FEMS Microbiol Rev* 38(5), pp. 996-1047. doi: 10.1111/1574-6976.12075
- Ramanathan, R. K. et al. 2004. Low overexpression of HER-2/neu in advanced colorectal cancer limits the usefulness of trastuzumab (Herceptin) and irinotecan as therapy. A phase II trial. *Cancer Invest* 22(6), pp. 858-865. doi: 10.1081/cnv-200039645
- Rather, G. M. et al. 2021. In cancer, all roads lead to NADPH. *Pharmacol Ther* 226, p. 107864. doi: 10.1016/j.pharmthera.2021.107864
- Rennoll, S. and Yochum, G. 2015. Regulation of MYC gene expression by aberrant Wnt/beta-catenin signaling in colorectal cancer. *World J Biol Chem* 6(4), pp. 290-300. doi: 10.4331/wjbc.v6.i4.290
- Robichaud, N. et al. 2015. Phosphorylation of eIF4E promotes EMT and metastasis via translational control of SNAIL and MMP-3. *Oncogene* 34(16), pp. 2032-2042. doi: 10.1038/onc.2014.146
- Rodriguez-Salas, N. et al. 2017. Clinical relevance of colorectal cancer molecular subtypes. *Crit Rev Oncol Hematol* 109, pp. 9-19. doi: 10.1016/j.critrevonc.2016.11.007
- Roepman, P. et al. 2014. Colorectal cancer intrinsic subtypes predict chemotherapy benefit, deficient mismatch repair and epithelial-to-mesenchymal transition. *Int J Cancer* 134(3), pp. 552-562. doi: 10.1002/ijc.28387
- Roma-Rodrigues, C. et al. 2019. Targeting Tumor Microenvironment for Cancer Therapy. *Int J Mol Sci* 20(4), doi: 10.3390/ijms20040840
- Rombouts, A. J. M. et al. 2018. Does pelvic radiation increase rectal cancer incidence? - A systematic review and meta-analysis. *Cancer Treat Rev* 68, pp. 136-144. doi: 10.1016/j.ctrv.2018.05.008
- Roskoski, R., Jr. 2019. Small molecule inhibitors targeting the EGFR/ErbB family of protein-tyrosine kinases in human cancers. *Pharmacol Res* 139, pp. 395-411. doi: 10.1016/j.phrs.2018.11.014
- Routy, B. et al. 2018. Gut microbiome influences efficacy of PD-1-based immunotherapy against epithelial tumors. *Science* 359(6371), pp. 91-97. doi: 10.1126/science.aan3706
- Ruiz-Casado, A. et al. 2017. Exercise and the Hallmarks of Cancer. *Trends Cancer* 3(6), pp. 423-441. doi: 10.1016/j.trecan.2017.04.007

Sadanandam, A. et al. 2013. A colorectal cancer classification system that associates cellular phenotype and responses to therapy. *Nat Med* 19(5), pp. 619-625. doi: 10.1038/nm.3175

Sadanandam, A. et al. 2014. Reconciliation of classification systems defining molecular subtypes of colorectal cancer: interrelationships and clinical implications. *Cell Cycle* 13(3), pp. 353-357. doi: 10.4161/cc.27769

Saitoh, S. et al. 2017. Rab5-regulated endocytosis plays a crucial role in apical extrusion of transformed cells. *Proc Natl Acad Sci U S A* 114(12), pp. E2327-E2336. doi: 10.1073/pnas.1602349114

Sanders, A. J. et al. 2011. EPLIN is a negative regulator of prostate cancer growth and invasion. *J Urol* 186(1), pp. 295-301. doi: 10.1016/j.juro.2011.03.038

Sanders, A. J. et al. 2010. The impact of EPLINalpha (Epithelial protein lost in neoplasm) on endothelial cells, angiogenesis and tumorigenesis. *Angiogenesis* 13(4), pp. 317-326. doi: 10.1007/s10456-010-9188-7

Sartore-Bianchi, A. et al. 2019. HER2 Positivity Predicts Unresponsiveness to EGFR-Targeted Treatment in Metastatic Colorectal Cancer. *Oncologist* 24(10), pp. 1395-1402. doi: 10.1634/theoncologist.2018-0785

Sartore-Bianchi, A. et al. 2016. Dual-targeted therapy with trastuzumab and lapatinib in treatment-refractory, KRAS codon 12/13 wild-type, HER2-positive metastatic colorectal cancer (HERACLES): a proof-of-concept, multicentre, open-label, phase 2 trial. *Lancet Oncol* 17(6), pp. 738-746. doi: 10.1016/S1470-2045(16)00150-9

Saville, M. K. and Watson, R. J. 1998. The cell-cycle regulated transcription factor B-Myb is phosphorylated by cyclin A/Cdk2 at sites that enhance its transactivation properties. *Oncogene* 17(21), pp. 2679-2689. doi: 10.1038/sj.onc.1202503

Schmid, D. and Leitzmann, M. F. 2014. Television viewing and time spent sedentary in relation to cancer risk: a meta-analysis. *J Natl Cancer Inst* 106(7), doi: 10.1093/jnci/dju098

Schuell, B. et al. 2006. HER 2/neu protein expression in colorectal cancer. *BMC Cancer* 6, p. 123. doi: 10.1186/1471-2407-6-123

Shih, H. P. et al. 2013. Pancreas organogenesis: from lineage determination to morphogenesis. *Annu Rev Cell Dev Biol* 29, pp. 81-105. doi: 10.1146/annurev-cellbio-101512-122405

Shook, D. and Keller, R. 2003. Mechanisms, mechanics and function of epithelial-mesenchymal transitions in early development. *Mech Dev* 120(11), pp. 1351-1383. doi: 10.1016/j.mod.2003.06.005

Siegel, R. et al. 2014. Colorectal cancer statistics, 2014. *CA Cancer J Clin* 64(2), pp. 104-117. doi: 10.3322/caac.21220

- Siegel, R. L. et al. 2020. Colorectal Cancer in the Young: Epidemiology, Prevention, Management. *Am Soc Clin Oncol Educ Book* 40, pp. 1-14. doi: 10.1200/EDBK_279901
- Siena, S. et al. 2018. Targeting the human epidermal growth factor receptor 2 (HER2) oncogene in colorectal cancer. *Ann Oncol* 29(5), pp. 1108-1119. doi: 10.1093/annonc/mdy100
- Slattery, M. L. et al. 2018a. The MAPK-Signaling Pathway in Colorectal Cancer: Dysregulated Genes and Their Association With MicroRNAs. *Cancer Inform* 17, p. 1176935118766522. doi: 10.1177/1176935118766522
- Slattery, M. L. et al. 2018b. The PI3K/AKT signaling pathway: Associations of miRNAs with dysregulated gene expression in colorectal cancer. *Mol Carcinog* 57(2), pp. 243-261. doi: 10.1002/mc.22752
- Sleeman, J. P. 2000. The lymph node as a bridgehead in the metastatic dissemination of tumors. *Recent Results Cancer Res* 157, pp. 55-81. doi: 10.1007/978-3-642-57151-0_6
- Sluiter, N. et al. 2016. Adhesion molecules in peritoneal dissemination: function, prognostic relevance and therapeutic options. *Clin Exp Metastasis* 33(5), pp. 401-416. doi: 10.1007/s10585-016-9791-0
- Smyrk, T. C. and Lynch, H. T. 1999. Microsatellite instability: impact on cancer progression in proximal and distal colorectal cancers. *Eur J Cancer* 35(2), pp. 171-172. doi: 10.1016/s0959-8049(98)00380-3
- Snyder, C. and Hampel, H. 2019. Hereditary Colorectal Cancer Syndromes. *Semin Oncol Nurs* 35(1), pp. 58-78. doi: 10.1016/j.soncn.2018.12.011
- Song, Y. et al. 2002. Inhibition of anchorage-independent growth of transformed NIH3T3 cells by epithelial protein lost in neoplasm (EPLIN) requires localization of EPLIN to actin cytoskeleton. *Mol Biol Cell* 13(4), pp. 1408-1416. doi: 10.1091/mbc.01-08-0414
- Staudacher, J. J. et al. 2017. Activin signaling is an essential component of the TGF-beta induced pro-metastatic phenotype in colorectal cancer. *Sci Rep* 7(1), p. 5569. doi: 10.1038/s41598-017-05907-8
- Steder, M. et al. 2013. DNp73 exerts function in metastasis initiation by disconnecting the inhibitory role of EPLIN on IGF1R-AKT/STAT3 signaling. *Cancer Cell* 24(4), pp. 512-527. doi: 10.1016/j.ccr.2013.08.023
- Steinke, V. et al. 2013. Hereditary nonpolyposis colorectal cancer (HNPCC)/Lynch syndrome. *Dtsch Arztebl Int* 110(3), pp. 32-38. doi: 10.3238/arztebl.2013.0032
- Sundvold, H. et al. 2016. Arv1 promotes cell division by recruiting IQGAP1 and myosin to the cleavage furrow. *Cell Cycle* 15(5), pp. 628-643. doi: 10.1080/15384101.2016.1146834
- Szklarczyk, D. et al. 2021. The STRING database in 2021: customizable protein-protein networks, and functional characterization of user-uploaded gene/measurement sets. *Nucleic Acids Res* 49(D1), pp. D605-D612. doi: 10.1093/nar/gkaa1074

- Taha, M. et al. 2019. EPLIN-alpha and -beta Isoforms Modulate Endothelial Cell Dynamics through a Spatiotemporally Differentiated Interaction with Actin. *Cell Rep* 29(4), pp. 1010-1026 e1016. doi: 10.1016/j.celrep.2019.09.043
- Takayama, T. et al. 2006. Colorectal cancer: genetics of development and metastasis. *J Gastroenterol* 41(3), pp. 185-192. doi: 10.1007/s00535-006-1801-6
- Toon, C. W. et al. 2014. Immunohistochemistry for myc predicts survival in colorectal cancer. *PLoS One* 9(2), p. e87456. doi: 10.1371/journal.pone.0087456
- Tsoi, K. K. et al. 2009. Cigarette smoking and the risk of colorectal cancer: a meta-analysis of prospective cohort studies. *Clin Gastroenterol Hepatol* 7(6), pp. 682-688 e681-685. doi: 10.1016/j.cgh.2009.02.016
- Tsurumi, H. et al. 2014. Epithelial protein lost in neoplasm modulates platelet-derived growth factor-mediated adhesion and motility of mesangial cells. *Kidney Int* 86(3), pp. 548-557. doi: 10.1038/ki.2014.85
- Turner, B. C. et al. 1998. Expression of AP-2 transcription factors in human breast cancer correlates with the regulation of multiple growth factor signalling pathways. *Cancer Res* 58(23), pp. 5466-5472.
- Van der Jeught, K. et al. 2018. Drug resistance and new therapies in colorectal cancer. *World J Gastroenterol* 24(34), pp. 3834-3848. doi: 10.3748/wjg.v24.i34.3834
- Verweij, J. et al. 1994. Paclitaxel (Taxol) and docetaxel (Taxotere): not simply two of a kind. *Ann Oncol* 5(6), pp. 495-505. doi: 10.1093/oxfordjournals.annonc.a058903
- Vieira, A. R. et al. 2017. Foods and beverages and colorectal cancer risk: a systematic review and meta-analysis of cohort studies, an update of the evidence of the WCRF-AICR Continuous Update Project. *Ann Oncol* 28(8), pp. 1788-1802. doi: 10.1093/annonc/mdx171
- Villalba, M. et al. 2017. Role of TGF-beta in metastatic colon cancer: it is finally time for targeted therapy. *Cell Tissue Res* 370(1), pp. 29-39. doi: 10.1007/s00441-017-2633-9
- Vocka, M. et al. 2019. Novel serum markers HSP60, CHI3L1, and IGFBP-2 in metastatic colorectal cancer. *Oncol Lett* 18(6), pp. 6284-6292. doi: 10.3892/ol.2019.10925
- Vogelstein, B. et al. 1988. Genetic alterations during colorectal-tumor development. *N Engl J Med* 319(9), pp. 525-532. doi: 10.1056/NEJM198809013190901
- Vu, T. and Datta, P. K. 2017. Regulation of EMT in Colorectal Cancer: A Culprit in Metastasis. *Cancers (Basel)* 9(12), doi: 10.3390/cancers9120171
- Vuik, F. E. et al. 2019. Increasing incidence of colorectal cancer in young adults in Europe over the last 25 years. *Gut* 68(10), pp. 1820-1826. doi: 10.1136/gutjnl-2018-317592

- Wang, H. et al. 2007. Characterization of porcine EPLIN gene revealed distinct expression patterns for the two isoforms. *Anim Biotechnol* 18(2), pp. 101-108. doi: 10.1080/10495390600864660
- Wang, J. and Nakamura, F. 2019. Identification of Filamin A Mechanobinding Partner II: Fimbacin Is a Novel Actin Cross-Linking and Filamin A Binding Protein. *Biochemistry* 58(47), pp. 4737-4743. doi: 10.1021/acs.biochem.9b00101
- Wang, Q. et al. 2018. PIK3CA mutations confer resistance to first-line chemotherapy in colorectal cancer. *Cell Death Dis* 9(7), p. 739. doi: 10.1038/s41419-018-0776-6
- Wang, Y. et al. 2020. Inhibition of fatty acid catabolism augments the efficacy of oxaliplatin-based chemotherapy in gastrointestinal cancers. *Cancer Lett* 473, pp. 74-89. doi: 10.1016/j.canlet.2019.12.036
- Wang, Y. et al. 2013. HAVcR-1 expression in human colorectal cancer and its effects on colorectal cancer cells in vitro. *Anticancer Res* 33(1), pp. 207-214.
- Ward, P. S. and Thompson, C. B. 2012. Metabolic reprogramming: a cancer hallmark even warburg did not anticipate. *Cancer Cell* 21(3), pp. 297-308. doi: 10.1016/j.ccr.2012.02.014
- Weis, S. M. and Cheresch, D. A. 2011. Tumor angiogenesis: molecular pathways and therapeutic targets. *Nat Med* 17(11), pp. 1359-1370. doi: 10.1038/nm.2537
- Weisenberger, D. J. et al. 2006. CpG island methylator phenotype underlies sporadic microsatellite instability and is tightly associated with BRAF mutation in colorectal cancer. *Nat Genet* 38(7), pp. 787-793. doi: 10.1038/ng1834
- Williams, R. D. and Dickey, J. W., Jr. 1969. Physiology of the colon and rectum. *Am J Surg* 117(6), pp. 849-853. doi: 10.1016/0002-9610(69)90074-9
- Wilschut, J. A. et al. 2010. Increased risk of adenomas in individuals with a family history of colorectal cancer: results of a meta-analysis. *Cancer Causes Control* 21(12), pp. 2287-2293. doi: 10.1007/s10552-010-9654-y
- Wong, C. S. et al. 2008. Identification of 5-fluorouracil response proteins in colorectal carcinoma cell line SW480 by two-dimensional electrophoresis and MALDI-TOF mass spectrometry. *Oncol Rep* 20(1), pp. 89-98.
- Wu, D. 2017. Epithelial protein lost in neoplasm (EPLIN): Beyond a tumor suppressor. *Genes Dis* 4(2), pp. 100-107. doi: 10.1016/j.gendis.2017.03.002
- Wu, L. et al. 2013. Diabetes mellitus and the occurrence of colorectal cancer: an updated meta-analysis of cohort studies. *Diabetes Technol Ther* 15(5), pp. 419-427. doi: 10.1089/dia.2012.0263
- Wu, X. et al. 2020. The 60-kDa heat shock protein regulates energy rearrangement and protein synthesis to promote proliferation of multiple myeloma cells. *Br J Haematol* 190(5), pp. 741-752. doi: 10.1111/bjh.16569

- Xie, B. et al. 2019. Cyclin B1/CDK1-regulated mitochondrial bioenergetics in cell cycle progression and tumor resistance. *Cancer Lett* 443, pp. 56-66. doi: 10.1016/j.canlet.2018.11.019
- Xie, P. et al. 2014. Genetic demonstration of intestinal NPC1L1 as a major determinant of hepatic cholesterol and blood atherogenic lipoprotein levels. *Atherosclerosis* 237(2), pp. 609-617. doi: 10.1016/j.atherosclerosis.2014.09.036
- Xu, S. et al. 2020. Foes or Friends? Bacteria Enriched in the Tumor Microenvironment of Colorectal Cancer. *Cancers (Basel)* 12(2), doi: 10.3390/cancers12020372
- Yam, A. Y. et al. 2008. Defining the TRiC/CCT interactome links chaperonin function to stabilization of newly made proteins with complex topologies. *Nat Struct Mol Biol* 15(12), pp. 1255-1262. doi: 10.1038/nsmb.1515
- Yang, H. et al. 2021. Exosomal IDH1 increases the resistance of colorectal cancer cells to 5-Fluorouracil. *J Cancer* 12(16), pp. 4862-4872. doi: 10.7150/jca.58846
- Yonesaka, K. 2021. HER2-/HER3-Targeting Antibody-Drug Conjugates for Treating Lung and Colorectal Cancers Resistant to EGFR Inhibitors. *Cancers (Basel)* 13(5), doi: 10.3390/cancers13051047
- Yonesaka, K. et al. 2011. Activation of ERBB2 signaling causes resistance to the EGFR-directed therapeutic antibody cetuximab. *Sci Transl Med* 3(99), p. 99ra86. doi: 10.1126/scitranslmed.3002442
- Yu, J. S. and Cui, W. 2016. Proliferation, survival and metabolism: the role of PI3K/AKT/mTOR signalling in pluripotency and cell fate determination. *Development* 143(17), pp. 3050-3060. doi: 10.1242/dev.137075
- Zeng, S. et al. 2019. Chemoresistance in Pancreatic Cancer. *Int J Mol Sci* 20(18), doi: 10.3390/ijms20184504
- Zhan, T. et al. 2017. Wnt signaling in cancer. *Oncogene* 36(11), pp. 1461-1473. doi: 10.1038/onc.2016.304
- Zhang, L. L. et al. 2018a. miR-24 inhibited the killing effect of natural killer cells to colorectal cancer cells by downregulating Paxillin. *Biomed Pharmacother* 101, pp. 257-263. doi: 10.1016/j.biopha.2018.02.024
- Zhang, S. et al. 2013. Epidermal growth factor promotes protein degradation of epithelial protein lost in neoplasm (EPLIN), a putative metastasis suppressor, during epithelial-mesenchymal transition. *J Biol Chem* 288(3), pp. 1469-1479. doi: 10.1074/jbc.M112.438341
- Zhang, S. et al. 2011. EPLIN downregulation promotes epithelial-mesenchymal transition in prostate cancer cells and correlates with clinical lymph node metastasis. *Oncogene* 30(50), pp. 4941-4952. doi: 10.1038/onc.2011.199

Zhang, Y. et al. 2015. Stromal Cells Derived from Visceral and Obese Adipose Tissue Promote Growth of Ovarian Cancers. *PLoS One* 10(8), p. e0136361. doi: 10.1371/journal.pone.0136361

Zhang, Y. Y. et al. 2018b. A LIMA1 variant promotes low plasma LDL cholesterol and decreases intestinal cholesterol absorption. *Science* 360(6393), pp. 1087-1092. doi: 10.1126/science.aao6575

Zhitnyak, I. Y. et al. 2020. Early Events in Actin Cytoskeleton Dynamics and E-Cadherin-Mediated Cell-Cell Adhesion during Epithelial-Mesenchymal Transition. *Cells* 9(3), doi: 10.3390/cells9030578

Zubeldia, I. G. et al. 2013. Epithelial to mesenchymal transition and cancer stem cell phenotypes leading to liver metastasis are abrogated by the novel TGFbeta1-targeting peptides P17 and P144. *Exp Cell Res* 319(3), pp. 12-22. doi: 10.1016/j.yexcr.2012.11.004

Supplement materials

Supplement-1. Human Colorectal cancer TMA

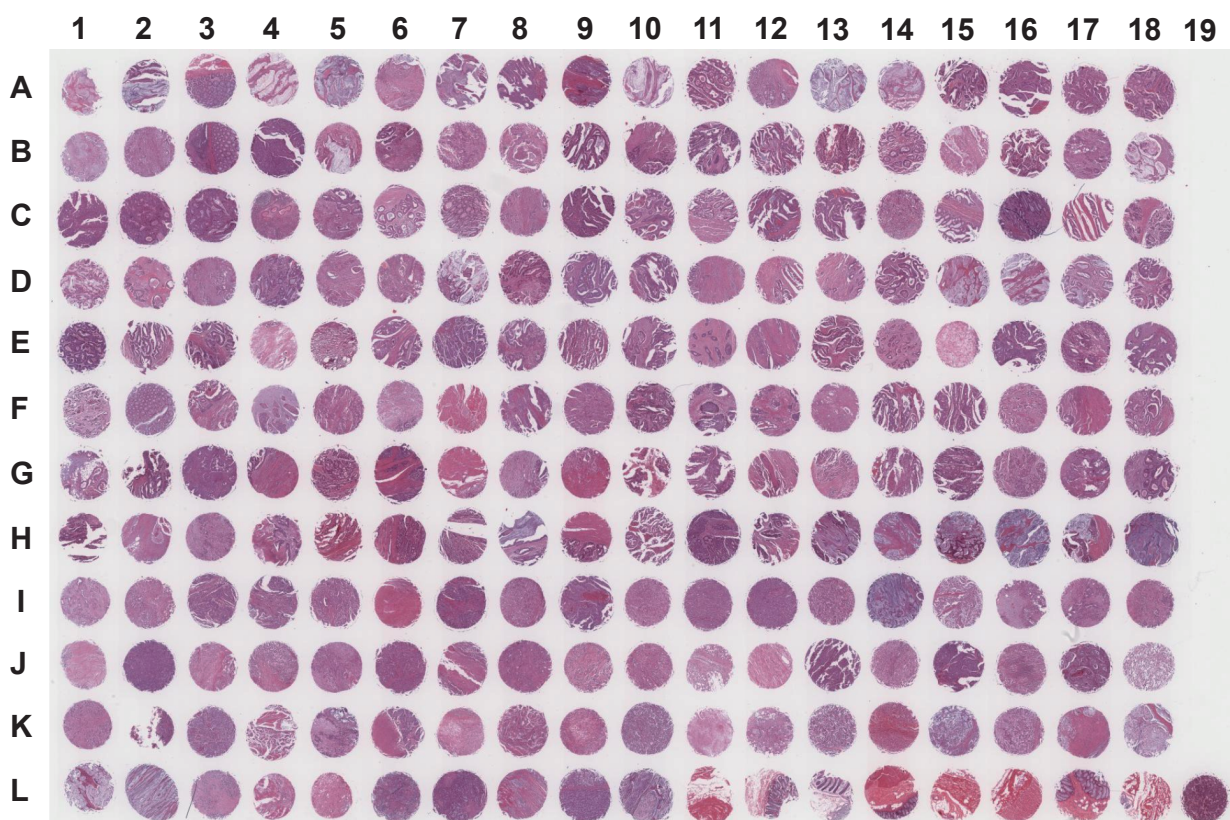


Figure S1 TMA of colon carcinoma and normal colon tissue. The TMA (CO2161a) (<https://www.biomax.us/tissue-arrays/Colon/CO2161a>) includes 205 cases of adenocarcinoma, 3 signet-ring cell carcinoma, 8 normal tissue, single core per case including pathology grade, TNM and clinical stage.

Table S1 Information about TMA (TNM, Grade, Stage and Tissue type)

Position	TNM	Grade	Stage	Type
A1	T3N1M0	-	IIIB	Malignant
A2	T4N1M0	1	IIIB	Malignant
A3	T3N0M0	-	IIA	Malignant
A4	T3N0M0	1	IIA	Malignant
A5	T3N2M0	1	IIIB	Malignant
A6	T2N1M0	1	IIIA	Malignant
A7	T3N1M0	1	IIIB	Malignant
A8	T2N0M0	1	I	Malignant
A9	T4N0M0	1	IIB	Malignant
A10	T3N0M0	-	IIA	Malignant
A11	T3N0M0	1	IIA	Malignant

A12	T2N0M0	2-3	I	Malignant
A13	T2N0M0	1	I	Malignant
A14	T4N0M1	1		Malignant
A15	T4N0M0	1	IIB	Malignant
A16	T4N0M0	2	IIB	Malignant
A17	T4N0M0	2	IIB	Malignant
A18	T4N0M0	2	IIB	Malignant
B1	T4N0M0	1	IIB	Malignant
B2	T3N0M0	2	IIA	Malignant
B3	T4N0M0	1	IIB	Malignant
B4	T3N2M0	2	IIIB	Malignant
B5	T2N0M0	1	I	Malignant
B6	T3N0M0	1	IIA	Malignant
B7	T2N0M0	2	I	Malignant
B8	T4N0M0	2	IIB	Malignant
B9	T3N0M0	1	IIA	Malignant
B10	T4N2M0	1	IIIC	Malignant
B11	T2N0M0	1	I	Malignant
B12	T2N0M0	1	I	Malignant
B13	T2N1M0	2	IIIA	Malignant
B14	T4N0M0	1	IIB	Malignant
B15	T3N0M0	1	IIA	Malignant
B16	T3N0M0	1	IIA	Malignant
B17	T4N0M0	1	IIB	Malignant
B18	T3N0M0	3	IIA	Malignant
C1	T3N1M0	2	IIIB	Malignant
C2	T4N1M0	2	IIIB	Malignant
C3	T3N0M0	2	IIA	Malignant
C4	T4N2M0	2	IIIC	Malignant
C5	T3N0M0	2	IIA	Malignant
C6	T4N0M0	1	IIB	Malignant
C7	T2N0M0	-	I	Malignant
C8	T4N2M0	2	IIIC	Malignant
C9	T3N0M0	2	IIA	Malignant
C10	T4N0M0	2	IIB	Malignant
C11	T2N0M0	2	I	Malignant
C12	T3N0M0	1	IIA	Malignant
C13	T3N0M0	2	IIA	Malignant
C14	T4N1M0	2	IIIB	Malignant

C15	T4N0M0	1	IIB	Malignant
C16	T1N0M0	2	I	Malignant
C17	T3N0M0	2	IIA	Malignant
C18	T3N0M0	2	IIA	Malignant
D1	T4N0M0	2	IIB	Malignant
D2	T4N0M0	2	IIB	Malignant
D3	T4N0M0	2	IIB	Malignant
D4	T3N0M0	2	IIA	Malignant
D5	T3N0M0	2	IIA	Malignant
D6	T3N0M0	2	IIA	Malignant
D7	T3N0M0	2	IIA	Malignant
D8	T3N0M0	2	IIA	Malignant
D9	T3N0M0	2	IIA	Malignant
D10	T4N0M0	1	IIB	Malignant
D11	T3N1M0	2	IIIB	Malignant
D12	T4N1M0	2	IIIB	Malignant
D13	T4N0M0	1	IIB	Malignant
D14	T2N0M0	1	I	Malignant
D15	T3N0M0	1-2	IIA	Malignant
D16	T3N0M0	1-2	IIA	Malignant
D17	T4N2M0	1-2	IIIC	Malignant
D18	T4N0M0	2	IIB	Malignant
E1	T4N2M0	2	IIIC	Malignant
E2	T3N1M0	1	IIIB	Malignant
E3	T3N1M0	1	IIIB	Malignant
E4	T3N1M0	1	IIIB	Malignant
E5	T4N2M0	2	IIIC	Malignant
E6	T3N1M0	2	IIIB	Malignant
E7	T4N0M0	2	IIB	Malignant
E8	T3N0M0	2	IIA	Malignant
E9	T4N0M1	2	IV	Malignant
E10	T3N0M0	2	IIA	Malignant
E11	T4N2M0	2	IIIC	Malignant
E12	T4N0M0	2	IIB	Malignant
E13	T3N0M0	2	IIA	Malignant
E14	T4N0M0	2	IIB	Malignant
E15	T3N2M0	2	IIIB	Malignant
E16	T2N0M0	2	I	Malignant
E17	T4N2M0	2	IIIC	Malignant

E18	T3N0M0	2	IIA	Malignant
F1	T4N1M0	2	IIIB	Malignant
F2	T4N2M0	-	IIIC	Malignant
F3	T3N1M0	2	IIIB	Malignant
F4	T4N0M0	3	IIB	Malignant
F5	T4N1M0	2	IIIB	Malignant
F6	T3N0M0	2	IIA	Malignant
F7	T3N0M0	-	IIA	Malignant
F8	T3N1M0	2-3	IIIB	Malignant
F9	T4N0M0	2	IIB	Malignant
F10	T3N0M0	2	IIA	Malignant
F11	T4N0M0	3	IIB	Malignant
F12	T3N0M0	2	IIA	Malignant
F13	T4N1M0	2	IIIB	Malignant
F14	T4N1M0	2	IIIB	Malignant
F15	T3N1M0	2	IIIB	Malignant
F16	T4N1M0	2	IIIB	Malignant
F17	T3N2M0	2	IIIB	Malignant
F18	T3N0M0	2	IIA	Malignant
G1	T3N0M0	2	IIA	Malignant
G2	T3N1M0	2	IIIB	Malignant
G3	T3N0M0	2	IIA	Malignant
G4	T3N1M0	2	IIIB	Malignant
G5	T4N0M0	2	IIB	Malignant
G6	T3N1M0	2	IIIB	Malignant
G7	T3N0M0	2	IIA	Malignant
G8	T4N0M0	2	IIB	Malignant
G9	T3N0M0	3	IIA	Malignant
G10	T3N0M0	1	IIA	Malignant
G11	T4N0M0	2	IIB	Malignant
G12	T3N0M0	2	IIA	Malignant
G13	T4N1M0	2	IIIB	Malignant
G14	T3N0M0	2	IIA	Malignant
G15	T3N0M0	2	IIA	Malignant
G16	T3N0M0	2	IIA	Malignant
G17	T3N0M0	2	IIA	Malignant
G18	T4N2M0	2	IIIC	Malignant
H1	T2N0M0	2	I	Malignant
H2	T4N1M0	2	IIIB	Malignant

H3	T3N0M0	2	IIA	Malignant
H4	T3N0M0	2	IIA	Malignant
H5	T3N1M0	2	IIIB	Malignant
H6	T2N0M0	2	I	Malignant
H7	T2N2M0	3	IIIB	Malignant
H8	T3N1M0	2	IIIB	Malignant
H9	T3N0M0	2	IIA	Malignant
H10	T2N0M0	2	I	Malignant
H11	T4N0M0	2	IIB	Malignant
H12	T3N1M0	2	IIIB	Malignant
H13	T4N0M0	2	IIB	Malignant
H14	T3N0M0	2	IIA	Malignant
H15	T3N0M0	2	IIA	Malignant
H16	T3N0M0	2	IIA	Malignant
H17	T3N1M0	2	IIIB	Malignant
H18	T3N0M0	2	IIA	Malignant
I1	T4N0M0	2-3	IIB	Malignant
I2	T3N1M0	3	IIIB	Malignant
I3	T3N1M0	3	IIIB	Malignant
I4	T3N0M0	2	IIA	Malignant
I5	T3N1M0	2-3	IIIB	Malignant
I6	T3N1M0	-	IIIB	Malignant
I7	T3N1M0	3	IIIB	Malignant
I8	T2N0M0	3	I	Malignant
I9	T3N0M0	2	IIA	Malignant
I10	T3N0M0	3	IIA	Malignant
I11	T3N0M0	3	IIA	Malignant
I12	T3N0M0	3	IIA	Malignant
I13	T3N1M0	3	IIIB	Malignant
I14	T3N1M0	2-3	IIIB	Malignant
I15	T3N0M0	3	IIA	Malignant
I16	T4N2M0	3	IIIC	Malignant
I17	T4N0M0	3	IIB	Malignant
I18	T3N0M0	3	IIA	Malignant
J1	T3N1M0	3	IIIB	Malignant
J2	T3N0M0	3	IIA	Malignant
J3	T4N1M1	3	IV	Malignant
J4	T3N0M0	3	IIA	Malignant
J5	T4N2M0	3	IIIC	Malignant

J6	T3N0M0	3	IIA	Malignant
J7	T3N0M0	3	IIA	Malignant
J8	T3N0M0	3	IIA	Malignant
J9	T3N0M0	3	IIA	Malignant
J10	T4N2M0	3	IIIC	Malignant
J11	T3N0M0	3	IIA	Malignant
J12	T4N1M0	-	IIIB	Malignant
J13	T4N0M0	3	IIB	Malignant
J14	T4N0M0	3	IIB	Malignant
J15	T2N0M0	3	I	Malignant
J16	T4N2M0	3	IIIC	Malignant
J17	T3N0M0	2-3	IIA	Malignant
J18	T3N0M0	3	IIA	Malignant
K1	T3N0M0	3	IIA	Malignant
K2	T3N0M0	3	IIA	Malignant
K3	T3N0M0	3	IIA	Malignant
K4	T4N0M0	3	IIB	Malignant
K5	T4N0M0	3	IIB	Malignant
K6	T3N1M0	3	IIIB	Malignant
K7	T4N0M0	3	IIB	Malignant
K8	T4N0M0	-	IIB	Malignant
K9	T3N2M1	3	IV	Malignant
K10	T4N2M0	3	IIIC	Malignant
K11	T3N1M0	-	IIIB	Malignant
K12	T4N2M0	3	IIIC	Malignant
K13	T3N1M0	3	IIIB	Malignant
K14	T2N0M0	3	I	Malignant
K15	T4N2M0	3	IIIC	Malignant
K16	T3N1M0	3	IIIB	Malignant
K17	T3N0M0	3	IIA	Malignant
K18	T3N1M0	3	IIIB	Malignant
L1	T3N0M0	3	IIA	Malignant
L2	T3N0M0	3	IIA	Malignant
L3	T4N2M0	3	IIIC	Malignant
L4	T4N1M0	3	IIIB	Malignant
L5	T3N0M0	3	IIA	Malignant
L6	T3N1M0	3	IIIB	Malignant
L7	T4N0M0	2	IIB	Malignant
L8	T3N0M0	-	IIA	Malignant

L9	T3N0M0	-	IIA	Malignant
L10	T4N0M1	-	IV	Malignant
L11	-	-	-	Normal
L12	-	-	-	Normal
L13	-	-	-	Normal
L14	-	-	-	Normal
L15	-	-	-	Normal
L16	-	-	-	Normal
L17	-	-	-	Normal

Supplement-2. TMA of human pancreatic cancer.

Table S2 Information about pancreatic cancer TMA (PA2081a) (TNM, Grade, Stage and Tissue type). The TMA contains 42 cases of pancreatic duct adenocarcinoma, 3 pancreatic adenosquamous carcinoma, 1 pancreatic islet cell carcinoma, 6 pancreatic metastatic carcinoma, 10 pancreatic islet cell tumor, 11 pancreatic inflammation, 21 adjacent normal pancreatic tissue and 10 normal pancreatic tissue (from autopsy), duplicated cores per case.

Position	Organ (Anatomic Site)	Pathology diagnosis	TNM	Grade	Stage	Type
A1	Pancreas	Duct adenocarcinoma (chronic inflammation of fibrofatty tissue and blood vessel)	T2N0M0	-	I	malignant
A2	Pancreas	Duct adenocarcinoma (chronic pancreatitis)	T2N0M0	-	I	malignant
A3	Pancreas	Duct adenocarcinoma	T3N0M0	1	II	malignant
A4	Pancreas	Duct adenocarcinoma	T3N0M0	1	II	malignant
A5	Pancreas	Duct adenocarcinoma (pancreatic tissue)	T2N0M0	-	I	malignant
A6	Pancreas	Duct adenocarcinoma	T2N0M0	1	I	malignant
A7	Pancreas	Duct adenocarcinoma (tumoral necrosis)	T2N0M0	-	I	malignant
A8	Pancreas	Duct adenocarcinoma (tumoral necrosis)	T2N0M0	-	I	malignant
A9	Pancreas	Duct adenocarcinoma	T3N0M0	1--2	II	malignant
A10	Pancreas	Duct adenocarcinoma	T3N0M0	1--2	II	malignant
A11	Pancreas	Duct adenocarcinoma	T3N0M0	1	II	malignant
A12	Pancreas	Duct adenocarcinoma	T3N0M0	1	II	malignant
A13	Pancreas	Duct adenocarcinoma	T3N0M0	1	II	malignant
A14	Pancreas	Duct adenocarcinoma	T3N0M0	1	II	malignant
A15	Pancreas	Duct adenocarcinoma	T3N0M0	1	II	malignant
A16	Pancreas	Duct adenocarcinoma	T3N0M0	1	II	malignant
B1	Pancreas	Duct adenocarcinoma	T2N0M0	2	I	malignant
B2	Pancreas	Duct adenocarcinoma	T2N0M0	2	I	malignant
B3	Pancreas	Duct adenocarcinoma	T3N0M0	2	II	malignant
B4	Pancreas	Duct adenocarcinoma	T3N0M0	2	II	malignant
B5	Pancreas	Duct adenocarcinoma	T4N1M0	2	III	malignant
B6	Pancreas	Duct adenocarcinoma	T4N1M0	2	III	malignant
B7	Pancreas	Duct adenocarcinoma	T2N0M0	2	I	malignant

B8	Pancreas	Duct adenocarcinoma	T2N0M0	2	I	malignant
B9	Pancreas	Duct adenocarcinoma	T2N0M0	2	I	malignant
B10	Pancreas	Duct adenocarcinoma	T2N0M0	2	I	malignant
B11	Pancreas	Duct adenocarcinoma	T3N0M0	2	II	malignant
B12	Pancreas	Duct adenocarcinoma	T3N0M0	2	II	malignant
B13	Pancreas	Duct adenocarcinoma	T4N0M0	2	III	malignant
B14	Pancreas	Duct adenocarcinoma (sparse)	T4N0M0	1	III	malignant
B15	Pancreas	Duct adenocarcinoma	T3N1M0	1	III	malignant
B16	Pancreas	Duct adenocarcinoma	T3N1M0	1	III	malignant
C1	Pancreas	Duct adenocarcinoma (fibrofatty tissue and blood vessel)	T2N0M0	-	I	malignant
C2	Pancreas	Duct adenocarcinoma (fibrofatty tissue and blood vessel)	T2N0M0	-	I	malignant
C3	Pancreas	Duct adenocarcinoma	T3N0M0	2	II	malignant
C4	Pancreas	Duct adenocarcinoma	T3N0M0	2	II	malignant
C5	Pancreas	Duct adenocarcinoma	T3N0M1	2	IV	malignant
C6	Pancreas	Duct adenocarcinoma	T3N0M1	2	IV	malignant
C7	Pancreas	Duct adenocarcinoma (sparse)	T2N0M0	2	I	malignant
C8	Pancreas	Duct adenocarcinoma (sparse)	T2N0M0	2	I	malignant
C9	Pancreas	Duct adenocarcinoma	T2N0M0	2	I	malignant
C10	Pancreas	Duct adenocarcinoma	T2N0M0	2	I	malignant
C11	Pancreas	Duct adenocarcinoma	T2N1M0	2	III	malignant
C12	Pancreas	Duct adenocarcinoma	T2N1M0	2	III	malignant
C13	Pancreas	Duct adenocarcinoma	T2N0M0	2	I	malignant
C14	Pancreas	Duct adenocarcinoma	T2N0M0	2	I	malignant
C15	Pancreas	Duct adenocarcinoma	T2N0M0	3	I	malignant
C16	Pancreas	Duct adenocarcinoma	T2N0M0	3	I	malignant
D1	Pancreas	Duct adenocarcinoma	T3N1M0	3	III	malignant
D2	Pancreas	Duct adenocarcinoma	T3N1M0	3	III	malignant
D3	Pancreas	Duct adenocarcinoma	T2N0M0	1	I	malignant
D4	Pancreas	Duct adenocarcinoma	T2N0M0	1	I	malignant
D5	Pancreas	Duct adenocarcinoma	T2N0M0	3	I	malignant

D6	Pancreas	Duct adenocarcinoma	T2N0M0	3	I	malignant
D7	Pancreas	Duct adenocarcinoma	T4N1M1	3	IV	malignant
D8	Pancreas	Duct adenocarcinoma	T4N1M1	3	IV	malignant
D9	Pancreas	Duct adenocarcinoma	T2N0M0	3	I	malignant
D10	Pancreas	Duct adenocarcinoma	T2N0M0	3	I	malignant
D11	Pancreas	Duct adenocarcinoma (pancreatic tissue)	T1N0M0	-	I	malignant
D12	Pancreas	Duct adenocarcinoma (pancreatic tissue)	T1N0M0	-	I	malignant
D13	Pancreas	Duct adenocarcinoma	T3N0M0	3	II	malignant
D14	Pancreas	Duct adenocarcinoma	T3N0M0	3	II	malignant
D15	Pancreas	Duct adenocarcinoma	T2N0M0	3	I	malignant
D16	Pancreas	Duct adenocarcinoma	T2N0M0	3	I	malignant
E1	Pancreas	Duct adenocarcinoma	T2N0M0	3	I	malignant
E2	Pancreas	Duct adenocarcinoma	T2N0M0	3	I	malignant
E3	Pancreas	Duct adenocarcinoma with necrosis (sparse)	T2N0M0	3	I	malignant
E4	Pancreas	Duct adenocarcinoma with necrosis (sparse)	T2N0M0	3	I	malignant
E5	Pancreas	Duct adenocarcinoma	T2N0M0	3	I	malignant
E6	Pancreas	Duct adenocarcinoma	T2N0M0	3	I	malignant
E7	Pancreas	Duct adenocarcinoma (sparse)	T3N0M0	3	II	malignant
E8	Pancreas	Duct adenocarcinoma	T3N0M0	3	II	malignant
E9	Pancreas	Duct adenocarcinoma	T3N0M0	3	II	malignant
E10	Pancreas	Duct adenocarcinoma	T3N0M0	3	II	malignant
E11	Pancreas	Duct adenocarcinoma	T2N0M0	3	I	malignant
E12	Pancreas	Duct adenocarcinoma	T2N0M0	3	I	malignant
E13	Pancreas	Duct adenocarcinoma	T2N0M0	3	I	malignant
E14	Pancreas	Duct adenocarcinoma	T2N0M0	3	I	malignant
E15	Pancreas	Duct adenocarcinoma	T3N0M0	3	II	malignant
E16	Pancreas	Duct adenocarcinoma	T3N0M0	3	II	malignant
F1	Pancreas	Duct adenocarcinoma	T3N0M0	3	II	malignant
F2	Pancreas	Duct adenocarcinoma	T3N0M0	3	II	malignant
F3	Pancreas	Duct adenocarcinoma	T2N0M0	3	I	malignant

F4	Pancreas	Duct adenocarcinoma	T2N0M0	3	I	malignant
F5	Pancreas	Adenosquamous carcinoma	T3N1M0	-	III	malignant
F6	Pancreas	Adenosquamous carcinoma	T3N1M0	-	III	malignant
F7	Pancreas	Adenosquamous carcinoma	T3N0M0	-	II	malignant
F8	Pancreas	Adenosquamous carcinoma	T3N0M0	-	II	malignant
F9	Pancreas	Adenosquamous carcinoma	T3N0M0	-	II	malignant
F10	Pancreas	Adenosquamous carcinoma	T3N0M0	-	II	malignant
F11	Abdominal cavity	Islet cell carcinoma	-	-	-	malignant
F12	Abdominal cavity	Islet cell carcinoma	-	-	-	malignant
F13	Epiploon	Metastatic duct adenocarcinoma from pancreas	-	2	-	metastasis
F14	Epiploon	Metastatic duct adenocarcinoma from pancreas	-	2	-	metastasis
F15	Abdominal cavity	Metastatic duct adenocarcinoma from pancreas	-	3	-	metastasis
F16	Abdominal cavity	Metastatic duct adenocarcinoma from pancreas	-	3	-	metastasis
G1	Liver	Metastatic duct adenocarcinoma from pancreas	-	2	-	metastasis
G2	Liver	Metastatic duct adenocarcinoma from pancreas	-	2	-	metastasis
G3	Liver	Metastatic duct adenocarcinoma from pancreas	-	2	-	metastasis
G4	Liver	Metastatic duct adenocarcinoma from pancreas	-	2	-	metastasis
G5	Liver	Metastatic duct adenocarcinoma from pancreas	-	3	-	metastasis
G6	Liver	Metastatic duct adenocarcinoma from pancreas	-	3	-	metastasis
G7	Lymph node	Metastatic duct adenocarcinoma from pancreas	-	3	-	metastasis
G8	Lymph node	Metastatic duct adenocarcinoma from pancreas	-	3	-	metastasis
G9	Pancreas	Islet cell tumor	-	-	-	benign
G10	Pancreas	Islet cell tumor	-	-	-	benign
G11	Pancreas	Islet cell tumor	-	-	-	benign
G12	Pancreas	Islet cell tumor	-	-	-	benign
G13	Pancreas	Islet cell tumor	-	-	-	benign
G14	Pancreas	Islet cell tumor	-	-	-	benign
G15	Pancreas	Islet cell tumor	-	-	-	benign
G16	Pancreas	Islet cell tumor	-	-	-	benign
H1	Pancreas	Islet cell tumor	-	-	-	benign
H2	Pancreas	Islet cell tumor	-	-	-	benign
H3	Pancreas	Islet cell tumor	-	-	-	benign

H4	Pancreas	Islet cell tumor	-	-	-	benign
H5	Pancreas	Islet cell tumor	-	-	-	benign
H6	Pancreas	Islet cell tumor	-	-	-	benign
H7	Pancreas	Islet cell tumor (pancreatic tissue)	-	-	-	benign
H8	Pancreas	Islet cell tumor (pancreatic tissue)	-	-	-	benign
H9	Pancreas	Islet cell tumor	-	-	-	benign
H10	Pancreas	Islet cell tumor	-	-	-	benign
H11	Pancreas	Islet cell tumor	-	-	-	benign
H12	Pancreas	Islet cell tumor	-	-	-	benign
H13	Pancreas	Chronic pancreatitis	-	-	-	inflammation
H14	Pancreas	Chronic pancreatitis	-	-	-	inflammation
H15	Pancreas	Chronic pancreatitis	-	-	-	inflammation
H16	Pancreas	Chronic pancreatitis	-	-	-	inflammation
I1	Pancreas	Mild chronic inflammation	-	-	-	inflammation
I2	Pancreas	Mild chronic inflammation	-	-	-	inflammation
I3	Pancreas	Chronic pancreatitis	-	-	-	inflammation
I4	Pancreas	Chronic pancreatitis	-	-	-	inflammation
I5	Pancreas	Chronic inflammation (chronic inflammation of fibrous tissue and blood vessel)	-	-	-	inflammation
I6	Pancreas	Chronic pancreatitis	-	-	-	inflammation
I7	Pancreas	Chronic pancreatitis	-	-	-	inflammation
I8	Pancreas	Chronic pancreatitis	-	-	-	inflammation
I9	Pancreas	Mild chronic inflammation	-	-	-	inflammation
I10	Pancreas	Mild chronic inflammation	-	-	-	inflammation
I11	Pancreas	Chronic pancreatitis	-	-	-	inflammation
I12	Pancreas	Chronic pancreatitis	-	-	-	inflammation
I13	Pancreas	Chronic pancreatitis	-	-	-	inflammation
I14	Pancreas	Chronic pancreatitis	-	-	-	inflammation
I15	Pancreas	Mild chronic inflammation	-	-	-	inflammation
I16	Pancreas	Mild chronic inflammation	-	-	-	inflammation
J1	Pancreas	Mild chronic inflammation	-	-	-	inflammation
J2	Pancreas	Mild chronic inflammation	-	-	-	inflammation
J3	Pancreas	Cancer adjacent normal pancreatic tissue	-	-	-	NAT
J4	Pancreas	Cancer adjacent normal pancreatic tissue	-	-	-	NAT

J5	Pancreas	Cancer adjacent normal pancreatic tissue	-	-	-	NAT
J6	Pancreas	Cancer adjacent normal pancreatic tissue	-	-	-	NAT
J7	Pancreas	Cancer adjacent normal pancreatic tissue	-	-	-	NAT
J8	Pancreas	Cancer adjacent normal pancreatic tissue	-	-	-	NAT
J9	Pancreas	Cancer adjacent normal pancreatic tissue	-	-	-	NAT
J10	Pancreas	Cancer adjacent normal pancreatic tissue	-	-	-	NAT
J11	Pancreas	Cancer adjacent normal pancreatic tissue	-	-	-	NAT
J12	Pancreas	Cancer adjacent normal pancreatic tissue	-	-	-	NAT
J13	Pancreas	Cancer adjacent normal pancreatic tissue	-	-	-	NAT
J14	Pancreas	Cancer adjacent normal pancreatic tissue	-	-	-	NAT
J15	Pancreas	Cancer adjacent normal pancreatic tissue (sparse)	-	-	-	NAT
J16	Pancreas	Cancer adjacent normal pancreatic tissue	-	-	-	NAT
K1	Pancreas	Cancer adjacent normal pancreatic tissue	-	-	-	NAT
K2	Pancreas	Cancer adjacent normal pancreatic tissue	-	-	-	NAT
K3	Pancreas	Cancer adjacent normal pancreatic tissue	-	-	-	NAT
K4	Pancreas	Cancer adjacent normal pancreatic tissue	-	-	-	NAT
K5	Pancreas	Cancer adjacent normal pancreatic tissue with ductal hyperplasia (sparse)	-	-	-	NAT
K6	Pancreas	Cancer adjacent normal pancreatic tissue	-	-	-	NAT
K7	Pancreas	Cancer adjacent normal pancreatic tissue	-	-	-	NAT
K8	Pancreas	Cancer adjacent normal pancreatic tissue	-	-	-	NAT
K9	Pancreas	Cancer adjacent normal pancreatic tissue	-	-	-	NAT

K10	Pancreas	Cancer adjacent normal pancreatic tissue	-	-	-	NAT
K11	Pancreas	Cancer adjacent normal pancreatic tissue	-	-	-	NAT
K12	Pancreas	Cancer adjacent normal pancreatic tissue	-	-	-	NAT
K13	Pancreas	Cancer adjacent normal pancreatic tissue	-	-	-	NAT
K14	Pancreas	Cancer adjacent normal pancreatic tissue	-	-	-	NAT
K15	Pancreas	Cancer adjacent normal pancreatic tissue	-	-	-	NAT
K16	Pancreas	Cancer adjacent normal pancreatic tissue	-	-	-	NAT
L1	Pancreas	Cancer adjacent normal pancreatic tissue	-	-	-	NAT
L2	Pancreas	Cancer adjacent normal pancreatic tissue	-	-	-	NAT
L3	Pancreas	Cancer adjacent normal pancreatic tissue	-	-	-	NAT
L4	Pancreas	Cancer adjacent normal pancreatic tissue	-	-	-	NAT
L5	Pancreas	Cancer adjacent normal pancreatic tissue	-	-	-	NAT
L6	Pancreas	Cancer adjacent normal pancreatic tissue	-	-	-	NAT
L7	Pancreas	Cancer adjacent normal pancreatic tissue	-	-	-	NAT
L8	Pancreas	Cancer adjacent normal pancreatic tissue	-	-	-	NAT
L9	Pancreas	Cancer adjacent normal pancreatic tissue	-	-	-	NAT
L10	Pancreas	Cancer adjacent normal pancreatic tissue	-	-	-	NAT
L11	Pancreas	Cancer adjacent normal pancreatic tissue	-	-	-	NAT
L12	Pancreas	Cancer adjacent normal pancreatic tissue	-	-	-	NAT
L13	Pancreas	Normal pancreatic tissue	-	-	-	normal
L14	Pancreas	Normal pancreatic tissue	-	-	-	normal
L15	Pancreas	Normal pancreatic tissue	-	-	-	normal
L16	Pancreas	Normal pancreatic tissue	-	-	-	normal
M1	Pancreas	Normal pancreatic tissue	-	-	-	normal

M2	Pancreas	Normal pancreatic tissue	-	-	-	normal
M3	Pancreas	Normal pancreatic tissue	-	-	-	normal
M4	Pancreas	Normal pancreatic tissue	-	-	-	normal
M5	Pancreas	Normal pancreatic tissue (small intestine tissue)	-	-	-	normal
M6	Pancreas	Normal pancreatic tissue (chronic inflammation of fibrous tissue and blood vessel)	-	-	-	normal
M7	Pancreas	Normal pancreatic tissue	-	-	-	normal
M8	Pancreas	Normal pancreatic tissue	-	-	-	normal
M9	Pancreas	Normal pancreatic tissue	-	-	-	normal
M10	Pancreas	Normal pancreatic tissue	-	-	-	normal
M11	Pancreas	Normal pancreatic tissue	-	-	-	normal
M12	Pancreas	Normal pancreatic tissue	-	-	-	normal
M13	Pancreas	Normal pancreatic tissue	-	-	-	normal
M14	Pancreas	Normal pancreatic tissue	-	-	-	normal
M15	Pancreas	Normal pancreatic tissue	-	-	-	normal
M16	Pancreas	Normal pancreatic tissue	-	-	-	normal